Quantitative analysis of regulated proteolysis and protein dephosphorylation during mitotic exit



James Holder
St Edmund Hall
University of Oxford

A thesis submitted for the degree of
Doctor of Philosophy

Michaelmas 2018

This thesis is dedicated to my family and friends in recognition of all the support they have given me.

Acknowledgements

Having spent the last four years working towards the completion of a research-based Biochemistry DPhil here in Oxford, I would now like to recognise all those who encouraged and supported me during this period, and to acknowledge the organisations who provided the funding which supported my work.

I am indebted to both Oxford University for the generous bursary that first enabled me to take up my place as an undergraduate and to the Wellcome Trust and their programme director Matthew Whitby for offering me a place on their postgraduate research programme with the financial support this provided. Furthermore, it would not have been possible for this work to have been carried out without the funding awarded to the Barr Lab by Cancer Research UK.

I feel privileged to have worked in the Barr Lab, where I have benefitted greatly from the knowledge and expertise of all my colleagues, past and present. In particular, Dr Michael Cundell, Dr Ricardo Nunes-Bastos, Dr Andreas Gerondopoulos and Josip Ahel, who directed and supported me throughout my graduate studies. I am especially grateful for the unlimited guidance provided by my supervisor and mentor Professor Francis Barr. Considerable assistance has also been received from other sources: Professor Shabaz Mohammed for instructing me in the proficient use of the mass spectrometer; colleagues in the Gruneberg Lab for their collaborative work; and more recently, Professor Mike Goldberg of Cornell University for the opportunity to collaborate with him and join him in enlightening discussions. I would also like to thank Professor Jordan Raff and Professor Alison Woollard for their direction during two six-month rotation projects at the beginning of my DPhil.

The review and assessment of my research thesis was undertaken by Professor Chris Norbury and Dr Helfrid Hochegger and I am most grateful for their valuable feedback and input.

I would also like to thank my wife, Hillary, for her never-ending belief in me and her boundless patience regarding the long hours spent in the lab. Lastly, thanks go to my parents for their unwavering support throughout my time at university and especially for proof reading my thesis, an extremely difficult task for non-scientists.

The completion of this thesis would not have been possible without the contributions made by all the above-mentioned people and I would like to take this opportunity to sincerely thank everyone.

The work described in this thesis is the candidate’s own, except where stated to the contrary.

Abstract

The critical function of the cell cycle is to enable the faithful inheritance of genetic material. Correct attachment of chromosomes triggers degradation of cyclin B and entry into anaphase, the cell subsequently undergoing a series of rapidly occurring changes. Precise regulation of these events is necessary to ensure that they take place in the correct order and is crucial for the success of mitotic exit. This regulation has been attributed to the activity of both phosphatases and the anaphase-promoting complex/cyclosome (APC/C), but the relative contribution of each process remains unclear.

Using a quantitative, high-resolution mass spectrometric analysis, this work shows that the order of events in anaphase is controlled by a series of graded dephosphorylations whose rate is encoded into the system at the level of each individual phospho-site, based on the site's sequence characteristics. Phospho-serines surrounded by acidic residues are seen to be dephosphorylated more slowly than more basic phospho-threonine sites. This preference also applies to PP1 dependent dephosphorylations and is consistent with the previously identified substrate specificity of PP2A-B55. This indicates a general rate-determining principle of phospho-protein phosphatase-mediated dephosphorylation. In addition, the results presented in this thesis indicate that PP1 activates itself following CDK1 inactivation, promoting the dephosphorylation of over 1000 phospho-sites. Finally, in the absence of CDK activity, APC/C-dependent proteolysis is not necessary for ordered dephosphorylation. A single proteolytic event, the destruction of cyclin B, is therefore sufficient for orderly mitotic exit through relieving inhibition of phosphatase activity.

TABLE OF CONTENTS

1 INTRODUCTION 1

1.1 THE BALANCE OF KINASE AND PHOSPHATASE ACTIVITIES GOVERNS CELL CYCLE PROGRESSION 1

1.1.1 CDK1 ACTIVATION DRIVES ENTRY INTO MITOSIS 2

1.1.2 PHOSPHO-PROTEIN PHOSPHATASES 9

1.2 MITOTIC EXIT RELIES ON A PRECISELY TIMED SHIFT IN THE BALANCE BETWEEN KINASE AND PHOSPHATASE ACTIVITY 13

1.2.1 THE SPINDLE ASSEMBLY CHECKPOINT PREVENTS A PREMATURE SHIFT IN GLOBAL PHOSPHORYLATION STATUS 14

1.2.2 MITOTIC EXIT: THE REVERSAL OF CDK PHOSPHORYLATIONS 20

1.2.3 REGULATION OF PHOSPHO-PROTEIN PHOSPHATASES DURING MITOSIS 23

1.2.4 SUBSTRATE SPECIFICITY OF PP2A-B55 IMPOSES ORDER ON MITOTIC EXIT 32

1.3 UBIQUITIN DEPENDENT PROTEOLYSIS 33

1.3.1 CELL CYCLE CONTROL OF THE ANAPHASE PROMOTING COMPLEX/CYCLOSOME 37

1.3.2 THE ROLE OF ORDERED PROTEOLYSIS DURING MITOSIS AND MITOTIC EXIT 41

1.4 THESIS AIMS 45

2 RESULTS 47

2.1 ESTABLISHING A SYSTEM FOR *IN VIVO* ANALYSIS OF MITOTIC EXIT 47

2.1.1 PILOT PROTEOMIC ANALYSIS OF MITOTIC EXIT 47

2.1.2 OPTIMISATION OF MASS SPECTROMETRY PROTOCOLS 56

2.1.2.1 Proteins bound tightly to DNA are lost during clarification 56

2.1.2.2 Identifying optimal digestion conditions for both the phospho- and total-proteomes 58

2.1.3 OPTIMISED PROTEOMIC ANALYSIS OF MITOTIC EXIT 62

2.2 THE ROLE AND REGULATION OF PROTEOLYSIS DURING MITOTIC EXIT 78

2.2.1 DEGRADATION OF CCNB IS THE MINIMAL REQUIREMENT FOR PROTEOLYSIS DURING MITOTIC EXIT 78

2.2.2 THE BALANCE OF PROTEIN SYNTHESIS AND PROTEIN DEGRADATION DURING MITOSIS . 88

2.2.3 INHIBITION OF THE APC/C IS DEPENDENT ON CDK1 ACTIVITY 99

2.3 PP1 IS POSITIONED TO PLAY A CENTRAL ROLE IN THE REGULATION OF MITOSIS AND MITOTIC EXIT.....104
2.3.1 PP1 HELPS ACTIVATE THE APC/C DURING MITOTIC EXIT..... 104
2.3.2 UNDERSTANDING THE MITOTIC REGULATION OF PP1..... 118

3 DISCUSSION 133

3.1 A CASCADE OF DEPHOSPHORYLATIONS PROVIDE ORDER TO MITOTIC EXIT 133
3.1.1 PP1 OPPOSES ITS OWN CDK1-MEDIATED INHIBITION 134
3.1.2 PP1 LOCALLY OVERCOMES CDK1 REGULATION TO PROMOTE APC/C ACTIVATION ... 137
3.1.3 CDK1-INHIBITED PHOSPHATASES ARE ACTIVATED WITH DISTINCT TIMINGS TO CO-ORDINATE THE EVENTS OF EARLY ANAPHASE 140
3.1.4 IS THERE FUNCTIONAL EQUIVALENCY BETWEEN HUMAN AND YEAST REGULATION OF MITOTIC EXIT?..... 145
3.2 PROTEOLYSIS INITIATES MITOTIC EXIT..... 147
3.2.1 APC/C ACTIVITY CAN BE TEMPORALLY SPLIT INTO TWO DISTINCT FUNCTIONS..... 147
3.2.2 HOW DOES THE APC/C ACTIVITY PROMOTE DIFFERENT RATES OF PROTEOLYSIS? ... 150
3.2.3 CDC20 UBIQUITINATION BUT NOT DEGRADATION IS REQUIRED FOR RAPID APC/C ACTIVATION 153
3.3 CONCLUDING REMARKS..... 155

4 MATERIALS AND METHODS..... 156

4.1 REAGENTS AND ANTIBODIES..... 156
4.2 WESTERN BLOTTING..... 156
4.3 CLONING TECHNIQUES..... 158
4.4 CELL CULTURE..... 160
4.4.1 HIGH-RESOLUTION MITOTIC EXIT TIMECOURSES FOR WESTERN BLOT AND MASS SPECTROMETRY..... 160
4.4.2 MITOTIC EXIT TIMECOURSE COMPARING MPS1 AND CDK INHIBITION..... 163
4.4.3 TIMECOURSES ASSESSING CONTRIBUTION OF PROTEIN SYNTHESIS TO MITOSIS..... 164
4.5 IMMUNO-PRECIPITATION..... 166
4.6 MASS SPECTROMETRY PROTOCOLS 168
4.6.1 PROTEOLYTIC DIGESTION OF TIMECOURSE SAMPLES..... 168
4.6.2 DI-METHYL LABELLING AND TITANIUM DIOXIDE PHOSPHO-PEPTIDE ENRICHMENT 168
4.6.3 ONLINE NANO-LC AND TANDEM MASS SPECTROMETRY..... 169

4.6.4 COMPARISON OF LYSIS AND DIGESTION CONDITIONS FOR MASS SPECTROMETRY 170
4.6.5 HIGH PH FRACTIONATION OF TOTAL PROTEOME SAMPLES..... 172
4.6.6 FILTER ASSISTED SAMPLE PREPARATION 173
4.7 COMPUTATIONAL ANALYSIS 175
4.7.1 ANALYSIS OF MASS SPECTROMETRY TIMECOURSE DATA 175
4.7.2 CALCULATING THE STOICHIOMETRY OF PPP1CA-T320 PHOSPHORYLATION 177
4.7.3 ANALYSIS OF IMMUNO-PRECIPITATION MASS SPECTROMETRY DATA 178
4.8 ANNOTATION ANALYSIS OF TEST DIGESTS 179
4.9 IMAGING 179

5 BIBLIOGRAPHY 181

LIST OF FIGURES

FIGURE 1.1 THE BALANCE OF KINASE AND PHOSPHATASE ACTIVITY GOVERNS CELL CYCLE PROGRESSION 4
FIGURE 1.2 ACTIVATION OF CDK1 7
FIGURE 1.3 PHOSPHO-PROTEIN PHOSPHATASES 11
FIGURE 1.4 THE SPINDLE ASSEMBLY CHECKPOINT 16
FIGURE 1.5 INITIATION OF CYTOKINESIS AT THE CENTRAL SPINDLE 23
FIGURE 1.6 REGULATION OF CDK1-INHIBITED PHOSPHATASES DURING MITOSIS 25
FIGURE 1.7 PP2A-B55 RECOGNISES SUBSTRATES THROUGH A BIPARTITE BASIC MOTIF 31
FIGURE 1.8 REGULATION OF THE APC/C 36
FIGURE 2.1 PROTOCOL FOR A QUANTITATIVE MASS SPECTROMETRY ANALYSIS OF MITOTIC EXIT 49
FIGURE 2.2 CDK INHIBITION PROMOTES ORDERLY MITOTIC EXIT 51
FIGURE 2.3 QUANTIFICATION OF SECURIN BY MASS SPECTROMETRY 53
FIGURE 2.4 A PILOT QUANTITATIVE ANALYSIS OF MITOTIC EXIT 55
FIGURE 2.5 PROTEINS THAT ARE TIGHTLY BOUND TO DNA CAN REMAIN ASSOCIATED WITH CHROMATIN IN 5.3 M UREA EXTRACTS 58
FIGURE 2.6 UREA LYSIS WITHOUT CLARIFICATION PROVIDES OPTIMAL RECOVERY OF BOTH PHOSPHORYLATED AND NON-PHOSPHORYLATED PEPTIDES 61
FIGURE 2.7 ORDERED PROTEOLYSIS CANNOT ACCOUNT FOR THE EVENTS OF MITOTIC EXIT 64
FIGURE 2.8 AURORA A IS DEGRADED PRIOR TO PLK1 DURING MITOTIC EXIT 66
FIGURE 2.9 USING MPS1 INHIBITION TO DRIVE MITOTIC EXIT DOES NOT ALTER THE RELATIVE CONTRIBUTIONS OF DEPHOSPHORYLATION AND PROTEOLYSIS 67
FIGURE 2.10 FRACTIONATION ENABLES QUANTIFICATION OF LOWER ABUNDANCE PROTEINS 70
FIGURE 2.11 CHEMICAL INHIBITION OF THE APC/C CAN STABILISE CCNB1 DURING MITOTIC EXIT 79

FIGURE 2.12 DEPHOSPHORYLATION CAN OCCUR DURING MITOTIC EXIT IN THE ABSENCE OF APC/C OR PROTEASOME ACTIVITY 81
FIGURE 2.13 HIGH-RESOLUTION ANALYSIS OF MITOTIC EXIT UNDER CONDITIONS OF REDUCED APC/C ACTIVITY 85
FIGURE 2.14 APC/C DEPENDENT PROTEOLYSIS IS NOT NECESSARY FOR ORDERED DEPHOSPHORYLATION DURING MITOTIC EXIT 87
FIGURE 2.15 CONTINUED PROTEIN SYNTHESIS CANNOT ACCOUNT FOR DIFFERENT RATES OF PROTEOLYSIS DURING MITOTIC EXIT 90
FIGURE 2.16 PROTEIN SYNTHESIS IS REQUIRED FOR MITOTIC ENTRY BUT NOT MITOSIS 93
FIGURE 2.17 ONGOING PROTEIN SYNTHESIS IS NOT ESSENTIAL FOR SPINDLE CHECKPOINT-DEPENDENT ARREST IN MITOSIS 96
FIGURE 2.18 THE APC/C IS INHIBITED IN A CDK-DEPENDENT MANNER 100
FIGURE 2.19 CCNB1 IS DEGRADED IMMEDIATELY UPON CDK INHIBITION 101
FIGURE 2.20 OPTIMISATION OF CONDITIONS FOR EFFICIENT LARGE-SCALE PPP1C DEPLETION 105
FIGURE 2.21 PP1 CONTRIBUTES TO ACTIVATION OF THE APC/C DURING MITOTIC EXIT 107
FIGURE 2.22 RAPID ACTIVATION OF THE APC/C IS SENSITIVE TO THE LEVELS OF PP1 109
FIGURE 2.23 HISTOGRAMS HELP VISUALISE TRENDS WITHIN LARGE PROTEOMIC DATA SETS 111
FIGURE 2.24 PPP1CB HAS A LIMITED ROLE IN THE REGULATION OF MITOTIC EXIT 115
FIGURE 2.25 MANY DEPHOSPHORYLATIONS ARE DEPENDENT ON PPP1CA/C ACTIVITY DURING MITOTIC EXIT 117
FIGURE 2.26 PPP1CA/C-DEPENDENT DEPHOSPHORYLATIONS INCLUDE SITES INVOLVED IN REGULATION OF MITOTIC EXIT 119
FIGURE 2.27 CDK1 PHOSPHORYLATION OF PP1 PEAKS DURING MITOSIS AND IS RAPIDLY REMOVED UPON MITOTIC EXIT 121
FIGURE 2.28 PP1 IS AUTO-DEPHOSPHORYLATED UPON LOSS OF CDK1 ACTIVITY 124
FIGURE 2.29 CDK1 PHOSPHORYLATION DOES NOT ALTER THE LOCALISATION OF PP1 DURING MITOSIS 127

FIGURE 2.30 PP1 FORMS A VARIETY OF HOLOENZYME COMPLEXES 130
FIGURE 2.31 PP1 HOLOENZYME COMPLEXES DO NOT GENERALLY DISSOCIATE DURING MITOSIS 131
FIGURE 3.1 MODELS OF PP1 AUTO-DEPHOSPHORYLATION 135
FIGURE 3.2 CO-ORDINATED PHOSPHATASE ACTIVATION DETERMINES THE ORDER OF EVENTS DURING MITOTIC EXIT 141
FIGURE 3.3 REGULATION OF APC/C ACTIVITY BY CO-ACTIVATORS DURING MITOSIS AND MITOTIC EXIT 151

LIST OF TABLES

TABLE 4.1 ANTIBODY DETAILS....157
TABLE 4.2 SIRNA DUPLEXES....158
TABLE 4.3 ACCESSION NUMBERS....159
TABLE 4.4 PRIMER DETAILS....159
TABLE 4.5 SAMPLING FOR TIMECOURSES FOLLOWING CDK INHIBITION....163
TABLE 4.6 SAMPLING FOR TIMECOURSES COMPARING CDK AND MPS1 INHIBITION....165
TABLE 4.7 LYSIS BUFFER COMPOSITION....171
TABLE 4.8 SAMPLE DILUTION PRIOR TO PROTEOLYTIC DIGESTION....172
TABLE 4.9 HIGH PH FRACTIONATION BUFFERS....174
TABLE 4.10 FRACTION DILUTION AND MASS SPECTROMETRY ANALYSIS....174

LIST OF ABBREVIATIONS

ACN	Acetonitrile
AGC	Automatic gain control
AMBIC	Ammonium bicarbonate
ANLN	Annilin
ANOVA	Analysis of variance
APC/C	Anaphase promoting complex/cyclosome
ARPP-19	cAMP-regulated phosphoprotein 19
ATP	Adenosine triphosphate
AurA	Aurora A
AurB	Aurora B
BANF1	Barrier-to-autointegration factor 1
BEG	B55-ENSA-Greatwall pathway
BUB1	Budding uninhibited by benzimidazoles 1
BUB3	Budding uninhibited by benzimidazoles 3
BUBR1	Budding uninhibited by benzimidazoles related 1
CAA	Chloroacetamide
CAK	CDK-activating kinase
CCNA	Cyclin A
CCNB	Cyclin B
CCND	Cyclin D
CCNE	Cyclin E
Cdc14	Cell division control protein 14
Cdc2	Cell division control protein 2
CDC20	Cell division control protein 20
CDC25	Cell division control protein 25
CDC27	Cell division control protein 27
CDH1	CDC20 homologue 1
CDK1/2	Cyclin-dependent kinase 1/2
CENPF	Centromere protein F
CHX	Cycloheximide
CKAP2	Cytoskeleton-associated protein 2
CPC	Chromosomal passenger complex
CPI-17	Protein kinase C-potentiated inhibitor protein of 17 kDa
CRISPR	Clustered regularly interspaced short palindromic repeats
DMEM	Dulbecco’s modified eagle medium
DMSO	Dimethyl sulfoxide
DNA	Deoxyribonucleic acid
DTT	Dithiothreitol
ECT2	Epithelial cell-transforming sequence 2
EDTA	Ethylenediaminetetraacetic acid
EM	Electron microscopy
EM-CCD	Electron-multiplication charge-coupled device
ENSA	Endosulfine-α
FA	Formic acid
FEAR	Cdc14 early anaphase release
FCP1	Transcription Factor 2F-associating C-Terminal domain phosphatase 1

G1	Gap 1
G2	Gap 2
GdmCl	Guanidinium Chloride
GFP	Green fluorescent protein
GMNN	Geminin
HEAT	Huntingtin, elongation factor 3, A-subunit of PP2A, TOR1 yeast PI3-kinase
HEC1	Highly expressed in cancer 1
HMMR	Hyaluronan mediated motility receptor
HRP	Horseradish peroxidase
IAA	Iodoacetamide
INCENP	Inner centromere protein
KIF4A	Chromosome-associated kinesin 4A
KIF18A	Chromosome-associated kinesin 18A
KNL1	Kinetochore null protein 1
LC-MS	Liquid chromatography-mass spectrometry
M	Mitosis
MAD1	Mitotic arrest deficient 1
MAD2	Mitotic arrest deficient 2
MASTL	Microtubule-associated serine/threonine-protein kinase-like
MCC	Mitotic checkpoint complex
MEN	Mitotic exit network
MIS12	MIND kinetochore complex component, homolog
MKLP1	Mitotic kinesin like protein 1
MPF	Maturation/Mitosis promoting factor
MPS1	Mono-polar spindles 1
MYPT	Myosin phosphatase-targeting subunit 1
MYT	Membrane-associated tyrosine- and threonine-specific Cdc2-inhibitory kinase
NEBD	Nuclear envelope breakdown
NEK2	Never in Mitosis A' related kinase 2
NIPP1	Nuclear inhibitor of PP1
PAGE	Polyacrylamide gel electrophoresis
PBS	Phosphate-buffered saline
PLK1	Polo-like kinase 1
PNUTS	PP1 nuclear targeting subunit
PP1	Phospho-protein phosphatase 1
PP2A	Phospho-protein phosphatase 2A
PPM	Protein phosphatase Mg^{2+}- or Mn^{2+}-dependent
PPP	Phospho-protein phosphatases
PRC1	Protein regulator of cytokinesis 1
pro-TAME	pro-tosyl-L-arginine methyl ester
PSM	Peptide spectrum match
PSTP	Protein serine/threonine phosphatase
PTP	Protein tyrosine phosphatase
PTS	Phase transfer surfactant
RACGAP1	Rac GTPase-activating protein 1
RCS1	Regulator of chromosome segregation protein 1
ROCK	Rho associated protein kinase 1
S	Synthesis

SAC	Spindle assembly checkpoint
SAPS	SIT4 phosphatase-associated protein
SCF	SKP-Cullin-F box
SDC	Sodium deoxycholate
SDS	Sodium dodecyl sulfate
SEM	Standard error of the mean
siRNA	Small interfering ribonucleic acid
SLS	Sodium lauroyl sarcosinate
TACC3	Transforming acidic coiled-coil-containing protein 3
TEAB	Tetraethylammonium bicarbonate
TCEP	Tris(2-carboxyethyl)phosphine
TFA	Trifluoroacetic acid
TPX2	Targeting proteins for Xklp2
TRIP13	Thyroid hormone receptor interacting protein 13
USP44	Ubiquitin specific protease 44

1 Introduction

The critical function of the cell cycle is to allow the faithful inheritance of genetic material into two daughter cells. Mitotic exit, the final act of this cycle, encompasses a carefully choreographed series of events which occur in rapid succession. Ensuring that these events happen with the correct timing and order is vital for a successful division. Disruption of this order can be catastrophic to cell viability; causing DNA damage, aneuploidy and cell death. Central to these processes is the finely tuned balance of antagonistic activities; kinases with phosphatases; and protein synthesis with proteolysis. Yet the fundamental knowledge as to how these shifting equilibria correlate with the timing and ordering of events during mitotic exit remains limited.

Outlined within this work is a detailed study of how order is maintained within the mammalian cell cycle, particularly during mitosis and mitotic exit. Moreover, the intricate regulatory mechanisms used to ensure that these events are carried out with precise timing are examined.

1.1 The balance of kinase and phosphatase activities governs cell cycle progression

The cell cycle is split into discrete stages; gap 1 (G1), synthesis (S), gap 2 (G2) and mitosis (M), which can be further broken down into prophase, metaphase, anaphase and telophase. DNA is replicated during S phase, with cell growth and protein synthesis occurring in G2, to prepare a cell for mitosis. Cell cycle progression is surveyed by a series of checkpoints, ensuring that all the necessary processes are complete, and errors have been eliminated before continuing through the cycle. As a cell moves through each stage it undergoes a vast array of changes, both functional and morphological (Figure 1.1A).

Post-translational modifications are widespread throughout cell cycle control. Prominent amongst these modifications is phosphorylation, which is used to alter the localisation, activity and conformation of proteins. The enzymes responsible for this modification are kinases, which transfer a phosphate moiety from adenosine triphosphate (ATP) onto a target protein. This modification is removed by phosphatase enzymes, catalysing the release of inorganic phosphate from the substrate protein. The balance between these two activities governs the phosphorylation status of the cell. In particular, the activities of cyclin-dependent kinases (CDKs) and the opposing phospho-protein phosphatases (PPPs) are critical to mitotic progression (Figure 1.1). Cells contain a series of feedback loops to prevent premature activation of the master mitotic kinase, cyclin-dependent kinase 1 (CDK1) (Figure 1.2) (Novak and Tyson, 1993; Morgan 1995). While the addition of a specific inhibitor of PPPs, an algal toxin named okadaic acid, leads to many of the changes associated with mitosis (Felix et al., 1990; Lucocq et al., 1991; Picard et al., 1989; Yamashita et al., 1990).

1.1.1 CDK1 activation drives entry into mitosis

Entry into mitosis triggers a global increase in the phosphorylation status throughout the cell; primarily carried out by CDK1. Additional kinases of the Aurora and Polo family, namely Aurora A (AurA), Aurora B (AurB) and Polo-like kinase 1 (PLK1), also play important roles in centrosome maturation, spindle formation and the spindle assembly checkpoint (SAC) (Combes et al., 2017; Fu et al., 2007; Barr et al., 2004). Moreover, ‘Never in Mitosis A’ related kinase 2 (NEK2) localises to centrosomes and promotes splitting of the mother and daughter centriole. This occurs early in the G2/M transition prior to Aurora and Polo-dependent

centrosome maturation and enables the formation of a bi-polar spindle (Faragher and Fry, 2003; Fry et al., 1998a; Fry et al., 1998b).

The initial work on CDK and cyclins was done whilst characterising the maturation or mitosis promoting factor (MPF), which was identified in *Xenopus* oocytes as a cytoplasmic factor which can induce meiotic entry. MPF was then subsequently shown to induce mitosis in somatic cells. Prior to this, the yeast gene product $p34^{cdc2/28}$ was found to be a serine/threonine kinase which promotes mitotic entry (Beach et al., 1982; Hindley and Phear, 1984; Reed et al., 1985). Subsequent mutational studies in both yeast and *Xenopus* found that the MPF consists of two subunits. The first is cell division cycle 2 (Cdc2), a homologue of CDK1, which phosphorylates proteins during mitosis (Arion et al., 1988; Dunphy et al., 1988; Gautier et al., 1988). The second are cyclins, identified as periodically expressed proteins, which bind to and activate Cdc2 specifically during mitosis (Draetta et al., 1989; Gautier et al., 1990; Labbe et al., 1989; Meijer et al., 1989; Solomon et al., 1990). Furthermore, a non-degradable form of cyclin prevents Cdc2 inactivation and mitotic exit (Murray et al., 1989). A number of studies demonstrated the distinctions between A and B type cyclins (Lehner and O'Farrell, 1990; Pines and Hunt, 1987; Pines and Hunter, 1989; Swenson et al., 1986), and furthermore that these cyclins are expressed at different times and show preferential binding to particular CDKs (Desai et al., 1995; Minshull et al., 1990). Once formed, CDK:Cyclin complexes are stable and the CDK substrate specificity is altered by this cyclin binding (Peeper et al., 1993). Consequently, each stage of the cell cycle is defined by a particular CDK:Cyclin activity, with mitosis being defined by the activity of CDK1:Cyclin B (CCNB) (Figure 1.1A). CCNB synthesis

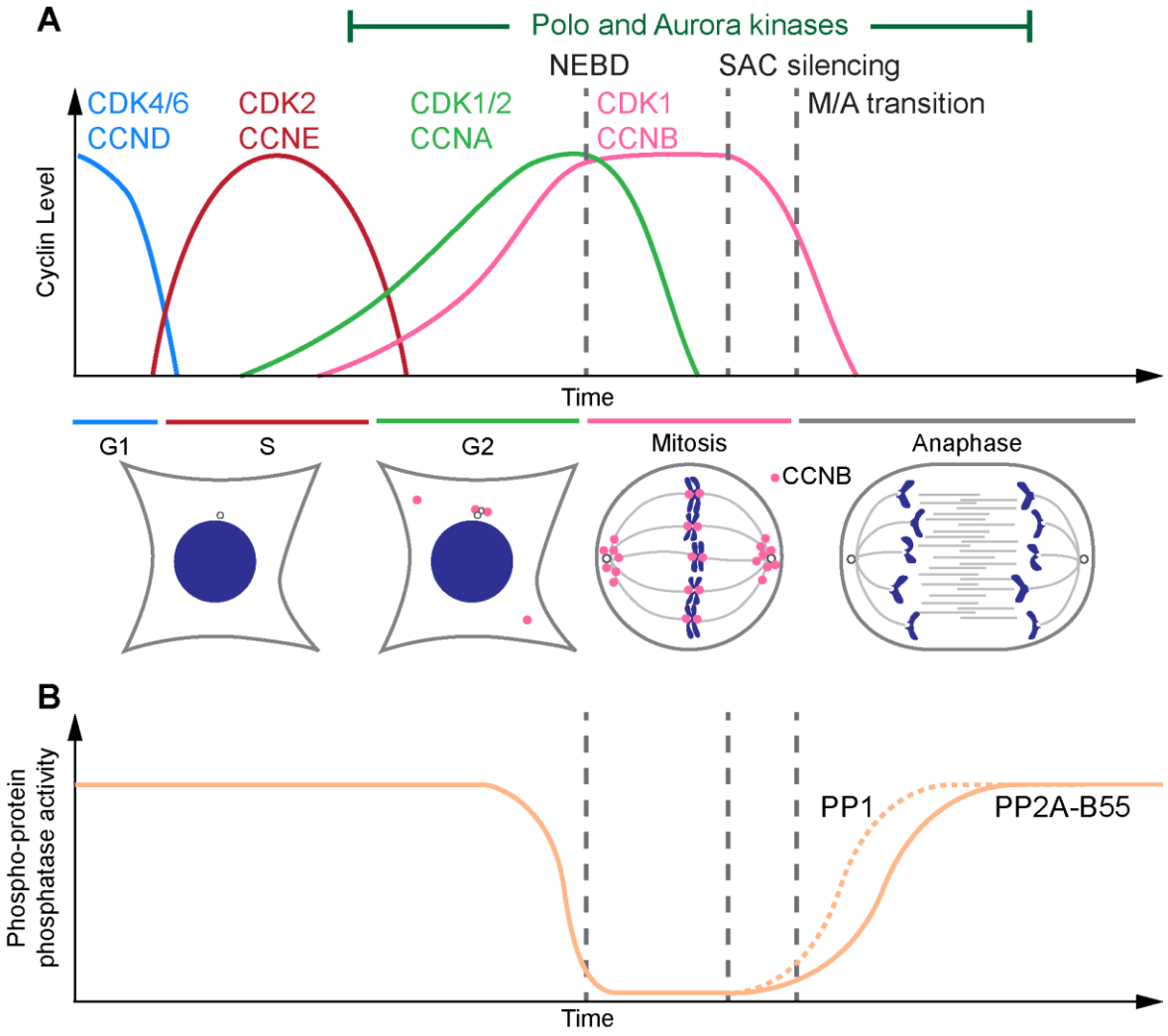


Figure 1.1 The balance of kinase and phosphatase activity governs cell cycle progression

(A) Levels of cyclin oscillate throughout the cell cycle, binding to and activating cyclin-dependent kinases (CDK). The specific CDK:cyclin complexes formed are shown and coloured coded according to their cyclin. The window during which Polo and Aurora kinases are active is marked above the graph. Cell cycle stages are noted beneath the graph, along with cartoons depicting the morphological changes occurring within the cell. (B) The activity of CDK1-inhibited phospho-protein phosphatases, PP1 and PP2A-B55, drops sharply during mitosis, allowing a global increase in phosphorylation status throughout the cell. As cyclin B (CCNB) is degraded, the inhibition of these phosphatases is released.

peaks during the G2 phase (Minshull et al., 1990; Pines and Hunter, 1989) initiating CDK1 activation. Interestingly, the factors required for transcription of CCNB all need prior CDK activation. This means that CCNB transcription only commences once sufficient CDK2:Cyclin A (CCNA) activity has accumulated in the late S, early G2 phase (Chae et al., 2004; Dynlacht et al., 1994; Laoukili et al., 2008; Major et al., 2004; Saville and Watson, 1998).

During G2, despite constant shuttling, CCNB is found predominantly in the cytoplasm due to high rates of nuclear export (Hagting et al., 1998; Toyoshima et al., 1998; Yang et al., 1998), before accumulating at the centrosomes simultaneously with their maturation (Hirota et al., 2003). Binding of CCNB alone is insufficient to activate CDK1; it does however position the activating T-loop in an open conformation available for phosphorylation (Jeffrey et al., 1995). The T-loop phosphorylation of CDK1-T161 by CDK-activating kinases (CAK) further promotes CDK activity (Russo et al., 1996). It is thought that cyclin binding and T-loop phosphorylation of CDK1 happen in concert (Figure 1.2). The level and activity of CAK remains constant throughout the cell cycle (Brown et al., 1994; Poon et al., 1994; Tassan et al., 1995; Tassan et al., 1994) confirming that cell cycle-specific CDK activation is provided by cyclins. Other mitotic kinases are regulated in a similar manner; both Aurora and Polo kinases activity depend on T-loop phosphorylation: Aurora A-T288, Aurora B-T232 and PLK1-T210. Furthermore, full activation of Aurora A and B requires binding of their coactivators, the targeting protein for Xklp2 (TPX2) and inner centromere protein (INCENP), respectively (Bruinsma et al., 2012; Carmena et al., 2009).

During G2, CDK1 is also held inactive by the phosphorylation of T14 and Y15 by Wee1/MYT1 kinases (Gould and Nurse, 1989; Kellogg, 2003; Morla et al.,

1989). These inhibitory phosphorylations of CDK1 are opposed by the dual-specificity phosphatases cell division cycle 25A/B/C (CDC25A/B/C) (Figure 1.2) (Hoffmann et al., 1993). In particular, CDC25B and C are required for the G2/M transition (Lammer et al., 1998; Gabrielli et al., 1996). CDC25B assists in initiating CDK1:CCNB1 activation, while both are localised to the centrosome (Lindqvist et al., 2005; Gabrielli et al., 1996). The centrosomal targeting of CDK1:CCNB1 also requires the activity of the mitotic kinase, Aurora A (Hirota et al., 2003). Furthermore, Aurora A phosphorylates CDC25B, promoting the dephosphorylation of CDK1 (Dutertre et al., 2004). Following this initial activation at the centrosome, CDK1:CCNB1 begins to accumulate in the nucleus just prior to nuclear envelope breakdown (NEBD). This leads to the bulk activation of CDK1:CCNB1 (Gavet and Pines, 2010a; Gavet and Pines, 2010b) catalysed by CDC25C present in the nucleus (Gabrielli et al., 1997).

Once some CDK1:CCNB1 has been activated it can inhibit Wee1 and MYT1 through phosphorylation (Morgan, 1995). Additionally, CDK1:CCNB1 can activate CDC25B/C via phosphorylation, generating a self-amplifying positive feedback loop (Figure 1.2) (Gabrielli et al., 1997; Hoffmann et al., 1993; Lammer et al., 1998). This creates a bi-stable, switch-like transition from low steady state CDK1 activity to a high level of CDK1:CCNB1 activity. This ensures that once CDK1:CCNB1 activity has reached a certain threshold level, the transition into mitosis is irreversible (Novak and Tyson, 1993; Pomerening et al., 2003). Other mitotic kinases can also contribute to this bi-stability. Phosphorylation of CDC25C by PLK1 increases CDC25C activity and thus enhances the positive feedback loop promoting the amplification of CDK1:CCNB1 activity (Karaiskou et al., 1999; Roshak et al., 2000). Moreover, PLK1 counteracts the negative feedback loop

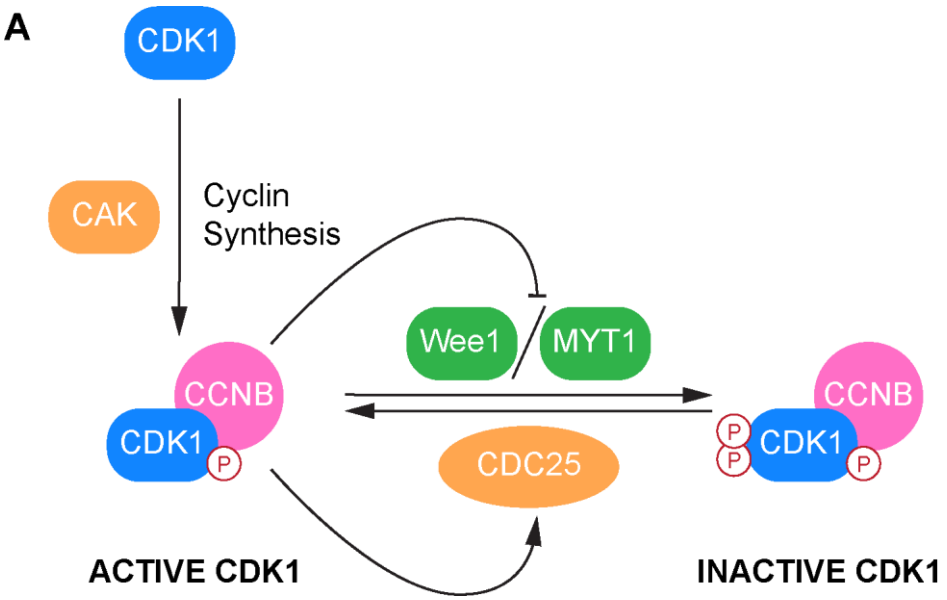


Figure 1.2 Activation of CDK1

CDK1 is simultaneously phosphorylated on its T-Loop by Cyclin activating kinase (CAK) and bound by Cyclin B (CCNB). During G2, these CDK1:CCNB complexes are kept inactive by Wee1 and MYT1 kinases, which inhibit CDK1:CCNB through phosphorylations at T14 and Y15. These phosphorylations are opposed by CDC25 phosphatases. CDK1:CCNB can activate CDC25 and inhibit Wee1/MYT1, both through phosphorylation. By regulating these pathways, CDK1:CCNB promotes activation of more CDK1:CCNB complexes. This feedback loop ensures the G2/M transition is switch-like and irreversible.

inhibiting CDK1 by phosphorylating both MYT1 and Wee1. This leads respectively to their inactivation and ubiquitin-dependent degradation, the latter being triggered by the beta transducin repeat protein (β-TrCP)/SKP-Cullin-F box (SCF), (Watanabe et al., 2004). In fact, the PLK1 phosphorylation of Wee1 is primed by prior phosphorylation via CDK1:CCNB1 (Watanabe et al., 2005). All the mechanisms described above function to ensure that CDK1 is not prematurely activated and that the triggering of mitosis is irreversible.

Kinases do not phosphorylate substrates indiscriminately; they recognise specific motifs, typically short linear sequences of amino acids. Both CDK1:CCNB and CDK2:CCNA are proline-directed kinases which phosphorylate S/T-P-X-K motifs (Nigg, 1993). An additional R-X-L motif has also been suggested to promote phosphorylation. In fact, the presence of this additional motif enables CDK1:CCNB complexes to phosphorylate non-ideal peptides lacking either the proline at +1 or the lysine at +3, relative to the phosphorylation site. CDK2:CCNA complexes do not show this flexibility in substrate specificity, always requiring a proline at +1 (Brown et al., 2015). However, not all kinases are proline-directed, with Aurora kinases recognizing the motif R/K-R-X-S/T-X, where X is preferentially any hydrophobic residue other than proline. A proline at the +1 position prevents Aurora-dependent phosphorylation (Ferrari et al., 2005), thus Aurora and CDK phosphorylations are mutually exclusive. The substrate specificity between Aurora A and B is thought to be largely down to differing localisation patterns (Carmena and Earnshaw, 2003). Furthermore, a single amino acid substitution has been seen to alter the localisation of Aurora A such that it can functionally rescue HeLa cells depleted of Aurora B (Fu et al., 2009). The substrate specificity of PLK1, another non-proline directed kinase, has been harder to pin down to a single motif, however it often demonstrates a preference for an acidic residue or asparagine two residues upstream from the phospho-acceptor site (Kettenbach et al., 2011). Interestingly, PLK1 localisation throughout the cell requires a priming phosphorylation on the docking target recognised by the conserved phospho-binding polo-box domain found in Polo-family kinases. This priming phosphorylation can be performed by different kinases including both CDKs and PLK1 itself (Neef et al., 2007; Park et al., 2010). Together, CDK, Polo and Aurora

kinases cooperate to specifically phosphorylate a wide variety of substrates upon mitotic entry, leading to a global increase in the phosphorylation status of the cell.

1.1.2 Phospho-protein phosphatases

It is evident that waves of phosphorylation promote cell cycle progression. However, the timing of dephosphorylation can be just as critical as the timing of the initial modification (Barr et al., 2011; Cundell et al., 2016; Hein et al., 2017). To explain this behaviour, it is necessary to identify the specific phosphatase activities required for different stages of the cell cycle and to understand their regulation.

Phosphatases can be split into two categories: phospho-tyrosine phosphatases (PTP) (Tonks, 2006) and serine/threonine-specific phosphatases (PSTP) (Barr et al., 2011). The former, other than the dual-specificity phosphatases CDC14 and CDC25, are less involved in cell cycle regulation (Dunphy and Kumagai, 1991). Activation of CDC14 is critical to the completion of mitotic exit in *Saccharomyces Cerevisiae*, through the removal of mitotic CDK1 phosphorylations (Stegmeier and Amon, 2004). While some of the functional properties of CDC14 have been conserved across species (Vazquez-Novelle et al., 2005) the requirement for CDC14 has not, with the role of human CDC14 homologues, CDC14A/B/C, not yet being clearly understood. CDC14A is proposed to have a role in the centrosome cycle (Kaiser et al., 2002; Mailand et al., 2002), while varying studies have implicated CDC14B in the regulation of mitotic spindle assembly, centriole duplication and mitotic exit (Cho et al., 2005; Dryden et al., 2003; Rodier et al., 2008; Wu et al., 2008). However, human cells lacking either CDC14A or B did not demonstrate any defects in the aforementioned processes (Berdougo et al., 2008; Mocciaro et al., 2010).

PSTPs however are involved in the regulation of many important events during mitosis and cytokinesis. All PSTPs are catalytically metal ion-dependent but can be split into two further categories, metallo-dependent phosphatases (PPM) and phospho-protein phosphatases (PPP). It is PPPs which are thought to be responsible for most mitotic regulation (Felix et al., 1990; Lucocq et al., 1991; Picard et al., 1989; Yamashita et al., 1990). Importantly, inhibition of an okadaic-acid-sensitive phosphatase, which opposes CDK1 phosphorylation, is necessary for proper mitotic progression (Burgess et al., 2010; Castilho et al., 2009; Vandre and Wills, 1992; Vigneron et al., 2009; Zhao et al., 2008b). Furthermore both PP1 and PP2A-B55 have been implicated in removing M-phase specific phosphorylation during mitotic exit (Castilho et al., 2009; Cundell et al., 2013; Mochida et al., 2009; Rodrigues et al., 2015; Trinkle-Mulcahy et al., 2006; Vagnarelli et al., 2011; Wu et al., 2009). The following work therefore focuses on the role and regulation of PPPs.

Unsurprisingly, given their shared susceptibility to okadaic acid inhibition, PPPs have very similar catalytic subunits, with three substrate binding grooves adjacent to the active site (Figure 1.3C) (Barr et al., 2011). The catalytic subunits of PP1 and PP2A do not show differing substrate specificities (Agostinis et al., 1992; Imaoka et al., 1983; Mumby et al., 1987), although PP2A is 100 times more sensitive to okadaic acid inhibition (Xing et al., 2006). There are three sub-families within the PPP family: PP5; PP2A which includes PPP2CA, PPP2CB, PPP6C, PPP4C; and PP1 consisting of PPP1CA, PPP1CB and PPP1CC (Figure 1.3A). PP1 holoenzymes generally consist of a single catalytic subunit and a single regulatory subunit, while PP2A holoenzymes are trimeric, consisting of a catalytic, scaffold and regulatory subunit (Figure 1.3B) (Janssens and Goris, 2001).

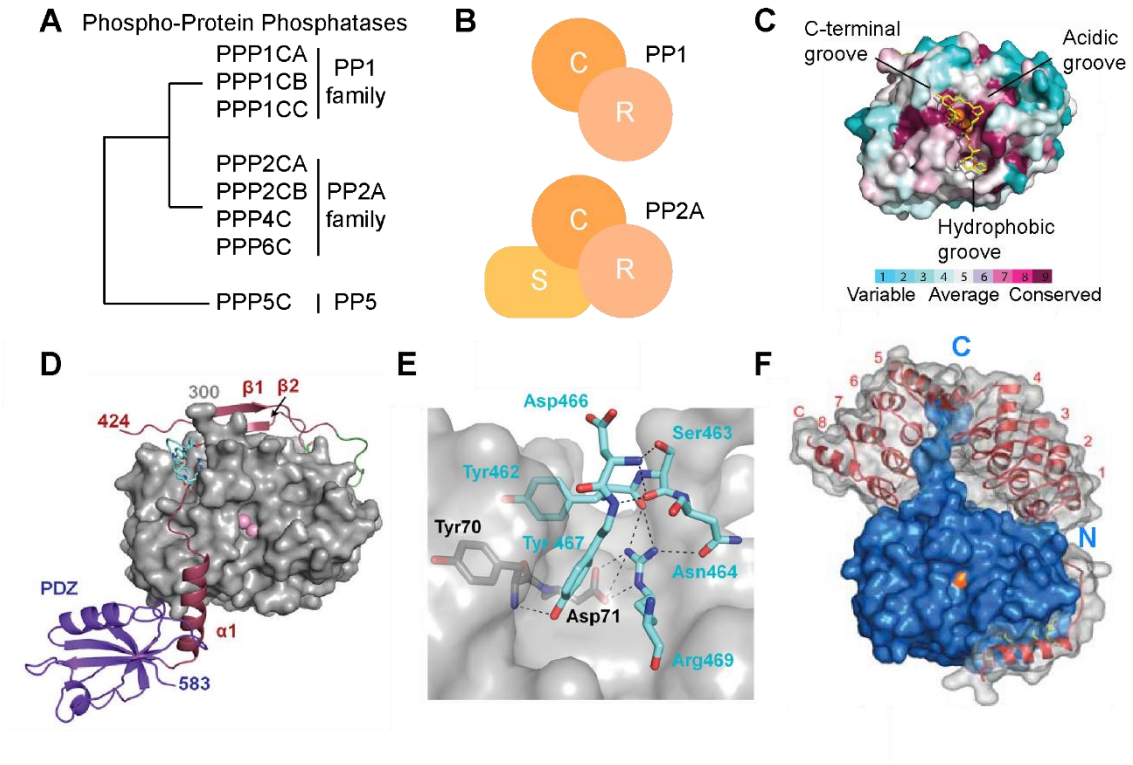


Figure 1.3 Phospho-protein phosphatases

(A) Schematic describing the relationship between the different phospho-protein phosphatase (PPP) sub-families. (B) Architecture of PPP holoenzymes, PP1 complexes form hetero-dimers containing a catalytic (C) and regulatory (R) subunit. PP2A holoenzymes are hetero-trimers containing a catalytic, regulatory and scaffold (S) subunit. (C) A surface map showing the conservation of the catalytic subunit across the PPP family. Both the active site and acidic groove of the catalytic subunit are highly conserved (purple). Orange spheres represent metal ions within the active site and the inhibitor okadaic acid is shown in yellow (Barr et al., 2011). (D) A 1.85 Å crystal structure of PPP1CA (grey, surface representation) in complex with spinophilin (cartoon). The PP1 binding domain of sphinophilin is shown in magenta, and makes extensive contacts with PP1 across four regions. Region IV occupies a substantial portion of the C-terminal groove of the catalytic site. (E) The interaction between PP1 and sphinophilin within region IV. Spinophilin residues (light blue) 462-469 interact with the C-terminal groove of PP1. PP1-D71 is an important residue for substrate interactions with the C-terminal groove of PP1. PP1-D71 forms a hydrogen bond with Spinophilin-R469, preventing substrate binding via this groove (Ragusa et al., 2010). (F) Crystal structure of PPP1CB (blue) with MYPT (grey/red cartoon). When bound to MYPT the C-terminus of PP1 (blue C) is extended out away from the catalytic site, marked by metal ions in the active site (orange) (Terrak et al., 2004).

PP6 enzymes have a similar structure to those of the PP2A family with: a catalytic subunit; an ankyrin repeat domain-containing subunit; and a SIT4 phosphatase-associated protein domain (SAPS) (Stefansson and Brautigan, 2006; Stefansson et al., 2008).

The substrate specificity of each holoenzyme is determined by the regulatory subunit (Agostinis et al., 1992; Imaoka et al., 1983; Mumby et al., 1987). These subunits direct the enzymes towards specific targets while inhibiting enzymatic activity against a different subset of phosphorylated proteins. Currently there are no structural data of a PP1 holoenzyme bound to substrate, so the relative contributions of the catalytic and regulatory subunits to substrate binding have only been inferred indirectly. For example, structural studies of the PP1-interacting protein (PIP) spinophilin shows that it binds close to the C-terminus of PP1, restricting access to the catalytic site (Figure 1.3D-E) (Ragusa et al., 2010). Additionally, crystal structures of PP1:myosin-phosphatase targeting subunit 1 (MYPT1/PPP1R12A) complexes show that binding of MYPT1 drastically restructures the catalytic site of PP1 specifically for interaction with myosin substrate (Figure 1.3F) (Terrak et al., 2004). Interestingly, it has been proposed that PP1 has between 100-200 interaction partners and it has been theorised that there may potentially be as many as 650 (Bollen et al., 2010). However, many of these require more rigorous experimental validation. Regardless, these regulatory subunits impart various properties to PP1 holoenzymes including cellular localisation and substrate specificity while some act as general inhibitors of PP1 activity (Cohen, 2002). PP2A holoenzymes contain one of four kinds of regulatory subunit; B/B55, B'/B56, B'' and B''' (Janssens and Goris, 2001), bound to one copy of the scaffold (PPP2R1A/B) subunit which contains 15 HEAT (Huntingtin,

elongation factor 3, A-subunit of PP2A, TOR1 yeast PI3-kinase) repeats, with the catalytic subunit binding to repeats 11-15. B56 regulatory subunits bind to repeats 2-8 (Xing et al., 2006; Xu et al., 2006) while B55α subunits bind to repeats 1-7 (Xu et al., 2008), impacting the properties required for a substrate to reach and interact with the catalytic site. These regulatory subunits enable the formation of many holoenzyme combinations with different specificities. This may go some way towards explaining the discrepancy between the number of kinases and phosphatases encoded in the genome, there being ~400 serine/threonine kinases and only ~40 serine/threonine phosphatases (Cohen, 2002; Manning et al., 2002).

1.2 Mitotic exit relies on a precisely timed shift in the balance between kinase and phosphatase activity

Activation of CDK1:CCNB triggers mitotic entry and activation of the spindle assembly checkpoint (SAC). This checkpoint prevents the loss of cohesion and premature chromosome separation in the presence of chromosomes that are not properly attached at the mitotic spindle. In the presence of unaligned chromosomes, the SAC generates the mitotic checkpoint complex (MCC). The MCC inhibits the anaphase-promoting complex/cyclosome (APC/C), an E3 ubiquitin ligase, stabilising the levels of CCNB and securin. This maintains CDK1 activity and chromosome cohesion, preventing mitotic exit. Once the chromosomes are attached the APC/C becomes active, promoting the ubiquitin-dependent degradation of CCNB and securin. The degradation of CCNB leads to the inactivation of CDK1. The removal of these CDK phosphorylations is necessary for the changes required for a proper mitotic exit.

1.2.1 The spindle assembly checkpoint prevents a premature shift in global phosphorylation status

The SAC assesses the attachment of kinetochores to microtubules, and the presence of any unattached kinetochores signals the checkpoint to remain on. Kinetochores are hierarchical structures with two functionally distinct regions. The inner layer of proteins, including various centromeric proteins (CENP), associate with CENP-A containing nucleosomes, to ensure the kinetochore is deposited correctly at the centromere (Cleveland et al., 2003; Meraldi et al., 2006). The outer layer of proteins is involved in microtubule attachment and acts as a platform to signal the status of each kinetochore (Cheeseman, 2014). Prior to mitosis the outer kinetochore proteins of the KMN network; KNL1, MIS12 and NDC80/HEC1, are recruited and define the site of attachment for microtubules (Cheeseman et al., 2006; DeLuca et al., 2006). While there are many other components of the kinetochore, these form the core platform from which signalling takes place.

As with other aspects of cell cycle control, SAC signalling is governed by changes in the phosphorylation state of key proteins. Mono-polar spindle 1 (MPS1) is central to this and considered to be the master kinase for spindle checkpoint activation. MPS1 is recruited by HEC1 to unattached kinetochores (Hiruma et al., 2015; Ji et al., 2015). This localisation is in part dependent on Aurora B activity at the kinetochore (Figure 1.4A) (Nijenhuis et al., 2014; Saurin et al., 2011; Zhu et al., 2013). It has recently been suggested that an MPS1-dependent phosphorylation cascade controls checkpoint signalling (Ji et al., 2017). MPS1 initially phosphorylates MELT motifs in KNL1 allowing the recruitment of BUB1 (budding uninhibited by benzimidazole 1) which also becomes phosphorylated by MPS1 (Ji et al., 2017; London et al., 2012; Shepperd

et al., 2012; Yamagishi et al., 2012). Phosphorylated BUB1 recruits mitotic arrest defective 1 (MAD1) and initiates a catalytic cycle which, together with the cell division cycle protein 20 (CDC20), MAD2 and BUB-related 1 (BUBR1), promotes the assembly of MCC to inhibit the APC/C (Figure 1.4A) (Faesen et al., 2017; Ji et al., 2017; Musacchio, 2015). In *Xenopus* extracts, MPS1 is directly regulated by CDK1 (Morin et al., 2012). Additionally, CDK1 phosphorylation of BUB1-S459 has been shown to prime the phosphorylation by MPS1 of the adjacent site, BUB1-T461 as a pseudo-MELT motif (Ji et al., 2017). These findings suggest that CDK activity is directly required in maintaining SAC activity.

Signal amplification is an important aspect of the SAC, ensuring that a single unattached kinetochore generates sufficient inhibitory signal to maintain the checkpoint. MAD2 is found in two different states: open (o-MAD2) and closed (c-MAD2), with the majority being in the checkpoint inactive open form during interphase (Luo et al., 2004; Musacchio and Salmon, 2007). During mitosis, the conversion of o-MAD2 to c-MAD2 is catalysed by MAD1:c-MAD2 complexes which are enriched at the unattached kinetochores. This kinetochore localisation is MPS1-dependent, as described previously (Hewitt et al., 2010; Tipton et al., 2013). The o→c-MAD2 transition is the signal amplification step referred to above (DeAntoni et al., 2005; Musacchio and Salmon, 2007). c-MAD2 can then interact with CDC20 and BUBR1 to form the MCC (Fang, 2002; Tipton et al., 2011), along with MAD2 and BUB3. CDC20 is unique amongst the MCC proteins in that it is simultaneously a coactivator and inhibitor of the APC/C (Izawa and Pines, 2015).

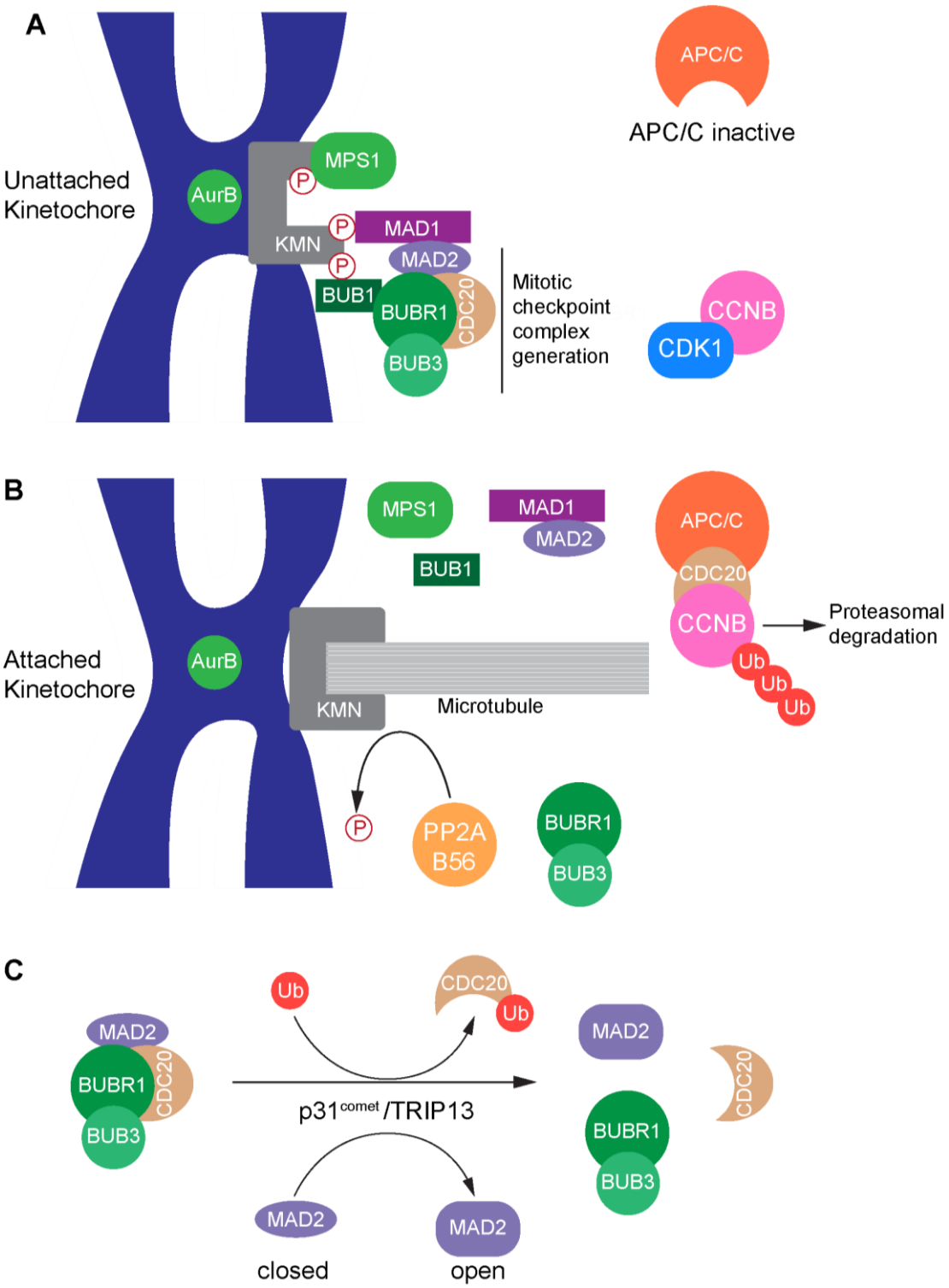


Figure 1.4 The spindle assembly checkpoint

(A) At unattached kinetochores, MPS1 is recruited to the kinetochore following phosphorylation by centromeric Aurora B (AurB). MPS1 phosphorylation of KNL1, part of the KMN network, and BUB1 drives a catalytic cycle which results in the production of mitotic checkpoint complex (MCC). This complex then acts as a diffusible inhibitor of the

APC/C, protecting CCNB from destruction. (B) Microtubule attachment to the kinetochore generates tension and pulls the kinetochore away from the centromere. PP2A-B56 then removes Aurora B phosphorylations. Together these events result in the dissociation of MPS1, BUB and MAD proteins from the kinetochore and cessation of MCC production. CDC20 then activates APC/C, promoting the ubiquitin-dependent destruction of CCNB and subsequently anaphase onset. (C) MCC must be disassembled to allow APC/C activation, this is thought to occur through $p31^{comet}$/TRIP mediated change in the MAD2 confirmation from closed to open, leading to dissociation of the complex. Alternatively, MCC disassembly can be promoted through CDC20 ubiquitination.

Microtubule binding to the kinetochore leads to the displacement of key SAC proteins, such as MAD1/2 and the BUBs (Figure 1.4B) (Funabiki and Wynne, 2013; Skoufias et al., 2001). MAD1 and MAD2 are moved away from the kinetochore along microtubules in a dynein-dependent manner (Howell et al., 2001; Wojcik et al., 2001). MPS1 is also lost from attached kinetochores due to direct competition with microtubule binding (Hiruma et al., 2015; Ji et al., 2015). However, inactivating the SAC requires that two conditions are met: that the kinetochores are attached to microtubules; and furthermore, are bi-orientated on the mitotic spindle (Nicklas, 1997; Nicklas et al., 1995). A key part of this is the error-correction system, which centres around the kinase Aurora B. Attachments which are not properly bi-orientated do not generate tension, meaning that the centromere and the kinetochore reside very close to each other. This enables the centromeric pool of Aurora B to phosphorylate components of the KMN network, reducing their affinity for microtubules and allowing a new attachment to be made (Cheeseman et al., 2006; DeLuca et al., 2006; Wei et al., 2007; Welburn et al., 2010). Due to the bipolar nature of the spindle and cohesed sister chromatids each bearing a kinetochore, correct attachments generate tension, physically separating the KMN network from Aurora B (Liu and Lampson, 2009). Potential

kinetochore-microtubule interactions are protected from premature destabilisation by the phosphatase PP2A-B56 which opposes Aurora B phosphorylation (Foley et al., 2011; Kruse et al., 2013). Furthermore, PP2A-B56 also removes the MPS1-dependent phosphorylation of KNL1, preventing further recruitment of SAC proteins at attached kinetochores and promoting SAC silencing (Figure 1.4B) (Espert et al., 2014). By contrast, PP1 in yeast has been shown to oppose both Aurora B and MPS1 at the kinetochore (Meadows et al., 2011; Pinsky et al., 2009; Rosenberg et al., 2011; Vanoosthuyse and Hardwick, 2009). A KNL1-bound pool of PP1 has been suggested to be involved in SAC silencing in metazoan cells (Espeut et al., 2012). However, PPP1CC can only bind to KNL1 once Aurora B phosphorylation of the PP1 binding motifs is removed, downstream of tension generation (Liu et al., 2010). This would mean that PP2A-B56 functions upstream of PP1, facilitating the latter's recruitment through removal of Aurora B sites. More recently, structural data have shown that KNL1 cannot simultaneously interact with PP1 and microtubules due to their overlapping binding sites (Bajaj et al., 2018). Additionally, KIF18A is bound and dephosphorylated by PP1, allowing its recruitment to microtubule plus ends, where it can supress microtubule dynamics. This stabilises kinetochore:microtubule attachments and promotes the formation of a tight metaphase plate (De Wever et al., 2014; Hafner et al., 2014). It is not clear whether KIF18A localises PP1 to the kinetochore or only interacts with PP1 already present at the kinetochore. Furthermore, transcription Factor 2F-associating C-Terminal domain phosphatase 1 (FCP1) is thought to promote SAC silencing through dephosphorylation of CDC20 and the deubiquitinase ubiquitin specific protease 44 (USP44) (Visconti et al., 2012). Consistent with this role, depletion of FCP1 causes a delay in the degradation of CCNB1 and subsequently

mitotic exit (Della Monica et al., 2015; Visconti et al., 2012). The mitotic regulation of FCP1 is not currently understood so it remains unclear whether FCP1-mediated SAC silencing is constitutive or correlated with the attachment status of kinetochores. Nevertheless, the relative roles of these phosphatases in SAC silencing still require further investigation.

To activate the APC/C, the MCC already generated prior to microtubule attachment and SAC silencing needs to be disassembled. One proposed mechanism involves the thyroid hormone receptor interacting protein 13 (TRIP13), an AAA ATPase, and its interaction partner $p31^{Comet}$. Together these proteins disassemble the MCC by destabilising the c-MAD2 conformation and promoting the transition back to o-MAD2 (Figure 1.4C) (Alfieri et al., 2018; Wang et al., 2014). It is unclear whether $p31^{Comet}$:TRIP13 function on free or APC/C bound MCC. Ubiquitination of CDC20 by the APC/C^{CDC20} itself has also been suggested to promote MCC disassembly (Kallio et al., 1998). It is thought that this ubiquitination would lead to dissociation of the MCC (Figure 1.4C) (Reddy et al., 2007), allowing the ubiquitinated CDC20 to be targeted for proteasomal degradation. The ubiquitination of CDC20 is opposed by USP44 to prevent premature APC/C activation and anaphase onset (Stegmeier et al., 2007; Zhang et al., 2011). How the $p31^{Comet}$:TRIP13 pathway and regulated CDC20 ubiquitination work together to achieve rapid APC/C activation upon SAC silencing is currently unknown.

Once the checkpoint is satisfied and the MCC is disassembled, APC/C^{CDC20} becomes active leading to ubiquitination and proteasomal degradation of many substrates. Critical amongst these targets are CCNB and securin, prompting the inactivation of CDK1 and loss of chromosome cohesion respectively (Figure 1.4B)

(Funabiki et al., 1996; King et al., 1995; Sudakin et al., 1995). Interestingly, the MCC only inhibits the APC/C against a subset of targets as degradation of CCNA begins swiftly following NEBD, independent of SAC activity (Di Fiore and Pines, 2010; Geley et al., 2001). The differential regulation of CCNA and CCNB is presumably reflective of their respective roles in the cell cycle.

1.2.2 Mitotic exit: The reversal of CDK phosphorylations

The loss of CDK1:CCNB activity triggers anaphase entry and a series of rapid changes throughout the cell including: chromosome separation; spindle morphology changes; organelle reformation; initiation of cytokinesis; and completion of abscission. All these events occur within a very narrow time window. In human cells, cytokinesis initiates ~8 min after anaphase onset (Bastos et al., 2012), with nuclear pore reformation and nuclear import occurring 8-9 and 12-13 min after chromosome separation, respectively (Cundell et al., 2016). It is therefore critical that CDK1 phosphorylations are removed in a timely manner during anaphase. As expected, multiple components crucial for cytokinesis have been shown to be negatively regulated by CDK1:CCNB (Barr and Gruneberg, 2007).

One of the most highly conserved anaphase spindle proteins and CDK1 substrates is the protein regulator of cytokinesis 1 (PRC1). Phosphorylation of PRC1-T470/481 by CDK1 prevents its ability to bundle anti-parallel, overlapping microtubules and promotes anaphase spindle-elongation (Jiang et al., 1998; Mollinari et al., 2002; Walczak and Shaw, 2010). Furthermore, CDK1 phosphorylation prevents the adjacent phosphorylation of PRC1-T602 by PLK1 until the former sites are removed (Cundell et al., 2013; Neef et al., 2007). Phosphorylation at PRC1-T602 primes the binding of PLK1. This PRC1

dependent recruitment of PLK1 to the central spindle is necessary for cytokinesis (Figure 1.5) (Neef et al., 2007). As such, CDK1:CCNB activity prevents premature central spindle formation and cytokinesis during mitosis. These CDK1 phosphorylations are removed by the CDK1-inhibited phosphatase PP2A-B55 (Cundell et al., 2013), ensuring that formation of the central spindle can only occur after CCNB is degraded.

Additionally, the centralspindlin complex is CDK1-regulated. Centralspindlin, consists of mitotic kinesin-like protein 1 (MKLP1) and RAC GTPase-activating protein (RACGAP1) and functions to position the Rho guanine nucleotide exchange factor ECT2 (epithelial cell transforming) at the cell equator (Su et al., 2011). Here, ECT2 is activated by PLK1 phosphorylation (Petronczki et al., 2007; Wolfe et al., 2009), leading to a tightly localised pool of activated $RhoA^{GTP}$ at the cell cortex (Figure 1.5). This pool of $RhoA^{GTP}$ then signals the initiation of cytokinesis by recruiting formins and Rho-associated protein kinase (ROCK) (Bassi et al., 2011; Castrillon and Wasserman, 1994; Hickson et al., 2006; Madaule et al., 1998). These effectors mediate cleavage furrow ingression and contractile ring formation through their actions on actin and myosin (Glotzer, 2005). CDK1 phosphorylation prevents MKLP1 binding to or moving along the microtubules (Mishima et al., 2004). Furthermore, CDK1 phosphorylation of ECT2 prevents its interaction with centralspindlin (Yuce et al., 2005). Together these phosphorylations prevent the positioning of ECT2 and the subsequent activation of RhoA at the cell equator until CDK1 is inactivated.

Although CDK1 becomes inactive, other mitotic kinase activities persist through anaphase into telophase. Aurora B localises mainly at the centromeres in metaphase and anaphase A, with recruitment to the central spindle in anaphase

B. This pool of Aurora B is required for regulation of anaphase spindle extension and central spindle formation. Aurora B is part of the chromosomal passenger complex (CPC) containing the inner centromere protein (INCENP), and two cofactors survivin and borealin (Ruchaud et al., 2007). The CPC relocalises from centromeres to the central spindle in anaphase, concomitant with the inactivation of CDK1 (Hummer and Mayer, 2009). Dephosphorylation of INCENP-T59, a CDK1 site, permits an interaction between the CPC and the kinesin motor MKLP2, enabling the accumulation of Aurora B at the central spindle (Gruneberg et al., 2004). This creates a restricted pool of Aurora B activity at the central spindle which is dependent on the loss of CDK1 activity. Subsequent Aurora B phosphorylation of MKLP1 at the anaphase spindle is required for microtubule bundling (Figure 1.5) (Douglas et al., 2010; Guse et al., 2005; Neef et al., 2006). Spindle midzone length is also regulated by Aurora B through phosphorylation of chromosome-associated kinesin 4A (KIF4A), stabilising microtubule length (Bastos et al., 2014). Furthermore, a gradient of Aurora B activity emanating from the central spindle is thought to ensure that nuclear envelope reformation occurs only after sister chromosomes have sufficiently separated (Afonso et al., 2014). This idea was predicated on Aurora B substrates only becoming dephosphorylated once out of range of Aurora B at the midzone. As discussed earlier, PLK1 activity and localisation to the central spindle is required for cytokinesis. Interestingly, PLK1 has two pools of docking partners, pro/metaphase docking partners whose PLK1 binding is primed by CDK1 and anaphase-specific partners whose priming is inhibited by CDK1 phosphorylation (Neef et al., 2007). This demonstrates that prior CDK1 activity has important consequences downstream of its own inactivation. Furthermore, the removal of these

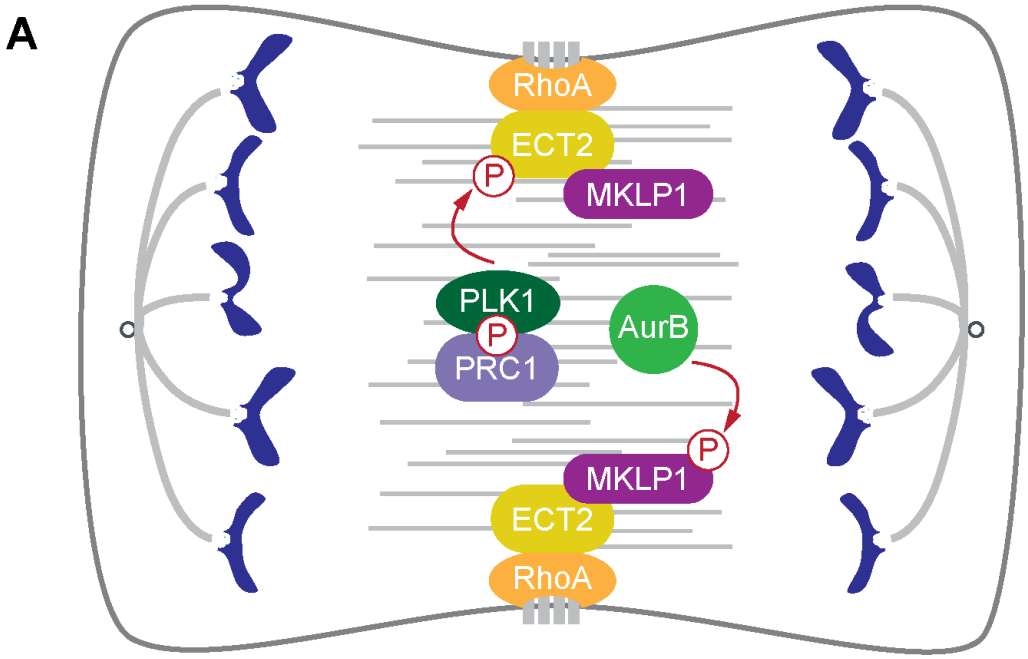


Figure 1.5 Initiation of cytokinesis at the central spindle

(A) Aurora B (AurB) is relocalised to the spindle midzone following CDK1 inactivation, where it phosphorylates and activates the kinesin MKLP1. Following removal of a CDK1 phosphorylation, PRC1 binds to microtubules where it is phosphorylated and subsequently bound by PLK1. ECT2 is positioned at the cell equator by MKLP1 and activated through PLK1 phosphorylation. This leads to tightly localised RhoA activity which induces furrowing.

phosphorylations, in concert with the continued activity of Aurora and Polo kinases, is crucial to the timing and order of mitotic exit.

1.2.3 Regulation of phospho-protein phosphatases during mitosis

PPPs show differential regulation during the cell cycle. PP2A-B55 and PP1 are inhibited by CDK1:CCNB during mitosis (Figure 1.1B and 1.6), however not all PPPs are subject to CDK1-dependent inhibition. Additionally, PPP activity is directed and targeted by binding of regulatory subunits. As previously mentioned, PP2A-B56 activity is required during mitosis to oppose Aurora B and MPS1

phosphorylation at the kinetochore. Furthermore, PP2A-B56 has a role in maintaining centromere cohesion during mitosis. Centromere localised Shugoshin 1 (SGO1) recruits PP2A-B56 to the kinetochore to oppose PLK1 and Aurora B phosphorylation and prevent cohesin removal from the centromere (Hauf et al., 2005; Kitajima et al., 2006; Riedel et al., 2006; Tang et al., 2006). Given these mitotic functions, it follows that PP2A-B56 is not inhibited by CDK1:CCNB. PP2A-B56 holoenzymes can be targeted to binding partners through a short binding motif, the LxxIxE (Hertz et al., 2016). These binding partners can be substrates themselves as is the case with RACGAP1 and Repo-man (Hertz et al., 2016; Qian et al., 2013), or simply bring PP2A-B56 activity to a specific location, as with BUBR1 and kinetochore localisation (Suijkerbuijk et al., 2012). It has been suggested that phosphorylation of particular residues within the LxxIxE motif increases the affinity of the interaction with PP2A-B56 (Hertz et al., 2016; Wang et al., 2016). This creates the exciting prospect of PP2A-B56 acting as a phosphorylation-directed phosphatase. There are also likely to be other motifs which enable PP2A-B56 to interact with binding partners, since SGO1 makes alternative contacts with PP2A-B56 (Xu et al., 2009).

PP1 catalytic subunits also use short motifs to interact with many regulatory subunits. The most common, RVxF, binds to the hydrophobic groove of PP1 catalytic subunits, however this binding does not generally impact PP1 activity or conformation (Bollen, 2001; Cohen, 2002; Egloff et al., 1997). While the RVxF

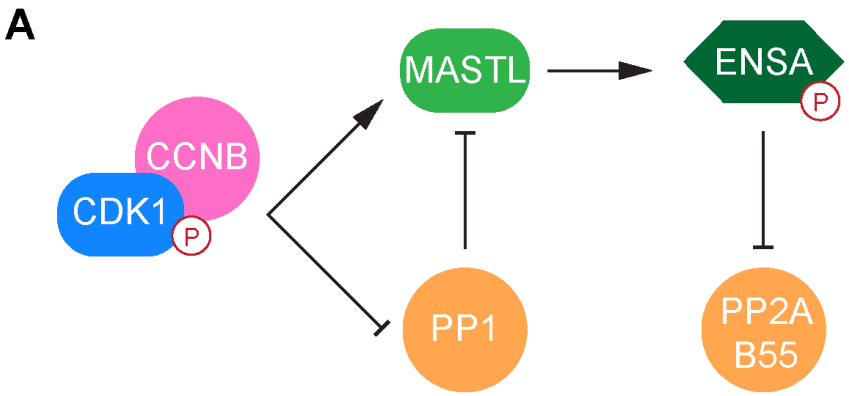


Figure 1.6 Regulation of CDK1-inhibited phosphatases during mitosis

(A) CDK1:Cyclin B (CCNB)-mediated inhibition of PP1 and PP2A-B55 is required for the rapid transition between G2 and mitosis. CDK1:Cyclin B directly inhibits PP1 through phosphorylation, whereas PP2A-B55 is indirectly inhibited via the BEG pathway. MASTL is activated by CDK1:CCNB and then phosphorylates ENSA, which can then specifically inhibit PP2A-B55 holoenzymes by acting as an unfair substrate. PP1 is able to dephosphorylate and inactivate MASTL, therefore inhibition of PP1 reinforces the activation of the BEG pathway.

consensus is K/R-x_{0-1}-V/I-x-F/W, in practice motifs often deviate away from this (Hurley et al., 2007). Nevertheless, RVxF motifs are functionally interchangeable as demonstrated with the motifs of known PP1 interacting proteins: nuclear inhibitor of PP1 (NIPP1); and inhibitor 1 (PPP1R1). Following motif exchange, both proteins still interact with PP1 and it is seen that their relative inhibitory potency is dependent on the strength of their respective RVxF motif (Wakula et al., 2003). A small number of interactors have an additional G/S-I-L-K/R motif which can provide secondary contacts to the catalytic subunit.

Besides helping to localise PP1 correctly, many of its interactors demonstrate some level of inhibitory activity towards PP1. More accurately these could be described as substrate specifiers since they only prevent

dephosphorylation of a select group of PP1 substrates. There are, however, true PP1 inhibitors such as inhibitor-1 and protein kinase C-potentiated inhibitor of 17 kDa (CPI-17/PPP1R14A) which act as pseudo-substrates once phosphorylated (Ceulemans and Bollen, 2004; Eto, 2009). CPI-17 is seen to specifically inhibit PPP1CB:MYPT1 (Eto, 2009). Conversely, inhibitor-2 does not require phosphorylation to demonstrate inhibitory activity towards PP1.

The interaction between PP1 and several binding partners, including NIPP1 and PP1 nuclear targeting subunit (PNUTS), are regulated by phosphorylation (Beullens et al., 2000; Kim et al., 2003). This has been well established in the case of the PPP1CC:Repo-man complex (Qian et al., 2015; Qian et al., 2013; Vagnarelli et al., 2011). CDK1 and Aurora B phosphorylation of Repo-man prevent its interaction with PPP1CC and histones, respectively. Once CDK1 is inactivated and Aurora B has relocalised to the midzone, the PPP1CC:Repo-man complex can form and bind to histones, where it can dephosphorylate several substrates including Histone 3 (H3)-S10 (Murnion et al., 2001), which has been linked to the timing of chromatin decondensation. H3-T3 is also dephosphorylated, preventing further Aurora B recruitment to the chromatin (Qian et al., 2015; Qian et al., 2013), thus reversing mitotic chromosome condensation. Finally, PPP1CC:Repo-man complexes have also been shown to recruit Importin-β to chromatin during anaphase and to promote early events in nuclear envelope reformation (Vagnarelli et al., 2011). Aurora B phosphorylation of the RVSF motif within KNL1 modulates recruitment of PPP1CC to the kinetochore (Liu et al., 2010). Recent work has built upon these ideas by suggesting the binding between PP1 and a subset of RVxF proteins is negatively regulated by Aurora B phosphorylation of the motif during mitosis (Nasa et al., 2018). However, the significance of these findings is unclear

due to limitations in the pan R-V-pS/T-F antibody used for the mass spectrometry interactome analysis. This approach significantly enriched 40 proteins, however only five were previously identified as known PP1 interactors when compared to an already extensive accepted list (Bollen et al., 2010). Moreover, only half showed any reduction upon the use of Aurora B inhibitor during mitosis, suggesting that only a subset were Aurora B sites. This group, however, did include KNL1. It therefore remains to be seen how entry into mitosis and more specifically mitotic phosphorylation globally affect PP1's ability to interact with other proteins.

PP1 is nevertheless still subject to direct regulation by CDK1:CCNB during mitosis, via inhibitory phosphorylation of PPP1CA-T320 (Figure 1.6) (Dohadwala et al., 1994; Yamano et al., 1994). This site is conserved in the other human PP1 catalytic isoforms (PPP1CB-T316, PPP1CC-T311) and is highly conserved throughout evolution, except in the case of plants. T320 phosphorylation peaks during mitosis and is thought to prevent premature substrate dephosphorylation during mitotic entry and in mitosis (Wu et al., 2009). In *Xenopus* extracts, it has been reported that dephosphorylation of PP1 substrates is prevented during mitosis, correlating with phosphorylation of PP1-T320. Upon CDK1 inhibition these PP1 substrates were rapidly dephosphorylated (Wu et al., 2009). It follows that dephosphorylation of PP1-T320 must be an important early event of mitotic exit (Figure 1.1B) (Grallert et al., 2015; Wu et al., 2009; Yamano et al., 1994). *In vitro* data show that PP1 is capable of auto-dephosphorylating *in vivo*, however this has not yet been shown conclusively in human cells (Dohadwala et al., 1994; Watanabe et al., 2003; Wu et al., 2009; Yamano et al., 1994). It remains plausible that other phosphatases could be responsible for dephosphorylating this site *in*

vivo. The situation is further complicated by the proposed functions of PP1 during mitosis in checkpoint silencing (Moura et al., 2017; Vanoosthuyse and Hardwick, 2009; Winkler et al., 2015). This would imply that CDK phosphorylation cannot completely abrogate the activity of PP1. A crystal structure of PPP1CB:MYPT1 shows that when complexed with a binding partner, the C-terminal tail of PP1 is positioned away from the catalytic site (Terrak et al., 2004), suggesting that CDK inhibition can be overcome through holoenzyme formation.

The relative contribution of the three PP1 isoforms to mitotic regulation remains unclear, and it is unknown whether the consequences of CDK regulation are the same for all PP1 isoforms. Depletion of PPP1CA or PPP1CC individually does not result in an obvious phenotype (Zeng et al., 2010a), suggesting some level of functional redundancy between PPP1C isoforms. By contrast, depletion of PPP1CB almost exactly recapitulates the phenotype observed upon depletion of its canonical binding partner, MYPT1, leading to nuclear deformation and impaired envelope integrity (Takaki et al., 2017; Zeng et al., 2010a). However, this is thought to be caused by diminished control of actomyosin contraction in interphase cells which results in genome instability (Takaki et al., 2017), rather than a perturbed mitosis. This suggests that PPP1CB-MPYT1 is a highly specific activity, discrete from PPP1CA- and 1CC- containing enzymes, which may be involved in mitotic regulation.

PP2A-B55 is the other CDK1-inhibited PPP, this inhibition occurring indirectly through the B55-ENSA-Greatwall (BEG) pathway (Figure 1.6) (Cundell et al., 2013). Greatwall, a serine/threonine kinase, was first identified as a regulator of the cell cycle in *Drosophila melanogaster*, where mutation of Greatwall resulted in impaired mitotic progression and improper chromosome condensation

(Archambault et al., 2007; Yu et al., 2004). The human homologue, microtubule-associated serine/threonine-protein kinase-like enzyme (MASTL), has been shown to have similar effects via analogous experiments (Burgess et al., 2010; Voets and Wolthuis, 2010) and is activated by CDK1:CCNB (Blake-Hodek et al., 2012; Vigneron et al., 2011; Yu et al., 2006). Once active, MASTL phosphorylates the small molecules endosulfine-α (ENSA) and c-AMP regulated phosphoprotein 19 (ARPP19) at Ser67, a highly conserved residue, allowing them to bind to and specifically inhibit PP2A-B55 holoenyzmes (Figure 1.6) (Gharbi-Ayachi et al., 2010; Mochida et al., 2010). Other PP2A holoenzymes are not inhibited by these molecules. Phosphorylated ENSA inhibits PP2A-B55 through an unfair competition model, binding tightly to the active site and preventing dephosphorylation of other substrates (Williams et al., 2014). ENSA itself is only slowly dephosphorylated. This means that the activation of PP2A-B55 is delayed, occurring only after CDK1 and, subsequently, MASTL have been inactivated and the remaining ENSA has been dephosphorylated. Consequently, PP2A-B55 substrates such as PRC1-pT481 are not dephosphorylated immediately as CDK1 becomes inactive following checkpoint silencing. Separation of chromosomes is inhibited stoichiometrically by CCNB and securin, whereas PP2A-B55 is inhibited by CDK1:CCNB enzyme activity. This creates two thresholds of CCNB degradation during mitotic exit. The first threshold reached relieves inhibition of chromosome separation but keeps PP2A-B55 inactive until the second threshold is achieved when CDK1:CCNB activity is no longer high enough to maintain PP2A-B55 inhibition. This ensures that chromosome separation occurs prior to initiation of cytokinesis (Cundell et al., 2013). In fact, depletion of MASTL leads to a cut phenotype whereby the cell initiates cytokinesis before the chromosomes

have separated. Furthermore, although complete inactivation of MASTL requires PP2A-B55 (Hegarat et al., 2014; Mochida et al., 2016), inactivation of MASTL is initiated by other phosphatases. During mitotic exit, FCP1 has been shown to oppose CDK1-dependent phosphorylation of MASTL (Della Monica et al., 2015), while PP1 dephosphorylates auto-activatory sites within MASTL (Blake-Hodek et al., 2012; Heim et al., 2015; Rogers et al., 2016). Although the FCP1-dependent inactivation of MASTL is proposed to occur upstream of PP1 activity the relative timings of these dephosphorylations have not yet been described. Moreover, while logical, it has not been conclusively shown that the direct CDK1-mediated inhibition of PP1 allows it to become active prior to PP2A-B55.

The timing of phosphatase activation is also important in determining SAC responsiveness during mitotic exit. CDK1:CCNB phosphorylation of MPS1-S281 is necessary for its kinetochore localisation and this site is dephosphorylated by PP2A-B55 (Hayward et al., 2018). This finding is surprising given the CDK1-dependent inhibition of PP2A-B55 during mitosis. However, the characteristic delay in PP2A-B55 activation prior to dephosphorylation of this site ensures that checkpoint reactivation is possible should kinetochore attachment errors occur early in mitotic exit. These examples demonstrate the importance of regulating phosphatase activity and how it ensures the correct order and timing during mitosis and mitotic exit. They may also explain how the checkpoint remains responsive to errors in kinetochore attachment for some time after the initial silencing events (Dick and Gerlich, 2013; Vazquez-Novelle et al., 2014).

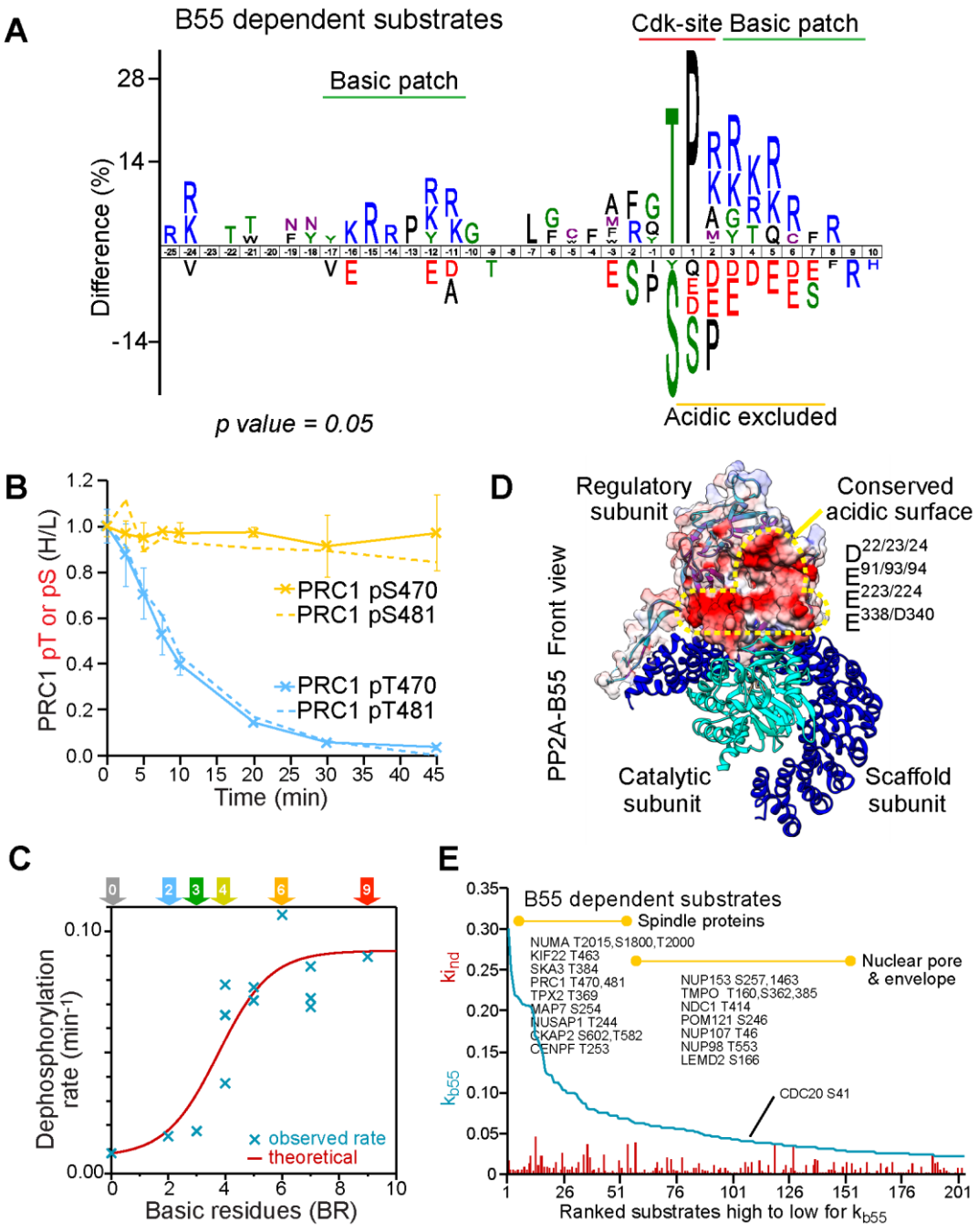


Figure 1.7 PP2A-B55 recognises substrates through a bipartite basic motif

(A) Alignment of high-confidence PP2A-B55 substrates shows a preference for dephosphorylating CDK1 sites, especially phospho-threonine. These substrates are characteristically enriched for two basic patches either side of the phospho-site. This was termed the bipartite polybasic recognition determinant (BPR). (B) Mutation of PRC1-T481 to S481 prevents dephosphorylation by PP2A-B55. (C) Modelled and experimental rate of PRC1-T481 dephosphorylation decreases as basic residues within the BPR are

sequentially mutated. (D) Crystal structure of PP2A-B55 holoenzyme, with the conserved acidic surface highlighted (yellow dotted line). Mutation of these residues prevents PP2A-B55 from dephosphorylating its substrates. (E) High confidence PP2A-B55 substrates ranked according to their rate of B55-dependent dephosphorylation. The more rapidly dephosphorylated substrates are spindle proteins whilst later substrates are nuclear pore and envelope proteins (Cundell et al., 2016).

1.2.4 Substrate specificity of PP2A-B55 imposes order on mitotic exit

A combined approach using mass spectrometry and modelling across the three conditions: control; B55 depletion; and MASTL depletion, identifies approximately 2500 PP2A-B55 mitotic exit substrates (Cundell et al., 2016). Alignment of the high confidence PP2A-B55 substrate phospho-sites reveals several important characteristics. PP2A-B55 substrates are enriched for CDK sites, pS/T-P, with a preference for phospho-threonine (Figure 1.7A). PRC1-pS481 mutant is unable to be dephosphorylated by PP2A-B55 (Figure 1.7B), unless the site is mutated to match the YFDS67 motif found in ENSA. These show that the phospho-preference of these phosphatases can impact on the timing of events during mitotic exit (Cundell et al., 2016; Hein et al., 2017).

The presence of two basic patches which flank the phosphorylation site, termed a bipartite basic region (BPR), is another characteristic feature of PP2A-B55 sites (Figure 1.7A) (Cundell et al., 2016). Acidic residues are also excluded from this region. Sequential alanine mutation of the basic residues of PRC1-pT481, shows that the rate of dephosphorylation correlates with the basicity of the phospho-site (Figure 1.7C). Impaired dephosphorylation impacts the timings of events in anaphase, with BPR mutant PRC1-T481 causing a delay in initiating cytokinesis. A complementary acidic region on the surface of the B55 regulatory subunit necessitates the presence of basic residues in the substrates (Figure

1.7D). These principles also hold true when applied to the unfair inhibitor phosphorylated-ENSA. Significantly, the substrates with the highest rates of B55-dependent dephosphorylation are the most basic, typically the proteins involved in spindle morphology changes such as PRC1 and TPX2. Conversely the slowest dephosphorylated substrates are less basic and include nuclear pore and envelope proteins such as nuclear pore complex protein 153 (NUP153) (Figure 1.7E). In fact, nuclear pore reformation and nuclear import are both under the control of PP2A-B55, ensuring that they occur downstream of chromosome segregation (Cundell et al., 2016).

Evidently, PP2A-B55 contributes to the order and timing of mitotic exit, and the sequence characteristics of each substrate phospho-site impact the rate of dephosphorylation. What remains unclear is whether this is a general principle governing dephosphorylation during mitotic exit or whether this is a specific property of PP2A-B55 holoenzymes. Regardless, this is an interesting prospect given that 3000 B55-independent dephosphorylations were identified during the same study. PP1 would appear to be the likeliest candidate responsible for many of these dephosphorylations given its CDK1-dependent inhibition. However, given the number of potential holoenzymes, finding any holoenzyme substrate specificities would prove difficult.

1.3 Ubiquitin dependent proteolysis

Progression through the cell cycle is coupled to the destruction of key proteins such as cyclins. Typically, this entails ubiquitin-dependent proteolysis where ubiquitin chains are covalently linked to lysines (Lys) in the substrate, targeting the protein to the 26S proteasome where it is degraded. Ubiquitination is carried out by the co-ordinated actions of ubiquitin-activating (E1), ubiquitin-conjugating (E2)

and ubiquitin ligating (E3) enzymes. This can result in the mono or poly-ubiquitination of target substrates. These chains of ubiquitin can be linear or branched and linked through the different Lys contained within ubiquitin (Komander and Rape, 2012). Typically, Lys11 and Lys48 linked chains signal a protein for degradation (Jin et al., 2008b; Matsumoto et al., 2010). While there are other E3 ubiquitin ligases in a cell, the following discussion will focus primarily on APC/C and its role in cell cycle control. However, an alternative E3 ligase, SKP1-Cullin1-F box protein (SCF) also plays an important role early in the cell cycle.

The SCF complex has been well studied. It consists of a Cullin1, a scaffold, Rbx1, an E2 recruiter, and SKP1, which binds to F-box proteins (Skaar et al., 2014). There are over 50 F-box proteins in the human genome and here they recognise substrates for the SCF, often through phosphorylation of a substrate's degron motif (Skaar et al., 2013; Wang et al., 2014). The F-box protein β-TRCP, which recognises D-pS-G-X-X-pS degrons, targets several important cell cycle regulators for degradation via the SCF (Wertz et al., 2011). These include Cyclin D1, early mitotic inhibitor 1 (EMI1) and Wee1, and enable progression through S phase and the G2/M transition respectively (Margottin-Goguet et al., 2003; Watanabe et al., 2004; Wei et al., 2008). F-box with the WD40 motif 7 (FBXW7) also contributes to cell cycle control by promoting ubiquitination of Cyclin E (Koepp et al., 2001). Phosphorylation of the consensus degron, (L)-X-pT/pS-P-(P)-X-pS/pT/E/D, is required for recognition by FBXW7 (Welcker and Clurman, 2008). Other F-box proteins have also been implicated in cyclin ubiquitination. Unsurprisingly, dysregulation of F-box proteins has been observed in a variety of cancers (Wang et al., 2014; Zheng et al., 2016).

The APC/C is also a multi-subunit complex, consisting of a core of 14 proteins (Hutchins et al., 2010; Zachariae et al., 1996) with a coactivator, either CDC20 or CDH1 (Kramer et al., 1998; Visintin et al., 1997). APC11 and APC2 form the minimal catalytic core of the APC/C (Tang et al., 2001) while the coactivator together with the APC10 subunit form the main platform for recognition of degron motifs in the substrate (Chao et al., 2012; Kraft et al., 2005; Pfleger et al., 2001). The classical degron motif is the D-box, whose presence is necessary and sufficient for APC/C to mediate ubiquitination of particular substrates (Glotzer et al., 1991; King et al., 1996). The minimal consensus motif is RxxLxxxxN, where mutation of any of the three key residues can prevent substrate targeting for degradation (Glotzer et al., 1991). Structural studies have revealed that D-boxes are bipartite in nature, with the N-terminus interacting with the coactivators and the C-terminus interacting with a hydrophilic surface of APC10 (Chang et al., 2015; Zhang et al., 2016). Alternatively, proteins can be targeted through the KEN box, named after its consensus sequence (Pfleger and Kirschner, 2000). In substrates containing both KEN and D-boxes their degradation is dependent on both sequences (Burton and Solomon, 2001; Passmore et al., 2003). The KEN box is often found immediately downstream of acidic residues, while a proline to the C-terminus of the motif helps position substrates appropriately. Other degron motifs have also been identified, for example the ABBA motif found in CCNA, BUBR1 and BUB1 is recognised by human CDC20 (Davey and Morgan, 2016; Lu et al., 2014).

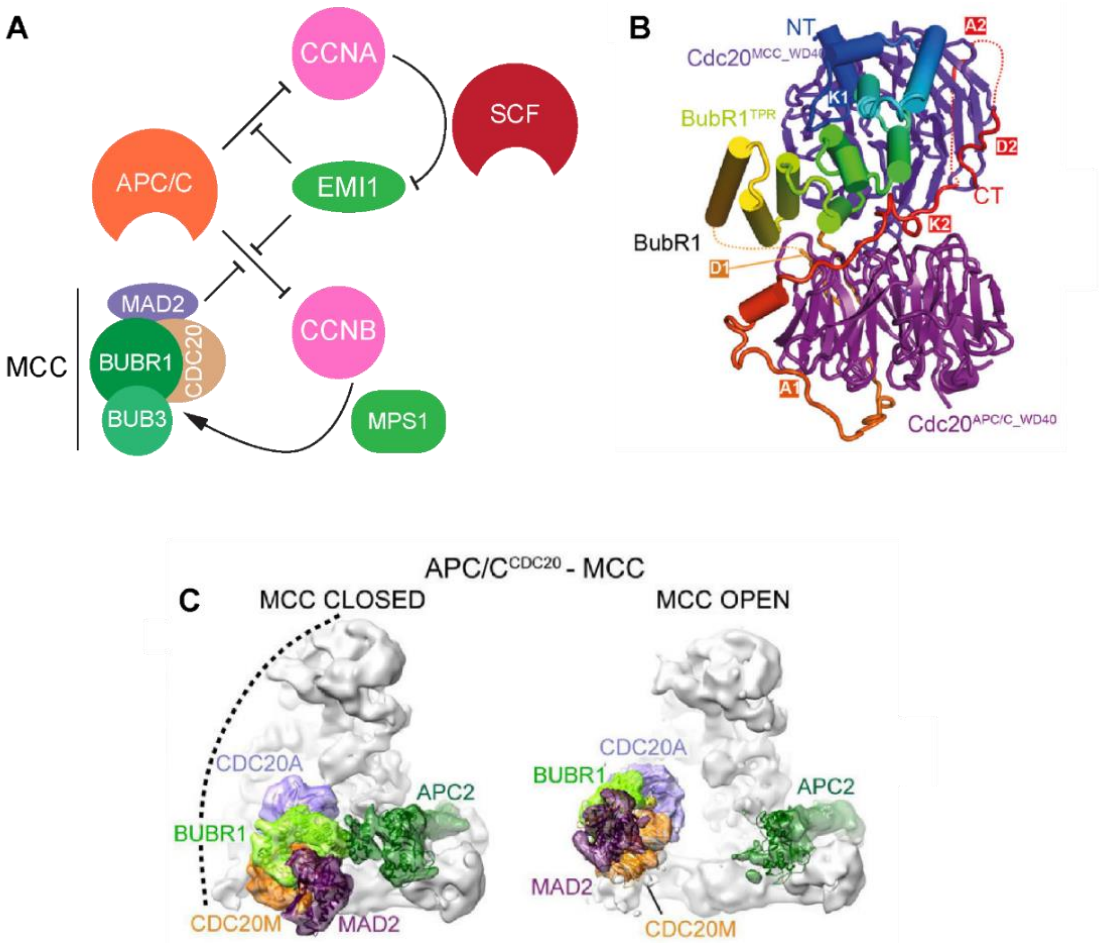


Figure 1.8 Regulation of the APC/C

(A) During S and G2 phases, the APC/C is kept inhibited by early mitotic inhibitor 1 (EMI1), allowing the accumulation of Cyclin A (CCNA) and B (CCNB). Upon entry into mitosis EMI1 is rapidly degraded by the SCF, a ubiquitin ligase, in a phosphorylation-dependent manner, leading to the activation of the APC/C and the degradation of CCNA during prometaphase. Meanwhile, the spindle assembly checkpoint (SAC) generates mitotic checkpoint complex (MCC) which inhibits the APC/C towards anaphase substrates, including CCNB. CDK1:CCNB activity is required for a functional SAC and the correct localisation of MPS1, promoting stabilisation of CCNB. Once all kinetochores are attached, MCC production ceases, allowing APC/C mediated destruction of CCNB. (B) Cartoon generated from Cryo-EM data showing that BUBR1 interacts with two molecules of CDC20 (dark and light purple), using two sets of degron motifs (A,D,K 1 and 2). CDC20M and CDC20A refer to CDC20 molecules either incorporated into MCC or bound to the APC/C as a coactivator, respectively (Yamaguchi et al., 2016). (C) Cryo-EM structure of the APC/C^{CDC20}:MCC complex, in the open and closed conformations. In the open conformation, CDC20M is positioned appropriately for ubiquitination (Alfieri et al., 2016).

In addition to substrate recognition, coactivator subunits are required to stimulate catalytic activity. The interaction between APC10 and the E2 enzyme ubiquitin conjugating enzyme E2C (UBE2C), responsible for substrate mono-ubiquitination, requires the conformational changes elicited by coactivator binding to the APC/C (Chang et al., 2015; Li et al., 2016). UBE2S, another E2, is responsible for poly-ubiquitination of substrates through Lys11 connected chains. UBE2S does not compete for binding with UBE2C and does not appear to interact with the RING domain of APC11 (Wickliffe et al., 2011; Williamson et al., 2009). However, the APC11 RING domain is necessary for enhancing the catalytic activity of UBE2S (Chang et al., 2015). Together these interactions position UBE2C and UBE2S to fulfil their roles of priming and elongation respectively. Neither E2 enzyme is essential, however UBE2S is required for optimal mitotic exit, potentially because of its specificity for producing K11-linked ubiquitin chains (Garnett et al., 2009; Matsumoto et al., 2010; Wickliffe et al., 2011).

1.3.1 Cell cycle control of the anaphase promoting complex/cyclosome

From late S-phase and in G2, the early mitotic inhibitor 1 (EMI1) keeps the APC/C inactive (Di Fiore and Pines, 2008; Grosskortenhaus and Sprenger, 2002; Hsu et al., 2002b) by preventing APC/C-coactivator interaction with substrate D-boxes and opposing ubiquitin chain elongation (Figure 1.8A) (Frye et al., 2013; Miller et al., 2006; Wang and Kirschner, 2013). This enables the accumulation of mitotic proteins, such as CCNB and CDC20. At the G2/M transition, PLK1 phosphorylates EMI1, targeting it for degradation by $SCF^{\beta TRCP}$ (Hansen et al., 2004), allowing APC/C association with CDC20 and in principle its activation. Once in mitosis the APC/C is subjected to regulation through MCC binding and phosphorylation (Figure 1.8A).

CDC20 was initially thought to be sequestered into MCC to prevent its association with the APC/C. However, it is now known that whilst the MCC exists as a 1:1:1:1 subunit stoichiometry, it can bind to a second molecule of CDC20 complexed to the APC/C. Recent structural studies support this work and confirm that two molecules of CDC20 are present in the MCC-APC/C^{CDC20} complex (Alfieri et al., 2016; Yamaguchi et al., 2016). One CDC20 was part of the MCC ($CDC20_M$), as expected, while the second was bound as a coactivator of the APC/C ($CDC20_A$) (Figure 1.8B). The interaction with BUBR1 altered the position of $CDC20_A$, preventing activation of the APC/C. BUBR1, the largest subunit of the MCC, contains two sets of degron motifs each set consisting of a D box, Ken box, and ABBA motif. One set interacts with CDC20 and MAD2 to promote MCC formation while the other set blocks all three of these degron binding sites on $CDC20_A$ (Figure 1.8B). BUBR1 can be thought of as a pseudo-substrate inhibitor of the APC/C, since their interaction is mediated by the motifs normally used for APC/C substrate recognition (Alfieri et al., 2016; Izawa and Pines, 2015; Lara-Gonzalez et al., 2011; Lischetti et al., 2014; Yamaguchi et al., 2016). Furthermore, tetratricopeptide repeating (TPR) motifs of BUBR1 interact directly with APC2 preventing UBE2C gaining access to the catalytic core of the APC/C (Herzog et al., 2009). This means the APC/C^{CDC20}:MCC can neither bind substrates nor initiate their ubiquitination. However, UBE2S is still able to bind to the MCC-APC/C^{CDC20} complex, meaning that the chain elongation of pre-ubiquitinated substrates is possible (Kelly et al., 2014; Yamaguchi et al., 2016). The presence of two CDC20 molecules also explains how CDC20 is ubiquitinated. Data suggest that CDC20 which is part of the MCC is preferentially ubiquitinated over free or APC/C-bound CDC20 (Alfieri et al., 2016; Yamaguchi et al., 2016). Moreover, the

APC/C^{CDC20}:MCC complexes can adopt two conformations, a closed fully inhibited form and an open state (Figure 1.8C). When open, $CDC20_A$:MCC swings away from the main body of the APC/C, and the space created enables the E2 ubiquitin ligases UBE2C and UBE2S to access $CDC20_M$ and allows its mono or poly-ubiquitination, respectively (Alfieri et al., 2016; Yamaguchi et al., 2016). CDC20 ubiquitination is dependent on the APC/C subunit, APC15, which promotes formation of the open state and thus the ubiquitination of $CDC20_M$ without affecting the degradation of CCNB and securin (Figure 1.8C) (Alfieri et al., 2016; Uzunova et al., 2012; Yamaguchi et al., 2016). Auto-ubiquitination of $CDC20_A$ has also been shown to occur (Foe et al., 2011) but the structural flexibility of $CDC20_A$ without the MCC is unknown.

Modification of degron motifs can also modulate the substrate-APC/C interaction. Phosphorylation of the D-box at position 6 can increase substrate ubiquitination (Hellmuth et al., 2014) while at position 2 it can interfere with APC substrate binding (Lu et al., 2014). This is also reflected in the preference for an acidic residue at position 6 and a basic residue at position 2 of the D-box consensus motif (Alfieri et al., 2017). Many core APC/C subunits are phosphorylated during mitosis, promoting binding of CDC20 and activation of the APC/C^{CDC20} (Fujimitsu et al., 2016; Kraft et al., 2003) but these phosphorylations are not necessary for CDH1 binding (Kramer et al., 2000; Zhang et al., 2016). Of particular note is the fact that APC1 and APC3/CDC27 are hyper-phosphorylated (Herzog et al., 2005; Kraft et al., 2003; Qiao et al., 2016). Structural studies reveal that phosphorylation of APC1 moves an auto-inhibitory loop to allow binding and activation of CDC20 (Zhang 2016). The phosphorylation of APC3/CDC27 is

thought to recruit CDK complexes and promote the phosphorylation of APC1 (Fujimitsu et al., 2016; van Zon et al., 2010).

Despite CDC20 and CDH1 making similar contacts with the APC/C, only CDC20 binding is promoted by APC/C phosphorylation. It is thought that the more extensive contacts made by CDH1 with the APC/C can overcome the auto-inhibition of APC1 without prior phosphorylation. Furthermore, CDK-phosphorylation of CDH1 on four residues has been seen to interfere with APC/C^{CDH1} binding (Chang et al., 2015). Likewise, CDK phosphorylation of CDC20's N-terminus also attenuates APC/C binding (Labit et al., 2012). CDK2:CCNA phosphorylation of CDC20 is thought to prevent premature APC/C^{CDC20} formation, promoting mitotic entry though CCNB stabilisation (Hein et al., 2017). Moreover, CDK1:CCNB phosphorylation of CDC20 is thought to prevent interaction with APC8 (Chang et al., 2015; Zhang et al., 2016). An additional PLK1 phosphorylation of CDC20 interferes with the association between UBE2S and the APC/C, but the mechanism of this inhibition is unclear (Jia et al., 2016). Both PP1 and PP2A have been implicated in the removal of these phospho-sites and the subsequent activation of the APC/C^{CDC20}, however precise details of the specific holoenzymes and their regulation were lacking until recently. It has now been shown that PP2A-B55 rapidly dephosphorylates inhibitory phospho-threonine residues located toward the N-terminus of CDC20. Conversely, PP2A-B55 relieves the phospho-serine-mediated inhibition of CDH1 much more slowly. In this way the substrate preferences of PP2A-B55 impacts the timing of both APC/C activation and co-factor binding during mitotic exit (Hein et al., 2017).

1.3.2 The role of ordered proteolysis during mitosis and mitotic exit

Following EMI1 degradation at mitotic entry, the APC/C is able to degrade CCNA and NEK2A during prometaphase, despite MCC binding (Hames et al., 2001). These substrates must therefore interact with the APC/C distinctly from CCNB and securin. Consequently, NEK2A can bind to the APC/C in the absence of a coactivator, however one is required for NEK2A ubiquitination (Boekhout and Wolthuis, 2015; Hayes et al., 2006; Kimata et al., 2008). CCNA's resistance to SAC-dependent APC/C inhibition is one of the key differences between CCNA and CCNB. As such CCNA is degraded directly after NEBD occurs and ~20 min before CCNB. Furthermore, inhibiting the SAC by using MPS1 inhibitors collapses this delay causing both cyclins to show similar destruction kinetics (Mansfeld et al., 2011). The degradation of CCNA is not dependent on its D-box, instead a C-terminal region containing the ABBA motif targets CCNA for degradation by binding directly to CDC20 (Di Fiore et al., 2015; Jacobs et al., 2001). Thus, the MCC ensures ordered cyclin proteolysis during mitosis.

It is also proposed that ordered proteolysis contributes to a proper mitotic exit (Lindon and Pines, 2004). A central feature of G2 is the synthesis of factors required for mitosis, including CCNB, Aurora and Polo kinases, as well as many factors required for mitotic spindle formation (Whitfield et al., 2002). A detailed analysis of cell cycle regulated transcripts identifies approximately 50 genes whose transcription peaks in G2 and approaching a further 160 with transcript levels peaking in mitosis. While this isn't a direct measure of protein synthesis during the cell cycle it is probably a representative view of the changes that occur, given the function of the proteins identified. In essence, it is reasonable to hypothesise that these proteins must be degraded in a timely manner following

APC/C activation. In fact, 55 human proteins were identified as APC/C substrates in a 2011 review (Meyer and Rape, 2011).

Once activated, the APC/C^{CDC20} rapidly ubiquitinates CCNB and securin, targeting them for degradation (Glotzer et al., 1991). The APC/C^{CDH1} complex can form as CCNB is degraded and CDK1 activity falls (Kotani et al., 1999; Visintin et al., 1997). APC/C^{CDH1} can then target CDC20 for destruction (Pfleger and Kirschner, 2000). Dephosphorylation of the APC/C itself contributes to this switch by weakening the APC/C^{CDC20} interaction (Zachariae et al., 1998). This rapid change in APC/C coactivator alters substrate specificity and further contributes to ordered proteolysis during mitotic exit. Once active, APC/C^{CDH1} can target cytokinesis regulators, such as Aurora kinases, TPX2, PLK1, anillin and cytoskeletal associated protein 2 (CKAP2), for degradation (Seki and Fang, 2007; Stewart and Fang, 2005b; Taylor and Peters, 2008; Zhao and Fang, 2005). Interestingly, the degradation of only a few proteins, beside Aurora kinases, has been shown to be completely dependent on APC/C^{CDH1} (Floyd et al., 2008), which raises questions regarding the importance of switching coactivators during mitotic exit in human cells. It has been demonstrated that PLK1 is degraded prior to Aurora A (Lindon and Pines, 2004), to ensure proper spindle dynamics and organisation during anaphase (Floyd et al., 2008). Following on, it was proposed that PLK1 phosphorylation helps activate CDC14A prior to checkpoint silencing, promoting CDH1 activation in anaphase. Interestingly, the inhibition of PLK1 does not stabilise Aurora A as well as PLK1 depletion, suggesting that the presence and not just the activity of PLK1 is required for CDH1 activation (van Leuken et al., 2009). Depletion of CDH1 stabilises levels of anillin but does not affect the kinetics of mitotic exit or cytokinesis (Zhao and Fang, 2005). Anillin is required for the

completion of furrow ingression, meaning its stabilisation would more likely have effects downstream of abscission. This is supported by work suggesting that the destruction of CKAP2 does not impact completion of mitotic exit and that post-translational modification may inactivate CKAP2 prior to its degradation (Seki and Fang, 2007). Consistently, the addition of the proteasome inhibitor MG-132 did not alter the rate of dephosphorylation of PPP1CA-pT320 or PRC1-pT481 in HeLa cells following CDK inhibition (Cundell et al., 2013). Furthermore, a global proteomic analysis of meiotic exit in *Xenopus* eggs, which lack CDH1, showed that proteolysis was limited to a few key rapidly degraded targets such as CCNB1/2 and securin (Presler et al., 2017). These latter results suggest that APC/C-dependent proteolysis fulfils a more limited role than previously thought and may be more important for resetting cell status in G1 rather than implicitly impacting the order and timing of mitotic exit.

One final consideration is the role of ongoing protein synthesis during mitosis and mitotic exit. Translation was initially thought to be globally repressed upon mitotic entry (Fan and Penman, 1970). It is now thought that a small number of proteins escape this repression using cap-independent translation which is dependent on an internal ribosome entry site (IRES) (Cornelis et al., 2000; Pyronnet et al., 2000; Qin and Sarnow, 2004; Wilker et al., 2007). It has also been suggested that CDK1 can actually promote canonical cap-dependent translation during mitosis, functionally substituting for RAPTOR-mTOR kinase and phosphorylating translation initiation factors (Shuda et al., 2015). Furthermore, it has been proposed that continued synthesis and degradation of CDC20 is necessary to enable rapid activation of the APC/C^{CDC20} upon checkpoint satisfaction (Nilsson et al., 2008). This degradation of CDC20 was dependent on a

functional SAC. Subsequently, this turnover was shown to take place via the APC15-mediated ubiquitination of CDC20 (Uzunova et al., 2012). Nilsson et al. also showed slower rates of both CCNB and BUBR1 turnover during mitosis. However, this synthesis of CDC20 has not been proven directly, only inferred from the degradation of CDC20. Additionally, transcription continues at low levels during mitosis with a further burst during late mitotic exit (Palozola et al., 2017; Vankova Hausnerova and Lanctot, 2017). How this spike of transcription correlates with protein synthesis remains unclear and it is not yet known if ongoing protein synthesis contributes to differential rates of proteolysis during mitotic exit.

The quantitative model of Cdc2 control, which was developed in fission yeast by Stern and Nurse, places protein synthesis at the centre of cell cycle progression. In this model, the G1, S and mitotic cyclins ensure that Cdc2/CDK1 goes through stages of increasing activity, as each cyclin is synthesised, degraded and replaced by the next. This leads to increasing widespread phosphorylation, peaking in mitosis, before the system is reset through cyclin degradation during mitotic exit. A single CDK:cyclin complex is therefore sufficient for orderly progression of the cell cycle (Stern and Nurse, 1996; Uhlmann et al., 2011). Furthermore, this model also necessitates a balance between kinase and phosphatase activities, particularly the presence of a CDK-inhibited phosphatase. This inhibition would peak during mitosis enabling the global increase in phosphorylation. As such phosphatase activity is just as important in substrate phosphorylation status as the kinase it opposes: in budding yeast this phosphatase is Cdc14. To reset the cell status during mitotic exit the inhibition of this phosphatase must be relieved. The Cdc14 early anaphase release (FEAR) and mitotic exit network (MEN) act sequentially to release Cdc14 from the inhibitor

Net1 (Queralt et al., 2006; Queralt and Uhlmann, 2008; Stegmeier and Amon, 2004). It has been proposed that FEAR-activated Cdc14 could dephosphorylate sites early in mitotic exit (Jin et al., 2008a) but it is more likely that these pathways function together to gradually relieve Cdc14 inhibition, initially, while Cdc2 is active through FEAR and later, when Cdc2 is inactive, using MEN (Queralt et al., 2006; Stegmeier et al., 2002). This would gradually shift the balance of kinase and phosphatase activity during mitotic exit. In human cells, however, the activation of the CDK1-inhibited phosphatases PP1 and PP2A-B55 bears little resemblance to FEAR and MEN (Cundell et al., 2013). Nevertheless, it remains to be seen whether the direct and indirect CDK1-mediated inhibition of these two phosphatases has similar implications for regulation of mitotic exit.

1.4 Thesis aims

A fundamental question in cell biology is, ‘How do cells coordinate chromosome segregation with cytoplasmic division to create new cells?’ It is clear, from decades of published literature, that progression through the cell cycle is tightly regulated, with mitosis depending on decisive switches in the balance between kinase and phosphatase activity. These transitions are coupled to the synthesis and destruction of key proteins such as cyclins. Furthermore, the order of events is critical to successful division, with incorrect timing being highly injurious to cell survival. This is most obvious when considering the rapid, sequential changes a cell undergoes during mitotic exit.

The relative contributions of phosphatase activity and targeted proteolysis to the regulation of mitotic exit are currently unclear. Furthermore, current analysis of mitotic exit is often protein-specific and lacking the time resolution to properly dissect the events of early anaphase. With this in mind, the use of a mass

spectrometry-based approach to obtain a global vantage point of the changes occurring during mitotic exit will be beneficial. Following these events with high time resolution, simultaneously at the level of protein turnover and phosphorylation status, will provide an unbiased view of mitotic exit. This knowledge will be invaluable to understanding the fundamental principles of cell cycle regulation and the importance of post-translational modifications.

2 Results

2.1 Establishing a system for *in vivo* analysis of mitotic exit

2.1.1 Pilot proteomic analysis of mitotic exit

To gain a full quantitative understanding of mitotic exit it is important to be able to follow changes in both protein abundance and phosphorylation state. Typical cell biological and Western blot methodologies allow investigation and confirmation of proteins and phosphorylation sites for which specific reagents are available but are unable to provide a global vantage point. Consequently, mass spectrometry is one of the preferred methods to observe general trends in data. The work by Cundell et al. serves as a clear example of the potential insights gained from taking a more global approach (Cundell et al., 2016). High-resolution, quantitative phospho-proteomic data allowed 1000s of phosphorylation sites to be followed simultaneously. Ultimately this yielded novel information regarding phosphatase substrate specificity, substrate identification and importantly the order and timing within mitotic exit. Therefore, the same quantitative strategy, di-methyl labelling, was used as described previously (Boersema et al., 2009). Each sample was labelled 'heavy', using deuterated formaldehyde with $NaBH_3CN$ to create a mass difference of 32 Da per N terminal amino-group or lysine side chain. The 'heavy' label was mixed in equal amounts with an aliquot of 0 min timepoint which had been labelled 'light', using formaldehyde and $NaBH_3CN$ for a mass difference of 28 Da. The ratio between the 'heavy' and 'light' labelled peptides reflected the change in that peptides abundance from 0 min (Methods 4.6.2) (Cundell et al., 2016). This enabled accurate, quantitative information to be obtained for thousands of peptides across the timecourse.

Nevertheless, the approach used by Cundell et al. had limitations since it was tailored specifically to interrogate PP2A-B55 function. These limitations were a consequence of experimental design, with the mitotically arrested cells being lysed, on ice, to create a mitotic extract. Firstly, low temperatures inactivate kinases, such as CDK1, PLK1 and Aurora kinases. While this helps to simplify the modelling parameters and interpretation of results, the activities of PLK1 and Aurora persist well into anaphase and are required for cytokinesis and abscission. Furthermore, PP1, a CDK1-inhibited phosphatase, known to be required alongside PP2A-B55 for mitotic exit, is inactive in these mitotic extracts; the reasons for this are poorly understood. Additionally, due to the inefficiency of APC/C dependent proteolysis under these conditions, there was a lack of proteomic information meaning that it was not possible to observe the contribution of proteolysis to mitotic exit.

To combat these limitations, the protocol from Cundell et al. was adapted as below (Figure 2.1). Firstly, the experiment was conducted *in vivo* at 37°C, 5% CO_2. This ensured that all the necessary components were present at physiological concentrations and functionally unperturbed. At this temperature, reactions occur much more rapidly and therefore an increased sampling rate was necessary. Initially, this was every 30 s for Western blot with every alternate timepoint being used for proteomic analysis (Figure 2.1A). In the previous work, cells were lysed, and dephosphorylation allowed to occur naturally, as PP2A-B55 was diluted away from its inhibitor, phosphorylated-ENSA. However, when working in cells, additional consideration is needed to ensure a high level of synchrony, a necessity for collecting meaningful results. This was achieved by arresting cells in mitosis using nocodazole, which was then washed out

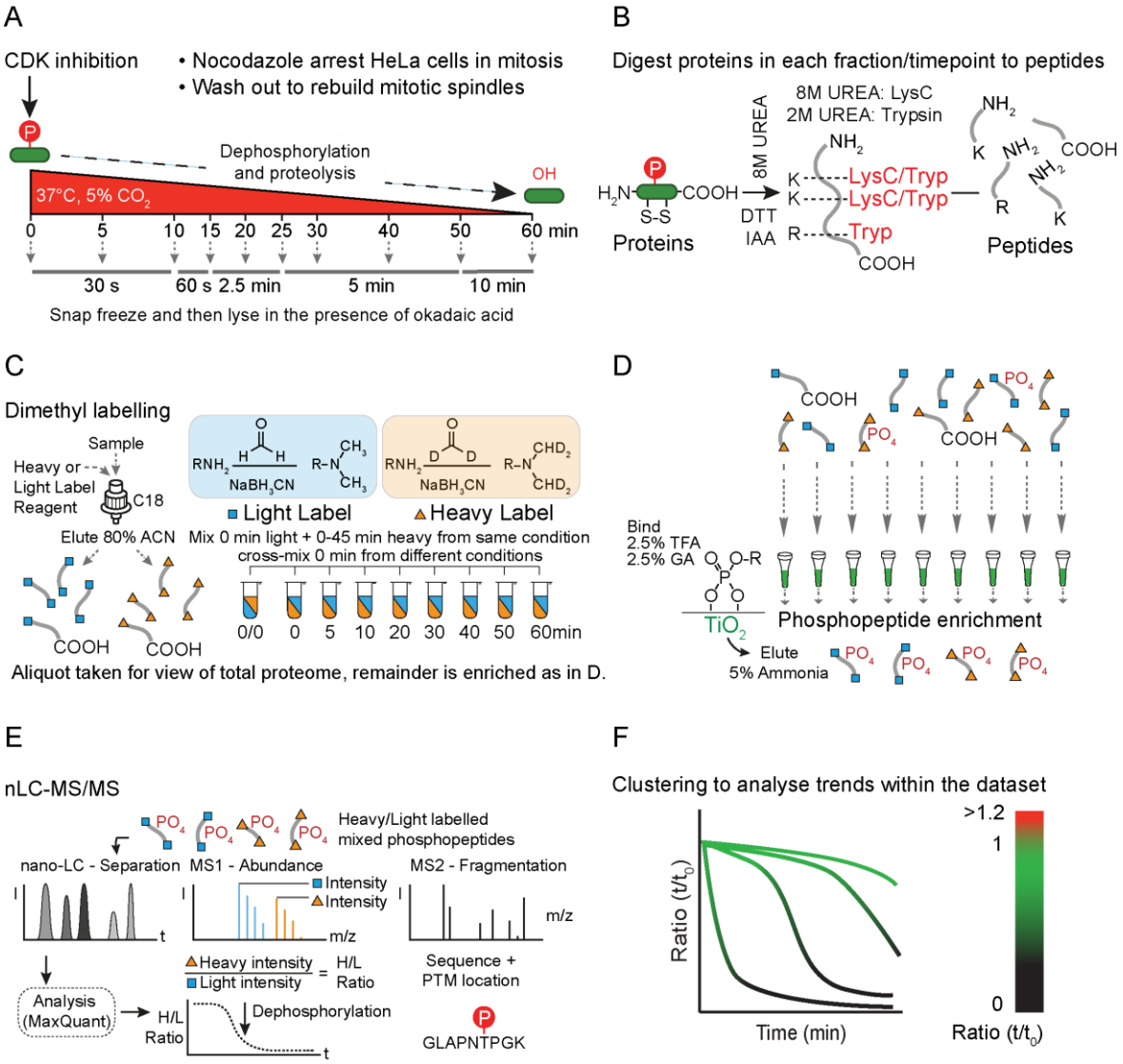


Figure 2.1 Protocol for a quantitative mass spectrometry analysis of mitotic exit

Protocol adapted from Cundell et al., 2016. (A) Cells are synchronised using nocodazole and flavopiridol, a CDK inhibitor, and sampled as indicated before lysis in 8 M Urea. (B) 500 µg proteins are digested using both Lys-C and trypsin. (C) Peptides are bound on a C18 column, labelled and a portion taken for total proteome analysis. (D) The remainder, 400 µg, is subjected to phospho-enrichment. (E) Samples are then run on an LC-MS/MS system and the intensity of 'heavy' and 'light' peptides is used to produce a ratio which can be used to follow changes in abundance over time. (F) Trends within the whole data-set are then examined using clustering within Perseus software, Methods 4.7.

allowing mitotic spindles to be rebuilt. Two procedural options were then available, the first being the inhibition of the checkpoint kinase, MPS1, using AZ3146. While providing the most physiological version of mitotic exit, cells do not demonstrate synchronous exit kinetics unless kept in 10% (v/v) serum containing DMEM media at 37°C, 5% CO_2 (unpublished data). This would have reduced the sampling rate significantly due to the need to centrifuge and remove the media from each sample before snap freezing. Alternatively, CDK inhibition, using flavopiridol, can be used to promote the highly synchronous progression into anaphase of cells resuspended in serum-free Opti-MEM media at 37°C. The use of Opti-MEM obviates the need for centrifugation and wash steps to remove serum proteins before sample processing. This change also enabled a 30 s timepoint resolution to be attained since the cells can be held in a 37°C water bath in the absence of 5% CO_2 (Figure 2.1-2). Therefore, because of the need for high temporal resolution for this work, CDK inhibition was used to trigger mitotic exit. However, this does create two caveats, both requiring consideration during analysis of the experimental data. Firstly, as CDK1 activity is uncoupled from the level of CCNB1, due to chemical inhibition, some dephosphorylation events will now take place earlier than under physiological conditions. For example, this system collapses the characteristic delay seen before dephosphorylation of PP2A-B55 sites, such as PRC1- pT481 (Figure 2.2B) (Cundell et al., 2013). Secondly, the level of CCNB1 now reflects the maximal rate of APC/C^{CDC20} activity. After generation of the cell samples, the procedure for mass spectrometry was almost identical to that used by Cundell et al., except that total proteome data were obtained for every sample generated, not just for label check conditions (Figure 2.1B-E). Global trends in the

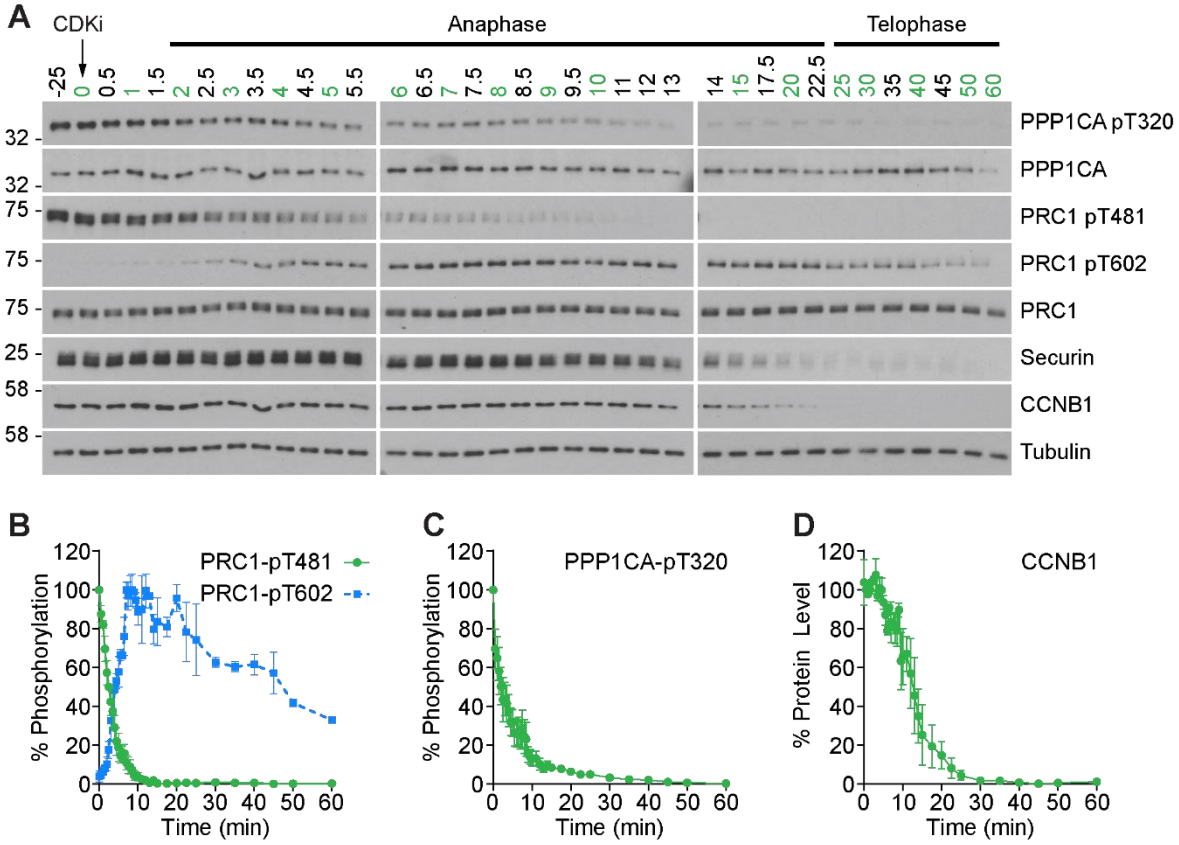


Figure 2.2 CDK inhibition promotes orderly mitotic exit

(A) Mitotically arrested cells were washed out from nocodazole, at 37°C 5% CO_2, and the CDK inhibitor (CDKi), flavopiridol, was added at 0 min. Samples were taken at the indicated timepoints, those used for mass spectrometry analysis are highlighted in green. Densitometric quantification of repeat experiments, as in (A) (Mean±SEM, n=2) is shown for (B) PRC1-pT481/pT602, (C) PPP1CA-pT320 and protein level for (D) CCNB1.

data were then identified through a clustering analysis, grouping proteolysis or dephosphorylation events into four categories: early, intermediate, late or stable (Figure 2.1F) (Methods 4.6).

Before proceeding further, it was important to establish that the experimental strategy described above accurately recapitulates orderly mitotic exit. For this purpose, specific markers of exit from mitosis and progression into

anaphase were analysed. As already explained, the central spindle protein PRC1 is inhibited by CDK1 phosphorylation at T481 in mitosis and phosphorylated at T602 by PLK1 in anaphase (Neef et al., 2007). The CDK inhibition protocol resulted in near complete dephosphorylation of PRC1-pT481 by 10 min, followed by accumulation of the PLK1 phosphorylation at PRC1-pT602 from 2.5 min (Figure 2.2A and B). Additionally, the inhibitory CDK1 phosphorylation of PP1 seen in mitosis, PPP1CA-pT320, was also lost by 10 min (Figure 2.2C), presumably indicative of PP1 activity in the system. Finally, APC/C-dependent proteolysis could be observed as highlighted by the falling levels of CCNB1 and securin starting from ~2.5 min and increasing in rate by 10 min and approaching a minimum from 20 min (Figure 2.2A and D; Figure 2.3A). Together these markers indicated that the cells had undergone mitotic exit and progressed into anaphase in an orderly fashion. Two repeats of these timecourse samples were then processed for mass spectrometry (Methods 4.6), identifying ~4500 proteins and ~15,000 phospho-sites, of which ~1/3 were reliably quantified. Ideally both CCNB1 and securin would be used as positive controls for identifying rapidly degraded proteins upon CDK inhibition, however only CCNB1 was consistently quantified at all timepoints by mass spectrometry. Securin was rarely identified and, when it was observed, it was poorly quantified. This can be explained by the distribution of basic residues within securin, which will be cleaved by Lys-C and trypsin, creating either short peptides, less than five amino acids, or very long peptides unsuitable for detection by the mass spectrometer and subsequent searching by MaxQuant software (Figure 2.3B). The MaxQuant output for quantitated proteins and phosphorylation sites was then analysed in Perseus and a clustering heat map generated (Methods 4.7.1). If a line remains green when moving horizontally along

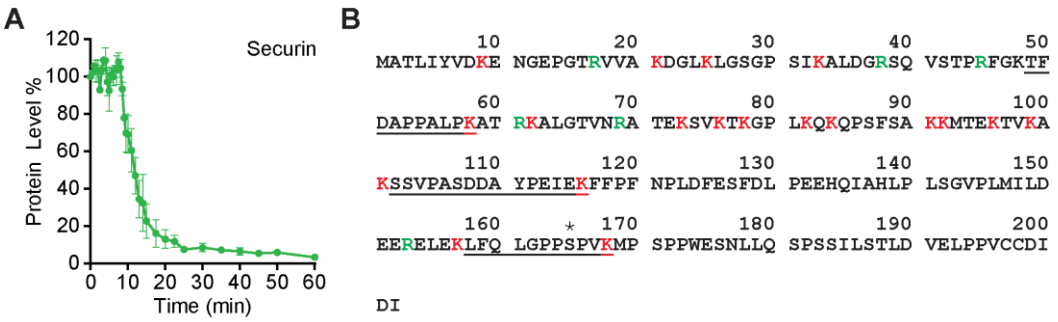


Figure 2.3 Quantification of securin by mass spectrometry

(A) Densitometric quantification of the Western blot from Figure 2.2 (Mean±SEM, n=2). (B) Amino acid sequence of securin with proteolytic cleavage sites marked: trypsin and Lys-C (K, red) or trypsin alone (R, green). Cleavage occurs to the C terminal side of each residue. Observable securin peptides are underlined, * denotes a phosphorylated residue.

the heatmap, that protein/phospho-site is stable. If the line turns black, the ratio has tended towards 0, indicating proteolysis or dephosphorylation.

Unexpectedly, the total proteome data did not cluster properly into four groups. In fact, except for one small cluster of noisier data, containing 91 proteins, the vast majority of the observed proteome, 1695 proteins, remained stable (Figure 2.4A). Given the number of proteins made in preparation for mitosis it had been assumed that these would be degraded with specific timings during mitotic exit (Whitfield et al., 2002). However, this initial analysis suggests that proteolysis plays a limited role during mitotic exit. By contrast, when subjected to the same analysis the phospho-proteomic data clustered into four groups (Figure 2.4B). These four groups correspond to early and intermediate dephosphorylations, stable phosphorylation and a final group of “noisy” data. Furthermore, when each of these phospho-site clusters was aligned it became clear that each group was enriched for particular sequence characteristics. Early dephosphorylations were enriched for phospho-threonine and basic residues while excluding phospho-

serine and acidic residues (Figure 2.4C, lower panel). Inverse residue preferences were seen for the stable phospho-sites, while the intermediate category didn't show any strong selection for specific sequence features (Figure 2.4C, upper panel). Taken together these preliminary analyses suggest that it is dephosphorylation and not proteolysis that helps determine the order of events during mitotic exit. Furthermore, it appears that the sequence characteristics of each phospho-site may encode rate determining information. Nevertheless, the dataset at present has its limitations. Firstly, the number of proteins present in a mitotic cell is ~9500 (Prof. Shabaz Mohammed, personal communication): here ~50% of these were identified and ~20% were reliably quantified over time. Due to the di-methyl labelling of peptides and the number of samples involved, the fractionation required to improve these numbers is far from trivial. Additionally, more repeats are necessary to account for noise, erroneous quantification and missing values. All these can impact the downstream clustering analysis. Therefore, optimisation and a more thorough analysis procedure was necessary to validate these pilot data.

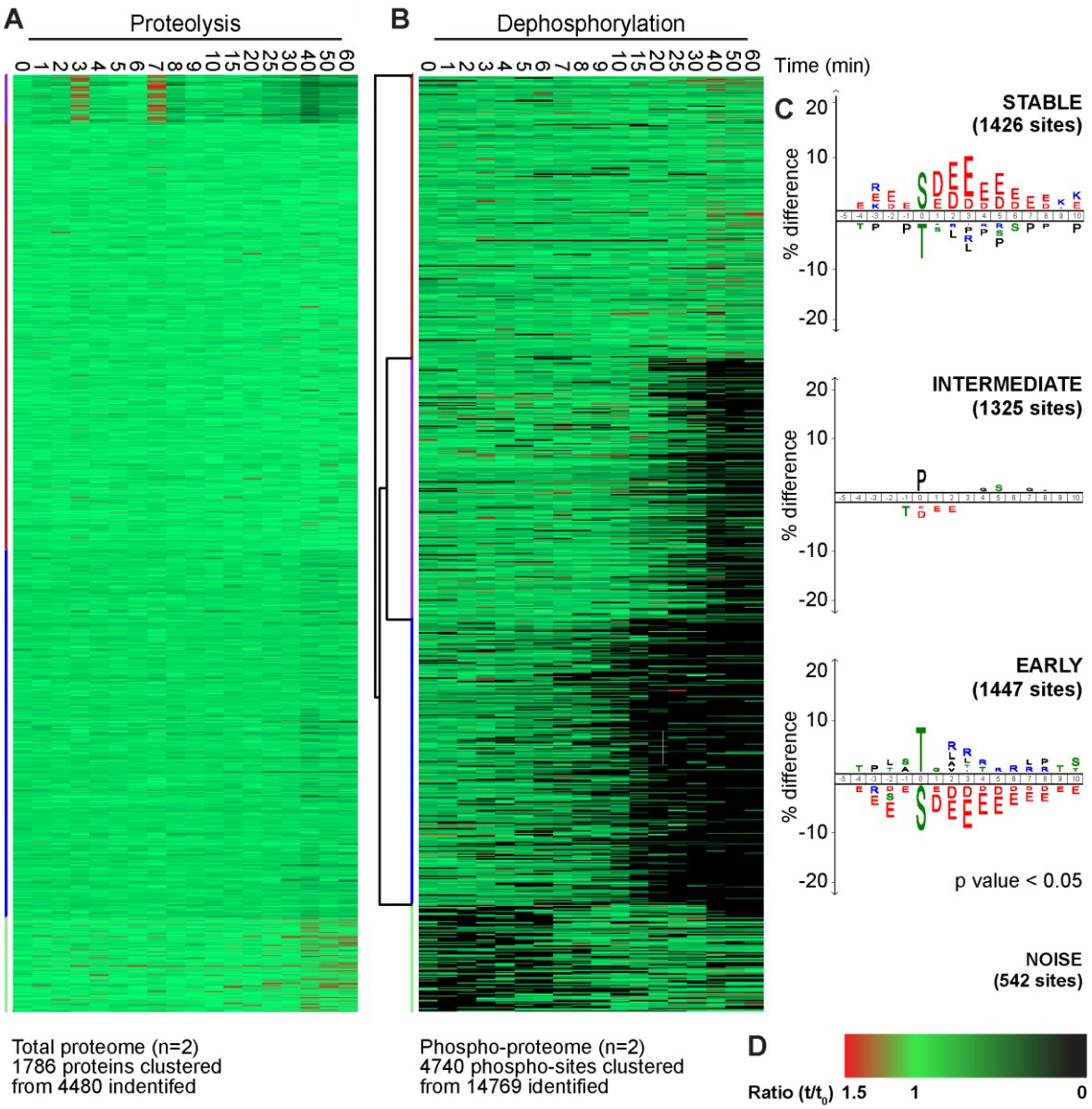


Figure 2.4 A pilot quantitative analysis of mitotic exit

Cells were arrested in mitosis and mitotic exit triggered with CDK inhibition. Heatmap of (A) protein groups or (B) phospho-sites clustered based on their behaviour over time. Time is shown in minutes. (C) Sequence logo analysis showing the relative enrichment of residues in the adjacent cluster from (B) when compared against the sequences of all clustered phospho-peptides. Number of phospho-sites in each cluster is in brackets. (D) Key linking heatmap colour with observed ratio.

2.1.2 Optimisation of mass spectrometry protocols

2.1.2.1 Proteins bound tightly to DNA are lost during clarification

Following the pilot analysis in 2.1.1, BANF1 was identified as a novel candidate for rapid degradation during mitotic exit. BANF1 was rapidly degraded following CDK inhibition, before recovering later in anaphase or early telophase (Figure 2.5A). This suggested a complex relationship between APC/C activity and the levels of protein synthesis during anaphase. Furthermore, BANF1 has been shown to cross-link distant segments of DNA forming a rigid chromatin barrier to promote the formation of a single nucleus (Samwer et al., 2017). Timing of the degradation and accumulation of BANF1 could be critical to the function as premature reformation of the nucleus would be unfavourable. Identification of BANF1 was especially interesting given that no other rapidly degraded proteins were identified in the mass spectrometry dataset besides CCNB1.

To validate this observation GFP-tagged BANF1 was transfected into HeLa cells and imaged during the course of a single mitosis. Prior to nuclear envelope breakdown (NEBD), BANF1 was present in the nucleus, partially enriched at the nuclear periphery (Figure 2.5D). As cells entered mitosis, BANF1 became evenly distributed in the cytoplasm. Following sister chromatid separation, BANF1 rapidly accumulated at the chromatin, initially at the edges before subsequently coating the whole surface. Later in anaphase the intensity of BANF1 observed on the chromatin appeared to decrease. These findings are consistent with published literature and are caused by changes in the phosphorylation state of BANF1 as determined by VRK1 and PP2A (Samwer et al., 2017). Importantly, the level of tagged BANF1 did not appear to decrease as expected during mitotic exit. In fact, the timing of rapid BANF1 accumulation at and partial release from chromatin

seemed to closely match the timing of changes in endogenous BANF1 level detected by mass spectrometry (Figure 2.5A).

This discrepancy between BANF1 levels during anaphase in the mass spectrometry data and by live cell imaging was explored further, focussing on the protocol used to create samples for mass spectrometry. Urea extracts produced from timecourses samples are clarified to remove insoluble cell debris from the lysate. Additionally, the chromatin is likely to be pelleted out of the sample at this stage. This can improve the quality and reproducibility of phospho-proteomics as nucleic acid molecules can interfere with the phospho-enrichment process (Potel et al., 2018). The assumption is that in 5.3 M urea proteins will be extracted from the chromatin and will not be lost. However, it is known that non-phosphorylated BANF1 can bind DNA with extremely high picomolar affinity (Skoko et al., 2009). This raises the possibility that BANF1 is pelleted out of the samples together with the chromatin when bound, at its tightest, to DNA. To test this HeLa cells were synchronised as shown in Figure 2.1A and samples collected at 0 min and 30 min following CDK inhibition. These samples were not clarified prior to digestion and were labelled ‘light’ and ‘heavy’, respectively. The samples were mixed in a 1:1 ratio and subjected to LC-MS analysis (Methods 4.6). CCNB1 could not be detected 30 min after CDK inhibition (Figure 2.5B, pink dot) whereas BANF1 was detected with equal intensity in both 0 and 30 min samples (Figure 2.5B, green dot). Individual peptides of BANF1 were also present with equal intensity in both samples (Figure 2.5C, green dots). The t_0/t_{30} ratio reflected the improved recovery of BANF1, increasing from 0.41 after clarification to 0.94 when samples were not clarified (Figure 2.5A and B). Together these observations confirmed that BANF1 was not degraded, but instead was removed from the sample through the

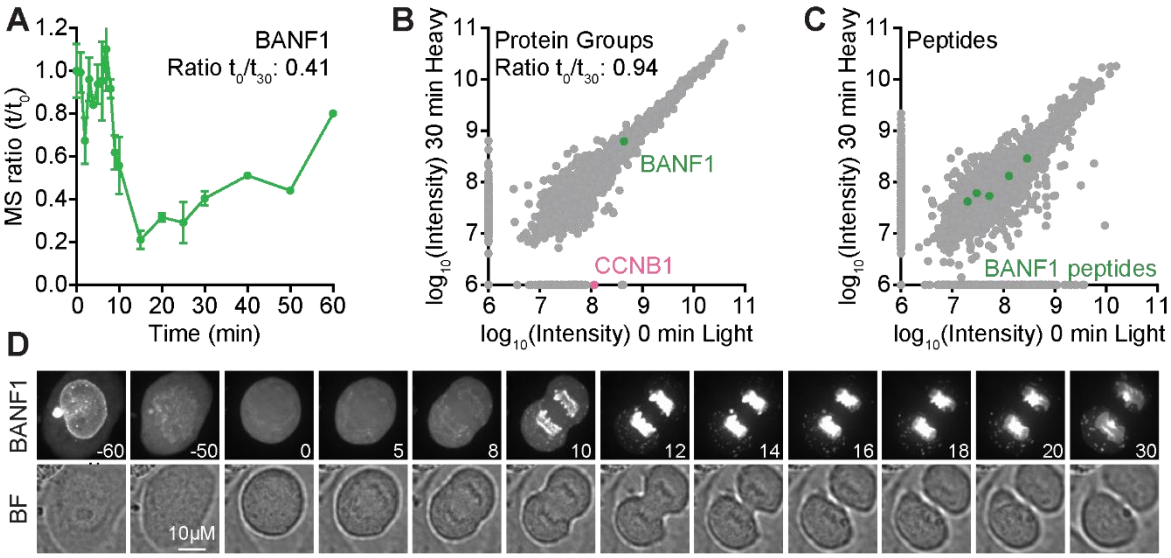


Figure 2.5 Proteins that are tightly bound to DNA can remain associated with chromatin in 5.3 M urea extracts

(A) The MS total protein ratio of BANF1 from data in Figure 2.4 (Mean±SEM, n=2). Cells were synchronised as in Figure 2.1 and harvested at 0 and 30 minutes after CDK inhibition. The lysates were left non-clarified and subsequently labelled 'light' and 'heavy', respectively. Log10 intensity plots of (B) protein group or (C) peptide MS data. (D) Live cell imaging of HeLa cells transfected with GFP-BANF1. Times shown are in minutes.

clarification. Furthermore, this demonstrates the importance of rigorous experimental design to ensure that results are representative, accurate and unbiased.

2.1.2.2 Identifying optimal digestion conditions for both the phospho- and total- proteomes

In light of the finding that some proteins could not be fully extracted by the standard protocol, a series of different conditions were tested to find the lysis and digestion protocol which gave best coverage of the proteome (Methods 4.6.4). Two conditions followed the standard urea lysis and digestion protocol used in Figure 2.4, one with and one without clarification (Figure 2.6A). The other conditions followed a simultaneous lysis, reduction and alkylation protocol (Figure

2.6A) (Methods 4.6.4) (Kulak et al., 2014). Here cells were lysed in either 8 M Urea, 1% sodium-deoxycholate (SDC) or 6 M guanidinium chloride (GdmCl), all supplemented with TCEP and chloroacetamide (CAA) for reduction and alkylation, respectively. TCEP and CAA were substituted in for dithiothreitol (DTT) and iodoacetamide (IAA), as the latter can cross-react. This allowed reduction and alkylation to be carried out simultaneously. For each condition, equal numbers of mitotically arrested cells were lysed and 100 µg digested. During the finished protocol samples were required to bind efficiently to C18 columns for di-methyl labelling. To ensure these steps were unaffected by changes in protocol, all conditions were bound to a C18 column, washed and eluted after digestion. Following this, 2 µg of each digest were run on a 120 min gradient (Methods 4.6.3).

The number of protein groups identified was similar in all samples, except for simultaneous digest with urea which showed a dramatically reduced number of identifications (Figure 2.6B). One issue with heating in urea at 95°C is that peptides become carbamylated, thus reducing the number of unmodified peptides. A subsequent search allowing for this as a modification provided some recovery of identifications, increasing from 1404 to 1934 protein groups but not to the same level as the other methods tested. Owing to the presence of non-specific modification this particular condition was discounted from further consideration. However, both GdmCl and SDC simultaneous digests identified more peptides and peptide-spectrum matches (PSM), which would result in better quality protein group identifications. Furthermore, all these digestion conditions had similar representation of cytoplasmic, membrane and nuclear proteins (Figure 2.6C) (Methods 4.7.4).

Since SDC simultaneous lysis produced the best identifications, this was chosen as the optimal condition to compare phospho-enrichment results against the original urea lysis protocol. Consistent with the previous digest test, SDC identified more protein groups than the original urea protocol (Figure 2.6E). However, when comparing phospho-enriched samples, the urea protocol identified ~30% more phospho-peptides than the SDC protocol (Figure 2.6D). Moreover, these phospho-peptides were often of greater intensity, as seen from the distribution of points away from the diagonal towards the x-axis (Figure 2.6D). The negative charge of a phosphate group can impair the ability of trypsin and Lys-C to cleave proteins, and it was possible this effect was enhanced in SDC. However, using a higher concentration of these enzymes did not improve recovery of phospho-peptides in the SDC condition (Figure 2.6F-G). The differences between the urea and SDC samples could in principle be explained by variability in enrichment efficiency as they were processed separately. Therefore, it was decided to differentially label the two conditions, 'heavy' and 'light', mixed in an equal ratio and then phospho-enrich together. The SDC was supplemented with sodium-N-lauroyl sarcosinate (SLS) (Methods 4.6.4) to closely replicate a phase transfer surfactant (PTS) buffer which had been used for high quality proteomics (Masuda et al., 2009). The urea sample was prepared as before, without clarification to obtain optimal results, and labelled 'light'. The PTS sample was labelled 'heavy'. As expected, both conditions identified similar numbers of proteins (Figure 2.6I), with considerable overlap. Nevertheless, the standard urea lysis again identified ~30% more phospho-peptides (Figure 2.6H). This result is especially surprising since SDC is routinely used in digests for phospho-proteomic analysis, although the comparison shown here does not support this choice.

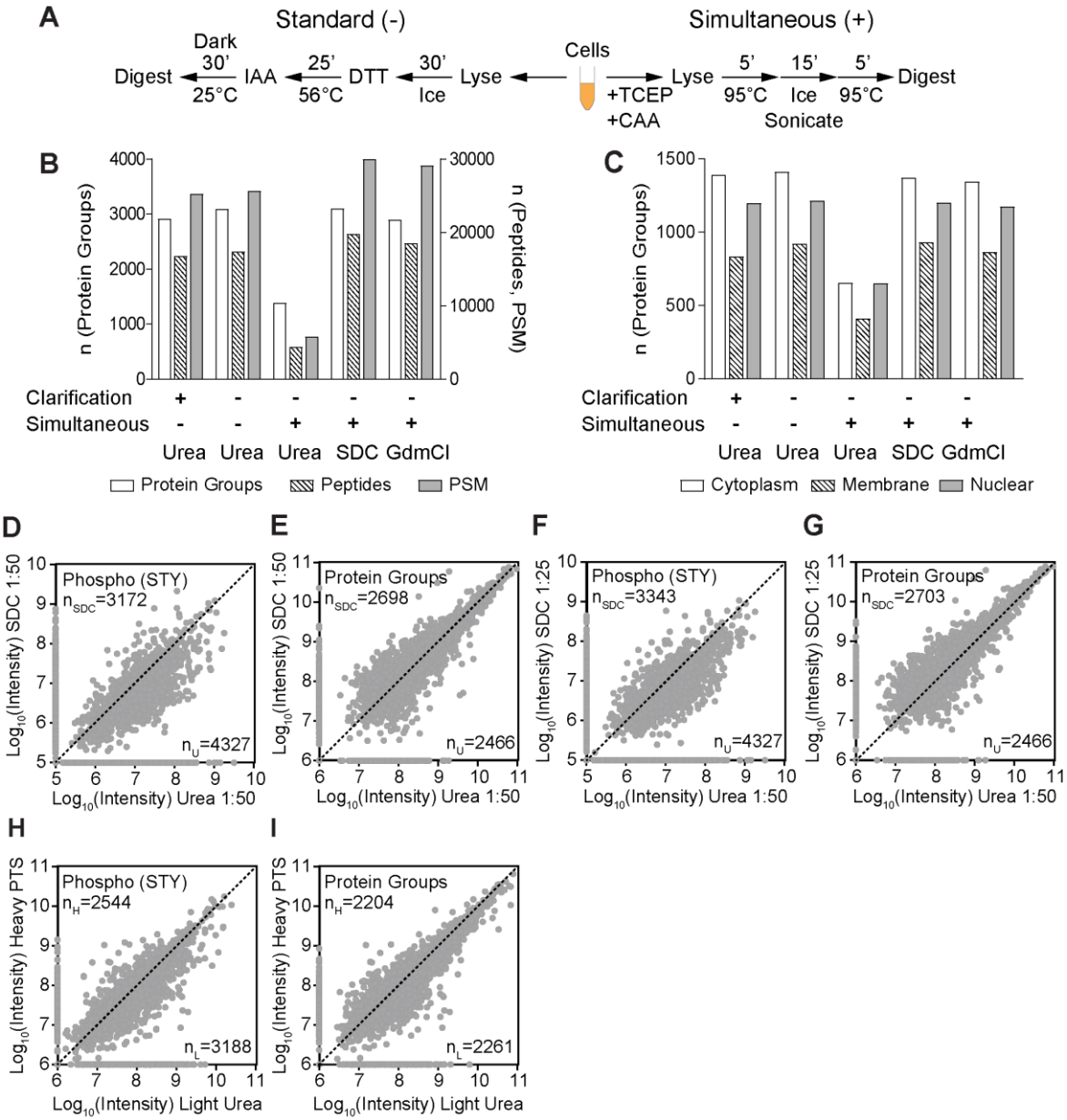


Figure 2.6 Urea lysis without clarification provides optimal recovery of both phosphorylated and non-phosphorylated peptides

(A) Schematic detailing the standard and simultaneous digestion protocols. (B) Number of identified protein groups, peptides and PSMs. Simplified sample preparation conditions are shown beneath the graph: clarification, digest type and lysis method. (C) Numbers of protein groups associated with GO Cellular Compartment-slim terms: cytoplasmic, membrane and nuclear. (D-G) Log10(Intensities) of phospho-peptides and protein groups from samples lysed under two different conditions. 1:50 and 1:25 denote the ratio of proteolytic enzyme to starting material. (F-G) Log10(Intensities) comparing 'light' and 'heavy' labelled phospho-peptides and protein groups. Samples lysed with urea were labelled 'light' and PTS lysed samples labelled 'heavy'. Dotted line denotes equal intensity

in the two samples. n represents the number of identifications in each condition. CAA (chloroacetamide), DTT (dithiothreitol), GdmCl (guanidinium chloride), IAA (iodoacetamide), PSM (peptide spectral match), PTS (phase-transfer surfactant): mixture of sodium deoxycholate and sodium N-lauroyl sarcosinate, SDC (sodium deoxycholate), TCEP (Tris(2-carboxyethyl)phosphine).

One important difference between the procedures, was the necessity to remove the SDC or SLS prior to C18 binding and phospho-enrichment. This involved rounds of vigorous shaking with ethyl acetate, centrifugation and removal of the organic layer which now contained the detergent. This could potentially have led to non-specific sample loss, and as phospho-peptides are generally of low abundance could have resulted in the reduced identifications observed. Nevertheless, the protocol that yielded the best results for both the total and phospho-proteomes was the standard urea lysis without clarification. This protocol was therefore used for all subsequent quantitative mass spectrometry experiments.

2.1.3 Optimised proteomic analysis of mitotic exit

Following the optimisation described above, a further two repeats of the control condition timecourse were performed and analysed by mass spectrometry. All four repeats were then searched and analysed together in MaxQuant and Perseus (Methods 4.7.1). For this analysis, at least two ratio values across the four repeats were required for any given protein/phospho-peptide and timepoint. One final constraint to aid clustering was that 15/18 values for the total, or 7/18 for the phospho-proteome, had to be present across the timecourse after averaging. Anything not reaching this minimum was discarded from further analysis. This was based on the reference profiles of CCNB1 and PRC1-pT481 (Figure 2.7E and G). The levels of PRC1 remained stable throughout the experiment (Figure 2.7F). This

resulted in 2165 proteins and 4,632 phospho-sites being clustered, from the 4813 and 18,675 identified, respectively. As seen in Figure 2.4A, the majority of the total proteome was stable and in fact the only protein seen to be degraded rapidly was CCNB1 (Figure 2.7A and E). A small number of proteins were degraded more slowly from late anaphase and telophase. This is typified by PLK1 where approximately 60% of the protein remained at 60 min following CDK inhibition (Figure 2.8A, red). The only proteins to show an intermediate rate of proteolysis were Aurora A and its coactivator TPX2 (Figure 2.8A, green). These proteins are found together in a complex and function together at the mitotic spindle (Bayliss et al., 2003; Kufer et al., 2002), so the observation that they were degraded together in anaphase is consistent with this. Contrary to the literature, it can clearly be seen that PLK1 was degraded after Aurora A (Figure 2.8A). This could be caused by premature activation of APC/C^{CDH1} through the chemical inhibition of CDK1. Since Aurora A degradation is entirely dependent on APC/C^{CDH1} (Floyd et al., 2008) this could preferentially alter the kinetics of Aurora A destruction. Therefore, total proteome MS data, previously generated by the lab, using MPS1 inhibition to trigger mitotic exit rather than CDK inhibition (Hayward et al., 2018) was inspected for the levels of Aurora A and PLK1. Inhibition of MPS1 triggers a more physiological mitotic exit due to a gradual decline in CDK1 activity rather than rapid inhibition. Under these conditions, Aurora A was still degraded prior to PLK1 (Figure 2.8B). This finding is consistent with PLK1 inhibition not stabilising Aurora A as effectively as PLK1 depletion (van Leuken et al., 2009). If the presence and not just the prior activity of PLK1 is required for Aurora A degradation, then it is logical that PLK1 degradation would occur later.

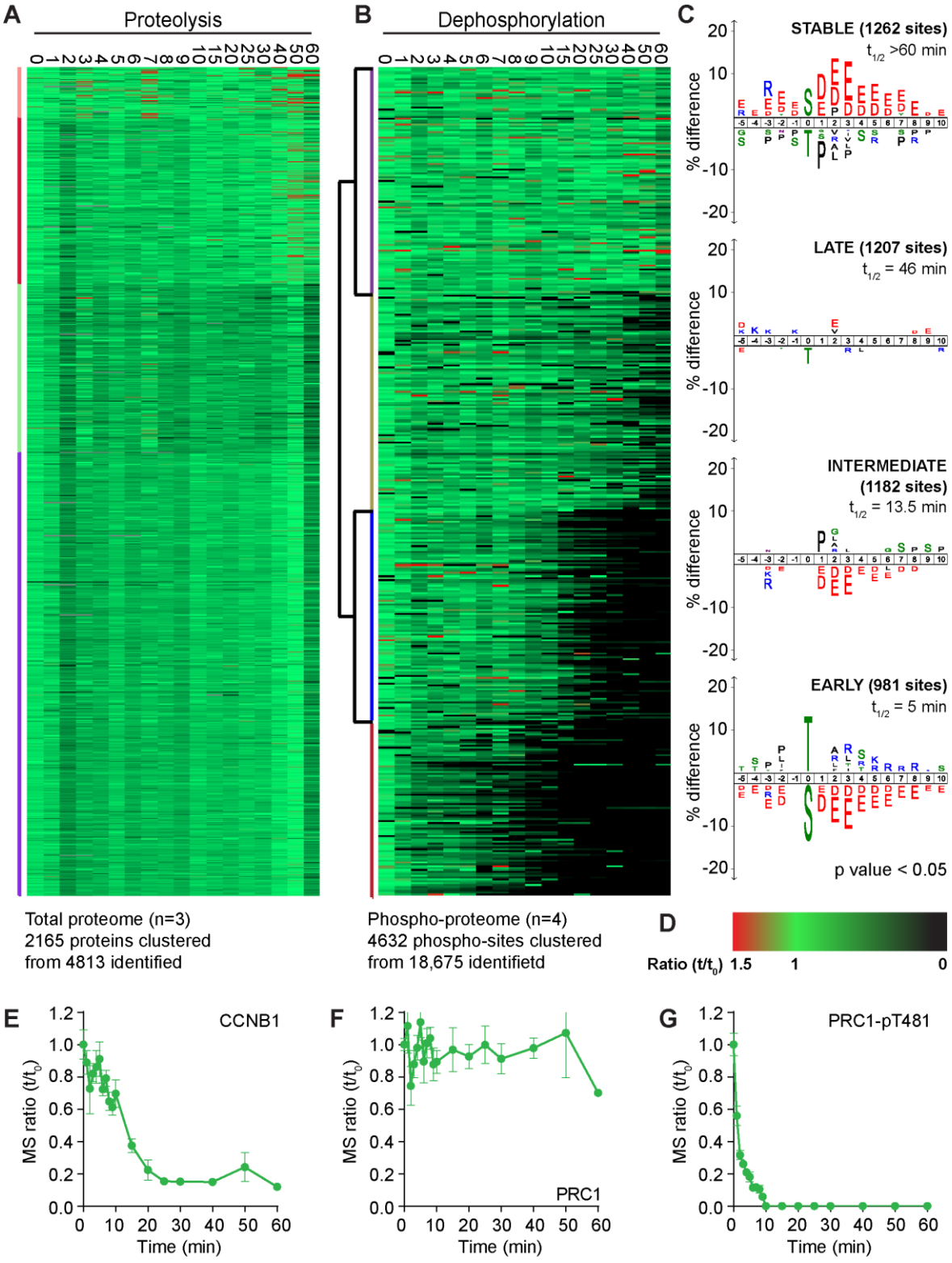


Figure 2.7 Ordered proteolysis cannot account for the events of mitotic exit

HeLa cells were arrested in mitosis and mitotic exit triggered as previously described. Heatmap of (A) protein groups or (B) phospho-sites clustered based on trends over time. Time is shown in minutes. (C) Sequence logo analysis showing the relative enrichment of residues in the adjacent cluster from (B). The number of phospho-sites and average half-

life for each cluster is indicated. (D) Key linking heatmap colour with observed ratio. Quantitative ratio of (E-F) protein level or (G) phosphorylation for CCNB1, PRC1 and PRC1-pT481 (Mean±SEM).

The MPS1 and CDK inhibition timecourse analyses were carried out in DMEM and Opti-MEM medium, respectively, and as such the timings between the experiments were not directly comparable. Nevertheless, the same clustering analysis was carried out on these data. Here, CCNB1 degradation followed more typical delayed sigmoidal kinetics during mitotic exit (Figure 2.9E). For further analysis, a filtering threshold of 12 timepoints was set for the total proteome. Because there were only two repeats it was necessary to accept more missing values than the CDK-inhibition experiments, and the final averaged data were also somewhat noisier. However, it was still clear that the proteome as a whole was stable (Figure 2.9A). This means that under conditions of either normal (MPS1i) or collapsed mitotic exit (CDKi) the detectable fraction of the proteome was stable for the window observed. This is logical given that only degradation kinetics should change between the two conditions, rather than the entire substrate specificity of the APC/C.

Under physiological conditions, chromosome separation, central spindle formation, initiation of cytokinesis, nuclear membrane reassembly and nuclear import all begin within 15 min of anaphase onset. By 60 min after anaphase onset, cells will have left anaphase and be co-ordinating abscission of the midbody. These data raise questions about the impact proteolysis could have on the order of events in anaphase. In fact, the data would suggest that the degradation of proteins like Aurora A, TPX2 or PLK1 will only be relevant for late events such as

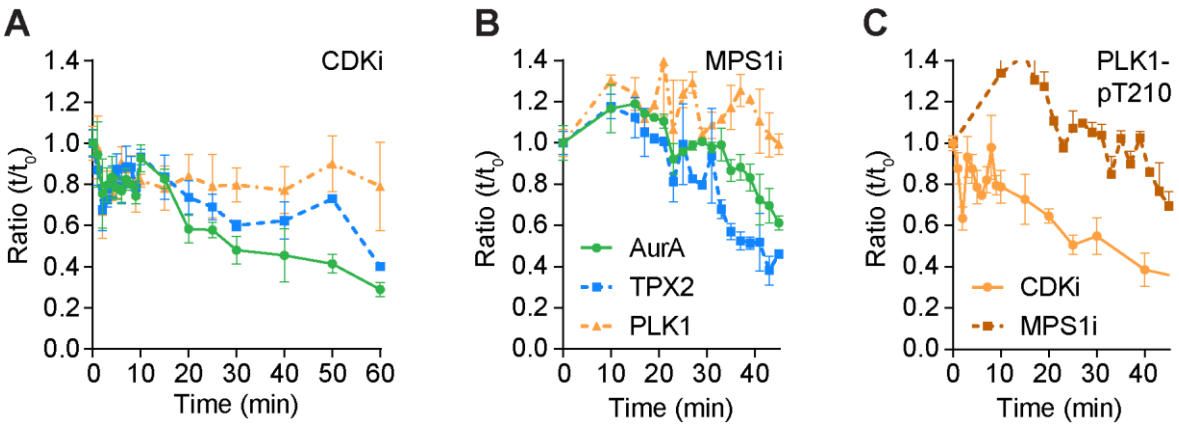


Figure 2.8 Aurora A is degraded prior to PLK1 during mitotic exit

Quantitative ratios of AurA, TPX2 and PLK1 protein levels, detected by mass spectrometry, over time following (A) CDK inhibition (CDKi) or (B) MPS1 inhibition (MPS1i). (C) PLK1-pT210 phosphorylation during mitotic exit, after either CDK or MPS1 inhibition.

abscission. Only the degradation of CCNB1 and securin were rapid enough to impact the events of anaphase. In unperturbed cells, this degradation is carried out prior to the events of anaphase.

Following CDK inhibition, nearly 5000 proteins were identified with over 2000 being reliably quantified across the whole timecourse. However, the two further repeats only provided small improvements in the total number of identifications and quantifications over the pilot analysis. This suggests that the current mass spectrometry protocol and set up is nearing the limit of its dynamic range and sequencing speed. Without entirely changing the protocol, further improvements would require fractionation, to reduce sample complexity, as has been demonstrated by many labs previously (Kulak et al., 2014). In fact, the single fractionation step, used by Cundell et al., to split each lysate into two fractions increased phospho-site identifications by ~30%. However, with the large number

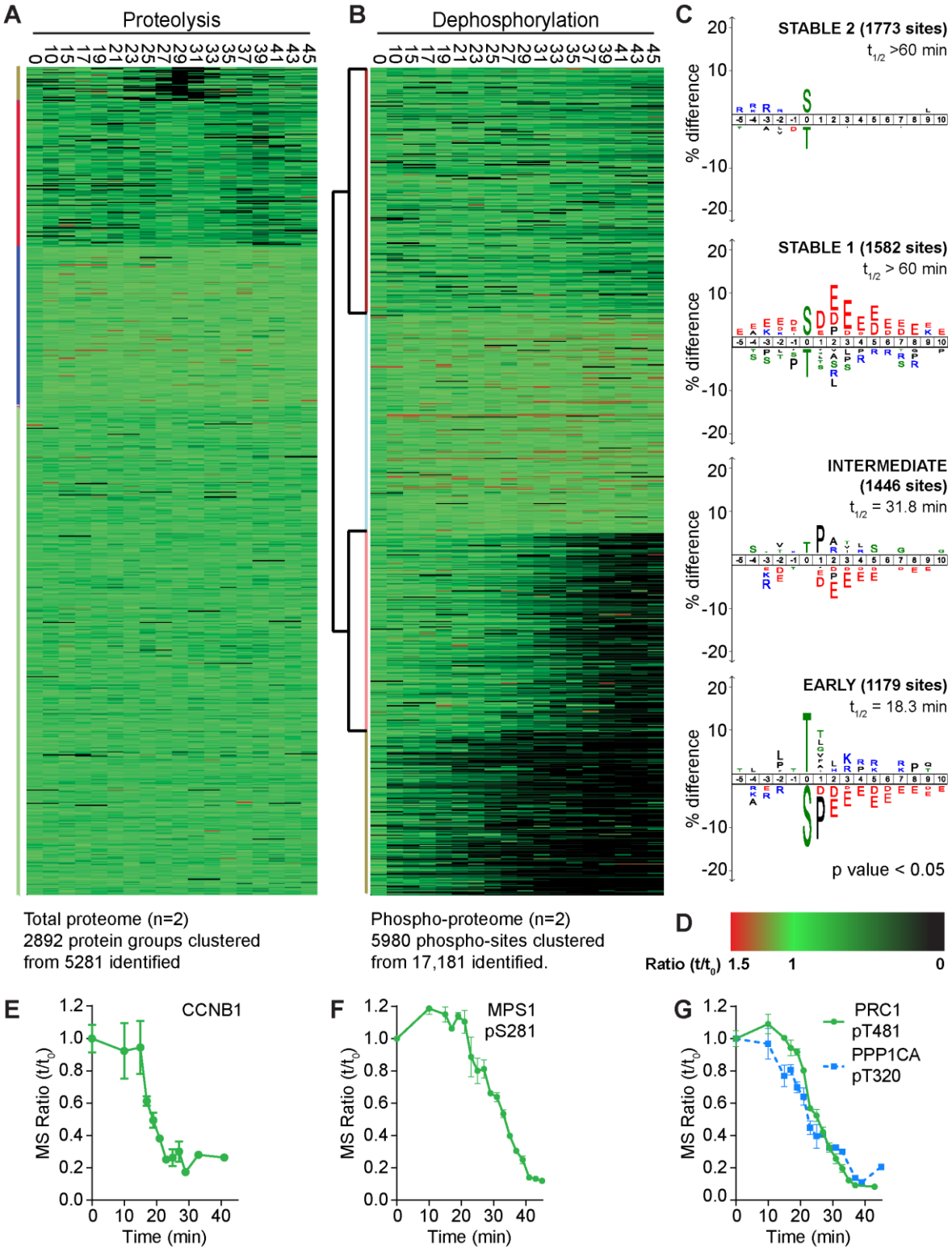


Figure 2.9 Using MPS1 inhibition to drive mitotic exit does not alter the relative contributions of dephosphorylation and proteolysis

HeLa cells were arrested in mitosis and mitotic exit triggered by MPS1 inhibition. Heatmap of (A) protein groups or (B) phospho-sites clustered based on trends over time. Time is shown in minutes. (C) Sequence logo analysis showing the relative enrichment of

residues in the adjacent cluster from (B). The number of phospho-sites and average half-life of each cluster is indicated. (D) Key linking heatmap colour with observed ratio. Quantitative ratio of (E) protein level or (F-G) phosphorylation for CCNB1, MPS1-pS281, PPP1CA-pT320, PRC1-pT481 (Mean±SEM, n=2). Mass spectrometry data obtained from Hayward et al., 2018 was reanalysed as detailed in Methods 4.7.1.

of samples involved fractionation would be costly in both time and mass spectrometry resources. Additionally, fractionation would have to take place downstream of labelling to minimise variation in labelling efficiency. As such, the total proteome samples, taken every 10 min, from the two optimised repeats were fractionated at high pH using stage tips. This entailed binding 25 µg of mixed, 'light':'heavy' labelled samples to C18 discs, which were eluted into seven fractions using a gradient of acetonitrile (Methods 4.6.5). It was necessary for fractionation to be carried out at high pH as the online liquid chromatography system attached to the mass spectrometer runs at low pH conditions. The current depth of the phospho-proteomic data was satisfactory, so these samples were not subjected to any fractionation.

Following fractionation of two timecourses, over 5600 proteins were identified, with 3749 being reliably quantitated. The profile of CCNB1 was consistent with previous data (Figure 2.10C). The clustering analysis still showed that the majority of the proteome was stable (Figure 2.10A). Furthermore, this greater sensitivity enabled the detection of lower abundance proteins such as CDC20 (Figure 2.9D), a coactivator of the APC/C. CDC20 is degraded upon entry into anaphase by newly active APC/C^{CDH1} complexes. This changes the substrate specificity of the APC/C allowing degradation of many proteins including Aurora A and B. However, here it can be seen that ~40% CDC20 was still present one hour

after CDK inhibition. This would suggest that the switch from CDC20- to CDH1-dependent degradation may not be as clear as was once thought. This improved sensitivity was not however reflected in the detection of securin, whose quantification is limited by the presence of suitable peptides following tryptic digest (Figure 2.3B).

This fractionated proteome identifies ~55% of the human mitotic proteome with close to 40% being quantitated. While it would be easy to focus on the raw number of proteins identified it may be more constructive to look at the proteins already reported to be degraded. One review listed 55 human proteins as substrates of the APC/C (Meyer and Rape, 2011), of which 34 were identified here (Figure 2.10F). Furthermore, in 2002, Whitfield et al. published a landmark paper outlining the list of human genes subject to cell cycle-dependent expression (Whitfield et al., 2002) . Of the ~210 genes under G2/M or M/G1 expression patterns, 120 are identified in the fractionated data set (Figure 2.10F). To ensure unbiased classification of whether a protein was degraded during the experimental window, a threshold value was set. This value was set at a maximum half-life of 2 hr or <75% of the protein remaining 60 min after CDK inhibition. This threshold does potentially allow proteins to be classified as being degraded whose proteolysis would occur beyond the window of an unperturbed anaphase, into telophase or the subsequent G1. Of the 25 reliably quantitated APC/C substrates (Figure 2.10F, triangles) only 9 were classified as being degraded during this experimental window (Figure 2.10G, green and yellow triangles). This 25 excluded securin but also CCNA2 and NEK2A which were degraded during nocodazole arrest prior to the start of this experiment. Of the mitotically transcribed genes, 90 additional proteins were quantified over time but only one, TACC3 (Figure 2.10G,

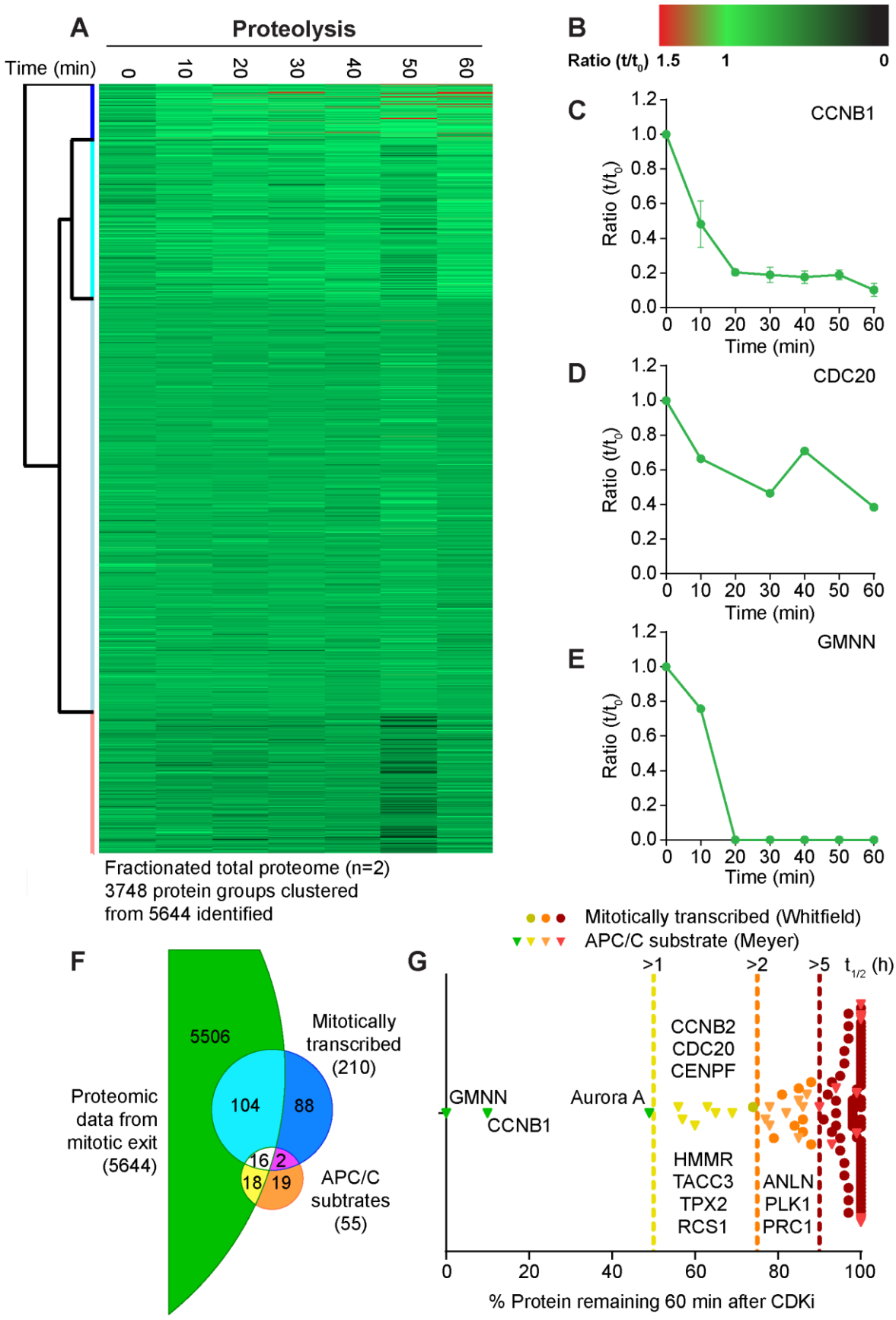


Figure 2.10 Fractionation enables quantification of lower abundance proteins

Figure 2.10 Fractionation enables quantification of lower abundance proteins (continued from previous page)

(A) Heatmap of clustered protein groups generated from fractionated total proteome samples. (B) Key linking heatmap colour with observed ratio. (C-E) Quantitative ratio of the protein levels of CCNB1, CDC20 and Geminin (GMNN). (F) Comparison of mitotically expressed genes and validated APC/C substrates with proteins identified by mass spectrometry. The reference lists were obtained from Whitfield et al., 2002 and Meyer et al., 2011, respectively. Numbers indicate how many protein identifications are in each region. (G) Proteins identified by mass spectrometry plotted according to the percentage of protein remaining 60 min after CDK inhibition. Vertical lines indicate various half-lives of degrading proteins. Proteins found in both the Whitfield and Meyer papers were classified as APC/C substrates.

gold circle), was seen to meet the degradation criterion, making a total of ten proteins being degraded during anaphase (Figure 2.10G, left of orange line). With the exception of geminin, these degraded proteins fall into two categories. The first group consists of SAC and kinetochore proteins: CCNB1/2, CDC20, CENPF (Glotzer et al., 1991; Gurden et al., 2010; Pfleger and Kirschner, 2000). The second includes mitotic spindle factors: Aurora A; Hyaluronan mediated motility receptor (HMMR); transforming acidic coiled-coil-containing protein 3 (TACC3); TPX2 and regulator of chromosome segregation protein 1 (RCS1) (Jeng et al., 2009; Lindon and Pines, 2004; Song and Rape, 2010; Stewart and Fang, 2005a; Zhao et al., 2008a). If the threshold was relaxed to allow half-lives of up to 5 hr, an additional 16 proteins would qualify as being degraded including PLK1, PRC1 and ANLN (Figure 2.10G, orange circles and triangles) (Juang et al., 1997; Neef et al., 2007; Zhao and Fang, 2005). However, this relaxed threshold allowed proteins which would be degraded in G1 to be included, while still excluding 89 proteins. A more stringent threshold, a half-life of 1 hr, would more realistically identify

proteins whose degradation could impact the timing of anaphase. When analysing both reference lists, only three proteins meet this criterion; Aurora A, CCNB1 and geminin (GMNN), and only the latter two are rapid enough to affect the events of early anaphase (Figure 2.10G, green triangles). Geminin, a DNA replication licensing factor, could not be observed prior to fractionation. The MS data shown here are consistent with the proposal that geminin is destroyed rapidly during mitotic exit (Figure 2.10E) (McGarry and Kirschner, 1998).

Since the Meyer review, other proteins such as FBXO31 (Choppara et al., 2018), have been reported to be APC/C substrates. Based on the analysis here it could be inferred that there are between 20-30 anaphase substrates of the APC/C. It has, however, been theorised that APC/C targets number into the hundreds (Meyer and Rape, 2011); it would seem likely that the majority of these are degraded in G1. This may help reset the cell status prior to entry into the next cycle. Furthermore, in the 55% of the proteome observed there were only three rapidly degraded proteins; CCNB1, securin and geminin. One would expect there to be a similar number in the remaining half of the proteome. These observations suggest that these mass spectrometric and clustering analyses provide a representative view of the proteome during mitotic exit. This additional background literature supports the conclusion that only a small portion of the mitotic proteome was subject to degradation and very few of these proteolytic events could impact the order of events in anaphase.

By contrast, when similarly analysed, dephosphorylations were clustered neatly into four groups; early, intermediate, late and stable (Figure 2.7B). The additional experimental repeats improved the clustering analysis on two fronts. Firstly, the noise cluster present in the initial analysis was no longer present, due

to more reliable quantification. Secondly, it became possible for the clustering analysis to distinguish between intermediate and late dephosphorylations which had previously been grouped together. These improvements made the trend in phospho-site sequence characteristics clearer. Early dephosphorylations, with an average half-life of 5 min, were strongly enriched for phospho-threonine over phospho-serine (Figure 2.7C, Early). Additionally, it was possible to observe a mild enrichment of basic residues and a strong de-enrichment of acidic residues close to the phospho-site (Figure 2.7C, Early). Intermediate dephosphorylations, with a typical half-life of 13.5 min, were also de-enriched of acidic residues, albeit to a lesser extent than the early cluster (Figure 2.7C, Intermediate). Late dephosphorylations with an average half-life of 46 min showed little dominant positive or negative selections, save for a mild selection against phospho-threonine (Figure 2.7C, Late). The stable phosphorylations, with a half-life greater than 60 min, had a very strong enrichment of acidic residues surrounding the phospho-site and some enrichment for phospho-serine (Figure 2.7C, stable). Phospho-threonine and basic residues were modestly selected against within this population. This analysis showed a gradual and continuous trend whereby the more acidic a phosphorylation site, the slower its dephosphorylation. Additionally, all else being equal, a phospho-threonine is more likely to be dephosphorylated rapidly than a phospho-serine. The additional methyl group of threonine could fulfil a steric requirement imposed by the catalytic site of the phosphatases. The T-loop phosphorylation of PLK1, PLK1-pT210, provided an interesting example of dephosphorylation and proteolysis regulating the same protein (Figure 2.8C), although at an individual substrate level the relative contributions of these two activities is unclear. However, such occurrences were rare in the dataset.

The substrate specificity of PP2A-B55, which preferentially dephosphorylated pT-P CDK sites flanked by a basic patch on either side, has been seen to determine the order of events during mitotic exit (Cundell et al., 2016). The results described here suggest that this is not a unique property of PP2A-B55 holoenzymes but of general phosphatase activity during mitotic exit. The dominant phosphatases during this period are proposed to be PP2A-B55 and PP1 (Wurzenberger and Gerlich, 2011). The catalytic subunits of PP1 and PP2A are highly conserved around the active site region, with little difference in substrate specificity without additional subunits (Agostinis et al., 1992; Barr et al., 2011; Imaoka et al., 1983; Mumby et al., 1987). It therefore follows that they would exhibit similar substrate preferences. The selection against acidic residues could in part be explained by a conserved acidic groove close to the active site. However, regulatory subunits also impact holoenzyme specificity. For instance, mutation of acidic residues on the surface of B55 can severely impair the activity of PP2A-B55 holoenzymes towards its substrates.

In contrast to Cundell et al., it was observed that the presence or absence of acidic residues appeared to be more strongly selected for than basic residues. One potential explanation for this outcome is that our analysis was likely to be biased against highly basic peptides since both Lys-C and trypsin cleave these residues. This means very basic regions were likely to be digested into peptides too small for detection by mass spectrometry, as exemplified by securin (Figure 2.3). Consequently, very basic phospho-sites were likely to be ‘under sampled’ resulting in their apparent importance being reduced. Additionally, the mitotic extract system utilised previously did not fully recapitulate PP1 activity. PP1 forms heterodimers which are highly variable in composition, containing one of three

catalytic subunits bound to one of over 100 proposed regulatory subunits (Bollen et al., 2010). This therefore means that the dephosphorylations observed here were carried out by a much broader pool of holoenzymes with varied specificities, reducing the contribution of PP2A-B55, and its preference for basicity, to the sequence analysis.

Since CDK inhibition was used to trigger anaphase it was logical that proline would be de-enriched at the +1 position, indicative of a CDK1 site (S/T-P), in the stable cluster. Interestingly, there was no proline enrichment at the +1 position in the early cluster and only small enrichment in the intermediate cluster. This would indicate that the nature of kinase responsible for a phosphorylation does not impact on its rate of dephosphorylation but rather that the sequence characteristics and their suitability for nucleophilic attack are more critical determinants of rate.

As with the total proteome, the same analysis was also conducted on the published phospho-proteomic data generated by MPS inhibition (Hayward et al., 2018). The clustering analysis produced the same trends in sequence characteristics (Figure 2.9B and C). Only two clusters of dephosphorylation could be observed in this analysis (Figure 2.9B and C, Intermediate and Early). Since MPS1 inhibition causes a gradual decline in CDK1 activity, via CCNB degradation, many dephosphorylations will be slower under these conditions. This could be seen in the dephosphorylation profiles of the CDK1 sites: MPS1-S281, PPP1CA-T320 and PRC1-T481, with a delay prior to dephosphorylation of these sites (Figure 2.9F and G). In fact, this was reflected in the sequence logo, with the early cluster of phospho-sites selecting against the proline at +1, whereas the intermediate cluster showed an enrichment of proline at +1, as CCNB1 had now

been degraded sufficiently to trigger loss of CDK1 activity and the subsequent dephosphorylation of its substrates. Two stable clusters of phospho-sites could be observed, one of which displayed the sequence traits expected (Figure 2.9C, Stable 1). The second stable cluster contained noisier data, as seen by randomly scattered black marks, representative of missing values (Figure 2.9C, Stable 2). This led to a logo without any apparent preferences. There was a small preference for phospho-serine which was indicative of these noisier sites being slower or more stable dephosphorylations. Further repeats of this timecourse would improve this analysis, as demonstrated by the CDK inhibition experiments (Figure 2.4B and 2.7B). Additionally, it was observed that dephosphorylation of PPP1CA-T320 began prior to PRC1-T481, indicative of PP1 activity accumulating prior to that of PP2A-B55 under MPS1 and spindle checkpoint-regulated mitotic exit. This is consistent with the requirement for PP1 to help inactivate MASTL kinase, promoting PP2A-B55 activity, during mitotic exit (Figure 2.9G).

These results suggest that the order of events in anaphase is determined by a graded series of dephosphorylations, the rate of which is pre-encoded into the system at the level of each individual phospho-site, based on the phospho-residue and the electrostatic characteristics of the surrounding amino acids. Furthermore, the majority of these dephosphorylations take place in the first 30 min following CDK inhibition. Conversely, only three proteins are seen to be sufficiently degraded in this window to effect anaphase events: CCNB1, securin and geminin. This would suggest that while APC/C dependent proteolysis plays a critical role in triggering anaphase onset, through degradation of CCNB1 and securin, it plays a limited role until much later in telophase and early G1. Moreover, it is known that cells can survive without securin, as CCNB can inhibit separase both directly and

through CDK1 activity (Huang et al., 2005; Stemmann et al., 2006; Gorr et al., 2005). Therefore, it can be proposed that the only APC/C-dependent proteolysis necessary for a normal anaphase is the degradation of CCNB1 (Rattani et al., 2014).

2.2 The role and regulation of proteolysis during mitotic exit

2.2.1 Degradation of CCNB is the minimal requirement for proteolysis during mitotic exit

To test the minimal requirement for APC/C-dependent proteolysis during mitotic exit it is necessary to selectively inhibit the APC/C. Owing to the presence of many ubiquitin ligases within the cell, direct inhibition of the proteasome, typically using MG132, is not specific enough to answer this question. The APC/C inhibitors, APC inhibitor (apcin) and pro-tosyl-L-arginine methyl ester (pro-TAME) have been shown to function synergistically, providing optimal results when used together (Sackton et al., 2014). Apcin binds to CDC20, acting as a competitive inhibitor to prevent ubiquitination of D-box containing substrates (Sackton et al., 2014), while pro-TAME prevents the interaction between the APC/C and its coactivators CDC20 and CDH1 (Figure 2.11A) (Zeng and King, 2012; Zeng et al., 2010b). Apcin can also prevent CDH1 interacting with substrates, albeit less efficiently than it interferes with CDC20 (Sackton et al., 2014). Due to the high number and concentration of cells used for these experiments it was necessary to titrate these inhibitors to find an optimal working concentration.

To do this, cells were arrested in mitosis, released and CDK inhibited as described (Method 4.4.1), with various concentrations of APC/C inhibitors or DMSO being added during the 25 min nocodazole wash out. The stability of CCNB1 and securin was then observed as a measure of APC/C inhibition (Figure 2.11). During the initial titration, the concentration found to be optimal in previous studies, 6 µM pro-TAME + 25 µM apcin (Sackton et al., 2014), did not provide sufficient stabilisation (Figure 2.11B, D and F, line 2). Increasing the concentration

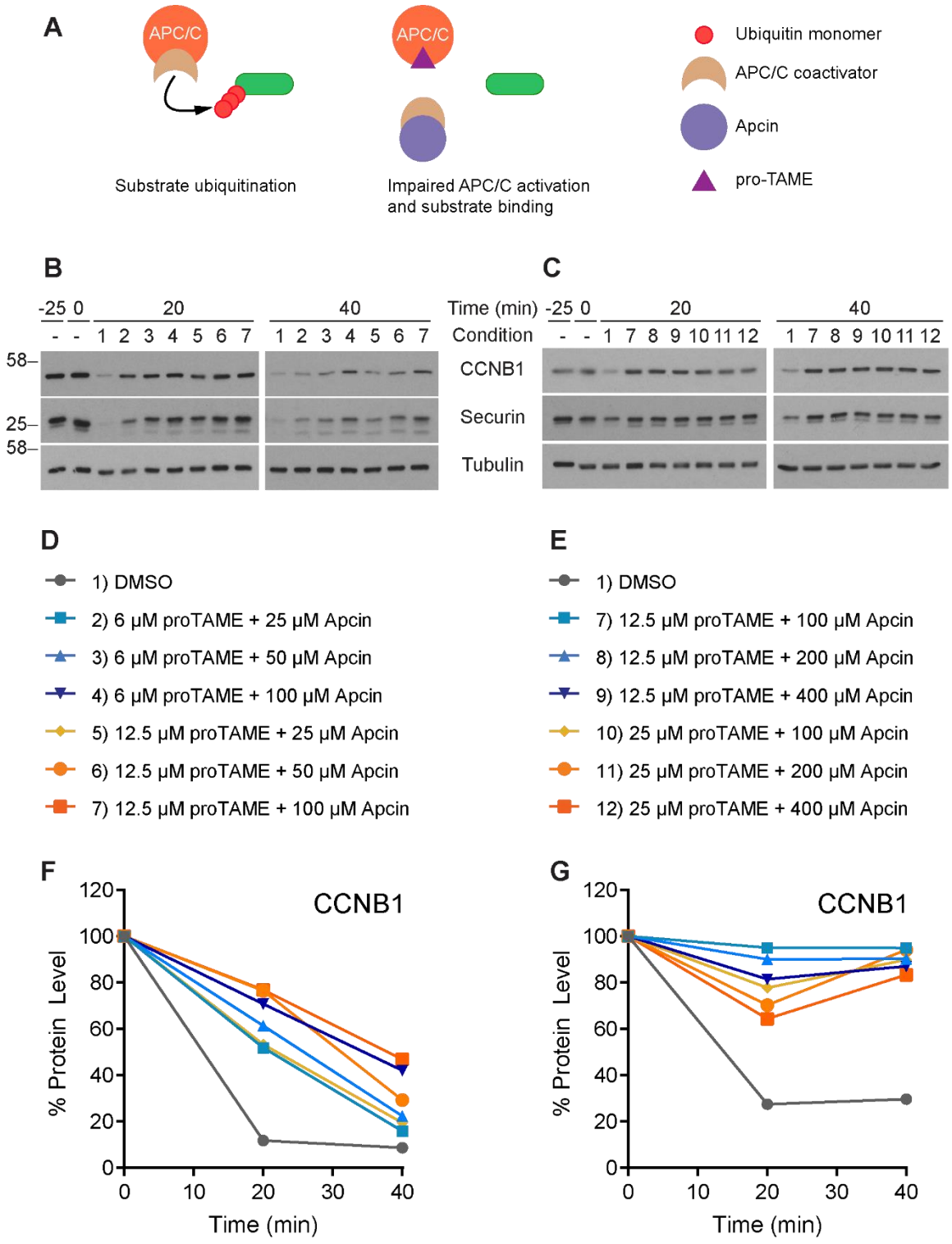


Figure 2.11 Chemical inhibition of the APC/C can stabilise CCNB1 during mitotic exit

HeLa cells were arrested in mitosis and CDK inhibited to trigger mitotic exit. (A) Schematic detailing the effects of apcin and pro-tosyl-L-arginine methyl ester (pro-TAME) on APC/C activity. (B-C) Titration of the APC/C inhibitors, apcin and pro-TAME, over a

range of concentrations. (D-E) Key relating the respective conditions from (A-B) to drug concentration used. (F-G) Densitometric quantification of CCNB1 levels in (B-C) following CDK inhibition.

of inhibitors up to 12.5 µM pro-TAME and 100 µM apcin did improve CCNB1 stabilisation but some degradation still occurred (Figure 2.11B, D and F, line 7). A second titration was carried out using this last concentration as a starting point (Figure 2.11C, E and G). Here all concentrations, including 12.5 µM pro-TAME and 100 µM apcin, showed near complete stabilisation of CCNB1 levels. However, the release into anaphase was not as efficient in this case, as shown by the rate of CCNB degradation in the DMSO control (Figure 2.11B-C and F-G, line 1). To be sure that effective inhibition was achieved, the highest concentration tested was taken forward for use in subsequent experiments. From now on APC/C inhibition refers to the use of 25 µM pro-TAME and 400 µM apcin.

An initial low-resolution timecourse was then carried out to see if dephosphorylation was at all possible under conditions of APC/C inhibition. Cells were prepared as before, with APC/C inhibitors added at the start of the 25 min nocodazole release. These conditions were DMSO control, APC/C inhibition, or APC/C and proteasome inhibition, the latter being supplemented with the proteasome inhibitor MG-132 at 40 µM. The functional consequences of these treatments are that under control conditions substrates can be targeted for proteolysis by APC/C dependent ubiquitination and subsequently destroyed by the proteasome (Figure 2.12A). When the APC/C is inhibited, APC/C substrates cannot be targeted to the proteasome but degradation can occur if mediated by

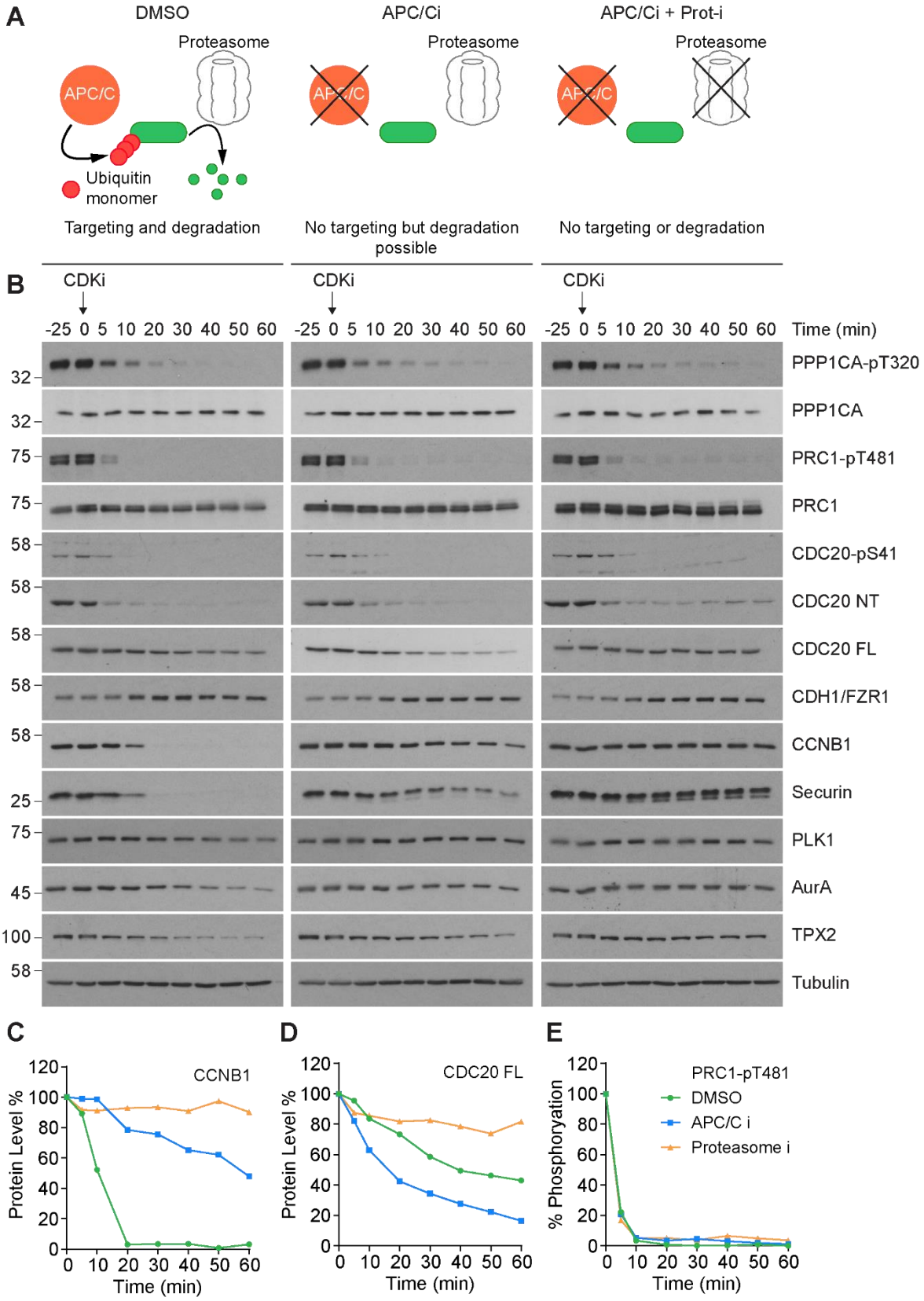


Figure 2.12 Dephosphorylation can occur during mitotic exit in the absence of APC/C or proteasome activity

Figure 2.12. Dephosphorylation can occur during mitotic exit in the absence of APC/C or proteasome activity (continued from previous page)

HeLa cells were arrested in mitosis as previously described. (A) Schematic detailing the APC/C and proteolytic activities in each condition. (B) Western blot showing the protein levels and phosphorylation state in mitotically arrested HeLa cells, following CDK inhibition, in the presence or absence of APC/C inhibitors (APC/Ci), 400 µM apcin and 25 µM pro-TAME, or APC/C and 40 µM MG-132 (Prot-i). Densitometric quantification of the levels of (C) CCNB1, (D) CDC20 and (E) PRC1-pT481.

other ubiquitin ligases. Finally, APC/C and proteasome inhibition means that no proteasome dependent proteolysis can occur, irrespective of targeting ligase. CCNB1 was completely degraded by 20 min in control conditions and was fully stabilised when both the APC/C and proteasome were inhibited (Figure 2.12B and C, green and orange lines). Complete stabilisation was not achieved through APC/C inhibition alone (Figure 2.12C, blue line). However, 80% of CCNB1 was stabilised during the first 20 min window in which CCNB1 is normally fully degraded. This was deemed a satisfactory level of inhibition given that using increasing amounts of drugs also increases the chance of unwanted, off-target effects. Similar trends are seen in the stability of securin, PLK1, Aurora A and TPX2. Consistent with earlier observations, PLK1 was degraded after Aurora A in the control conditions (Figure 2.12B). Furthermore, Aurora A, whose degradation is CDH1-dependent, was stabilised by the addition of APC/C inhibitors.

CDC20, which is thought to be degraded in a CDH1-dependent manner, levels were also examined. Under control conditions CDC20 was seen to be almost completely degraded by the 5 min mark (Figure 2.12B, left panel). This is in direct contradiction of the previous MS data which showed that ~50% of the protein remained 60 min after CDK inhibition (Figure 2.10D). Furthermore, the

levels of CDC20 were not stabilised by proteasome inhibition (Figure 2.12B, right panel), which suggests that a modification is interfering with or masking the epitope. The CDC20 antibody used was a polyclonal antibody generated using synthetic peptide of the residues surrounding Ala35, towards the N-terminus (CDC20 NT). Being just upstream of a phosphorylation site at Ser41, it is possible that the affinity of this antibody of CDC20 was affected by the presence of this phosphorylation. As a test a phospho-specific antibody against the CDC20-pS41 was used, and the disappearance of this phosphorylation signal closely matched the observed decrease in total protein signal (Figure 2.12B). Therefore, a new CDC20 antibody, generated through immunisation with full length CDC20 (CDC20 FL), was used. This antibody produced results much more in line with the MS data with ~50% degraded in 60 min (Figure 2.12B and D, green line). Interestingly, while CDC20 was stabilised by proteasome inhibition (Figure 2.12D, orange line), its levels were not stabilised by APC/C inhibitors (Figure 2.12D, blue line). This suggests CDC20 ubiquitination occurred prior to drug addition within this experiment and is consistent with this occurring while the SAC is active, in an APC15-dependent manner. This is, however, inconsistent with CDC20 degradation being dependent on APC/C^{CDH1} activity. As expected, the levels of CDH1 were stable throughout the timecourse, this being necessary for APC/C activity into the next G1 phase. Regardless, it is always necessary to validate antibodies thoroughly before use to ensure erroneous assumptions or observations are not made, as exemplified by the use of CDC20 antibodies here.

Importantly, under all conditions dephosphorylation of PP1 and PP2A-B55 substrates could be seen to occur equally rapidly, as typified by the PP2A-B55 substrate, PRC1-pT481, and the dephosphorylation of PPP1CA-pT320 (Figure

2.12B and E). A slight tail of phosphorylation could also be observed under conditions of APC/C or APC/C and proteasome inhibition. This was to be expected given that no inhibitor is 100% effective and CCNB1 persists for longer under these conditions. This would result in a residual amount of CDK1 activity persisting into anaphase which could allow small levels of phosphorylation to occur there. Nevertheless, these results are consistent with the hypothesis that the only proteolytic event necessary for mitotic exit is the degradation of CCNB1, to inactivate CDK1 and relieve separase inhibition. However, a more in-depth analysis was necessary to see if this holds true on a global level. This was achieved by combining the established MS protocol with the chemical inhibition of the APC/C described above.

Cells were seeded, harvested and the cell suspension separated into two halves following release from nocodazole arrest. The APC/C inhibitors were added to one half and an equal volume of DMSO added to the other (Methods 4.4.1). Anaphase onset was triggered 25 min later with CDK inhibition and samples taken as indicated (Figure 2.13A). This APC/C inhibition resulted in stabilisation of CCNB1 and securin, especially during the first 20 min following CDK inhibition (Figure 2.13A-C). Interestingly, while securin migrated as a single band under control conditions a smear above a single band was observed when APC/C was inhibited (Figure 2.13A and B). This could indicate multiple modification states of securin which are not normally observable under control conditions. Potentially, a priming modification was temporarily required prior to ubiquitination of securin, with inhibition of the APC/C trapping securin in this intermediate form. Levels of CDC20 were again seen to be independent of APC/C inhibition, supporting the idea that its destruction may not require APC/C^{CDH1} activity (Figure 2.13A and B).

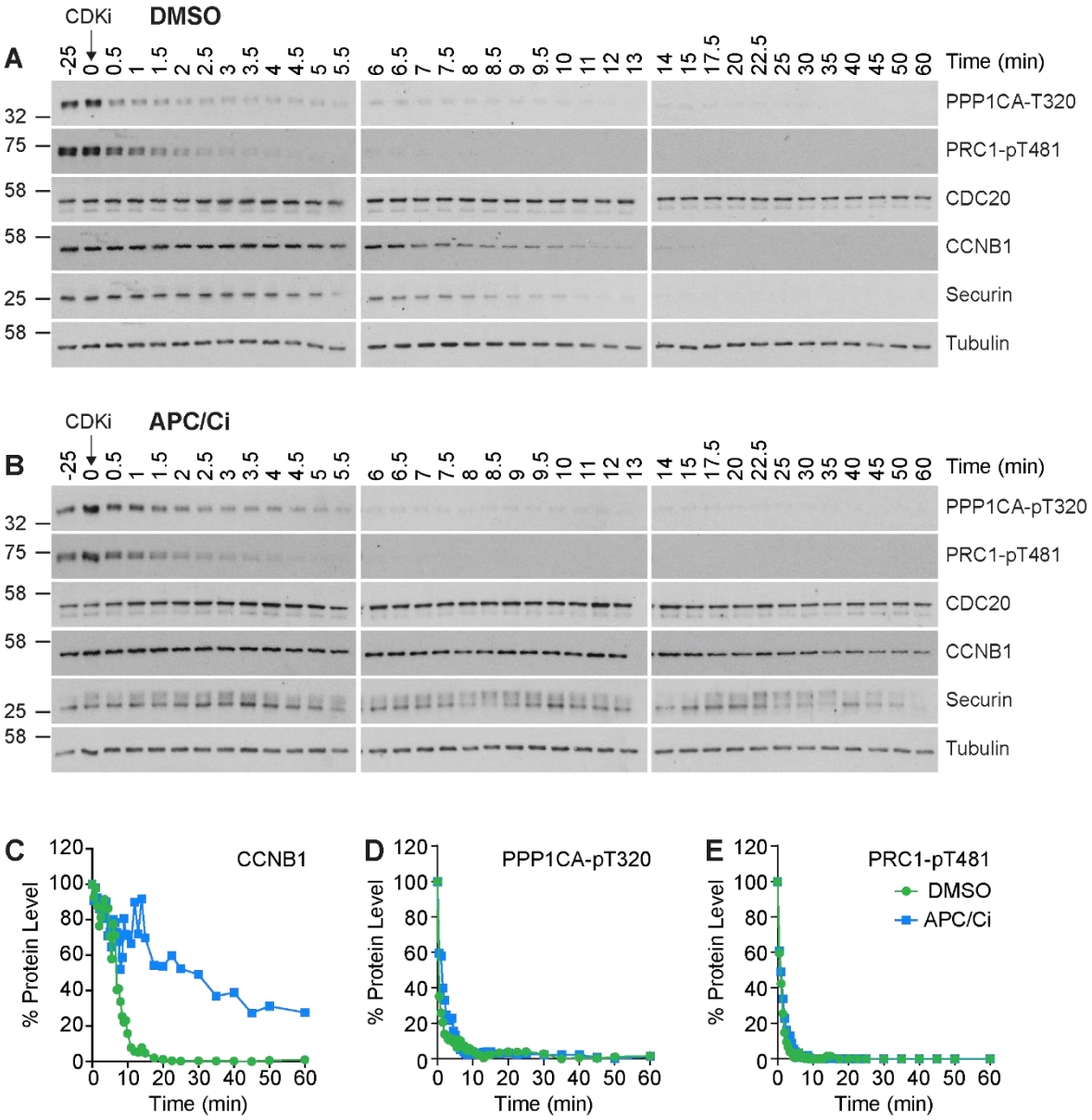


Figure 2.13 High-resolution analysis of mitotic exit under conditions of reduced APC/C activity

Western blot of samples generated from mitotically arrested HeLa cells which were treated with either (A) DMSO or (B) APC inhibitors (APC/Ci), 400 µM apcin and 25 µM pro-TAME, prior to CDK inhibition (CDKi). Samples were taken at the indicated timepoints. (C-E) Densitometric quantification of Western blot samples is shown for (C) CCNB1, (D) PPP1CA-pT320 and (E) PRC1-pT481.

Once again, dephosphorylation of PPP1CA-pT320 and PRC1-pT481 was equally rapid in control or APC/C-inhibited cells (Figure 2.13D and E). These samples

were then subjected to the same MS analysis previously described. (Figure 2.7) (Methods 4.6.1-3).

It was found that, since phospho-sites were clustered based on their behaviour across two timecourses, five clusters gave rise to the most sensible groupings. This allowed a category to be included for noisier data which was not quantified equally well in both conditions (Figure 2.14). The four remaining clusters followed the same pattern observed in the previous analysis (Figure 2.7B, Figure 2.14A), with phospho-site groupings of early, intermediate, late and stable. Furthermore, the average half-life of phospho-sites within each cluster was very similar in the control and APC/C inhibited conditions (Figure 2.14B). Predictably, the sequence logo of each of these clusters very closely matched those seen in the previous analysis of mitotic exit (Figure 2.7B, Figure 2.14B). This indicates that inhibition of APC/C-dependent proteolysis neither prevents dephosphorylation during mitotic exit nor affects the order in which they occur.

These results are consistent with dephosphorylation, rather than proteolysis, determining the order of events during anaphase. Furthermore, they support the idea that the only APC/C-dependent event necessary for anaphase is the degradation of CCNB1. One way to directly test this would be to repeat this experiment in cells expressing endogenous CCNB1, CRISPR tagged with auxin inducible degron (AID) sequence. Using a different ubiquitin ligase, the addition of auxin would target the AID-tagged CCNB1 for degradation. If carried out in the presence of APC/C inhibitors this would exclusively allow the destruction of CCNB1 to inactive CDK1. Timecourses carried out in the presence or absence of auxin could then be subjected to the sequence logo analysis done previously.

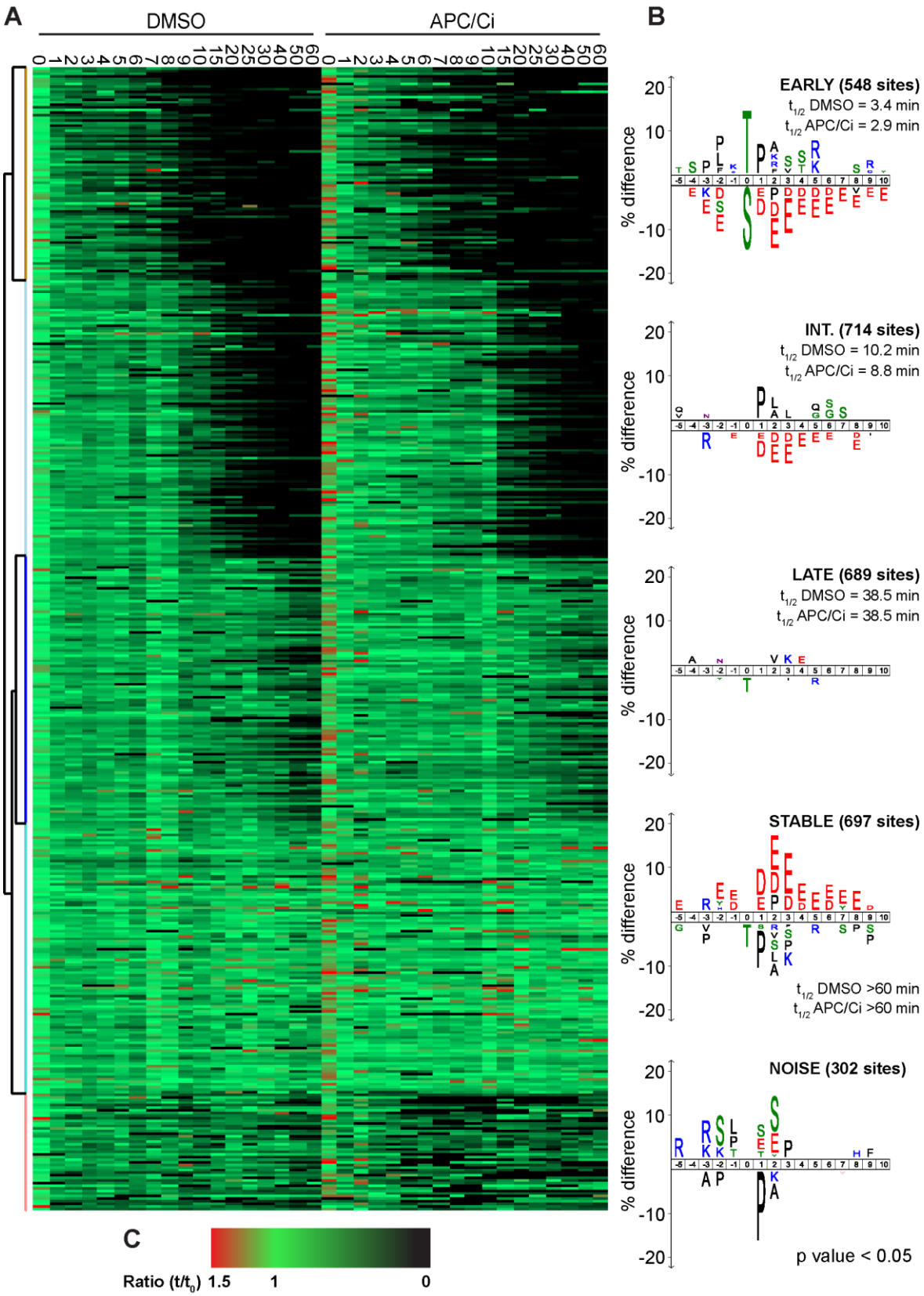


Figure 2.14 APC/C-dependent proteolysis is not necessary for ordered dephosphorylation during mitotic exit

Figure 2.14. APC/C-dependent proteolysis is not necessary for ordered dephosphorylation during mitotic exit (continued from previous page)

HeLa cells were arrested in mitosis and mitotic exit triggered as previously. (A) Heatmap of phospho-sites clustered based on their behaviour over time, following CDK inhibition, in the presence of either DMSO or APC/C inhibitors (APC/Ci), 400 µM apcin and 25 µM pro-TAME. (B) Sequence logo analysis showing the relative enrichment of residues in the adjacent cluster when compared against the sequences of all clustered phospho-peptides. Number of phospho-sites and the average half-life of each cluster is indicated. (C) Key linking heatmap colour with observed ratio.

2.2.2 The balance of protein synthesis and protein degradation during mitosis

As shown previously, very few proteins were degraded within the time window that could impact the order of events in anaphase (Figure 2.7, 2.9 and 2.10). Yet there were several proteins degraded later, whose proteolysis occurs at different rates. These results pose interesting questions. Why are different proteins degraded with different rates at all, if it is not to provide order to the events of anaphase? Moreover, how are these different rates achieved? It appears to be less straightforward than the simple switch from APC/C^{CDC20} to APC/C^{CDH1}, as CDC20 degradation can occur independently of CDH1 (Figure 2.12). Additionally, the degradation signals of CCNB1 and securin, two rapidly degraded proteins, were divergent from each other and bore little resemblance to those of PLK1 and PRC1 (Figure 2.15A). It is thought that key proteins such as CCNB1 and CDC20 are continually synthesised and degraded during mitosis (Nilsson et al., 2008) and it is this synthesis that keeps cells in mitosis. Perhaps synthesis of select proteins continuing into anaphase could explain how different rates of proteolysis occur.

To address this question, mitotically arrested cells were washed out of nocodazole into media containing 100 µg/ml cycloheximide (CHX) to inhibit protein synthesis 25 min before being treated with CDK inhibitor to trigger anaphase. Degradation of proteins at mitotic exit was unaffected by inhibition of protein synthesis (Figure 2.15C-D). This was confirmed by the quantification of CCNB1, CDC20 and Aurora A (Figure 2.15E-G, compare green and blue lines), meaning that differential rates of proteolysis could not be explained by ongoing protein synthesis. Given that these proteins fall under the same transcriptional control pathway for mitotic expression (Whitfield et al., 2002) it seems unlikely that they would then be individually and differentially regulated with respect to switching off gene expression. As previously, only CDC20 FL antibody recapitulated the proteomic data, with CDC20 NT over-estimating the level of CDC20 degradation (Figure 2.10D, Figure 2.12B, Figure 2.15C-D).

It has been previously shown that CDC20 is almost completely degraded 40 min after the addition of CHX to mitotic cells, with a half-life of around 20 min (Nilsson et al., 2008). Furthermore, the levels of BUBR1, CCNB1 and MAD2 also showed sizeable decrease within 60 to 120 min of CHX addition. If continued protein synthesis is critical to a normal mitosis it would follow that a 25 min treatment with CHX, equivalent to half a normal mitosis, should cause a measurable fall in protein levels. However, no difference was seen when comparing the levels of different mitotic proteins in the -25 and 0 min timepoints in either control or synthesis-inhibited conditions (Figure 2.15C-D). This poses questions about the importance of continued protein synthesis on a normal, unperturbed mitosis. Closer inspection of the Nilsson study raises two potential issues relevant to the interpretation of their experimental data. Firstly, a single

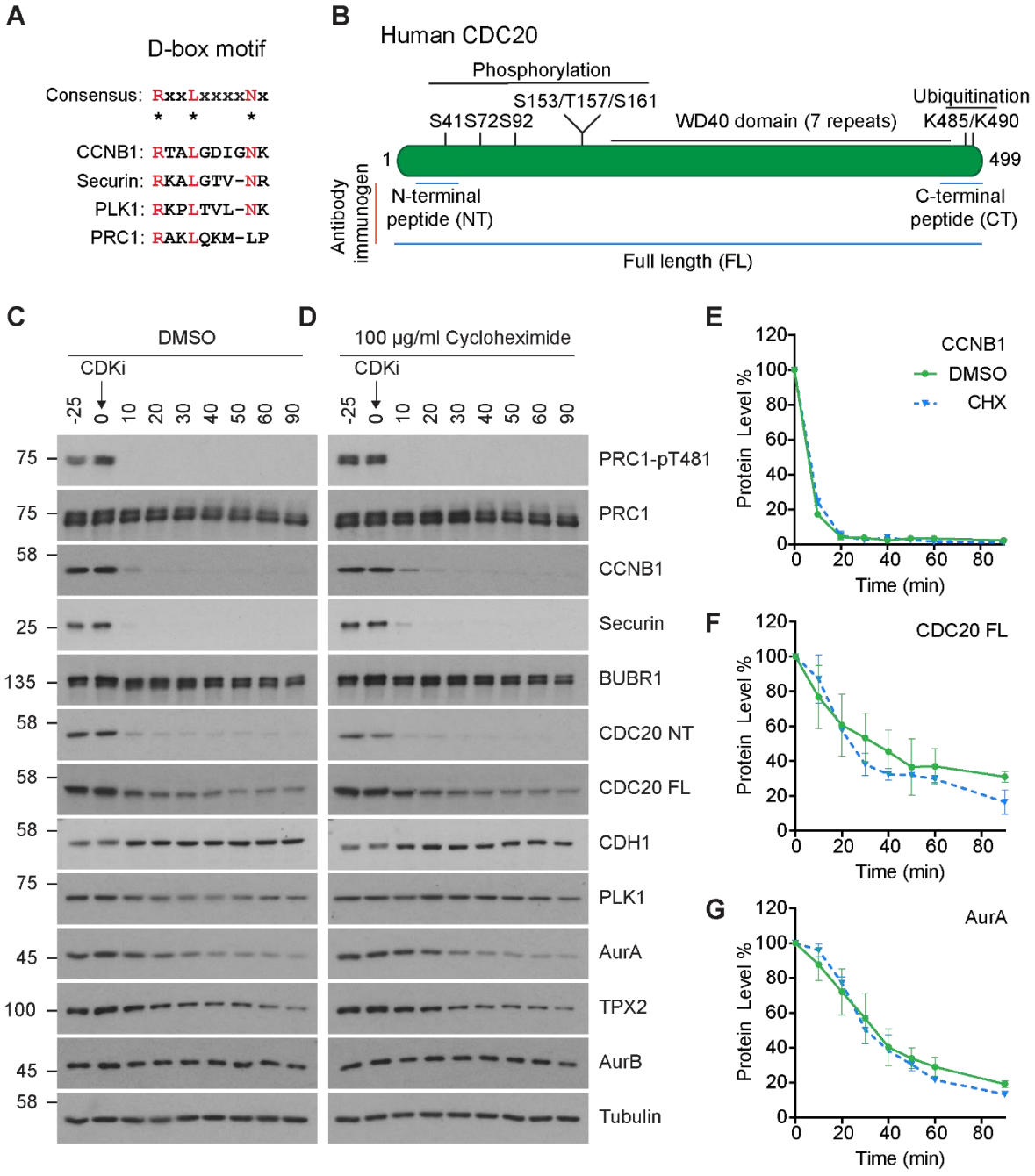


Figure 2.15 Continued protein synthesis cannot account for different rates of proteolysis during mitotic exit

(A) D-box motifs from anaphase substrates of the APC/C. (B) Schematic of CDC20, with modification sites noted. Regions of CDC20 used to generate commercially available antibodies are indicated. Mitotically arrested HeLa cells were washed out from nocodazole and treated with either (C) DMSO or (D) 100 µg/ml cycloheximide for 25 min prior to CDK inhibition. Samples were harvested as indicated and analysed by Western blot. Abbreviations following CDC20 denote the antibody epitope. (E-G) Densitometric

quantification of protein level, from Western blot data (C/D), for indicated protein (Mean ±SEM, n=2).

CDC20 antibody was used to probe levels of this protein and this antibody was generated against a C-terminal region of CDC20 which contained the lysines ubiquitinated by the APC/C (Figure 2.15B, C-terminal peptide). The CDC20 epitopes for antibodies used within this thesis are also marked on this schematic. As shown previously, antibodies can give misleading results, especially if targeted against an area which is readily modified (Figure 2.12). Secondly, their protocol used a thymidine and aphidicolin arrest to synchronise HeLa cells in S phase before washing out into media containing nocodazole or taxol. However, the authors added CHX 6 hr post wash-out, which would place the cells in early G2 and not mitosis. Together, the effects of post-translational modifications on recognition of CDC20 by antibodies and ongoing protein synthesis during G2 could account for the observed turnover of CDC20, rather than the proposed balance between continued synthesis and proteolysis in mitosis.

To test this idea, the Nilsson protocol was repeated, as described in the published paper (Methods 4.4.3) (Figure 2.16A), and the same proteins probed by Western blot. Under control conditions, the levels of mitotic proteins, such as CCNB1 and CDC20, increased throughout the experiment but few cells entered mitosis according to observations of the mitotic index, indicating that the cells were in G2 rather than mitosis (Figure 2.16B-D, green lines). Inhibition of protein synthesis led to a gradual decrease in the levels of CCNB1 and CDC20 over 120 min, falling to approximately 70% and 50% of their respective starting values (Figure 2.16B-D, blue lines). Again, few mitotic cells were observed. The rates of

proteolysis seen here are also much slower than those presented previously. Additionally, the percentage of cells in mitosis was calculated at the start and end of the experiment, 6 and 8 hr post wash-out respectively. Even by the end of the experiment the percentage of cells in mitosis had only risen to ~3% (Figure 2.16B). Therefore, while the authors interpreted their results in the context of mitosis they would be more accurately seen as a comment on protein homeostasis in G2.

The high levels of protein degradation seen by Nilsson et al. are inconsistent with the role of EMI1 in maintaining APC/C inhibition in G2. This level of degradation would necessitate continued and rapid levels of protein synthesis to allow sufficient accumulation of these proteins prior to mitosis. Furthermore, the futile cycles of synthesis and destruction would be energetically expensive. The lower rates of degradation, seen from our own account of their experimental work, suggest a CDC20 half-life of roughly 120 min (Figure 2.16B-C), much more consistent with EMI1 mediated inhibition of the APC/C prior to mitosis (Hsu et al., 2002b). Furthermore, during mitotic exit, when APC/C activity is maximal, the half-life for CDC20 was approximately 60 min (Figure 2.10D), while the published experiment suggested a half-life of ~20 min (Nilsson et al., 2008). This would imply that CDC20 is being degraded more quickly during a period of APC/C inhibition than when fully active during anaphase. An alternative conclusion would be that the high levels of CDC20 destruction observed previously are due to antibody epitope masking through modification.

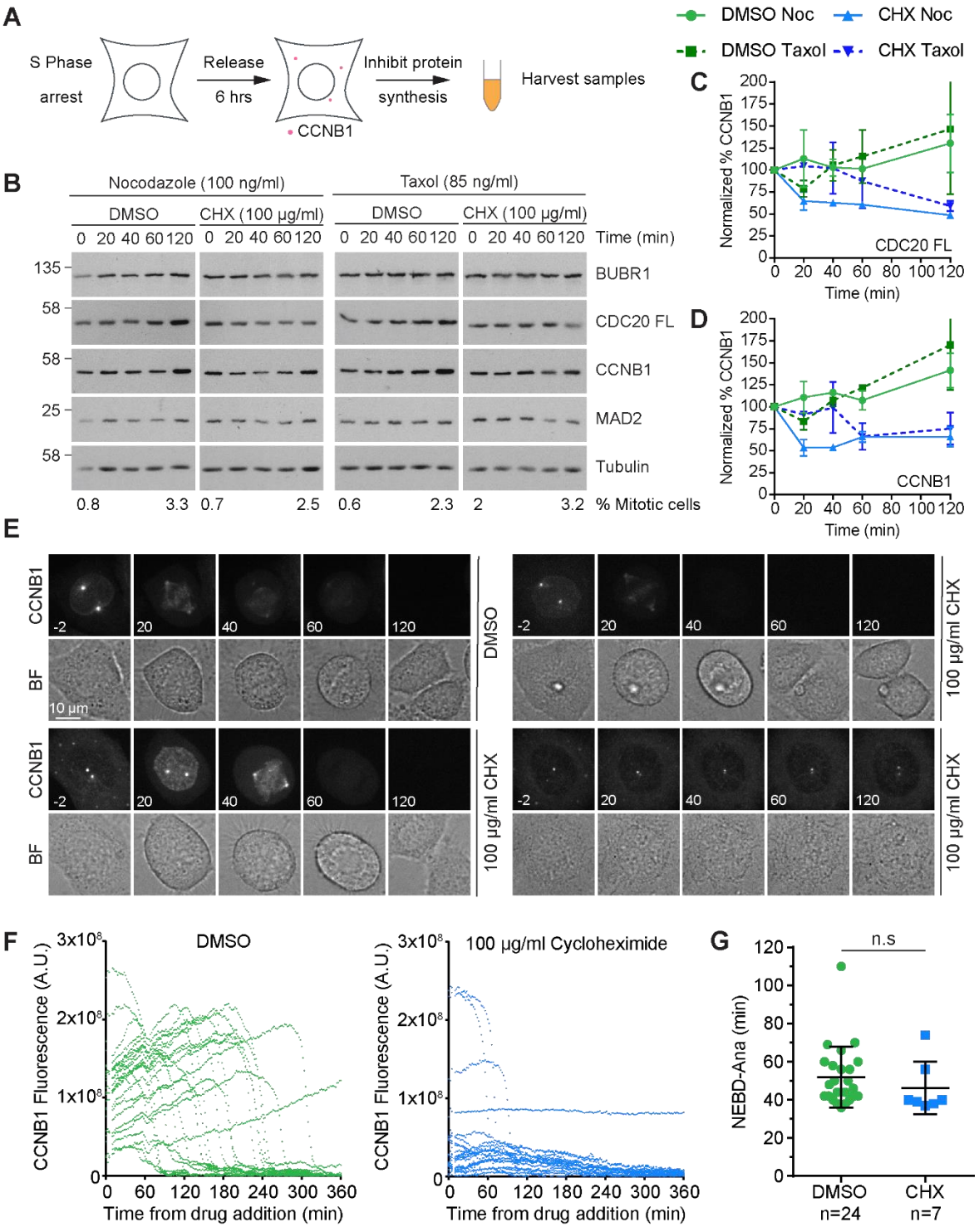


Figure 2.16 Protein synthesis is required for mitotic entry but not mitosis

(A) Cells were arrested in S phase using a double thymidine block and washed out into media containing either nocodazole or taxol. 6 hr later protein synthesis was inhibited using 100 µg/ml cycloheximide. (B) Western blot analysis of samples obtained from (A). The percentage of cells in mitosis at 0 and 120 min is shown beneath the western blots. Densitometric quantification of (C) CDC20 FL and (D) CCNB1 Western blot data from (B)

(Mean±SEM, n=2). (E) Live cell imaging of endogenously CRISPR tagged CCNB1, following addition of either DMSO or 100 µg/ml cycloheximide. (F) Raw fluorescence intensity plot of all cells following drug addition. (G) Statistical analysis of the time spent in mitosis using a ANOVA two-way T-test. Images shown are maximum intensity projections, quantification was carried out on sum intensity projections.

If proteins are being continually synthesised and destroyed during mitosis, the addition of CHX could have disastrous consequences. Levels of both CCNB1 and CDC20 would fall, with the former causing a decrease in CDK1 activity, allowing cells to leave mitosis. The consequence of CDC20 degradation is less clear since CDC20 is both a coactivator and inhibitor of the APC/C. However, if these proteins are not being continually synthesised the addition of CHX should have no impact on mitotic progression. To test this, the levels of endogenous CRISPR-tagged CCNB1-GFP (Alfonso-Perez et al., 2018) were followed by live cell microscopy. CHX or DMSO were then added just as cells were entering mitosis. Consistent with the literature, CCNB1 was predominantly cytoplasmic during G2 with some accumulation at the centrosomes. Following mitotic entry, CCNB localised to the spindle poles and the unattached kinetochores, as previously described for this cell line (Figure 2.16E) (Alfonso-Perez et al., 2018). In control cells the level of CCNB1 continued to climb throughout the experiment until cells entered mitosis (Figure 2.16E-F, left graph). CCNB1 levels peaked and plateaued, the plateau length varying with the time spent in mitosis, before rapidly decreasing. These features indicated that the cells had entered mitosis, satisfied the checkpoint and entered anaphase. This happened with nearly every cell within the fields of view. Importantly, the presence of a plateau indicates that levels of CCNB1 do not continue to rise throughout mitosis. Upon addition of CHX, levels of CCNB1 ceased to increase, confirming the activity of the drug (Figure

2.16E-F, right graph). As such, many of the cells imaged did not have the necessary levels of CCNB1 to enter mitosis. In these cells the CCNB1 fluorescence only gradually declined, more indicative of bleaching than of active degradation. Cells with the requisite level of CCNB1 did enter mitosis. The length of time spent in mitosis was compared to that of control cells. There was no statistically significant difference in the mean time spent in mitosis following addition of CHX (Figure 2.16G). These results are not consistent with the idea that proteins are being appreciably synthesised during mitosis. Cells which had accumulated CCNB1 at separated centrosomes but had not yet entered mitosis, proceeded to do so following inhibition of protein synthesis. However, the cells which had not yet accumulated high levels of CCNB1 at the centrosomes arrested in G2 and did not enter mitosis. No intermediate cells, which had accumulated CCNB1 at separated centrosomes, arrested in G2. This would suggest that the level of CCNB1 required to commit to mitosis is reached before the physical changes associated with mitotic entry occur. This would again argue against the requirement for continued synthesis of CCNB1 into mitosis. It would be interesting to examine the accumulation of CCNB1 at the centrosomes in order to determine the threshold level required for mitotic entry.

The requirement for ongoing protein synthesis during mitosis for checkpoint arrest was then tested directly. For this purpose, cells were synchronised in mitosis using nocodazole or taxol arrest rather than the thymidine arrest-release protocol (Figure 2.17A). The levels of BUBR1, CDH1 and MAD2 were all stable for two hours following inhibition of protein synthesis (Figure 2.17B). Furthermore, BUBR1 migrated as a doublet band whereas in the previous samples BUBR1 was a singlet (Figure 2.15A and 2.16B). The singlet band indicates the absence of

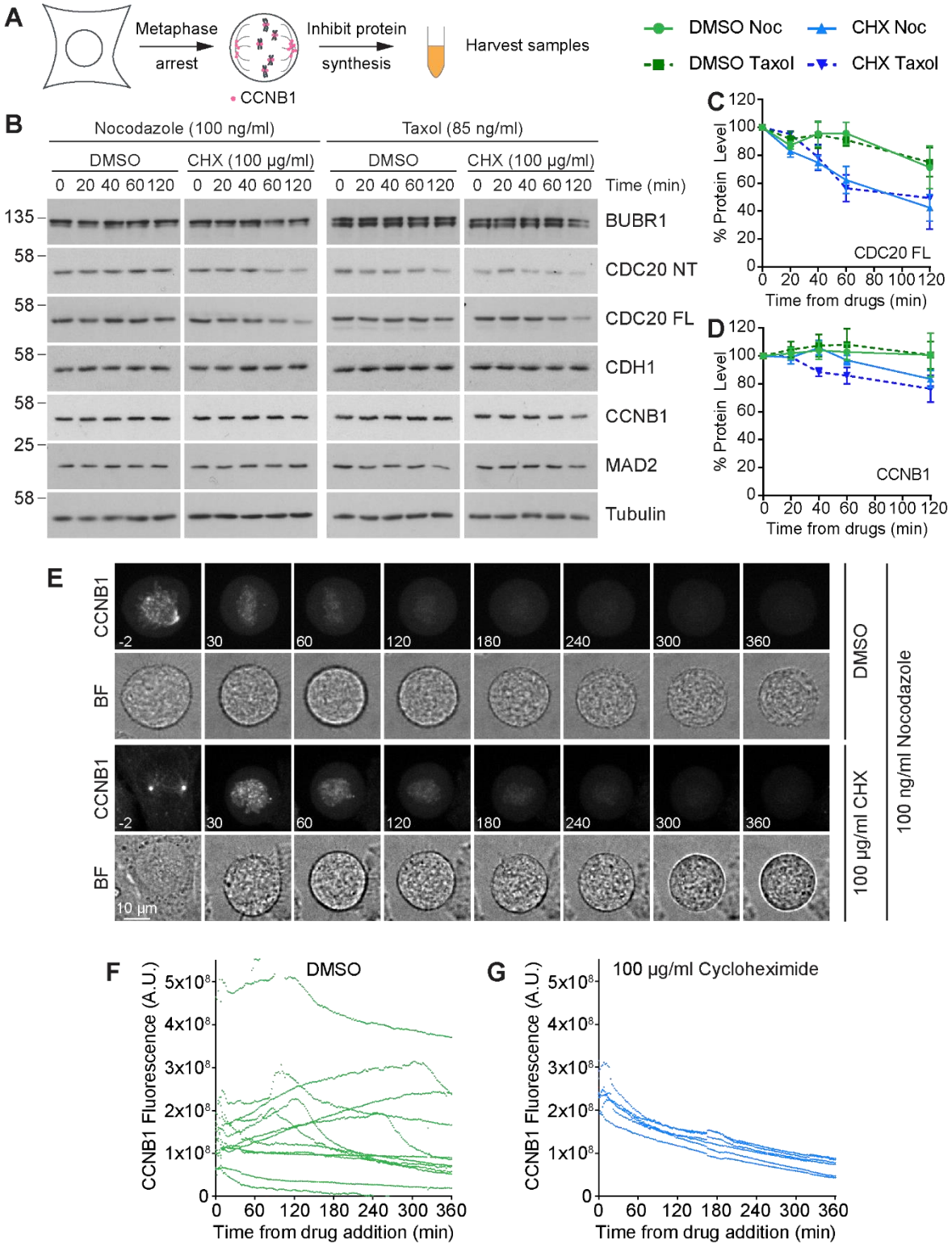


Figure 2.17 Ongoing protein synthesis is not essential for spindle checkpoint-dependent arrest in mitosis

(A) Cells were arrested in mitosis using either nocodazole or taxol prior to inhibition of protein synthesis using 100 µg/ml cycloheximide (CHX). (B) Western blot analysis of samples obtained from (A). Densitometric quantification of (C) CDC20 FL and (D) CCNB1

of Western blot data from (B) (Mean±SEM, n=3). (E) Live cell imaging of endogenously CRISPR-tagged CCNB1, following addition of 100 ng/ml nocodazole with either DMSO or 100 µg/ml cycloheximide. (E) Raw fluorescence intensity plot of cells over time, following drug addition (DMSO n=13, CHX n=6). Only cells which enter mitosis are shown. Images shown are maximum intensity projections, quantification was carried out on sum intensity projections.

BUBR1 modifications, typically phosphorylation, usually seen in mitosis; providing further confirmation that the published protocol was inadvertently observing G2 cells (Nilsson et al., 2008). During this period CCNB1 levels fell to 80% of their starting value, however the levels were barely different from the control during the first 60 min, (Figure 2.17D). As previously, two CDC20 antibodies were used. While the CDC20 NT antibody result is not as striking as in Nilsson et al., it does still appear to overestimate destruction of CDC20. Quantification of the signal from antibody against full-length CDC20 showed that around 50% is destroyed in two hours (Figure 2.17B-C), in line with the results from Figure 2.16. This is inconsistent with high rates of protein synthesis and turnover during mitosis. Importantly, the changes in protein level were followed over a 120 min period, whereas a normal mitosis typically takes 60 min. During the first 60 min after CHX addition, the levels of CCNB1 did not differ greatly from control, while CDC20 only began to diverge from control after 40 min (Figure 2.17C-D). Therefore, while it appears that protein synthesis may not be necessary for a normal mitosis, it may be required when mitotic progression is slowed.

Following on from this, CCNB1-GFP CRISPR cells were treated with CHX and nocodazole, to simultaneously inhibit protein synthesis and trigger spindle checkpoint-dependent mitotic arrest. This enabled the contribution of protein synthesis during a prolonged mitosis to be observed. As previously, in control

cells, CCNB1 fluorescence increased until mitotic entry and had a small plateau, after which the fluorescence gradually decreased. Since the cells did not leave mitosis, this decrease in signal is likely due to fluorophore bleaching rather than protein degradation (Figure 2.17E-F, Left graph). Other work in the laboratory, imaging CCNA2 and CCNB1, has estimated 25% bleaching occurs every 60min, under equivalent conditions, which would explain the reduction in signal observed here (Dr Tatiana Alfonso-Perez and Prof Francis A. Barr, personal communication). CCNB1 fluorescence, in the cells treated with cycloheximide and nocodazole, began decreasing immediately after drug addition at a similar rate to that seen in control cells (Figure 2.17E and G, right graph). However, these cells were still arrested in mitosis 360 min after drug addition, meaning CCNB1 must still be sufficiently present to maintain CDK1 activity and checkpoint function (Figure 2.17E, bottom row). This supports the idea that the fluorophore bleaching, rather than protein degradation, is responsible for the majority of signal loss; suggesting that ongoing protein synthesis and turnover is not essential for SAC-dependent arrest during mitosis.

Taken together, these results do not support the hypothesis that continued high levels of synthesis and degradation of certain mitotic factors have an important role in mitotic regulation. Rather they suggest that dynamic protein turnover is not necessary for an unperturbed mitosis. Furthermore, the ubiquitination, but not destruction, of CDC20 during mitosis could account for the results seen previously, given the antibody epitope. They do not however completely rule out a role for protein synthesis in maintaining the SAC in a prolonged mitosis. Additionally, protein synthesis cannot account for the differential rates of proteolysis seen during mitotic exit.

2.2.3 Inhibition of the APC/C is dependent on CDK1 activity

During mitosis, the inhibition of the APC/C towards anaphase substrates is maintained through MPS1 activity, which signals the presence of unattached kinetochores by promoting MCC generation. Recently it was seen that, during checkpoint signalling, CDK1-CCNB1 phosphorylation of MPS1-pS281 is required for MPS1 localisation to unattached kinetochores (Hayward et al., 2018). This is enhanced because CCNB1 is a *bona fide* spindle checkpoint protein dependent on MAD1 for its kinetochore localisation (Alfonso-Perez et al., 2018). MAD1 in turn requires MPS1 activity to interact with the kinetochore, setting up a spatial positive feedback loop enabling checkpoint signalling. MPS1-pS281 is removed by the phosphatase PP2A-B55, which is indirectly inhibited by CDK1:CCNB1 and its activation is delayed by the BEG pathway following CCNB1 degradation. Since CCNB1:CDK1 are important in maintaining checkpoint activity, it raises an important issue as to whether they additionally maintain inhibition of the APC/C (Figure 2.18A).

To confirm this, mitotically arrested cells were pushed into anaphase using either CDK inhibition or MPS1 inhibition. As expected, inhibition of CDK1 led to immediate, rapid dephosphorylation of PPP1CA-pT320 and PRC1-pT481 (Figure 2.18B and D). Removal of CDK1 sites is slower following MPS1 inhibition, due to the gradual inactivation of CDK1 (Figure 2.18C-D, top graph). Owing to incomplete sample recovery, the detection of phosphorylation in samples 5-17 min from the MPS1 condition was compromised, so the early behaviour of these phospho-sites is unclear. However, dephosphorylation of CDK sites did not begin immediately in the MPS1 phospho-proteomic data used for analysis earlier (Figure 2.9G). CCNB1 degradation was clearly faster under conditions of CDK inhibition than MPS1

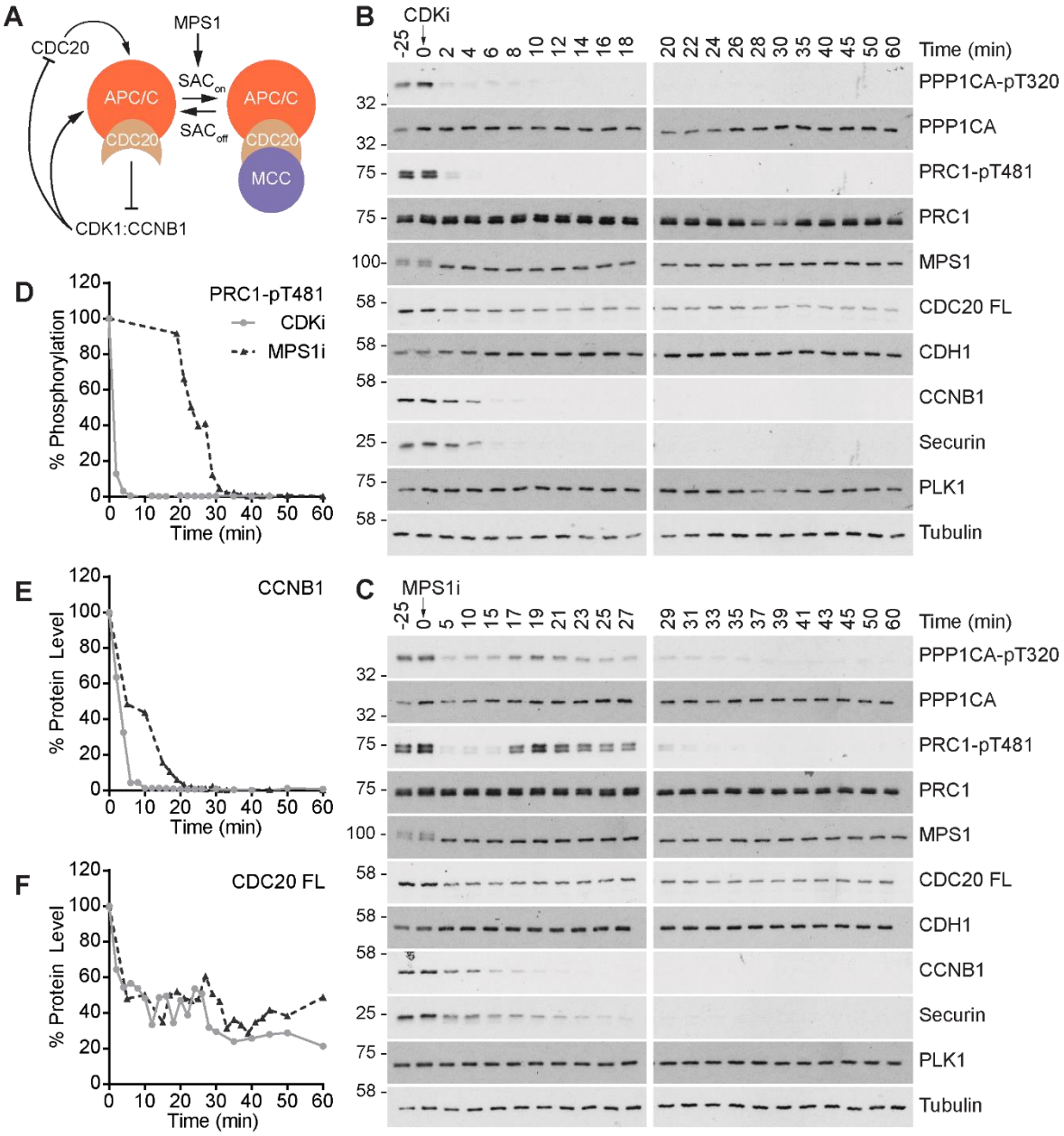


Figure 2.18 The APC/C is inhibited in a CDK-dependent manner

(A) Simple model depicting the regulation of the APC/C by CDK1-CCNB1. HeLa cells were arrested in mitosis, as previously described, and mitotic exit triggered through inhibition of either (B) CDK (CDKi) or (C) MPS1 (MPS1i). Each condition was sampled as indicated and probed via Western blot. Densitometric quantification of(D) PRC1-pT481, (E) CCNB1 and (F) CDC20 FL. SAC - spindle assembly checkpoint, MCC - mitotic checkpoint complex.

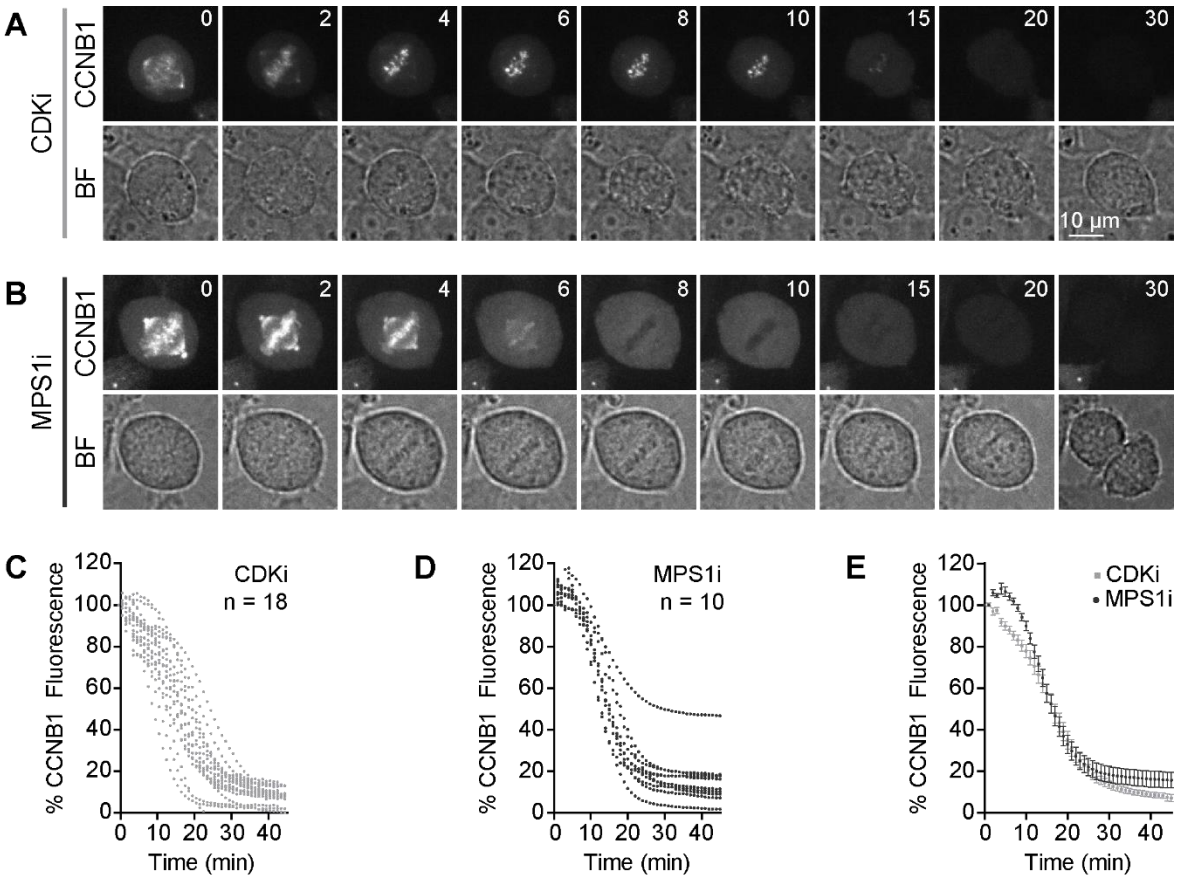


Figure 2.19 CCNB1 is degraded immediately upon CDK inhibition

The fluorescence of endogenous CCNB1-GFP was quantified over time following inhibition of (A) CDK (CDKi) or (B) MPS1 (MPS1i). Times indicated are in minutes. Drugs were added at 0 min. (C-D) Percentage fluorescence traces from individual cells following drug addition. n is number of cells quantified. (E) Average fluorescence percentage over time (Mean±SEM). Images shown are maximum intensity projections, quantification was carried out on sum intensity projections.

inhibition (Figure 2.18E). This was recapitulated when imaging endogenously tagged CCNB1-GFP following CDK-inhibition (Figure 2.19). Here, it can be seen that CCNB1 degradation began immediately upon CDK inhibition (Figure 2.19A and C), whereas there was a short delay seen upon MPS1 inhibition (Figure 2.19B and D). Interestingly, both the maximal rate and endpoint of CCNB1 degradation were very similar between the two conditions, showing that it was only the initiation of APC/C activity that was affected. The difference observed in the

imaging was smaller than that seen in the Western blot experiment. The microscope setup does not allow for vigorous mixing which could contribute to these discrepancies. In some cells, CCNB1 became trapped in the midbody following CDK inhibition, which persisted longer before degradation. Additionally, CCNB1 accumulated at kinetochores, after CDK inhibition, prior to being degraded. It is unclear whether these phenotypes are dependent on the alignment and checkpoint status of these cells or not.

Together these results show that CDK1 maintains APC/C inhibition separately to checkpoint activity. Moreover, depletion of PP2A-B55 does not lead to a delay in CCNB1 degradation (Hayward et al., 2018). This leaves PP1 as the likely candidate phosphatase to relieve this inhibition and allow activation of the APC/C. It is also unclear at this stage whether CDK1 inhibits the APC/C directly or whether phosphorylation of the MCC or another component prevents MCC turnover.

Destruction of CDC20 was similar under both conditions (Figure 2.18F). One possibility is that CDC20 bound to the APC/C, as part of the MCC, is ubiquitinated prior to mitotic exit and is destroyed rapidly upon checkpoint silencing. One assumption here would be that MCC disassembly is equally fast under both conditions. This hypothesis is consistent with the earlier result that CDC20 degradation was independent of APC/C activity during mitotic exit (Figure 2.12). CDC20 exists as three pools: free, in complex with the MCC and bound to the APC/C. To distinguish which of the three pools of CDC20 is being degraded would not be a simple task. However, a good place to start would be to assess the stability of MCC complexes by co-IP under conditions of CDK and MPS1 inhibition.

The results described so far show that much of what has been assumed about protein turnover in mitosis and mitotic exit may not be correct. Surprisingly, it appears that APC/C-dependent proteolysis, beyond the initial degradation of CCNB1, is not required for dephosphorylation and therefore order during anaphase. This would suggest that the APC/C functions to reset the cell status later in mitotic exit and the subsequent G1. Additionally, the described order of PLK1 and Aurora A destruction and the functional consequences of this need revisiting (Lindon and Pines, 2004). A role for CDK1 in inhibition of the APC/C supports the presence of a feedback loop, centred around levels of CCNB1, ensuring that commitment to anaphase is irreversible (He et al., 2011). Finally, these results question the role of continued protein synthesis and degradation during mitosis, perhaps limiting their contribution to abnormal mitosis following cell stress. More certainly, continued protein synthesis does not account for the differential rates of proteolysis during mitotic exit.

2.3 PP1 is positioned to play a central role in the regulation of mitosis and mitotic exit

2.3.1 PP1 helps activate the APC/C during mitotic exit

As described above, one likely function of CCNB1:CDK1 complexes is to maintain inhibition of the APC/C. To test whether APC/C inhibition is counteracted by PP1, HeLa cells were depleted of PP1, arrested in mitosis, released and their exit kinetics followed. Based on phenotype data, PPP1CA and PPP1CC were co-depleted while PPP1CB was depleted alone. Control cells exited mitosis as expected, with rapid dephosphorylation of PRC1-pT481, and CCNB1 degradation occurring in the first 15 min (Figure 2.20A, left). Cells depleted of PPP1CB showed the same behaviour upon mitotic exit (Figure 2.20A, right). PPP1CA/C depletion resulted in a shift in exit kinetics, with both PRC1-T481 dephosphorylation and CCNB1 degradation occurring slightly more slowly (Figure 2.20A, middle): this difference is, however, extremely subtle. Upon checking the siRNA efficiency, the depletion of the PP1 subunits was seen to be incomplete (Figure 2.20B). Regardless, this showed that the system was sensitive to the levels of PP1. The slightly slowed dephosphorylation of PRC1-pT481 could be explained by the requirement of PP1 in MASTL inactivation, placing PP1 upstream of PP2A-B55. Therefore, it would be expected that dephosphorylation of PP2A-B55 substrates is slowed upon efficient depletion of PP1. A small change could also be observed using the pan pS and pT pan-CDK1 phospho-site antibodies. This is consistent with PP1 being involved in the dephosphorylation of a wide range of substrates during mitotic exit. However, depletion conditions must be optimised before any further experiments are carried out.

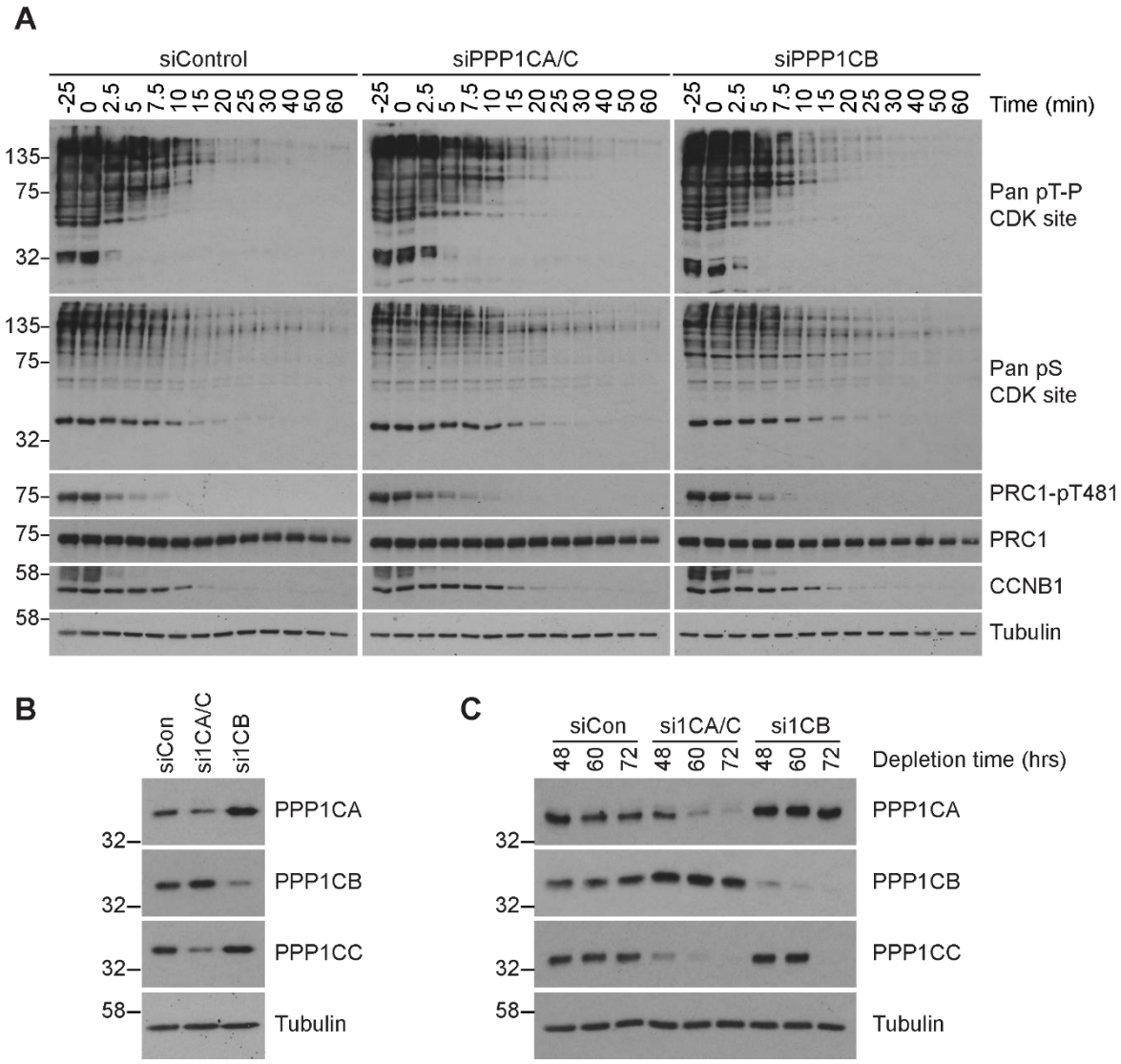


Figure 2.20 Optimisation of conditions for efficient large-scale PPP1C depletion

(A) Cells were depleted of control protein, PPP1CA and C or PPP1CB for 48 hr and simultaneously arrested in mitosis. CDK1 was then inhibited and cells were sampled as indicated and probed by Western blot. (B) Western blot checking depletion efficiency. (C) Cells were depleted for the times indicated and simultaneously arrested in mitosis, before harvesting. Samples were probed by Western blot.

Typically, a 48 hr depletion protocol was followed, to minimise accumulative stress of multiple cell cycles without PP1. This worked efficiently on small imaging dishes (not shown) but did not provide optimal depletion on the 15 cm dishes

required for large-scale experiments (Figure 2.20B). It was necessary to identify the minimum length of time required for efficient depletion of PP1. HeLa cells were depleted as before and harvested after either 48, 60 or 72 hours and probed for their levels of PP1 by Western blot. This established that 72 hours siRNA treatment was necessary to sufficiently deplete all three PPP1C isoforms (Figure 2.20C), and this was therefore used for subsequent large-scale experiments.

A high-resolution timecourse was run (Methods 4.4.1), using the optimised depletion protocol. As consistent with the previous experiment, both control and PPP1CB depletion behaved similarly (Figure 2.21A and C). However, simultaneous depletion of PPP1CA and PPP1CC doubled the time taken to completely dephosphorylate PRC1-pT481, from 6.5 to 13 min, confirming that PPP1CA/C lies upstream of PP2A-B55 (Figure 2.21A and B). CCNB1 degradation was also impaired, with completion of proteolysis occurring ~10 min later than in control conditions (Figure 2.21A, B and E orange line). Depletion efficiency was confirmed by Western blot (Figure 2.21D). To confirm these observations, cells expressing endogenous CCNB1-GFP were depleted of PP1 and the CCNB1 fluorescence followed over time. Control cells behaved consistently, with sister chromatid separation occurring, on average, approximately 62 min after nuclear envelope breakdown (NEBD) (Figure 2.22B siControl; Figure 2.22C siControl). Cells depleted of PPP1CB were not quite as consistent, but entered anaphase ~68 min after NEBD (Figure 2.22B siPPP1CB; Figure 2.22C siPPP1CB). However, this deviation from control cells is not significant. Both conditions showed similar profiles of CCNB1 fluorescence following NEBD (Figure 2.22D and F) but depletion of PPP1CA/C resulted in two populations of cells (Figure 2.22E siPPP1CA/C). One population appeared very similar to control cells, while the

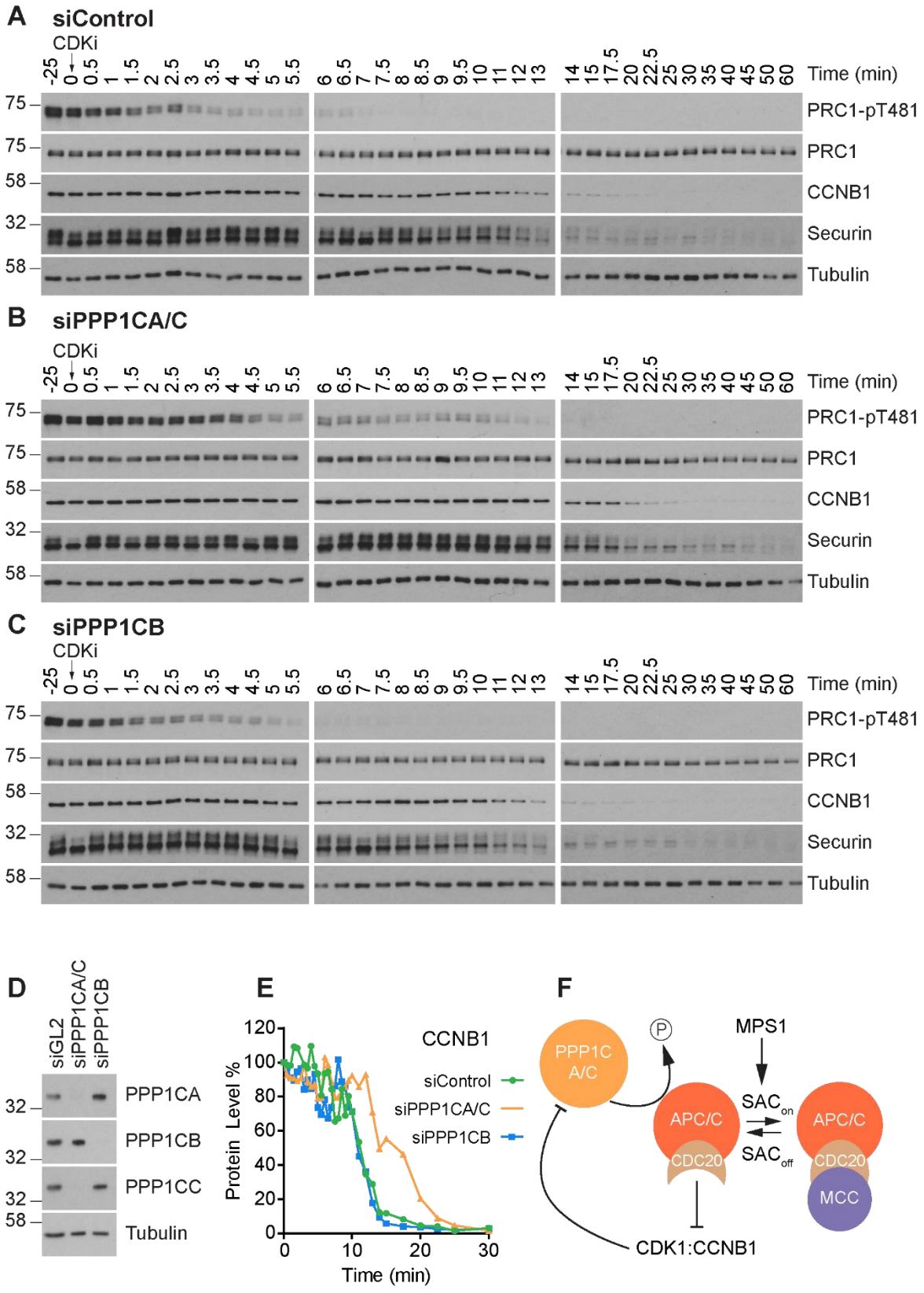


Figure 2.21 PP1 contributes to activation of the APC/C during mitotic exit

HeLa cells were depleted of PP1 catalytic subunits, either (A) control, (B) PPP1CA and C or (C) PPP1CB, and arrested in mitosis. Mitotic exit was then triggered using CDK

inhibition. Conditions were sampled and probed by Western blot as indicated. (D) Western blot confirming efficient depletion of PP1 catalytic subunits. (E) Densitometric quantification of CCNB1 levels across the three conditions. (F) A potential model of PP1's role in APC/C activation.

second reproduced the delay in CCNB1 degradation seen biochemically. When both populations are taken together, the average time from NEBD-anaphase onset is ~108 min; which is significantly different from that of control cells (Figure 2.22B siPPP1CA/C; Figure 2.22C si1PPPCA/C). As seen previously, near complete depletion of PPP1CA and 1CC was necessary to produce sizeable delays in APC/C activation (Figure 2.20A and 2.21A). Not every single cell in an experiment will be equally depleted of PP1. It is therefore likely that the two populations were created by variation in the level of PPP1CA/C left after depletion. If PPP1CA/C remains above a threshold, cells will exit mitosis normally; below this threshold a delay is observed. In the population presumably more fully depleted of PPP1CA/C, the rate of CCNB proteolysis was severely reduced to ~20% per hour. This would suggest that APC/C activation was not just delayed but also severely impaired. This novel finding shows that PPP1CA/C complexes are involved in activation of the APC/C prior to anaphase onset. It still remains unclear whether PP1 acts directly upon the APC/C (Figure 2.21F) or is in some way involved in MCC turnover.

The timecourse samples characterised in Figure 2.21 were processed for mass spectrometry. This helped to identify the contribution of PPP1CA/C to mitotic exit, as well as providing candidates for the PPP1CA/C-dependent dephosphorylations responsible for APC/C activation. These phospho-proteomic samples were subjected to the same analysis as before. On a technical level,

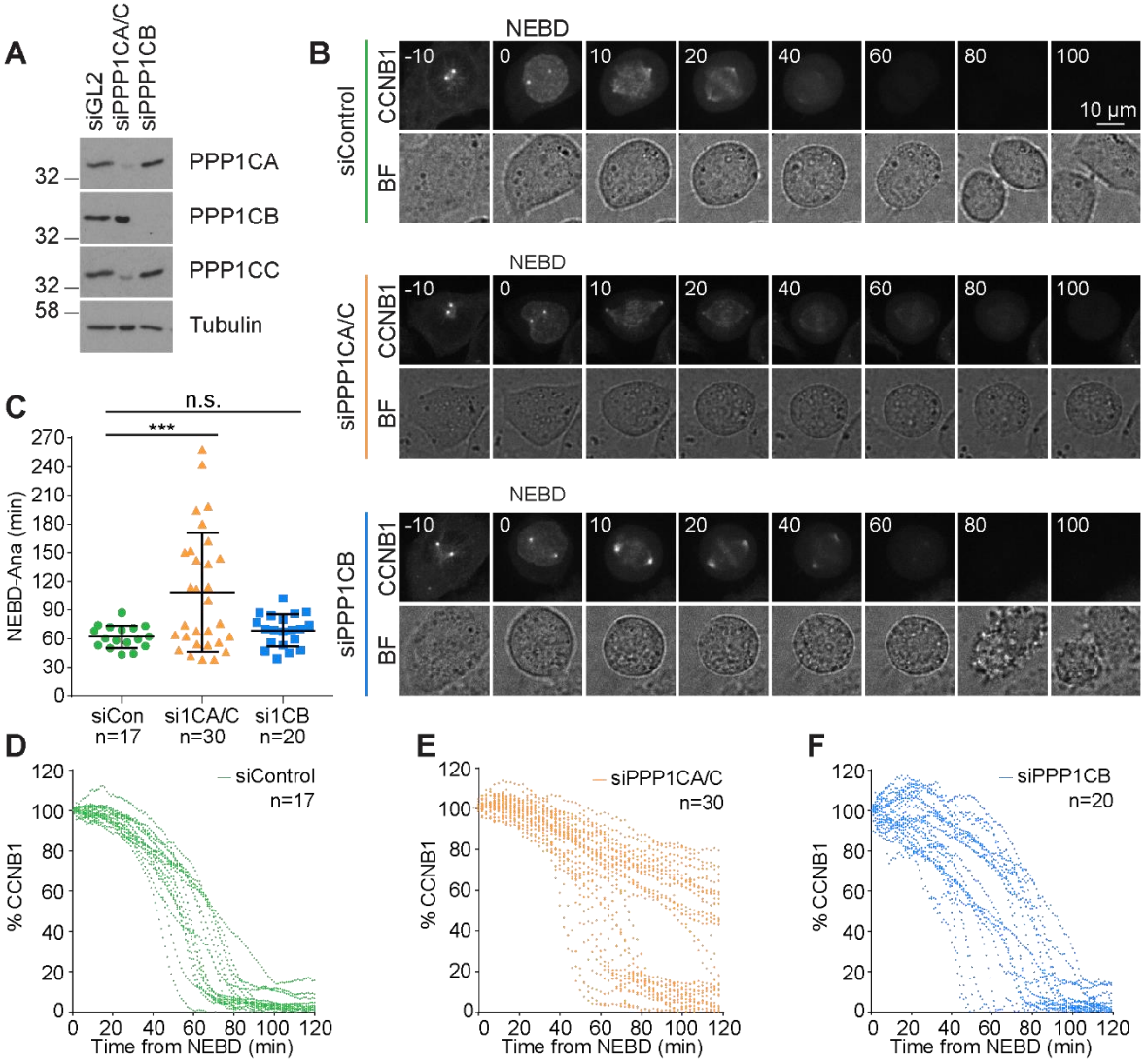


Figure 2.22 Rapid activation of the APC/C is sensitive to the levels of PP1

(A) Western blot confirming depletion efficiency of PP1 catalytic subunits from HeLa, CCNB1-GFP cells. (B) Live cell imaging of endogenous CRISPR tagged CCNB1-GFP cells depleted of control, PPP1CA/C and PPP1CB during mitosis. Times shown in minutes. (C) Comparison of time spent in mitosis by cells in each condition. Percentage CCNB1-GFP fluorescence following NEBD in (D) siControl, (E) siPPP1CA/C and (F) siPPP1CB cells. Images shown are maximum intensity projections, quantification was carried out on sum intensity projections.

there appeared to have been a problem with mixing ‘light’ and ‘heavy’ labelled peptides in a 1:1 ratio with the siPPP1CA/C timecourse. The ratios for both total and phospho-proteome upshifted away from the expected ratio of one

(Figure 2.23A-B). While cross-mixing did provide improvement, it did not completely fix the issue. Further repeats of this experiment will therefore be necessary to confirm the results obtained here.

A histogram plot of the ratios observed at each timepoint is an effective method of comparing the change over time between conditions. In control samples, the histogram peaked tightly around 1 with a Gaussian distribution. As time passed, the ratios were not grouped as tightly but collapsed towards 0 (Figure 2.23B, green). Depletion of PPP1CB had very little effect on bulk dephosphorylation over time (Figure 2.23C, compare green and blue). This would suggest that PPP1CB was not acting on a large number of substrates during mitotic exit and this is consistent with phenotype data (Zeng et al., 2010a; Takaki et al., 2017). However, depletion of PPP1CA/C drastically altered this behaviour (Figure 2.23B, compare green and orange) with a large spread of ratios, many still at or above 1, at the conclusion of the experiment. This shows that a large number of dephosphorylations during mitotic exit are dependent on the activity of PPP1CA/C. As this experiment was carried out *in vivo* it cannot be immediately claimed that any of these phospho-sites are direct PP1 substrates, due to the activity of other phosphatases such as PP2A-B55. It can, however, be assumed the contribution of proteolysis to this was minimal. These results highlight the global importance of PPP1CA/C function during mitotic exit.

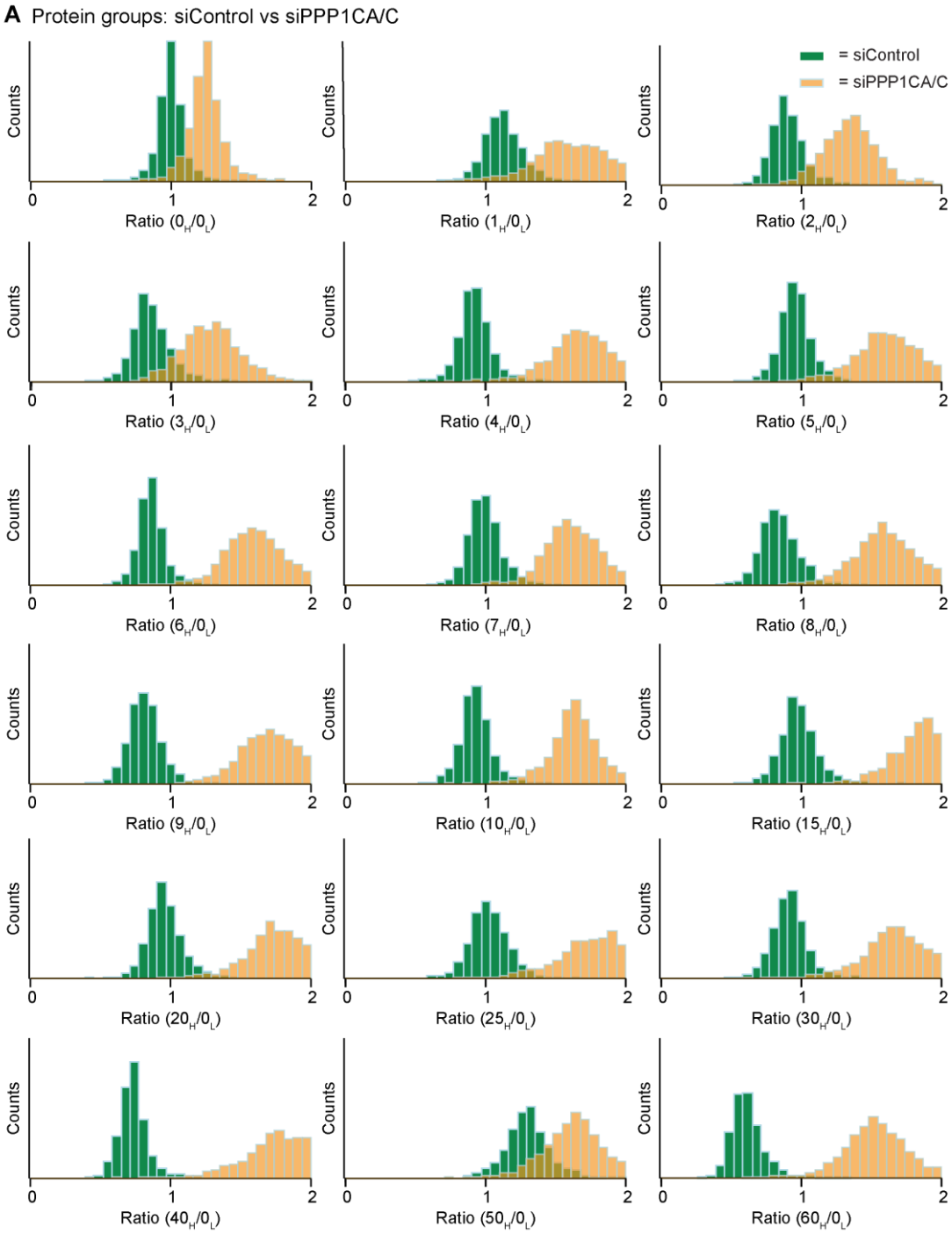


Figure 2.23 Histograms help visualise trends within large proteomic data sets

Samples from Figure 2.21 were prepared for mass spectrometry, Methods 4.6.1-3, and analysed as in Methods 4.7.1. (A) Quantitative ratios for the 3900 protein groups identified for control and PPP1CA/C depletion. Quantitative ratios for the >10,000 phospho-peptides, (B) PPP1CA/C- or (C) PPP1CB-depleted cells. Data was filtered for potential contaminants and false positives prior to this analysis.

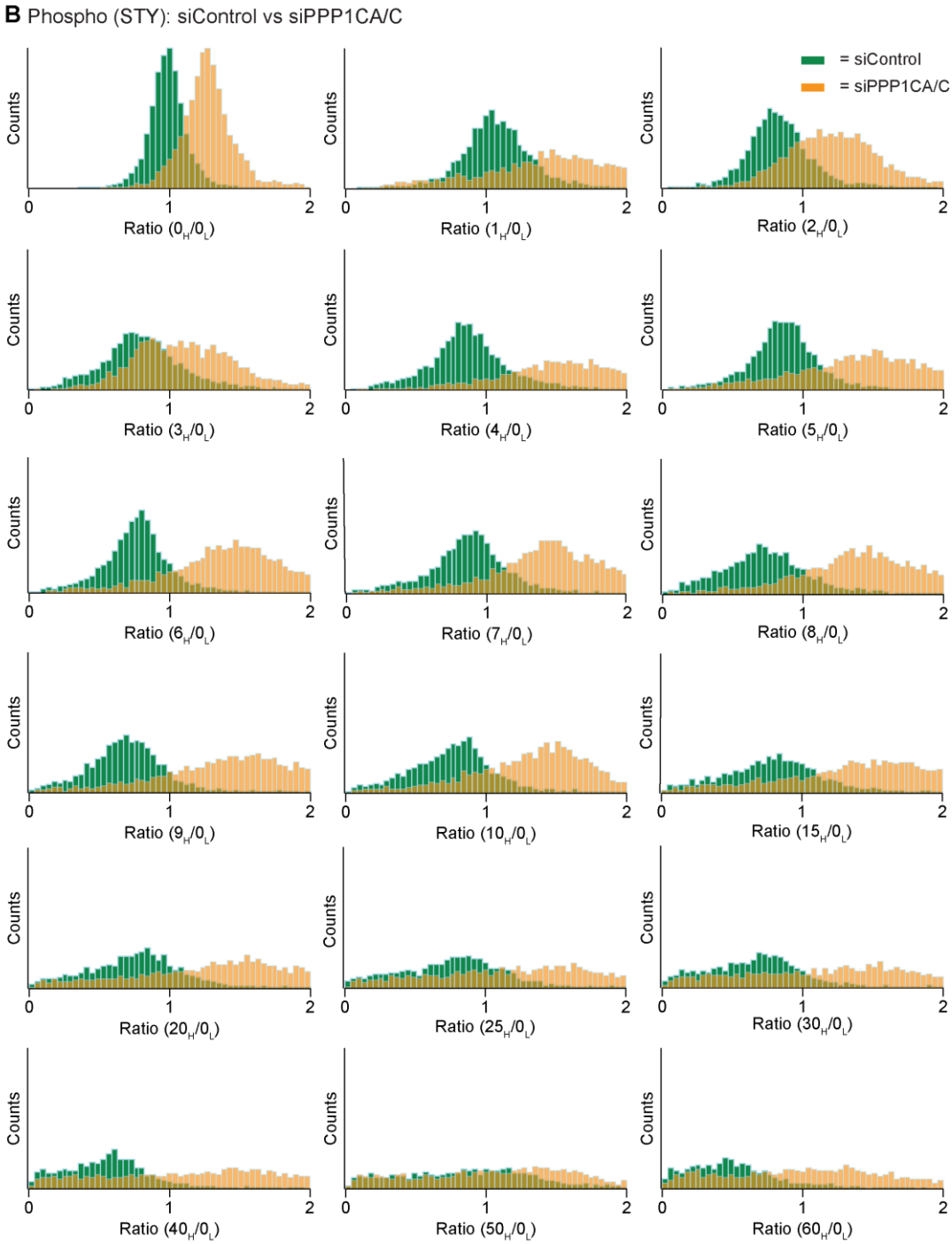


Figure 2.23 Histograms help visualise trends within large proteomic data sets (continued from previous page)

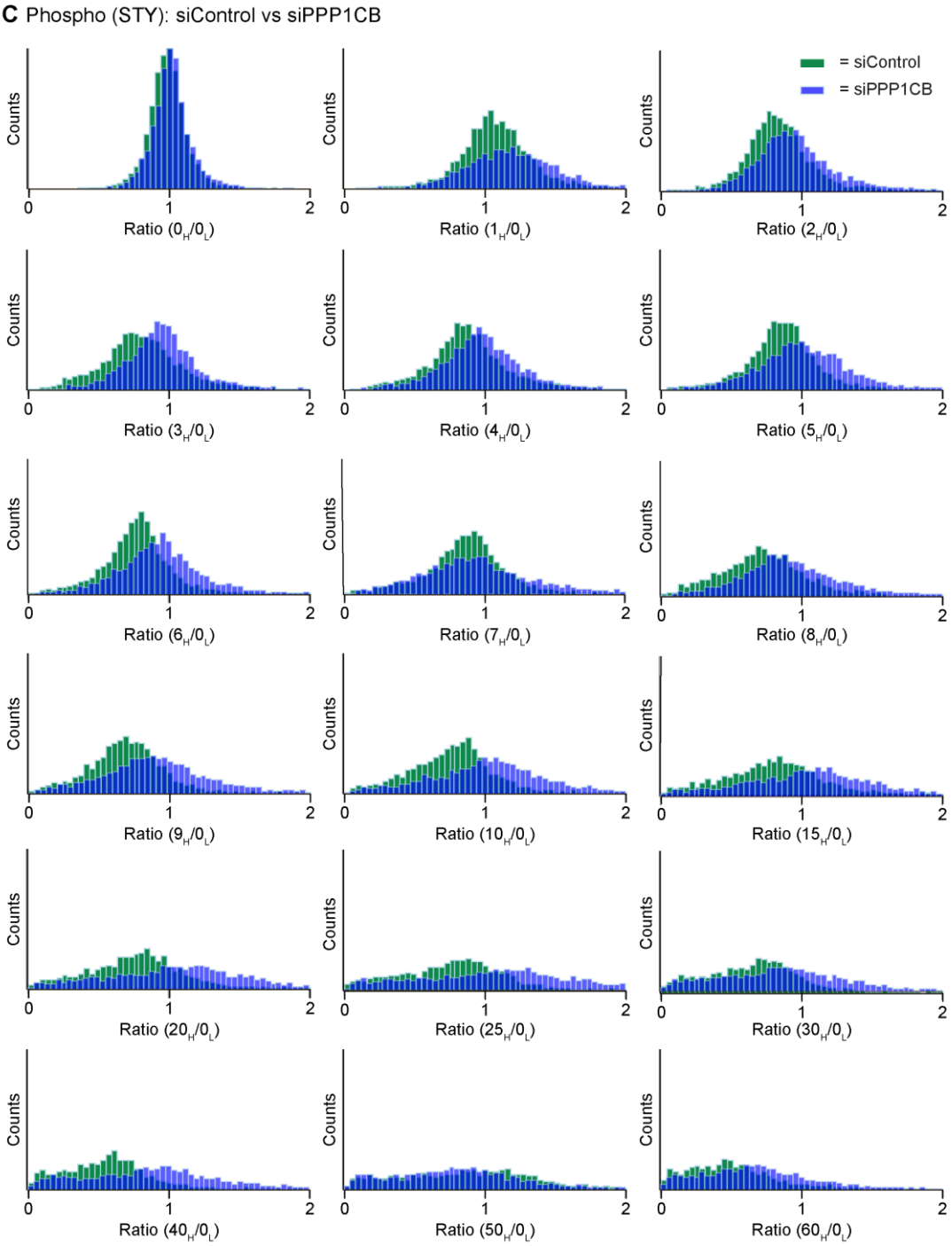


Figure 2.23 Histograms help visualise trends within large proteomic data sets (continued from previous page)

To identify PP1-dependent substrates, the behaviour of each phospho-site in control and depletion were clustered, as described previously (Methods 4.7.1). The average half-lives were calculated and compared to identify clusters containing potential substrates. Clusters where phospho-site half-life in the depleted condition was deemed longer than that of control were taken forward for further analysis. The clustering analysis of PPP1CB depletion and control was empirically found to require ten clusters (Figure 2.24A). However, only one of these clusters was found to have siPPP1CB half-lives that differed by more than 25% from the control conditions (Figure 2.24A and C). When looking at the sites contained within this cluster, very few showed a clear difference between the two conditions. It is likely that variation and noise in the data was the major contribution to the different half-lives observed. This supports a predominantly non-mitotic role for PPP1CB. The clustering comparison of control and PPP1CA/C required seven clusters, five of which were found to show a longer half-life following depletion (Figure 2.25A). These half-lives were all doubled or extended to beyond the window of the experiment. This more obvious effect was much more indicative of mitotic function than the data for PPP1CB. Furthermore, these clusters corresponded to nearly all of the non-stable phospho-sites used for the clustering analysis, a large number of which appeared to show different kinetics in the two conditions. The sequence characteristics of these clusters followed the trends observed previously (Figure 2.25B and 2.7). The more rapidly dephosphorylated PPP1CA/C-dependent phospho-sites were seen to have strong enrichment of phospho-threonine and de-enrichment of acidic residues (Figure 2.25B, Early). Conversely the less rapidly changing sites showed little sequence selection characteristics except for a mild de-enrichment of phospho-threonine.

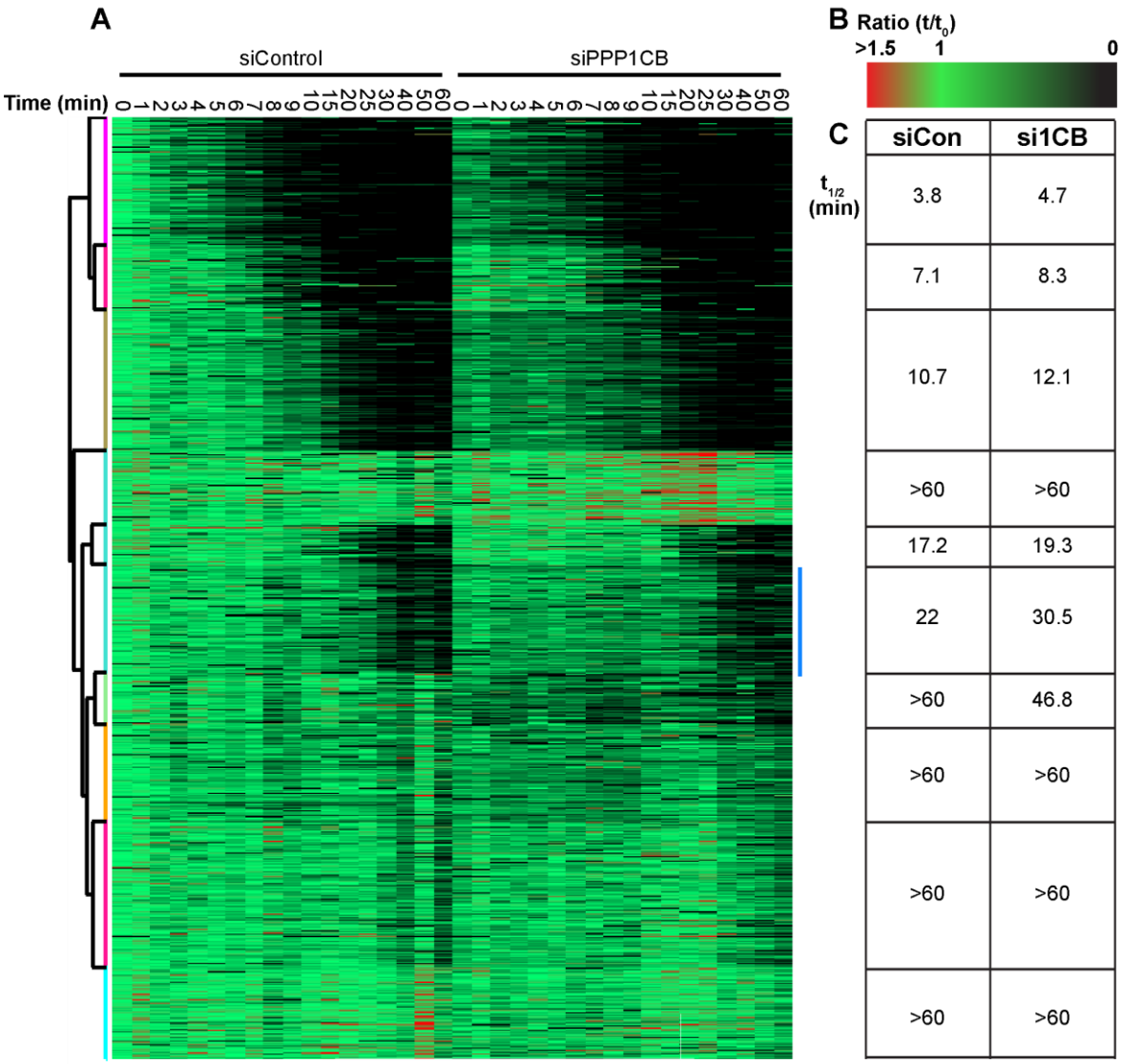


Figure 2.24 PPP1CB has a limited role in the regulation of mitotic exit

A) Clustering heat-map comparing the changes in phosphorylation over time in control and PPP1CB-depleted cells following CDK inhibition. Times shown are in minutes. Clusters where the average siPPP1CB half-life is >25% more than that of the siControl are marked with a blue line to the right of the heatmap. (B) Key linking heatmap colour with observed MS ratio. (C) The average half-life of a phospho-site for siControl and siPPP1CB are adjacent to their respective cluster.

Due to the number of potential PP1 holoenzymes in the cell the sequence characteristics seen here were indicative of the general preferences of PP1 catalytic subunits. This shows that the preference for phospho-threonine in the

absence of negative charge may be a general property of PPP holoenzymes not just PP2A-B55. This is unsurprising given the conservation surrounding the active sites of PPPs (Barr et al., 2011). Following this, phospho-sites with a siPPP1CA/C half-life which showed an increase of less than 50% over the control condition were discarded, as were overly noisy data. After this filtering, 1129 potential PPP1CA/C-dependent dephosphorylation events during mitotic exit remained. There are ~50,000 phosphorylations in a human cell, across all cell cycle stages (Marx et al., 2013). It is therefore probable that the ~17,000 phospho-sites identified here correspond to a large proportion of the mitotic phosphorylations. This suggests that the actual number of PPP1CA/C-dependent dephosphorylations is somewhat greater, highlighting just how important PPP1CA/C function is to proper mitotic exit.

There were several PPP1CA/C-dependent phospho-sites identified on SAC and APC/C proteins, which could be involved in APC/C activation (Figure 2.26A). Furthermore, phospho-sites on several cytokinesis factors were also seen to be dependent on PPP1CA/C (Figure 2.26B). These groups included PP2A-B55 substrates such as MPS1-pS281 and PRC1-pT481 (Figure 2.26C-D). However, many of these sites were not known PP2A-B55 substrates. This included several phosphorylations on an APC/C subunit, CDC27 (Figure 2.26A and F). Interestingly, BUB1-pS459 was also identified as a PPP1CA/C-dependent phospho-site. This site has been shown to be part of a sequential phosphorylation cascade that promotes MCC formation (Figure 2.26E) (Ji et al., 2017). In particular, pS459 primes BUB1 for phosphorylation by MPS1 at T461, which subsequently promotes formation of the MCC. It could be hypothesised that in the

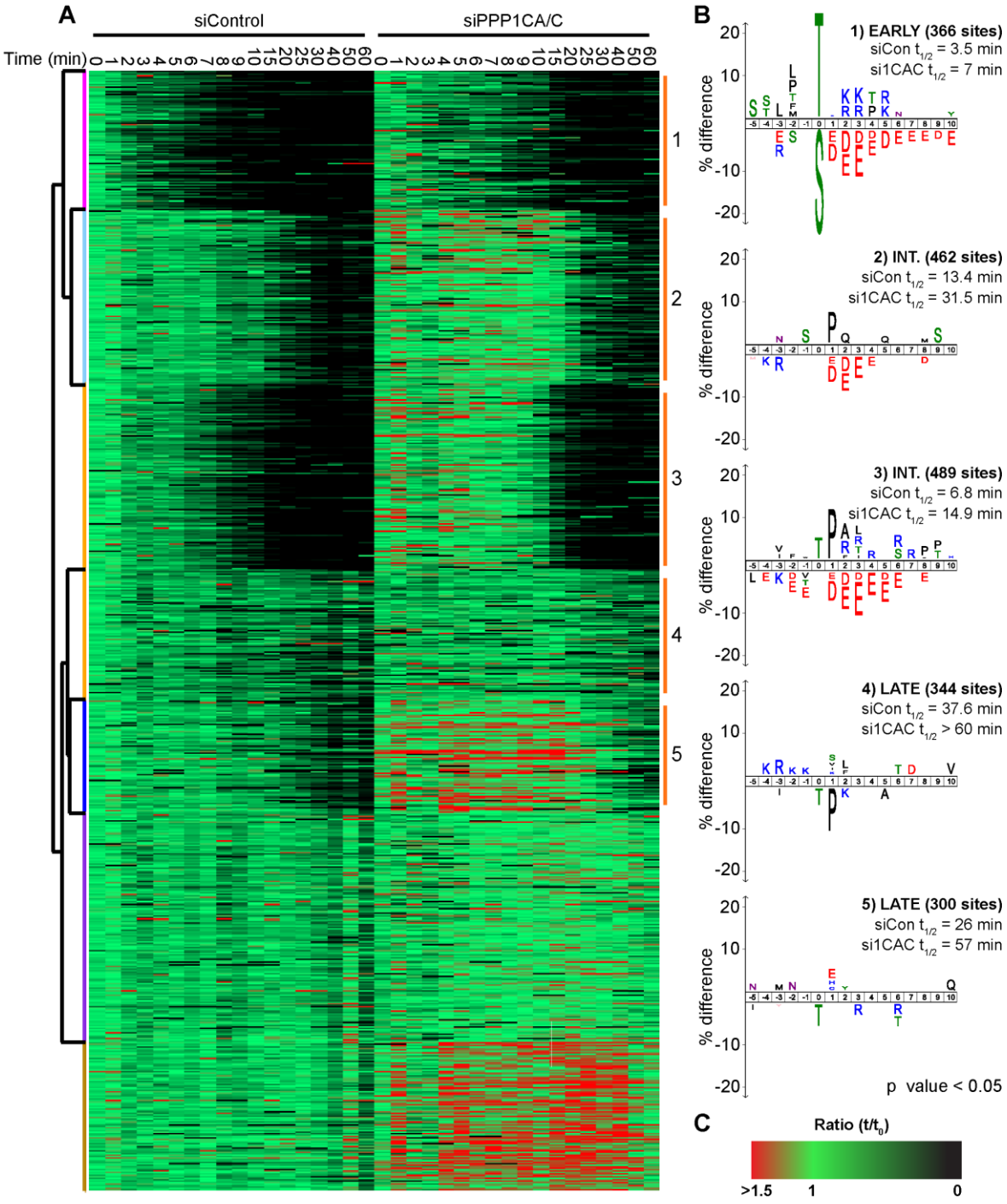


Figure 2.25 Many dephosphorylations are dependent on PPP1CA/C activity during mitotic exit

A) Clustering heat-map comparing the trends in phosphorylation over time in control and PPP1CA/C-depleted cells following CDK inhibition. Times shown are in minutes. Clusters where the average siPPP1CA/C half-life is >25% more than that of siControl are marked with an orange line to the right of the heatmap. The number of sites and the average

phospho-site half-life in each condition is indicated. C) Key linking heatmap colour with observed MS ratio.

absence of PPP1CA/C this site is removed more slowly upon kinetochore attachment, meaning that checkpoint reactivation is possible for longer. Whether this could account for the observed delay seen in APC/C activation upon PPP1CA/C depletion is unclear. Regardless, it is apparent that removal of the CDK1-dependent inhibition of the APC/C is dependent on PPP1CA/C.

2.3.2 Understanding the mitotic regulation of PP1

Given this apparent role of PPP1CA/C in APC/C activation following checkpoint silencing described above, it becomes important to understand more fully the CDK1-dependent inhibition of PP1 during mitosis. All three isoforms are thought to be phosphorylated by CDK1 at a conserved TP motif in the C-terminus, PPP1CA-pT320/PPP1CB-pT316/PPP1CC-pT311 (Figure 2.27A). To confirm that PP1 phosphorylation peaks during mitosis, GFP-tagged PPP1C subunits were immuno-precipitated from HeLa cells in different stages of the cell cycle and analysed by mass spectrometry (Methods 4.5 and 4.6.6). As expected, phosphorylation of both PPP1CA and PPP1CB was low in S phase, peaked in mitosis and decreased in anaphase (Figure 2.27B) (Methods 4.7.3). Unfortunately, PPP1CC-pT311 was not detected, likely due to the presence of additional basic residues close to the phospho-site (Figure 2.27A). These are cleavable by both Lys-C and trypsin and could potentially generate a peptide too small for detection by mass spectrometry. Nevertheless, these data are consistent with PP1 being phosphorylated during mitosis in a CDK-dependent manner.

A

SAC and APC/C	
Gene names	Phospho-residue
BUB1	459
BUB1	593
BUB1	596
BUB1	655
KNL1	1076
KNL1	539
KNL1	1773
CDC27	426
CDC27	434
CDC27	435
CDC27	438
CDC27	446
DSN1	30
DSN1	27
SPAG5	62
SPAG5	65
SPAG5	66
MPS1	281
MPS1	33

B

Cytokinesis factors	
Gene names	Phospho-residue
ANLN	320
ANLN	323
ANLN	364
ANLN	397
ANLN	401
ANLN	449
ANLN	485
ANLN	54
ANLN	927
ARHGEF2	163
ECT2	716
ECT2	861
ECT2	866
FHOD1	498
HAUS6	507
KIF23	450
KIF4A	1186
PRC1	470
PRC1	481
RACGAP1	628

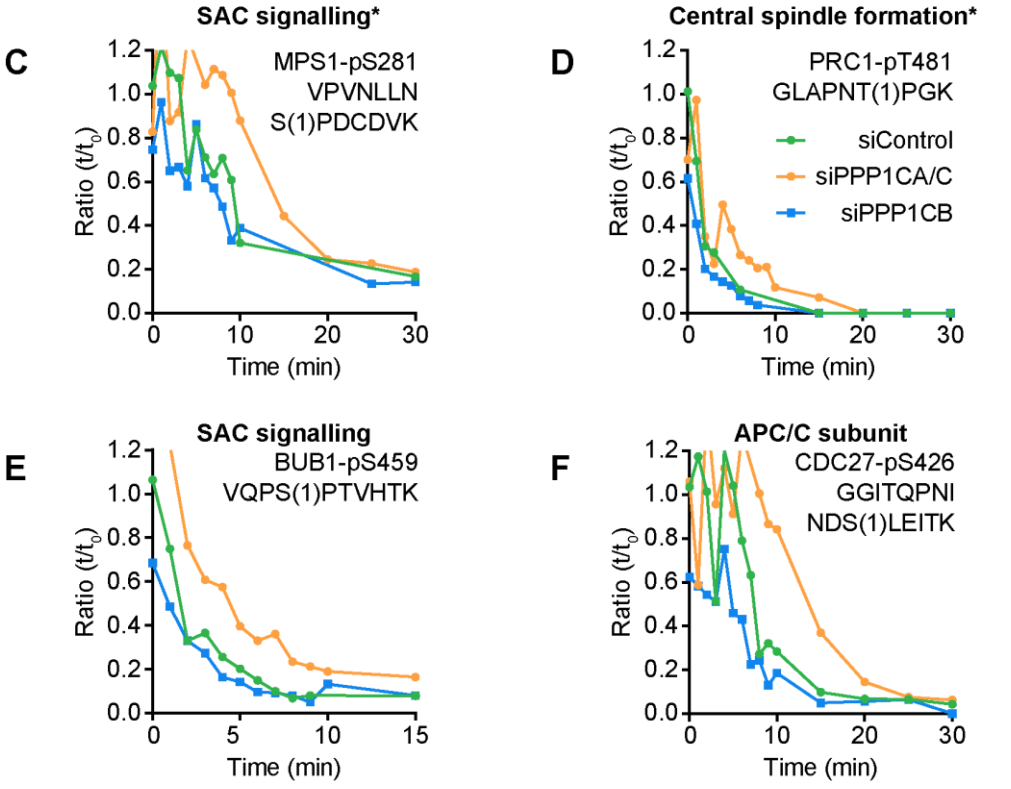


Figure 2.26 PPP1CA/C-dependent dephosphorylations include sites involved in regulation of mitotic exit

Identified PPP1CA/C-dependent dephosphorylations which are present on proteins involved in (A) Spindle assembly checkpoint (SAC) signalling and APC/C activity or (B)

cytokinesis. (C-F) Quantitative ratios of selected PPP1CA/C-dependent phospho-sites following CDK inhibition. The phosphorylated sequence observed is shown, with (1) denoting the phosphorylated residue. The protein function is stated above the graph. Asterisk indicates known PP2A-B55 substrates.

While testing the GFP-PPP1C constructs it became clear that the phospho-specific PPP1CA-pT320 antibody being used also detected PPP1CB-pT316 (Figure 2.27C). This was hardly unexpected given the sequence similarity surrounding the phospho-site (Figure 2.27A). Nevertheless, it was important to see whether these two phospho-sites would show similar changes during mitotic exit, so these sites were mined from the mass spectrometry data generated for Figure 2.7. Both sites can be seen to be dephosphorylated rapidly upon CDK inhibition (Figure 2.27D). However, based on the quantitative ratios it appeared that PPP1CA-pT320 was dephosphorylated more rapidly (Figure 2.27D). PPP1CB-pT316 had more of the characteristic tail of residual phosphorylation, as seen by Western blot (Figure 2.27D and 2.2). However, proteomic data would suggest that PPP1CB is roughly three times more abundant than PPP1CA (Cundell et al., 2016), and over ten times more than PPP1CC. Consistently, the intensity of the ‘heavy’ labelled PPP1CB-pT316 at 0 min was nearly three times more than that of PPP1CA-pT320 (Figure 2.27E). This difference remained constant throughout all timepoints where both phospho-sites were detected. The intensity of ‘heavy’ labelled PPP1CA-pT320 fell close to the detection limit of the MS within the first few minutes (Figure 2.27E). Consequently, these intensity measurements and the calculated ratios become less accurate. As such, a residual tail of 10-20% pT320 which is dephosphorylated slowly would fall below the detection threshold of the instrument. Furthermore, when using MPS1

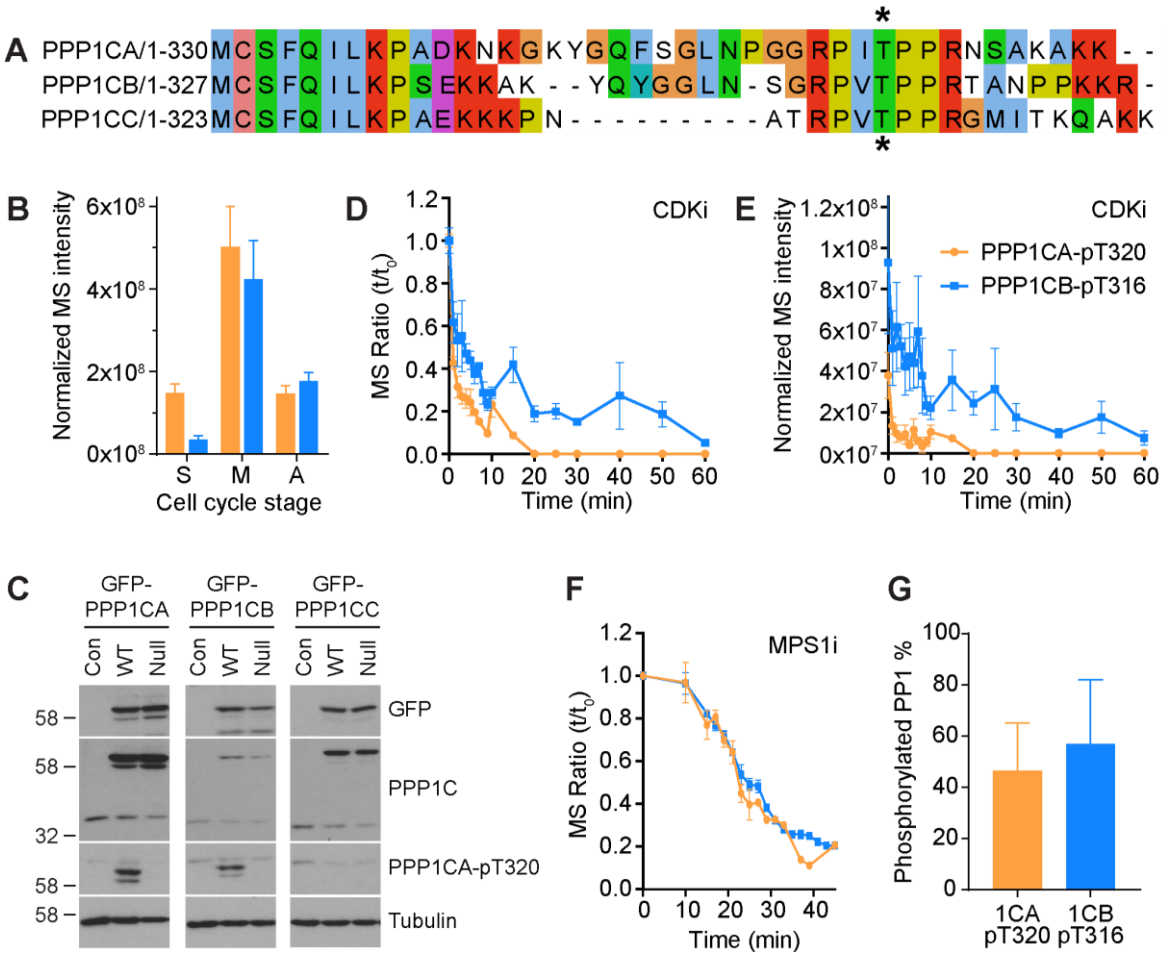


Figure 2.27 CDK1 phosphorylation of PP1 peaks during mitosis and is rapidly removed upon mitotic exit

(A) Alignment of the C-terminus of the three PP1 catalytic subunit isoforms found in *Homo sapiens*, asterisk marks the site of CDK phosphorylation. (B) Expression of GFP-PPP1C subunits was induced in HeLa-FRT cells prior to being synchronised in different cell cycle stages. Immuno-precipitated samples were analysed by mass spectrometry to find the intensity of PP1 phospho-peptides (mean±SEM, n=3). Intensities were normalised based on the level of non-modified PP1 peptides detected, Methods 4.7.3. (C) HeLa cells were transfected with empty vector (Con), wild type (WT) or CDK1 phospho-null mutant (Null) GFP-PPP1C subunits for 24 hr, synchronised with 2.5 mM thymidine and released. Cells were harvested 10 hr later. PPP1C indicates Western blot samples were probed with the respective isoform specific antibody. (D) Quantitative ratio or (E) 'heavy' labelled peptide intensity of PPP1CA/B CDK1 phosphorylation over time following CDK inhibition (CDKi), (mean±SEM, n=4). (F) Quantitative ratio of PPP1CA/B CDK1 phosphorylation following MPS1 inhibition (MPS1i), (mean±SEM, n=2). (G) Percentage stoichiometry of PPP1CA/B CDK1 phosphorylation during mitosis, calculated as in Methods 4.7.2 (mean±SEM, n=3). Proteomic data from Figure 2.7D, E and G and Figure 2.9F. For all graphs here PPP1CA-pT320 is shown in orange and PPP1CB-pT316 in blue.

inhibition to trigger mitotic exit, these two sites behaved almost identically (Figure 2.27F). From this it can be concluded that both PPP1CA and PPP1CB are rapidly dephosphorylated at a similar rate during mitotic exit, with half-lives of 23 and 24.5 min, respectively, following MPS1 inhibition.

The stoichiometry of a phosphorylation may have important implications for its dephosphorylation and can be a useful indicator here as to whether all PP1 is inhibited or only a portion of it. An attempt was therefore made to calculate this based on the change in the 'heavy' labelled non-phosphorylated form of the peptide over time using data from Figure 2.7 (Methods 4.7.2). Stoichiometry is difficult to measure accurately, especially when inferred from the levels of non-phosphorylated peptide, and the results obtained were highly variable. However, it can be concluded that not all PP1 was phosphorylated in mitosis, achieving only ~50% stoichiometry. This is consistent with previously published data (Sharma et al., 2014). While extra work is required to obtain a more reproducible stoichiometry measurement, these results show, as has been previously suggested, that some PP1 has the potential to be active during mitosis (Liu et al., 2010; Moura et al., 2017; Vanoosthuyse and Hardwick, 2009; Winkler et al., 2015).

While it is thought that PP1 can auto-dephosphorylate and thus self-activate upon mitotic exit, this has not yet been shown conclusively in human cells (Cundell et al., 2013; Cundell et al., 2016; Wu et al., 2009; Dohadwala et al., 1994; Yamano et al., 1994). A selective small molecule inhibitor of PP1, tautomycetin (TMC), was used to test this idea. TMC has been shown to inhibit PP1 ~40 times more effectively than PP2A (Mitsuhashi et al., 2001), and has been used at micro-molar concentrations to specifically inhibit PP1 in cells (Mitsuhashi et al., 2003). Therefore, HeLa cells were arrested in mitosis and 5 µM TMC was added during

the 25 min release from nocodazole prior to CDK inhibition. Under control conditions, the majority of the PPP1CA-pT320 signal was rapidly lost, with some residual phosphorylation remaining as the rate slowed over time, resembling an exponential decay (Figure 2.28A and C). PRC1-pT481 and CCNB1 levels were consistent with previous observations (Figure 2.2A and D; Figure 2.7E; Figure 2.28A). The addition of TMC resulted in a strong retention of PPP1CA-pT320, with approximately 70% remaining at the end of the experiment (Figure 2.28B-C). PRC1-pT481 dephosphorylation was also slowed but not to the same extent. If TMC was inhibiting PP2A directly, a larger delay would be expected. This delay is more consistent with PP1 inhibition preventing efficient inactivation of MASTL and the subsequent activation of PP2A-B55, following CDK inhibition. These results are consistent with the published literature and support a model wherein PP1 auto-dephosphorylates itself upon inactivation of CDK1 (Wu et al., 2009). The addition of TMC also delayed degradation of CCNB1, providing further confirmation of the role of PP1 in APC/C activation (Figure 2.28A-C).

Despite the high-resolution used during these timecourse experiments, dephosphorylation of PP1 occurred too rapidly to be able to extract much detail from the early timepoints. Therefore, HeLa cells were synchronised as previously, with the exception that the cells were incubated on ice 10 min prior to CDK inhibition. This was done to slow down the reaction sufficiently to get a clearer view of the early kinetics of this dephosphorylation. On ice about 80% of PPP1CA-pT320 was dephosphorylated in 60 min, compared to approximately 7-8 min at 37°C (Figure 2.27C, E and F). Both on ice and at 37°C, the rate of dephosphorylation gradually decreased over time (Figure 2.27C and F). If the

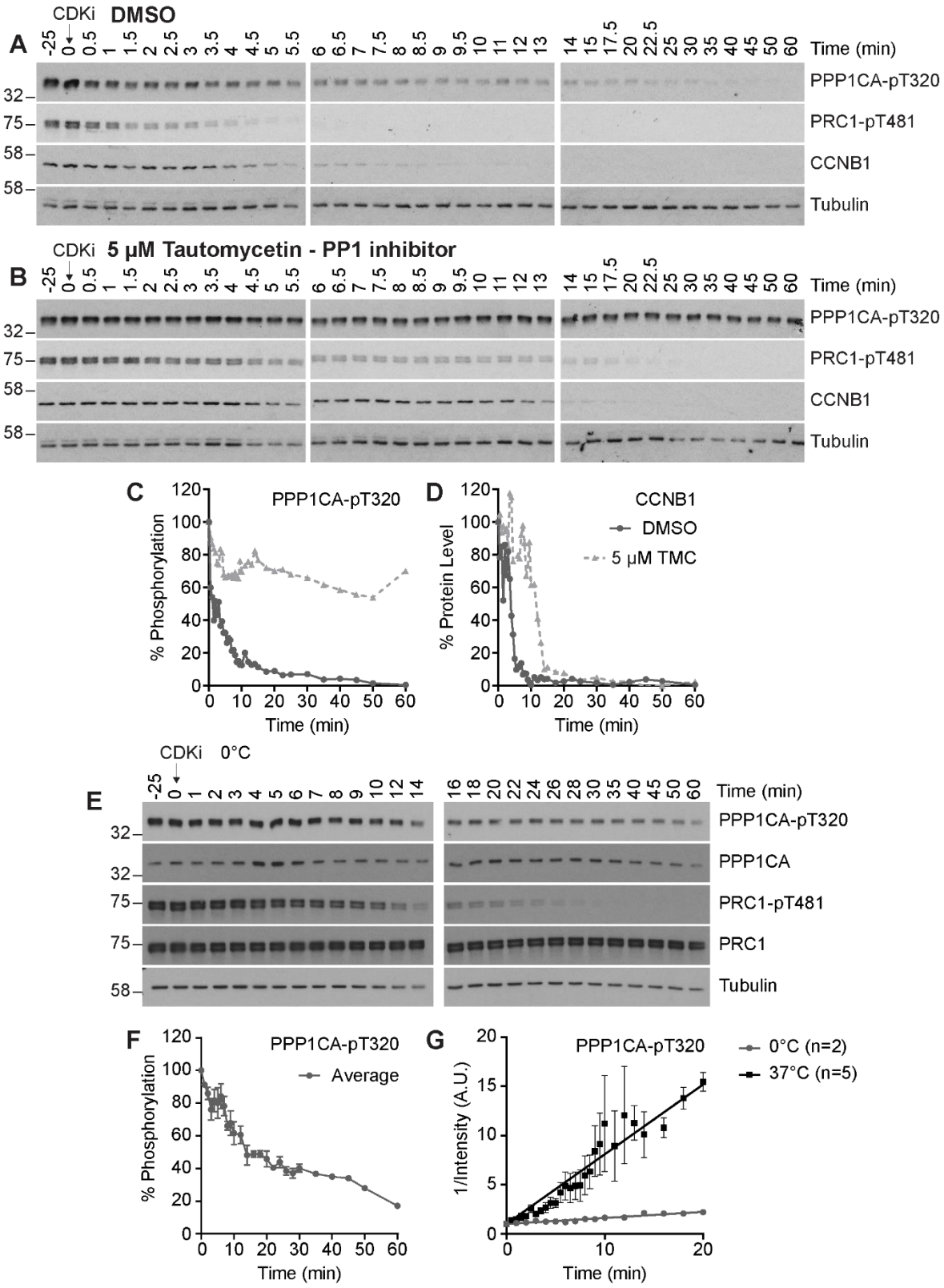


Figure 2.28 PP1 is auto-dephosphorylated upon loss of CDK1 activity

HeLa cells were arrested in mitosis and incubated for 25 min with either (A) DMSO or (B) PP1 inhibitor, 5 µM tautomycetin (TMC). CDK was inhibited and cells sampled at the times indicated. Densitometric quantification of samples from (A) and (B), is shown in (C)

PPP1CA-pT320 and (D) CCNB1. (E) HeLa cells were arrested in mitosis, as previously described, and placed on ice 10 min prior to CDK inhibition. Cells remained on ice for the duration of the experiment. (F) Densitometric quantification of samples from (E) (mean±SEM, n=2). (G) Inverse of the PPP1CA-pT320 signal intensity at 0°C and 37°C. (A) is representative of timecourses carried out at 37°C.

inverse of the pT320 signal is plotted, it fits a straight line at both 4°C and 37°C, indicative of a 2nd order reaction (Figure 2.28G). This perhaps suggests that two phosphorylated molecules of PP1 work to dephosphorylate each other in *trans*. This would explain the rapid initial rate of dephosphorylation which then slowed as the concentration of both reactants, phosphorylated PP1, decreased.

One further question remains concerning the mitotic regulation of PP1: does phosphorylation of PP1 itself affect its ability to interact with binding partners during mitosis and mitotic exit? HeLa FRT cell lines expressing either inducible GFP tagged wild type or CDK1 phospho-null mutant PPP1C subunits were generated and then imaged during mitosis (Figure 2.29). Consistent with published data, all three isoforms were predominantly nuclear during interphase, with PPP1CB and PPP1CC showing enrichment in the nucleoli (Figure 2.29). This behaviour was unaltered by mutation of the CDK1 site, which was unsurprising given that this phosphorylation is mitosis-specific. During mitosis, PPP1CA was enriched around the chromatin, potentially at the site of microtubule attachments (Figure 2.29A, top). As cells exited mitosis, PPP1CA remained at the chromatin before also localising to the central spindle. PPP1CB showed weak chromatin localisation in mitosis, which increased as the cells entered anaphase. It could also be seen to enrich weakly around the cortex and midbody (Figure 2.29C, top). PPP1CC was mainly cytoplasmic during mitosis before becoming enriched on

chromatin during mitotic exit. This is consistent with its proposed anaphase functions (Figure 2.29E, top) (Vagnarelli et al., 2011). Both PPP1CB and PPP1CC were incorporated into the newly formed nucleoli later in telophase. The behaviour of the PPP1C subunits was unaffected by mutation of the CDK1 site (Figure 2.29A, C and E, bottom). Furthermore, the timing of chromosome separation and cytokinesis was similar across the different cell lines. This would imply that the phospho-null mutants were not prematurely- or hyper-active during early anaphase. One conclusion might be that under normal conditions, dephosphorylation and activation of PP1 began prior to degradation of sufficient CCNB to trigger chromosome separation. This is consistent with the sensitivity and rapid response of PP1 to CDK inhibition. Additionally, dephosphorylation of PP1 may not be sufficient to trigger further dephosphorylations, requiring the binding of a regulating subunit. These modes of regulation need not be mutually exclusive.

It has been proposed that the interaction between PP1 and its binding partners is negatively regulated in mitosis, meaning that PP1 would need to rebind interaction partners following anaphase onset. It is not known if this is a general principle of PP1 regulation or only true of a specific subset of interactors. Inducible GFP-tagged PPP1C isoforms were expressed in HeLa-FRT cells (Figure 2.30A), with transfected GFP used as a control. These were immuno-precipitated from cell populations in three different cell cycle states: S phase following a thymidine arrest; metaphase from a nocodazole arrest and 25 min wash out; and an anaphase population treated with MPS1 inhibitor for 30 min following the nocodazole wash out (Figure 2.30A) (Methods 4.5). The use of a GFP pull-down

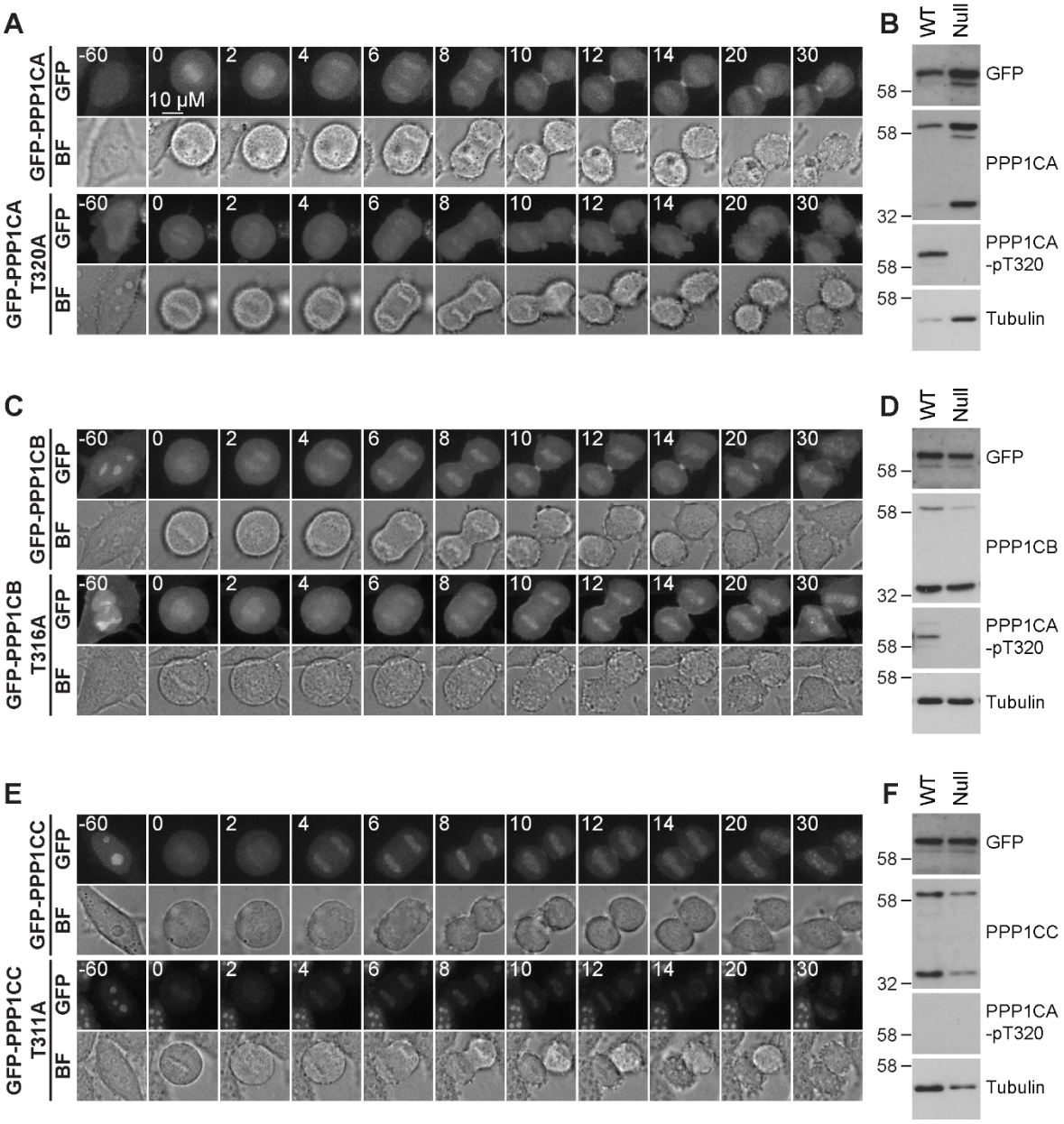


Figure 2.29 CDK1 phosphorylation does not alter the localisation of PP1 during mitosis

Expression of either wild-type (WT) of CDK1 phospho-null mutant (Null) GFP-PPP1C subunits was induced in HeLa-FRT cells for 20 hr. Cells were synchronised with 2.5 mM thymidine and released for 9 hr prior to the start of imaging either (A) PPP1CA, (C) PPP1CB or (E) PPP1CC subunits. Alternatively, cells were arrested in mitosis, using nocodazole, and harvested for Western blot for validation of (B) PPP1CA, (D) PPP1CB and (F) PPP1CC cell lines. Images shown are maximum intensity projections.

ensured specific PPP1C subunits were isolated, which is not trivial given the sequence similarity between the isoforms (Figure 2.30B). CCNB1 and tubulin blots confirmed the loading and cell cycle stage of each sample. SDS22 was seen to interact with all three PP1 isoforms, consistent with its proposed role as a chaperone (Figure 2.30B) (Cheng and Chen, 2015). Known PPP1CA and PPP1CB interactors, phostensin and MYPT, were seen to interact specifically with their respective binding partners. These validated samples were then prepared for mass spectrometry using filter assisted sample preparation (FASP) (Methods 4.6.6). The raw data were analysed as described in Methods 4.7.3. The average intensities of identified proteins in control and GFP-PP1 samples were plotted (Figure 2.30C-E). Many proteins were seen to be enriched over control, with several not being identified in the control sample at all (Figure 2.30C-E, dots lying on the y-axis). Proteins with over 100-fold enrichment in intensity over the control, when averaged across all samples, were deemed significant interactors for that particular PP1 isoform (Figure 2.30C-E). The enrichment factor and the isoform specificity are detailed in Figure 2.31A. To ensure that there was no bias against less abundant proteins a volcano plot analysis was carried out; this did not reveal any interactors previously unidentified in this experiment (not shown) (Methods 4.7.3). The proteins seen to have a 10-fold enrichment over control and a p value of <0.05 were clustered to identify trends in behaviour during the cell cycle, with example patterns of interaction shown in Figure 2.31C (Methods 4.7.3). This analysis showed that the majority of identified interactors bound with similar effectiveness to PP1 in all cell cycle stages (Figure 2.31D-F). While there were small changes in behaviour between cell cycle stages, these changes are not consistent with a binary mitotic regulation of PP1 holoenzymes. Interestingly,

some interactors seemed to show increased levels of interaction with PP1 during mitosis and anaphase (Figure 2.31D-F). Furthermore, statistical analysis of samples from the individual cell cycle stages did not reveal any cell-stage specific interactors that would have been overlooked by the previous analysis (data not shown). Most of the interactors identified had previously been seen to interact with PP1, often through similar proteomic screening. Various combinations of isoform specificity could be seen, with interactors binding to one, two or all three isoforms. This redundancy could explain why so few PPP1CB-dependent dephosphorylations were identified during mitotic exit (Figure 2.24). Nevertheless, it is clear that formation of PP1 holoenzyme complexes is not globally subjected to negative mitotic regulation.

Taken together these results show that PP1, in particular PPP1CA/C, is carefully positioned to play a central role in regulation of mitosis and mitotic exit. PPP1CA/C is involved in both the activation of the APC/C^{CDC20}, to trigger mitotic exit, and the subsequent dephosphorylation of many substrates. Furthermore, while CDK1 does phosphorylate PP1 during mitosis, this does not generally appear to interfere with its localisation or the ability of PP1 to interact with binding partners. Importantly, PP1 can auto-dephosphorylate this site, meaning its activity is directly linked to CCNB degradation rather than dependent on other enzymatic activities.

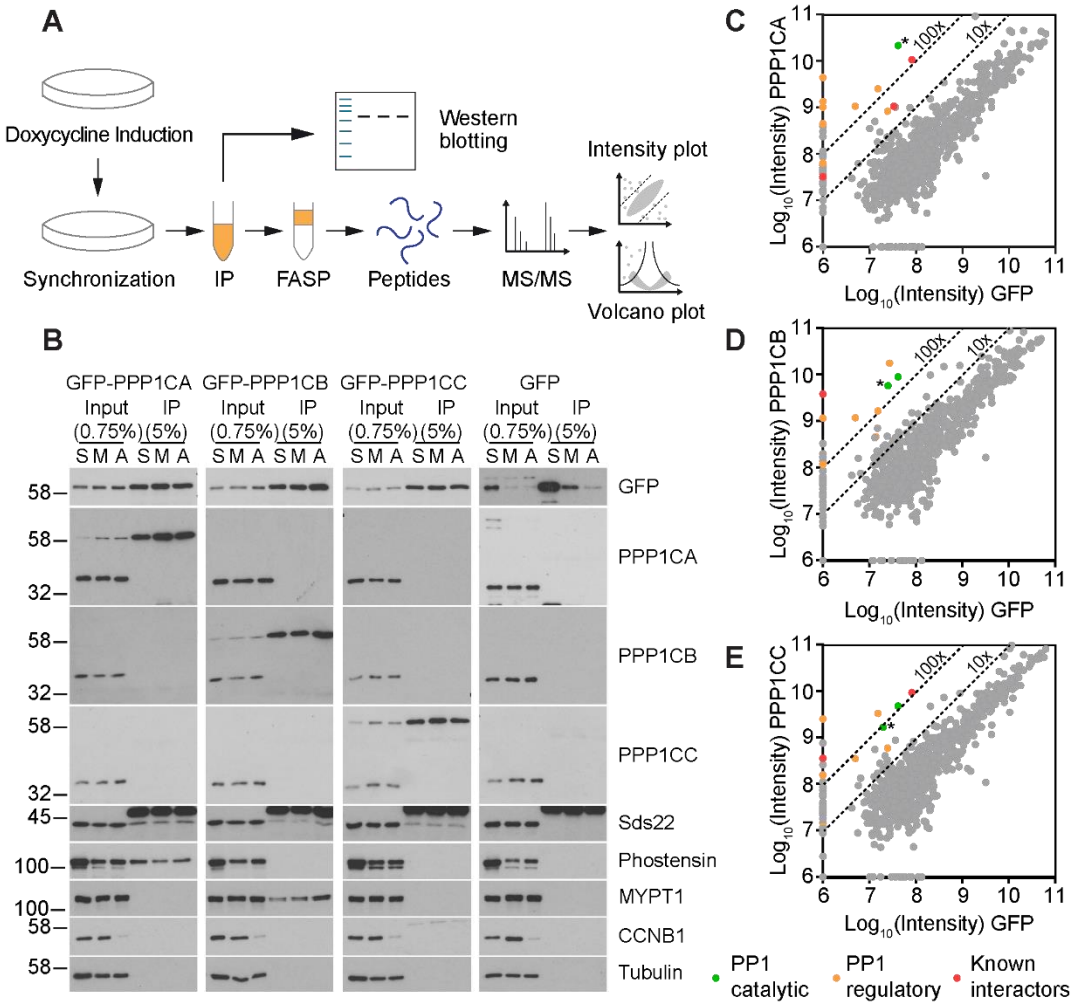


Figure 2.30 PP1 forms a variety of holoenzyme complexes

(A) Schematic outlining the cell culture, immuno-precipitation and mass spectrometry protocols. (B) Expression of GFP-PPP1C subunits was induced in HeLa-FRT cells prior to synchronisation in three cell cycle stages. GFP immuno-precipitations were used to pull down PP1 subunits for Western blot analysis. (C-E) Intensity plots from mass spectrometry analysis of the same samples. Each dot represents mean intensity across three repeats in all three cell cycle stages (n=9). All proteins must have been identified at least four times, each with three detected peptides, Methods 4.7.3. Asterisk marks the GFP-PP1 subunit used as bait. Cell cycle stages are denoted as S (S phase), M (metaphase) and A (anaphase).

A

	Gene Name	Alternative Name	Known Interactor	Fold Enrichment PPP1CA	PPP1CB	PPP1CC
Cat.	PPP1CA		-	519	214	115
	PPP1CB		-	1	230	1
	PPP1CC		-	2	1	85
1CA	CCDC85C		Y	306	6	9
	PPP1R18	Phostensin	Y	1028	1	1
	TOX4		Y	117	25	34
	TP53BP2	ASPP2	Y	1354	7	12
	TPRN		Y	118	1	1
1CB	H3F3A		N	1	171	1
	PPP1R12A	MYPT	Y	1	646	2
	RAI14		Y	1	200	1
	PPP1R38	SH2D4A	Y	33	3847	3
	SRRM1		N	22	121	58
1CC	ALPL		N	43	28	260
	CCDC85B		Y	17	9	158
A/C	NCOA5		Y	239	42	354
	YLPM1		Y	131	19	114
B/C	GSTP1		N	60	140	112
	H2AFX		N	37	117	83
All isoforms	NUCKS1		N	394	331	763
	PPP1R2	Inhibitor 2	Y	167	108	216
	PPP1R7	SDS22	Y	215	237	71
	PPP1R8	NIPP1	Y	4460	1161	2528
	PPP1R10	PNUTS	Y	453	118	155
	SLIRP		N	52	169	86

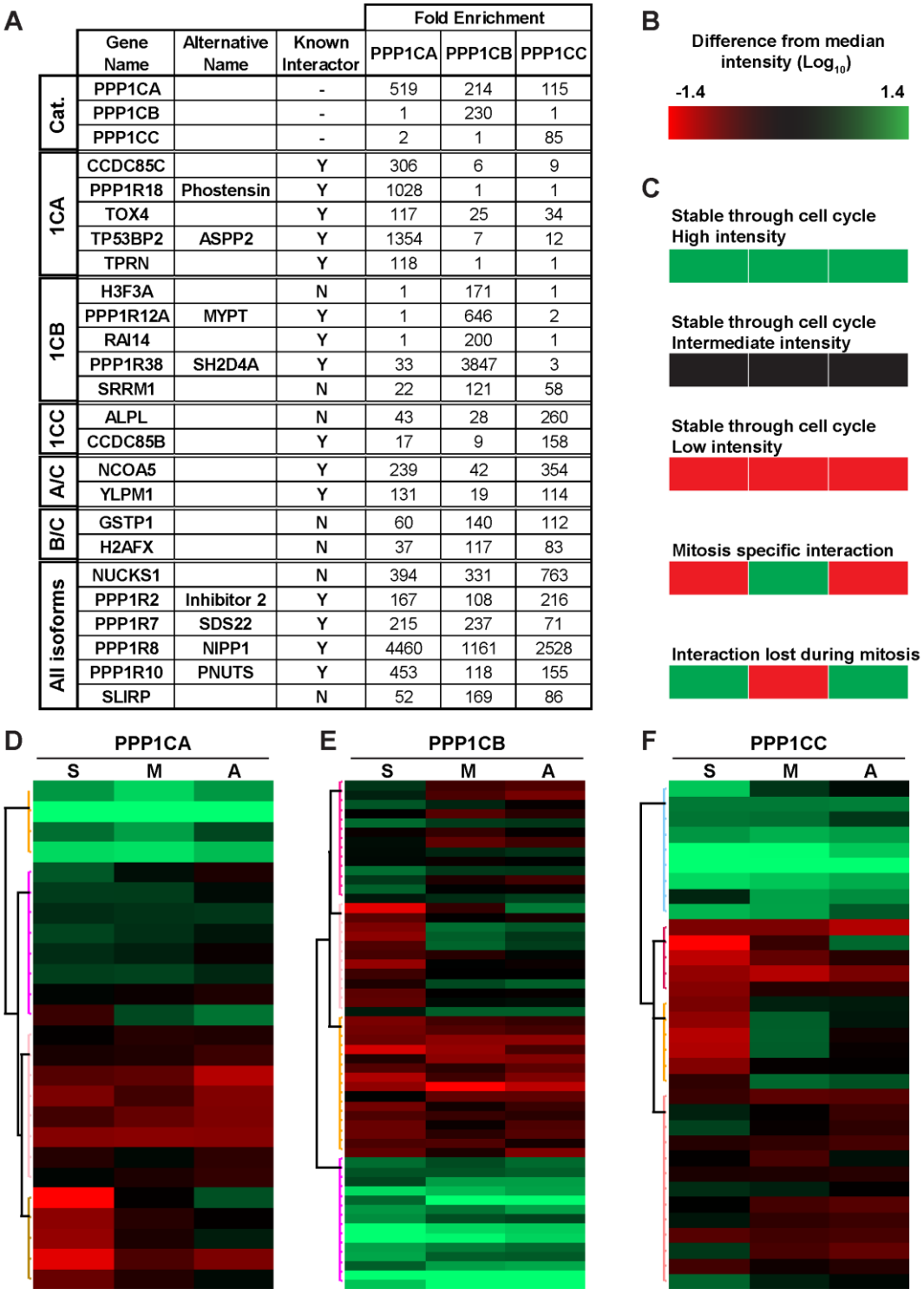


Figure 2.31 PP1 holoenzyme complexes do not generally dissociate during mitosis

(A) Mean fold enrichment of PPP1C interactors over control across all three cell cycle stages (n=9, 3 repeats across 3 stages). Only proteins with 100-fold enrichment with at least one PPP1C isoform are shown. (B) Key relating heatmap colour to difference from

median intensity of interactors. (C) Example patterns of interaction and their respective colour schemes. Clustering heatmap of interactors in each cell cycle stage for (D) PPP1CA, (E) PPP1CB and (F) PPP1CC. Data were analysed and clustered as described in Methods 4.7.3. Cell cycle stages are denoted as S (S phase), M (metaphase) and A (anaphase).

3 Discussion

For cells to exit mitosis correctly they must regulate protein activity through coordinated protein dephosphorylation and APC/C-mediated proteolysis. It is important to understand the relative contributions of these pathways since in many ways they are functionally equivalent. If a mitotic phosphorylation must be removed to inactivate a protein, it can be reversed either through phosphatase activity or destruction of the whole protein. A high-resolution analysis was used to clarify the regulatory principles that govern mitotic exit. The results presented suggest that ordered dephosphorylation, and not proteolysis, is the dominant mode of regulation during anaphase. Instead proteolysis is required to initiate anaphase through the destruction of CCNB. Moreover, the majority of the proteome was in fact stable during the window of anaphase examined, with only 10 proteins having a half-life of less than two hours. The broader implications of these findings, for the understanding of the cell cycle and the specific mechanisms which have evolved to regulate it, are considered below.

3.1 A cascade of dephosphorylations provide order to mitotic exit

The quantitative mass spectrometry analysis presented here suggests that regulated phosphatase activity co-ordinates the ordered progression of mitotic exit through sequential dephosphorylation of thousands of substrates. CDK1-mediated inhibition of the phosphatases PP1 and PP2A-B55 by different pathways, provides them with unique properties that ensure cells progress properly into the next cell cycle.

3.1.1 PP1 opposes its own CDK1-mediated inhibition

Exit from mitosis requires the regulated activation of two CDK1-inhibited phosphatases, PP1 and PP2A-B55. The indirect CDK1-mediated inhibition of PP2A-B55 is well understood and is responsible for the characteristic delay seen in its activation (Gharbi-Ayachi et al., 2010; Mochida et al., 2010). Ultimately this ensures that initiation of cytokinesis occurs after chromosomes have separated. Conversely, the direct inhibition of PP1 through direct CDK phosphorylation at T320 is less well characterised. Here the use of a specific PP1 inhibitor, tautomycetin, provides strong *in vivo* evidence that this inhibitory phosphorylation, PP1-T320, is removed by PP1 itself. Furthermore, the majority of PP1-T320 was dephosphorylated extremely rapidly upon CDK inhibition, highlighting a sensitivity to CDK activity and by extension the level of CCNB. Approximately 80% of PP1 was dephosphorylated in the first 8 min, at which point the rate rapidly diminished and the half-life increased accordingly. This would be inconsistent with a zero or first order reaction whereby a single molecule of PP1 dephosphorylates itself in *cis*. In fact, plotting the reciprocal of the PPP1CA-T320 signal intensity revealed that the early part of this timecourse was dominated by a rapid second order reaction before transitioning to slower kinetics (Figure 2.28G). The most parsimonious explanation for this would be that two phosphorylated molecules of PP1 interacted transiently to dephosphorylate one another in *trans* (Figure 3.1A). This would explain why PP1 dephosphorylation is rapid and then slows as the amount of PPP1CA-pT320 decreases but it does not explain what happens during the “slow” late phase of the reaction. A variation of this model would be that a

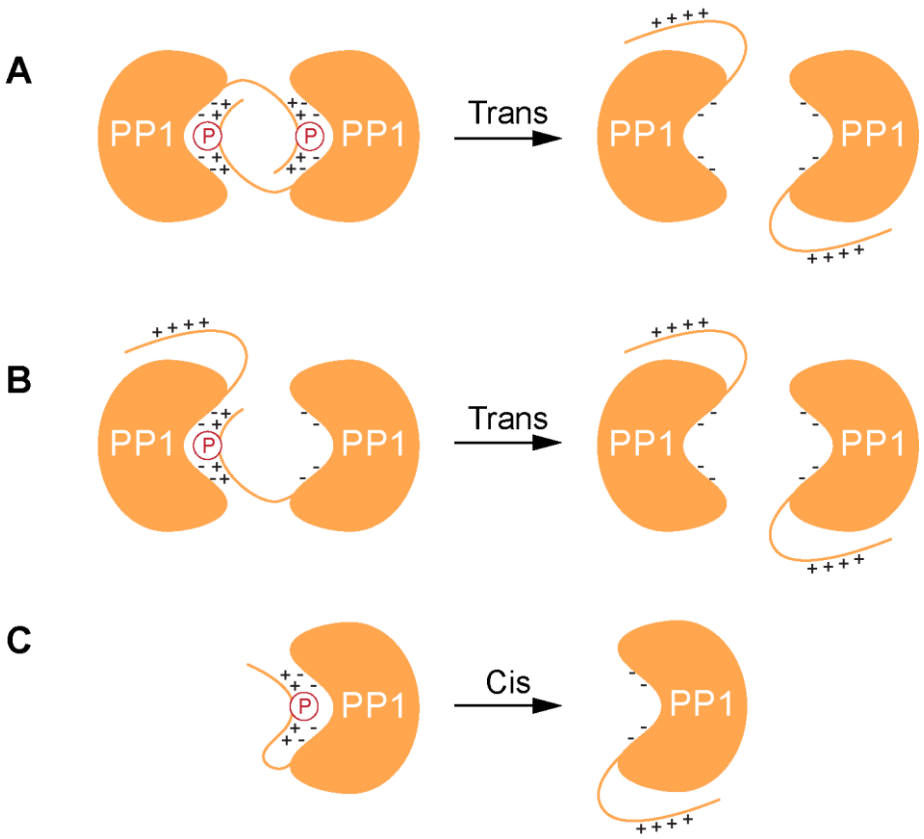


Figure 3.1 Models of PP1 auto-dephosphorylation

(A) Two molecules of phosphorylated-PP1 transiently interact to dephosphorylate each other in *trans*. Both molecules of PP1 are now unable to dephosphorylate further PP1. (B) A non-phosphorylated molecule of PP1 dephosphorylates a second molecule of PP1 in *trans*. Both molecules of PP1 are now active to dephosphorylate further PP1. (C) A single molecule of PP1 auto-dephosphorylates itself in *cis*.

molecule of unmodified “active” PP1 catalyses the dephosphorylation of the modified “inactive” PP1 in *trans* during the initial rapid dephosphorylation (Figure 3.1B). However, the occupancy data presented here would argue against this (Figure 2.27G). In the variant model the amount of active enzyme would accumulate over time and the rate of dephosphorylation would increase proportionally until the substrate became limiting. However, the results here did not show this behaviour (Figure 2.27). To explain the profile of PP1 dephosphorylation it is necessary to combine elements of both models. Thus, the

initial rapid dephosphorylation of PP1 is due to encounters between two molecules of PPP1CA-T320. As the rate of this initial reaction slows due to limiting concentrations of phosphorylated PP1, a linear reaction takes over, involving either unmodified PP1 acting in *trans* on PPP1CA-T320 or phosphorylated PP1 auto-dephosphorylating in *cis* (Figure 3.1).

Two phosphorylated molecules of PP1 acting in *trans* to initiate this process could provide an explanation for the observation that PP1 is not appreciably active in mitotic extracts (Cundell et al., 2013). There is an upper limit to the number of cells used to create an extract before lysis efficiency is impaired, the upper concentration limit being ~25 mg/ml (Cundell et al., 2013). This is well below the physiological concentration of protein in the cytoplasm of ~100 mg/ml, and places the concentration of phosphorylated PP1 at a point where the rate of its dephosphorylation due to a second order reaction would be greatly reduced (Figure 2.27). To further investigate this idea, cytostatic factor extracts from crushed *Xenopus laevis* eggs could be used to further test whether PP1 dephosphorylation occurs at higher protein concentrations. Additionally, purified non-phosphorylated and phosphorylated PP1 could be used to dephosphorylate PP1-T320 *in vitro* at a range of concentrations. This would not only confirm whether phosphorylated PP1 is capable of auto-dephosphorylation but also provide details of the reaction's concentration dependence.

One prediction based on these models is that during mitosis, while CDK1 activity persists, phosphorylated PP1 would continually auto-dephosphorylate before immediately being re-phosphorylated. This is analogous to the unfair substrate competition mechanism by which phosphorylated ENSA inhibits PP2A-B55 (Williams et al., 2014). This, together with the phosphorylation-dependent

inhibition of PP1 by Inhibitor-1 (Wu et al., 2009), would ensure that free PPP1C subunits cannot act unrestrainedly during mitosis. As CDK1 activity declines, the kinase:phosphatase equilibrium would shift allowing rapid accumulation of dephosphorylated PP1 which has the potential to be active. What remains unclear is how mitotic functions of PP1 are permitted despite CDK1-dependent inhibition. Clearly CDK phosphorylation cannot completely prevent PP1 activity, otherwise it would never become active. One possibility is that holoenzyme formation is able to circumvent this mode of inhibition. Indeed, PP1 holoenzyme formation was not globally reduced during mitosis (Figure 2.31) and published structural data suggest that the C-terminus of PP1 is repositioned away from the active site when part of a holoenzyme (Terrak et al., 2004). It is therefore plausible that holoenzyme formation interferes with the continual cycle of phosphorylation and dephosphorylation, targeting PP1 activity towards other substrates. The question still remains as to whether phosphorylation of PP1 can impact the activity of holoenzymes. Testing this would require a well characterised holoenzyme-substrate pairing, which is specific to mitosis. PPP1CC:Repo-man and Histone 3-pT3 meet these criteria and in addition the functional consequences for Aurora B localisation could be followed *in vivo*.

3.1.2 PP1 locally overcomes CDK1 regulation to promote APC/C activation

Mitosis and mitotic exit are tightly coupled to the levels of CCNB and the corresponding level of CDK1 activity. This necessitates that the timing of APC/C^{CDC20} activation must also be closely linked to this system through phosphorylation. As such, CDK inhibition led to more rapid activation of the APC/C than MPS1 inhibition, supporting direct regulation of the APC/C by CDK1 (Figure 2.18-19). This could theoretically be opposed by PP2A-B56, whose activity

is independent of CDK1. However, since PP2A-B56 is constitutively active during mitosis, there would be no way to prevent premature activation of the APC/C prior to checkpoint silencing and the subsequent accumulation of mis-segregated DNA. The same is likely true of FCP1 which is not currently thought to be regulated in a CDK1-dependent manner (Visconti et al., 2012). The presence of a functional SAC imposes a delay in APC/C activation, creating a requirement for a CDK-inhibited phosphatase. This would then create a feedback loop, ensuring the metaphase-anaphase transition is irreversible. How then does APC/C activation and mitotic exit ever occur if a CDK1-inhibited phosphatase is required whilst CDK1 activity is maximal? This would require a mode of CDK1 inhibition which can be specifically released with precise timing. PP2A-B55 does not meet this criterion given the indirect inhibition it experiences through the BEG pathway, the properties of which create the characteristic delay in PP2A-B55 (Cundell et al., 2013). Unsurprisingly, depletion of PP2A-B55 has no impact on the rate of CCNB1 proteolysis (Hayward et al., 2018).

By contrast, depletion of PPP1CA/C subunits did delay CCNB degradation. This was seen by live cell microscopy, timecourse experiments and confirmed through the use of a specific PP1 inhibitor (Figure 2.21-22). Furthermore, BUB1-pS459 was identified as a potential substrate of PPP1CA/C. This could provide redundancy in checkpoint silencing alongside the displacement of MPS1 from the kinetochore. Therefore, under normal conditions PP1 could help lock the kinetochore signalling status as “off”, as CCNB is being degraded. Nevertheless, this does not fully explain the observed delay in CCNB degradation.

APC/C activation must occur prior to degradation of CCNB, therefore it is likely that a specific pool of PP1 holoenzymes contributes to APC/C activation.

Given the nature of SAC signalling, this pool of PP1 is probably bound to the kinetochore. This could plausibly be recruitment of PP1 to KNL1, after microtubule attachment and the removal of Aurora B phosphorylations. However, recent structural data do not support this hypothesis, stating that KNL1 cannot simultaneously bind to both microtubules and PP1 (Bajaj et al., 2018). Alternatively, KIF18A may bring PP1 to the kinetochores, as it localises to microtubule plus ends at attached kinetochores. Here, dephosphorylation of KIF18A by PP1 is thought to stabilise kinetochore attachments (De Wever et al., 2014; Hafner et al., 2014). Thus, while the literature at present does not conclusively state when these binding partners localise PP1 to the kinetochore, it would seem likely that early recruitment of PP1 at unattached kinetochores would be via KNL1 and later recruitment to attached kinetochores via KIF18A. How these different mechanisms for PP1 localisation and their relationship to kinetochore attachment status link to regulation of APC/C activation remains unclear.

It has been suggested that the APC/C localises to the centromeres and kinetochores of unattached chromosomes, however this appears to be lost upon attachment (Acquaviva et al., 2004). Furthermore, MCC is a diffusible inhibitor of the APC/C with no apparent localisation. This creates a problem of scale; how does a local pool of PP1, which corresponds to a small proportion of total PP1, activate a freely diffusible complex pre-bound to its inhibitor? It is plausible that a small pool of PP1 initiates APC/C activation by signalling forward from attached kinetochores. As CCNB proteolysis begins, PP1 newly activated by dephosphorylation could then globally feed back onto the APC/C allowing maximal activation. This feedback could occur either through direct APC/C^{CDC20} dephosphorylation or through promoting MCC disassembly. Testing this may

prove difficult given the lack of information regarding mitotic regulation of PP1. However, identification of PPP1CA/C substrates which are removed prior to chromosome separation but downstream of kinetochore attachment may help resolve this paradox. Additionally, it will be necessary to understand the timing and control of PP1 localisation to kinetochores during mitosis more fully.

3.1.3 CDK1-inhibited phosphatases are activated with distinct timings to co-ordinate the events of early anaphase

PP1 and PP2A-B55 carry out distinct roles to ensure proper entry into mitotic exit; APC/C activation and initiation of cytokinesis, respectively. Furthermore, these functions can explain the requirement for two CDK1-inhibited phosphatases that are divergently regulated. Direct CDK1 inhibition ensures that the bulk of PP1 is inactive, allowing a global increase in phosphorylation status upon mitotic entry (Figure 3.2A). PP1 has the potential to form many different holoenzymes and it is likely that this can overcome the direct CDK1 inhibition of PP1, ensuring specific functions can be carried out with precise, defined timing during mitosis (Figure 2.30, 2.31 and 3.2B) (Bollen et al., 2010; Liu et al., 2010; Qian et al., 2015). PP2A holoenyzmes are stable and therefore are not afforded such flexibility in their regulation. Furthermore, while PP1 showed specific patterns of localisation throughout the cell cycle (Figure 2.29), PP2A-B55 remains diffuse throughout the cytoplasm and would argue against any specific, localised activation (Cundell et al., 2016). As CCNB is degraded, PP1 rapidly responds to the changes in CDK1 activity, through dephosphorylation in *trans* (Figure 3.2B). PP2A-B55 inhibition is maintained during this period by the BEG pathway. Once dephosphorylated, PP1 can then oppose the CDK1 phosphorylation of MASTL and initiate PP2A-B55 activation (Figure 3.2A-B).

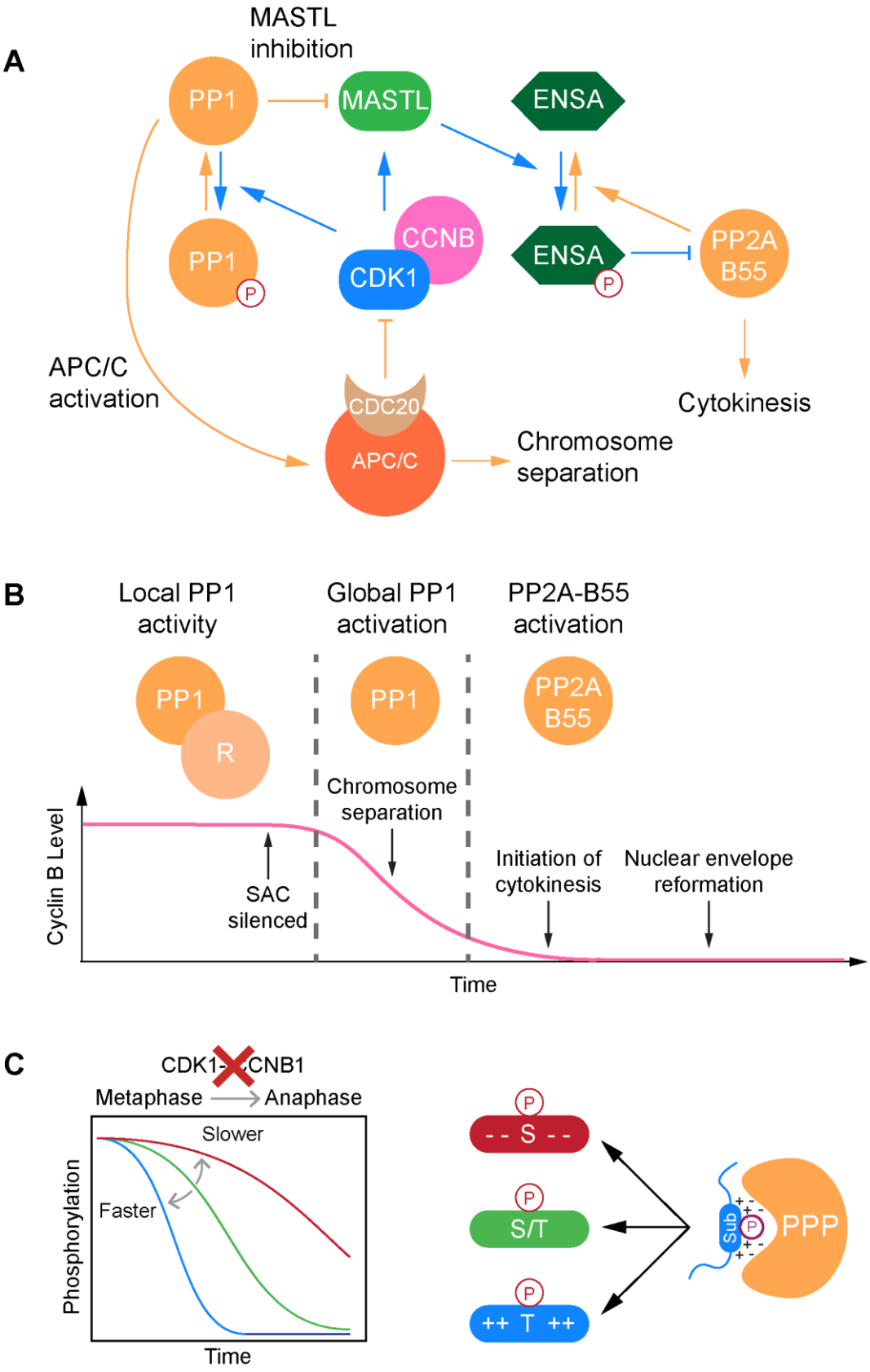


Figure 3.2 Co-ordinated phosphatase activation determines the order of events during mitotic exit

Figure 3.2. Co-ordinated phosphatase activation determines the order of events during mitotic exit (continued from previous page)

(A) Schematic comparing the CDK1-dependent regulation of PP1 and PP2A-B55 and the downstream consequences of their activation. Arrows denoting enzyme activity are colour coded according to cell cycle stage; metaphase (blue) and anaphase (orange). (B) The timing of PP1 and PP2A-B55 activation relative to the level of cyclin B. Important events of mitotic exit are marked with an arrow. (C) Model proposing how the rate of dephosphorylation during mitotic exit is encoded into the system, at the level of the sequence characteristics of each individual phospho-site.

This would create two waves of phosphatase activity to co-ordinate the early events of mitotic exit (Figure 3.2B). This is reflected in the mass spectrometry timecourse data following MPS1 inhibition. PPP1CA-pT320 dephosphorylation commenced ~5 min earlier than the model PP2A-B55 substrate PRC1-pT481. Moreover, the half-life of PRC1-pT481 was ~2 min longer than that of PPP1CA-pT320 (Figure 2.9G). These data are consistent with the delay of ~2-4 min observed between chromosome separation and central spindle formation (Cundell et al., 2013). It would be interesting to see whether many of the dephosphorylations seen in the early cluster following MPS1 inhibition, which were not CDK1 sites, would be catalysed by PP1 (Figure 2.9B-G). It is not yet known whether the PP1 which contributed to MASTL inactivation is the same pool that activated the APC/C. While this possibility is tempting to consider, it would risk activating PP2A-B55 prior to CCNB degradation. What is clear is that ordered activation of phosphatases is critical for proper co-ordination of mitotic exit.

The level of CCNB degradation which permits PP1 activation does not have to relate to that which allows chromosome separation. Knowing that PP2A-B56 is involved in the timing of separase activation (Hellmuth et al., 2014) it becomes

tempting to speculate whether PP1 may also help promote chromosome segregation beyond activation of the APC/C. However, the level of CCNB at which chromosomes separated was similar under both control and PPP1CA/C depletion, which is inconsistent with this hypothesis.

Once activated, both PP1 and PP2A-B55 lead to the dephosphorylation of many substrates during mitotic exit (Figure 2.25-26) (Cundell et al., 2016; Wu et al., 2009), the rate of which correlates with the sequence characteristics of each substrate (Figure 3.2C). This trend applies to the specificity of individual phosphatases, PP1 and PP2A-B55 (Figure 2.23-26) (Cundell et al., 2016) and also as a property of the system as a whole (Figure 2.7-9). Surprisingly, the only strong enrichment of a kinase motif is that of CDK; either in the intermediate cluster following MPS1 inhibition or in the stable cluster following CDK inhibition. Both of these observations can be explained by the use of their respective inhibitor. This suggests that the nature of the kinase which places a phosphorylation does not impart a specific timing to its dephosphorylation.

As predicted by structural data, the presence of particular regulatory subunits can impact the specificity of these phosphatases by altering which substrate binding grooves on the catalytic subunit are available (Ragusa et al., 2010). PP2A-B55 specifically recognises a bipartite basic motif rather than the general preference of basic residues observed here (Figure 2.7 and 2.9) (Cundell et al., 2016). Furthermore, mutation of acidic residues, found on the B55 regulatory subunit, drastically impairs substrate dephosphorylation. It is likely that PP1 holoenzymes also demonstrate such specificities. Due to the lack of structural data describing PPP holoenzymes bound to substrate, it is unclear how much the catalytic subunit can contribute to substrate binding. The work here suggests that

the catalytic subunit of these holoenzymes does impact substrate specificity. It appears that acidic residues are key determinants of dephosphorylation rate, which is influenced more by the presence or absence of acidic residues than basic residues (Figure 2.7, 2.9 and 2.25). An acidic groove close to the active site is conserved between both PP1 and PP2A catalytic subunits (Figure 1.3C). A phosphate represents a dense region of negative charge. Substrates containing additional negativity provided by acidic residues, would be electrostatically repelled from this binding groove. Conversely, the presence of basic residues surrounding the active site would help neutralise the charge of the phosphate moiety enabling more efficient substrate binding and phosphorylation (Figure 3.2C). Mutating this acidic groove might help to identify residues important for substrate binding. However, it would be essential to ensure that these mutations did not impact upon the protein folding of the catalytic site or the ability to be incorporated into holoenzymes.

It is clear that the nature of the phosphorylated residue is important: PRC1-T481S mutants cannot be dephosphorylated by PP2A-B55. The rationale behind the more rapid dephosphorylation of phospho-threonine over phospho-serine remains unknown, although the additional methyl group of threonine may confer steric properties which could improve the efficiency of dephosphorylation. Crystal structures of holoenzyme bound to substrate would be an important step towards understanding this distinction. Likewise, mutation of PPP1CA-T320S or the surrounding basic residues to alanine could help clarify exactly how CDK1 phosphorylation inhibits PP1. Severe impairment of this dephosphorylation could suggest that PP1 is inhibited by unfair competition through cycles of continuous phosphorylation and dephosphorylation during mitosis. This same process would

explain the sensitivity and rapid response to fluctuations in the level of CDK1 activity.

Taking the above into consideration, the following model is proposed with regard to how CDK-inhibited phosphatases co-operate to ensure orderly progression through mitotic exit (Figure 3.2). Late in mitosis, PP1 is recruited to attached kinetochores where it can dephosphorylate BUB1-pS459, among other substrates. This promotes activation of the APC/C^{CDC20} (Figure 3.2A). Multiple thresholds of CCNB degradation then ensure an ordered activation of phosphatases relative to chromosome separation (Figure 3.2B). Almost immediately following initiation of CCNB proteolysis, decreasing CDK1 activity permits the dephosphorylation and activation of PP1. PP1 can then begin dephosphorylation of less acidic substrates and initiate activation of PP2A-B55. As CCNB1 degradation continues, sister chromatid cohesion is lost. Further degradation then allows the full inactivation of MASTL. PP2A-B55 can then dephosphorylate ENSA, permitting subsequent activity against other substrates (Figure 3.2A). Once both phosphatases are active, thousands of phosphorylations can be removed helping to reset the system for the next cell cycle. The order of these dephosphorylations is determined by the suitability of each substrate for interactions with PPP active sites through charge interactions (Figure 3.2C).

3.1.4 Is there functional equivalency between human and yeast regulation of mitotic exit?

Saccharomyces cerevisiae divide through closed mitosis, where the nuclear envelope remains intact throughout chromosome separation. Here the phosphatase Cdc14 removes phosphorylations created by Cdc28, a CDK1 homologue (Visintin et al., 1998). During mitosis, Cdc14 is kept inactive through

interactions with an inhibitor, Net1. This inhibition is relieved by phosphorylation of Net1, leading to dissociation of Cdc14 and its release from the nucleolus throughout the cell. Two pathways, FEAR and MEN, co-ordinate the initial and sustained activation of Cdc14, respectively. The active Cdc14 generated by these two pathways is thought to fulfil specific functions. FEAR-activated Cdc14 stabilises the anaphase spindle, regulates nuclear positioning through control of microtubule dynamics, helps complete chromosome separation and promotes the activation of further Cdc14 through the MEN (D'Amours and Amon, 2004). Cdc14 activated via MEN is thought to promote mitotic exit through mediating Cdc28 inhibition, and the degradation of Clb2 late in mitosis (Jaspersen et al., 1998). Furthermore, there is some evidence that suggests MEN may regulate cytokinesis. While these events all occur during mammalian mitotic exit, current data would suggest that PP1 and PP2A-B55 fulfil these same regulatory roles rather than CDC14 homologues (Mocciaro and Schiebel, 2010; Wurzenberger and Gerlich, 2011). However, division of labour between PP1 and PP2A-B55 does not reflect the differences between FEAR and MEN. Both FEAR and MEN pathways integrate functions from mammalian PP2A-B55/B56 as well as PP1. The largest distinction here is that Cdc14 activation, by either pathway, falls downstream of APC/C activation and degradation of securin. While Cdc14 does feed back to the APC/C and promote cyclin degradation, this only occurs in late anaphase, long after initial phosphatase activation. In mammalian cells, specific activation of PP1 triggers APC/C activation against CCNB and securin, which subsequently leads to global phosphatase activation. Importantly, the two waves of Cdc14 activation are similar to the temporally distinct activation of PP1 and PP2A-B55. This ensures

that certain functions, such as central spindle formation and initiation of cytokinesis, are carried out with precise timing.

Collectively this would imply that phosphatase activity dominates the regulation of events within anaphase during closed mitosis and moreover, that the relative contributions of proteolysis and dephosphorylation arose early during eukaryotic evolution.

3.2 Proteolysis initiates mitotic exit

The results contained within this work highlight findings critical to the understanding of ubiquitin-mediated proteolysis within mitotic regulation. Firstly, that ordered proteolysis cannot account for the rapid series of events taking place during anaphase (Figure 2.7-10). Secondly, in the absence of CDK activity, APC/C-dependent proteolysis is not necessary to trigger dephosphorylation, and therefore order, throughout mitotic exit (Figure 2.13-14). From this it can be inferred that the only proteolytic event required for cells to exit mitosis is CCNB degradation.

3.2.1 APC/C activity can be temporally split into two distinct functions

Previously it has been suggested that APC/C coactivators have functionally distinct roles in regulating the licensing of DNA replication, whereby GMNN, an inhibitor of DNA replication, is degraded rapidly by APC/C^{CDC20}, while later APC/C^{CDH1} degrades CDC6 (Clijsters et al., 2013). The results described in this thesis expand upon this to suggest that globally CDC20 and CDH1 satisfy different requirements of mitotic exit (Figure 3.3A). These temporally separated functions of the APC/C can be described as follows: firstly, the creation of a cell state free from CDK:cyclin activity to permit mitotic exit through phosphatase activation; secondly, the degradation of mitotic factors to re-set the cell status for the subsequent cell

cycle. A simple view would be to separate these functions based on the APC/C coactivator, CDC20 for cyclin destruction and CDH1 for resetting cell status. This is supported by a proteomic analysis of meiotic exit in *Xenopus* eggs which found that wide-spread dephosphorylation was triggered by the degradation of a small number of proteins, typified by the APC/C^{CDC20} substrates: CCNB1/2, securin and GMNN (Presler et al., 2017). These eggs lack CDH1, therefore typical APC/C^{CDH1} substrates such as CDC20 and Aurora kinases were, unsurprisingly, stable. The absence of CDH1-dependent degradation is thought to help bypass G1 and promote rapid divisions within the early embryo (Presler et al., 2017), highlighting a role for APC/C^{CDH1} activity in promoting the formation of a stable G1 state. Nevertheless, it has been suggested that the switch from CDC20 to CDH1 may not be as clear as previously thought. APC/C^{CDC20} is required for the degradation of BUBR1, CENPF and PLK1 late in anaphase (Choi et al., 2009; Floyd et al., 2008; Gurden et al., 2010). In support of this, CDC20 is not rapidly degraded during mitotic exit (Figure 2.10D) suggesting that both CDC20 and CDH1 function during late anaphase/telophase to degrade mitotic proteins (Figure 3.3A).

The first function of the APC/C relates to the quantitative model of Cdc2 control, which places cyclins at the centre of cell cycle regulation. Rounds of cyclin synthesis and destruction govern transitions to successive cell cycle stages of increasing Cdc2/CDK activity which peaks in mitosis. CCNA and CCNB are sequentially degraded during mitosis, in an APC/C-dependent manner. CCNA destruction begins following NEBD while CCNB proteolysis occurs downstream of SAC silencing. Early mitotic inhibitor 1 (EMI1) prevents premature degradation of these mitotic cyclins by inhibiting the APC/C prior to mitotic entry (Grosskortenhaus and Sprenger, 2002; Hsu et al., 2002a). The destruction of

CCNA and CCNB creates a state free of cyclins and consequently CDK activity, during mitotic exit.

One important question to ask is, “Why has CCNA proteolysis evolved to escape SAC-dependent inhibition of the APC/C^{CDC20}?” CCNA is sufficient to trigger mitotic entry in the absence of CCNB (Furuno et al., 1999; Gong and Ferrell, 2010; Swenson et al., 1986). Furthermore, CCNA can bind to and activate CDK1 (Desai et al., 1995). Therefore, understanding the relative substrate specificities of CDK1/2:CCNA and CDK1:CCNB complexes could help to find the answer. Cells depleted of CCNB rapidly exit mitosis following entry, as they cannot activate the SAC (Hayward et al., 2018). Therefore a unique feature of CDK1:CCNB is to inhibit anaphase onset. It is likely that this also occurs through inhibition of cytokinesis since PRC1 and the CDK-dependent regulation of its function are evolutionarily conserved. These findings show that CDK1:CCNA cannot fully substitute for CDK1:CCNB, and it is likely that it is these functional differences which necessitates their differential proteolysis.

Prior destruction of CCNA could potentially ensure that degradation of CCNB creates a state fundamentally different to G2, which is governed by CDK:CCNA activity. This inherent asymmetry would drive the cell cycle forward into anaphase rather than reverting back to a G2 state. Simultaneous degradation of CCNA and B, following checkpoint silencing, could interfere with this asymmetry depending on the relative rates of cyclin destruction. Engineering a situation where CCNB proteolysis overtakes that of CCNA could be used to test the consequences of CCNA persisting into anaphase. Potentially a CCNA mutant whose degradation is impaired but not prevented could be used. Nevertheless, it

is APC/C^{CDC20} which drives this asymmetry pushing cells into mitotic exit, through CCNB degradation and the phosphatase activation downstream of this.

Later during mitotic exit, the APC/C^{CDH1} becomes active. Here the function of the APC/C also changes from driving the cell cycle forward through asymmetry to resetting cell status through proteolysis of mitotic factors (Figure 3.3A). In a 2011 review, 55 human proteins were identified as APC/C substrates of which 34 were identified here (Figure 2.10) (Meyer and Rape, 2011). Of these only nine were seen to have a half-life of less than two hours and categorised as being degraded during the window of the experiment. In fact, when comparing the proteomic data here to the list of genes expressed for mitosis, only one additional protein was classified as being degraded (Whitfield et al., 2002). It is likely that the degradation of many of these proteins therefore occurred in the following G1 and could not impact the regulation of mitotic exit.

3.2.2 How does the APC/C activity promote different rates of proteolysis?

The two categories of APC/C function discussed above highlight the necessity for different rates of proteolysis. Rapidly degraded proteins fulfil functions necessary to trigger mitotic exit whereas slow turnover is used for resetting cell status. How these differences in kinetics are achieved is poorly understood. This could be explained by varying rates of continued protein synthesis into anaphase, but the timing and rate of proteolysis were unchanged for the APC/C substrates probed by Western blot following cycloheximide addition (Figure 2.15). One alternative is that degron motifs themselves encode some rate information. Under normal circumstances D and KEN box sequences are required for efficient proteolysis, and even when a substrate is tethered to the APC/C the presence of degron

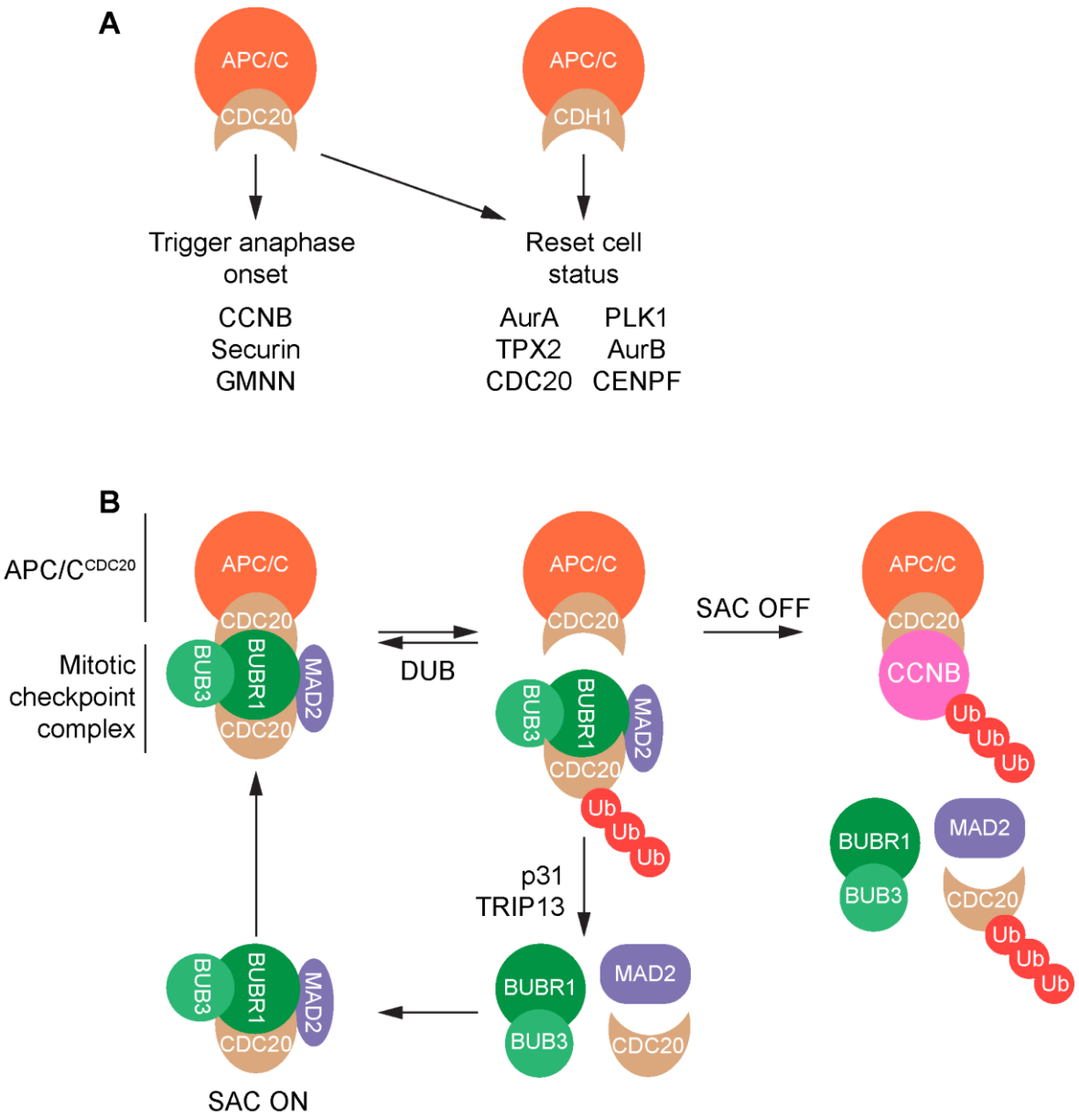


Figure 3.3 Regulation of APC/C activity by co-activators during mitosis and mitotic exit

(A) APC/C activity can be split into two functional categories: triggering mitotic exit or resetting cell status for a subsequent G1 phase, example APC/C substrates are noted. (B) A model detailing the role of CDC20 ubiquitination during mitosis. While kinetochores are unattached, the spindle assembly checkpoint (SAC) generates mitotic checkpoint complex (MCC), which can bind to and inhibit the APC/C^{CDC20}. The molecule of CDC20 within the MCC is ubiquitinated by the APC/C^{CDC20}, causing the MCC to dissociate. Deubiquitinases (DUB) can then act on CDC20, allowing the MCC to rebind the APC/C^{CDC20}. Any MCC which is disassembled by the p31/TRIP13 pathway is regenerated by an active SAC. Ubiquitination of CDC20 ensures rapid APC/C activation once the SAC

is silenced by lowering the affinity of the MCC for APC/C^{CDC20} and promoting efficient disassembly of the MCC.

motifs increases the rate of ubiquitin transfer to the substrate (Van Voorhis and Morgan, 2014). Computer modelling of APC/C^{CDC20}-substrate interactions has previously shown that both binding efficiency and suitability of ubiquitin transfer are important determinants in the rate and timing of degradation. In fact, in a two-substrate system model competing for the same APC/C^{CDC20}, the substrate with greater affinity for the APC/C^{CDC20} is degraded more quickly. However, when tested *in vivo*, the expression of an additional copy of Clb5 in *S.cerevisiae* did not reduce the rate of proteolysis of the downstream substrate securin (Lu et al., 2015). Timecourse data presented here would suggest that APC/C^{CDC20} has few early substrates including CCNB, securin and GMNN, all of which were degraded rapidly and with similar timing (Figure 2.2, 2.3, 2.7 and 2.10). While it would seem likely that degron-APC/C interactions would naturally result in differing rates of proteolysis, direct competition between substrates cannot be a fundamental principle of APC/C regulation. Furthermore, there are no clear characteristics contained within the degron motifs of these proteins which would indicate rapid or slow proteolysis (Figure 2.15A). Given that the sequence characteristics surrounding a particular phospho-site govern the rate of dephosphorylation, it seems probable that additional sequences or features of known motifs govern interaction with the APC/C. This would require bioinformatics and sequence analysis of a validated list of APC/C substrates. Identifying a list of substrates degraded *in viv*o during mitotic exit would require deep-proteomic analysis over a longer time window than used here, extending into the subsequent G1 stage.

It is also possible that regulated post-translational modification of APC/C substrates can modulate their interaction with the APC/C and their rate of ubiquitination. This has been described for BUBR1 by acetylation and for CENPF by farnesylation (Choi et al., 2009; Gurden et al., 2010). Furthermore, recent work has shown that APC/C-mediated ubiquitination of substrates is opposed by deubiquitination. Cezanne, a deubiquitinase, binds to APC/C substrates and specifically removes K11-linked ubiquitin chains. Depletion of Cezanne accelerates the rate of proteolysis for both CCNB and AurA. Furthermore, the levels of Cezanne are proposed to be cell cycle regulated, peaking in mitosis before also being degraded during mitotic exit (Bonacci et al., 2018). Here, the level of Cezanne was stable during the window of anaphase observed (Figure 2.7 and 2.10). The action of deubiquitinases, such as Cezanne, could retard the proteolysis of certain proteins but they are unlikely to account for the large differences in rate observed between early and late APC/C substrates.

3.2.3 CDC20 ubiquitination but not degradation is required for rapid APC/C activation

CDC20 is unique in its position as both an inhibitor and activator of the APC/C. Previous work suggests that continual synthesis and degradation of CDC20 is required to maintain a mitotic state and for the rapid APC/C activation following SAC silencing. The work presented here argues against a requirement for protein synthesis during mitosis (Figure 2.16-17). Inhibition of protein synthesis did not cause cells to leave mitosis prematurely, while in cells unable to exit mitosis, inhibition of protein synthesis did not lead to rapid degradation of CCNB. Furthermore, if proteins such as CDC20 were continually turning over at high levels during mitosis the levels of synthesis and destruction would have needed to

be evenly matched to ensure levels of CDC20 are correct. Depending on the relative levels of CDC20 required for activation and inhibition of the APC/C, an imbalance between the synthesis and destruction of CDC20 could cause cells to either arrest in mitosis or trigger anaphase prematurely. Currently, there is no known feedback between protein synthesis and APC/C activity. Furthermore, there is no direct evidence of CDC20 synthesis during mitosis, only that inferred from CDC20 degradation. The measurements made here were of endogenous CCNB levels and not those of CDC20, which was proposed to have a much shorter half-life than CCNB (Nilsson et al., 2008). Therefore, generation of cells expressing endogenous levels of CRISPR-tagged Halo-CDC20 could be used to image cells during mitosis with two different Halo ligands. This type of pulse-chase experiment would then allow any newly synthesised molecules of CDC20 to be visualised, fully testing the requirement for protein synthesis in mitosis.

CDC20 degradation is thought to be a consequence of APC/C switching coactivators to CDH1, following CDK1 inactivation. Conversely, here it was seen that CDC20 degradation was independent of APC/C activity during mitotic exit, suggesting that the ubiquitination of CDC20 occurs prior to checkpoint silencing (Figure 2.12, 2.13 and 3.3B). While surprising, this still agrees with the finding that CDC20 can be ubiquitinated when part of MCC which is bound to APC/C^{CDC20}. Nevertheless, the functional consequences of this regulation need further examination. A situation could be envisaged where CDC20 ubiquitination could enable rapid APC/C activation following SAC silencing through modulating the affinity of the MCC for APC/C^{CDC20} and promoting efficient disassembly of the MCC (Figure 3.3B). Given that ~50% of CDC20 still remained one hour after CDK inhibition, it is important to understand whether any particular pools of CDC20 are

indeed preferentially degraded during mitosis. This would require a time series of immuno-precipitations during mitotic exit, pulling down either endogenous APC/C or MCC subunits or CDC20 itself.

3.3 Concluding remarks

The combination of high-resolution mass spectrometry with the biochemical and cell biological techniques used in this research work has provided a novel insight into one of the fundamental questions of biology. It presents a clear view of how the cells co-ordinate the events of mitotic exit: with proteolysis of a single substrate, CCNB, triggering a graded series of dephosphorylations whose rate is encoded into the system at the level of individual phospho-sites. Due to their differing modes of regulation, ordered activation of CDK-inhibited phosphatases additionally contributes to the timing of events within mitotic exit. Furthermore, while individual PPP holoenzymes demonstrate differing substrate specificity they still follow the same governing principles based on the sequence characteristics surrounding the phospho-site. Overall, the findings presented here suggest a general mechanism of cell cycle control where proteolysis plays a crucial but limited role driving transitions through cell cycle checkpoints while phosphatase activity is required for fine regulation of components within the system. Most importantly, these results can be explained by the chemical and physical properties of the amino acid constituents of these proteins. This provides a foundation for the tightly choreographed, rapid series of events which occur during mitotic exit and ensures that faithful inheritance of genetic material is pre-programmed into the fundamental building blocks of a cell.

4 Materials and Methods

4.1 Reagents and Antibodies

Standard lab reagents and stocks were purchased from Sigma Aldrich, Thermo Scientific and VWR. The antibodies and siRNA duplexes used are listed in Tables 4.1 and 4.2. Inhibitors and drugs were bought from Tocris (flavopiridol, AZ3146, apcin, pro-TAME, tautomycetin), Cell signalling (cycloheximide), CalBiochem (nocodazole, taxol, MG-132), Sigma (protease inhibitor cocktail C, phosphatase inhibitor cocktail 3) and resuspended in DMSO. Thymidine was purchased from CalBiochem and resuspended in sterile Millipore filtered water. Centrifugation steps were carried out in Eppendorf 5427-R and 5417-R models.

4.2 Western blotting

Samples were run on SDS-PAGE gels (mini protean, Bio-Rad) and transferred to nitrocellulose membranes, using semi-dry transfer protocol (trans-blot turbo, Bio-Rad): 2.5 A, 25 V, 7 min for two gels. Membranes were blocked in 5% cow's milk in phosphatase buffered saline (PBS), 0.1% Tween-20 (PBST), antibodies were incubated in milk/PBST for 2-24 hr. Species-specific 2^{o} antibodies conjugated to horseradish peroxidase (HRP) were obtained from Jackson ImmunoResearch Laboratories, Inc. and used at 1 µg/ml. PBST was used to wash membranes for an hour, between antibody incubations and prior to developing. All Western blots were revealed using ECL (GE Healthcare) on films.

Table 4.1 Antibody details

Antibody	1^0 Ab species	Ab producer	Gel %	Dilution
Aurora A	Rb	Cell Signalling, 4718S	10	1:2000
Aurora B	Mo	BD Transduction Labs, 611083	10	1:2000
BUBR1	Rb	Bethyl, A300-386A	7.5	1:2000
CDC20 Full length (FL)	Rb	Proteintech, Polyclonal, 10252-1-AP	10	1:1000
CDC20 N-terminal (NT)	Rb	Cell Signalling, monoclonal, 4823S	10	1:1000
CDH1	Mo	Santa Cruz, sc-56312	10	1:500
Cyclin B1	Mo	Millipore, 05-373	10	1:5000
DM1A (Tubulin)	Mo	Sigma, Cat T6199-200UL	10	1:10,000
GFP	Sh	Barr Lab	-	1:2500
MAD2	Sh	Sh MAD1, Gruneberg Lab	12.5	1:1000
MPS1	Sh	Sh MPS1, Gruneberg Lab	7.5	1:1000
MYPT1	Rb	Epitomics, 1519-1	7.5	1:1000
Pan Cdk1 pSP	Rb	Cell Signalling, 9477S	10	1:1000
Pan Cdk1 pTP	Mo	Cell Signalling, 9391S	10	1:1000
Phostensin	Mo	Santa Cruz Biotech, sc-365099	7.5	1:2000
PLK1	Go	Go PLK1, Barr Lab	10	1:2000
PPP1CA	Rb	Bethyl, A300-904A	10	1:1000
PPP1CA-pT320	Rb	AbCam, Ab62334	10	1:2000
PPP1CB	Rb	Bethyl, A300-905A	10	1:750
PPP1CC	Go	Santa Cruz Biotechnology, sc-6108	10	1:1000
PRC1	Rb	Rb PRC1, Barr Lab	7.5	1:2000
PRC1-pT481	Rb	Epitomics, 2189-1	7.5	1:4000
PRC1-pT602	Rb	Rb 602, Barr Lab	7.5	1:2000
Sds22	Go	Santa Cruz Biotech, sc-162164	10	1:1000
Securin	Rb	AbCam, Ab79546	12.5	1:2000
TPX2	Mo	AbCam, Ab32795	7.5	1:2000
Rb = Rabbit; Mo = Mouse; Sh = Sheep; Go = Goat				

Table 4.2 siRNA duplexes

Sense sequence of siRNA duplexes used. All sequences target the 3'UTR of specified genes. All duplexes were designed and purchased from Dharmacon using the siDESIGN tool.

Target	Sense sequence (5'-3')
GL2	cguacgcggaauacuucgauu
PPP1CA	uggauugauuguacagaaauu
PPP1CB	gggaagagcuuuacagacauu
PPP1CC	gcggugaaguugaggcuuauu

4.3 Cloning techniques

Pfu-HotStart polymerase (Agilent Technologies) was used for all PCR reactions, with 25 ng template DNA, 0.2 mM dNTPs and 4 µM primers. When conducting Quickchange mutagenesis 50 ng of template DNA and 2.5 µM primers were used. Agarose gel (0.8-2%) electrophoresis was used to separate PCR products, after which they were gel extracted (Qiagen). This product was then TA tailed with Taq polymerase (New England Biolabs) and ligated into the pSC-A vector which contained ampicillin/kanamycin resistance (Agilent Technologies). Accession numbers from which the DNA sequences were derived are detailed in Table 4.3. All primers used are listed below in Table 4.4.

Restriction digests were incubated at 37˚C with the chosen restriction enzyme for 2 hr with 2 µg DNA used as starting material. This was analysed by agarose gel electrophoresis. Gel bands were extracted and ligated using a 3:1 insert/vector molar ratio with T4 DNA ligase (New England Biolabs). For GFP-tagging inserts were ligated into pcDNA5-FRT-TO-eGFP-N vectors. Resulting

plasmids were transformed into XL1-blue Rb^{+}-Ca^{2+} competent bacterial cells and then the DNA extracted using Qiagen miniprep or maxiprep kits.

Table 4.3 Accession Numbers

Accession numbers were obtained from NCBI, and used to generate DNA and protein sequences for cloning and amino acid sequence alignments.

Target	Accession numbers
BANF1	NM_001143985.1
PPP1CA	NM_002708.3
PPP1CB	NM_002709.2
PPP1CC	NM_002710.3

Table 4.4 Primer details

Cloning primers used as described in Methods 4.3.

Primer name	DNA sequence (5'-3')
PPP1CA_T320A_F	ggaggccgacccatcgccccaccccgcaattcc
PPP1CA_T320A_R	ggaattgcggggtggggcgatgggtcggcctcc
PPP1CB_T316A_F	aattctggacgtcctgtcgctccacctcgaacagct
PPP1CB_T316A_R	agctgttcgaggtggagcgacaggacgtccagaatt
PPP1CC_T311A_F	gccacgagacctgtagcgcctccaaggggtatg
PPP1CC_T311A_R	catacccctggaggcgctacaggtctcgtggc
BANF1_Upstream_F1	ggaagtggaagaaagttctagtgg
BANF1_Upstream_F2	ggaaaggagcgcctactaagg
BANF1_BamH_F1	GGGATCCCCatgacaacctcccaaaagcacc
BANF1_Xho1_R1	CCTCGAGtcacaagaaggcgtcgcacc
BANF1_Downstream_R1	ctactcggctgcaaactctgg
BANF1_Downstream_R2	cttcgtagaggacaggggagg

4.4 Cell culture

HeLa-S3 and HeLa-FRT cells were grown in DMEM, 10% FBS medium (DMEM/FBS) and incubated at 37°C, 5% CO_2. Mirus LT1 (Mirus Bio LLC) and oligofectamine (Invitrogen) were used, per well as specified below, for the transfection of plasmid DNA or siRNA, respectively, in 3 cm dishes:

- DNA: 200 ng expression plasmid + 800 ng empty vector plasmid + 3 µL LT1 + 200 µl Opti-MEM
- siRNA: 60 pmol siRNA duplex + 3 µl oligofectamine + 200 µl Opti-MEM

For co-depletion 40 pmol of each siRNA duplex was used. Selection drugs blasticidin and hygromycin were purchased from InVivogen and used at 4 µg/ml and 200 µg/ml, respectively. Expression in HeLa-FRT cells was induced using doxycycline at 1 µg/ml. Doxycyline was resuspended in water and sterile filtered prior to aliquoting and storage.

4.4.1 High-resolution mitotic exit timecourses for Western blot and mass spectrometry

HeLa cells were seeded at 1,200,000 cells/dish onto 15x 15 cm dishes per condition and grown for 72 hr**.** Nocodazole, a microtubule depolymerisation agent, was added to 100 ng/ml, for 20 hr, to arrest the cells in mitosis. If depletion was necessary, cells were seeded at 600,000 cells/dish and grown for 24 hr before transfection with the appropriate siRNA for 72 hr. Nocodazole was added to the dishes for the final 20 hr of depletion. Dishes were depleted with 600 pmol siRNA duplex + 30 µl oligofectamine + 1000 µl Opti-MEM, or 400 pmol per siRNA duplex was used for co-depletion.

The mitotic cells were harvested by shake-off, washed in 2x 25 ml 1x PBS, 1x 25 ml Opti-MEM, both of which had been pre-equilibrated to 37°C, 5% CO_2.

Wash centrifugations were carried out for 5 min at 200 g_{av}, 37°C. Cells were counted prior to the last wash and resuspended in pre-equilibrated Opti-MEM to give 15,000,000 cells/ml. A 100 µl sample of cells was taken and added to a tube pre-aliquoted with 200 µl ice cold urea buffer (8 M urea, 100 mM ammonium-bicarbonate (AMBIC)) and immediately snap frozen. The urea buffer was supplemented with protease inhibitors (Sigma cocktail C, 1:250 dilution), phosphatase inhibitors (Sigma cocktail 3, 1:100 dilution) and 100 nM okadaic acid.

The cells were incubated for 25 min (37˚C, 5% CO_2) to allow cells to rebuild bipolar mitotic spindles, with gentle mixing every ~5 min. While the cells were incubating, 500 µl of flavopiridol buffer (see below) was made and pre-warmed to 37°C. Where more than 500 µl of flavopiridol was required, this was scaled accordingly. Flavopiridol is a broad spectrum CDK inhibitor and will trigger mitotic exit when added to mitotic cells.

- Flavopiridol buffer: 480 µl pre-equilibrated Opti-MEM + 20 µl, 5 mM flavopiridol (resuspended in DMSO)

After the 25 min incubation, a 300 µl sample was taken and added to a tube pre-aliquoted with 600 µl ice cold urea buffer. This t_0 sample was immediately snap frozen and represented after cells had rebuilt mitotic spindles. Where samples were for mass spectrometry, 15 of these t_0 samples were taken to act as a reference. One experiment required the cells to be incubated on ice for 10 min prior to addition of flavopiridol (Figure 2.28).

Flavopiridol buffer was added to the cells at a 1:10 dilution, giving a final flavopiridol concentration of 20 µM. The cells were immediately mixed through inversion and pipetting before being split in half. Owing to the frequency of early timepoints, one 2 ml aliquot was kept incubating at 37°C, 5% CO_2, gently mixed

every 5 min, to ensure stable conditions. The other half was placed in a 37°C water bath and sampled accordingly. At each timepoint, 100 µl of cells was added to 200 µl ice-cold urea buffer and then snap frozen. If the first half of cells ran out, the second half was sampled for the remainder of the timecourse. Once the sampling rate decreased cells were placed at 37°C, 5% CO_2 for optimal conditions. Sampling is described in Table 4.5.

Samples were thawed on ice, with intermittent vortexing and incubated on ice for 20 min. In the initial timecourse, the lysate was clarified (20,000 g_{av}, 15 min, 4°C) and the supernatant isolated. Later timecourses skipped this clarification step. A 50 µl aliquot of lysate was taken for Western blotting and 25 µl of 3x sample buffer was added (to a final concentration of 1x) and samples boiled for 5 min and loaded on Western blots. Typically, 6 µg was loaded on each Western blot but when necessary increased to 10 µg. The concentration of the remaining lysates was measured by Bradford assay.

Low-resolution timecourses for Western blot were set up in an identical fashion to that described above. 50 µl of cells were taken at each timepoint before immediate lysis in 25 µl of 3x sample buffer. Samples were diluted 1:2 with 1x sample buffer prior to Western blotting.

Where necessary, drugs were added at the start of the 25 min incubation, to ensure maximal inhibition prior to the addition of flavopiridol. All of the following drugs were resuspended in DMSO prior to use. MG132, a proteasome inhibitor, was used at 40 µM while apcin and proTAME, APC/C inhibitors, were used at 400 µM and 25 µM, respectively. Cycloheximide (CHX) was used at 100 µg/ml. Tautomycetin, a PP1 inhibitor was used at 5 µM.

Table 4.5 Sampling for timecourses following CDK inhibition

Times shown are relative to CDK inhibition

Time (min)		
-25	6	14
0	6.5	15
0.5	7	17.5
1	7.5	20
1.5	8	22.5
2	8.5	25
2.5	9	30
3	9.5	35
3.5	10	40
4	11	45
4.5	12	50
5	13	60
5.5	14	

4.4.2 Mitotic exit timecourse comparing MPS1 and CDK inhibition

Cells were seeded, synchronised and harvested as in Methods 4.4.1. Harvested cells were washed three times in 25 ml 1x PBS and 1x 25 ml DMEM/FBS, both pre-equilibrated to 37°C, 5% CO_2. Cells were counted prior to the last wash and resuspended in DMEM/FBS to give 15,000,000 cells/ml. 25 µl of cells were added to 975 µl of pre-equilibrated Opti-MEM and then pelleted (1200 g_{av}, 30 s, 37°C) and lysed in 100 µl 1.5x sample buffer. The Opti-MEM was supplemented with 100 nM calyculin to immediately stop dephosphorylation. All samples were collected this way. Cells were incubated for 25 min at 37°C, 5% CO_2. Flavopiridol buffer was made as previously described. AZ3146, an MPS1 inhibitor, was diluted in the same way.

After the 25 min incubation, the t_0 sample was collected. The flavopiridol or AZ3146 buffers were then added to a 1:10 dilution, giving a final concentration of 20 µM. Cells were immediately mixed through inversion and pipetting and placed at 37°C, 5% CO_2. This was critical to ensure proper mitotic exit when using MPS1 inhibition. Conditions were sampled as specified in Table 4.6.

4.4.3 Timecourses assessing contribution of protein synthesis to mitosis

HeLa cells were seeded at 50, 000 cells/well on six well plates in DMEM/FBS and grown for 72 hr. These cells were arrested in mitosis using either a 100 ng/ml nocodazole, 20 hr or 80 ng/ml, 16 hr taxol arrest. Cells for t_0 were collected by shake-off and pelleted 400 g_{av}, 60 s and then resuspended in 1 ml 1x PBS, 37°C and spun 1000 g_{av}, 30 s. The washed pellet was lysed in 50 µl of 1.5x sample buffer. Time was started following addition of either 100 µg/ml cycloheximide or an equal volume of DMSO to the remaining wells. Samples were harvested, as above, at 20/40/60 and 120 min and diluted 1:3 with 1x sample buffer and 5 µl loaded for Western blotting.

Alternatively, a double thymidine synchronisation was used to achieve a high degree of synchronicity without arresting in mitosis. Cells were seeded as above and grown for 48 hr before being synchronised in S phase with 2.5 mM thymidine, 18 hr. Following this, dishes were washed three times, once with 1x PBS and twice with DMEM/FBS, both pre-equilibrated to 37°C, 5% CO_2, before being incubated for 10 hr at 37°C, 5% CO_2. At this point, there should be an enrichment of mitotic cells. A second synchronisation with 2.5 mM thymidine, 12 hr was then carried out. Cells were washed as above and then released into DMEM/FBS supplemented with either 100 ng/ml nocodazole or 85 ng/ml taxol.

Table 4.6 Sampling for timecourses comparing CDK and MPS1 inhibition

Times shown are relative to drug addition, either CDK (CDKi) or MPS1 inhibition (MPS1i).

Time (min)	
CDKi	**MPS1i**
-25	-25
0	0
2	5
4	10
6	15
8	17
10	19
12	21
14	23
16	25
18	27
20	29
22	31
24	33
26	35
28	37
30	39
35	41
40	43
45	45
50	50
60	60

After a 6 hr incubation at 37°C, 5% CO_2, t_0 sample was as harvested as follows. Any mitotic cells were collected by shake-off and pipetting and placed on ice, alongside the media from the well. 1 ml of ice-cold 1x PBS, supplemented with 1 mM EDTA, was added to the well and left on ice for 10 min. Cells were harvested by pipetting, pooled with previously collected media and pelleted (300 g_{av}, 60 s) and washed in 1x ice cold PBS, without EDTA (600 g_{av}, 60 s). Cells were lysed in 50 µl 1.5x sample buffer. Time was started following the addition of cycloheximide or DMSO and harvested as above. Samples were again diluted 1:3 in 1x sample buffer prior to Western blotting.

4.5 Immuno-precipitation

HeLa-FRT cells, with inducible GFP-PPP1C expression, were seeded on three 15 cm dishes per condition at a density of 1,200,000 cells/dish and left to incubate at 37°C, 5% CO_2 for 48 hr. Expression of GFP tagged PPP1C was induced with doxycycline, 2 µg/ml and left for a further 24 hr. Alternatively, pcDNA5-eGFP empty vector construct was transfected 20 hr prior to synchronisation, as follows: 1 µg pcDNA5-eGFP + 9 µg pBluescript + 30 µl LT1 + 1000 µl Opti-MEM. Cells for S phase samples were then synchronised using 2.5 mM thymidine for 18 hr, whereas cells for metaphase and anaphase extracts were synchronised with 100 ng/ml nocodazole, for 20 hr.

S phase cells were washed in 2x 25 ml PBS (200 g_{av}, 5 min, 37°C). Cells were then incubated in 10 ml 1x PBS, 1 mM EDTA for 10 min at 37°C and harvested from the dish. 2x 20 ml of 1x PBS, 37°C was used for washing before the cells were counted, pelleted (200 g_{av}, 5 min, 4°C) and snap frozen.

Metaphase and anaphase cells were then collected via shake-off in DMEM media and washed in 3x 20 ml DMEM medium, 10% FBS, 0.1% sucrose (200 g_{av},

5 min, 37°C). Cells were resuspended in 10 ml DMEM medium, counted and incubated to rebuild mitotic spindles (25 min, 37°C, 5% CO_2) with gentle mixing every 5 min. 20 ml ice-cold PBS was then added to metaphase cells, spun (200 g_{av}, 5 min, 4°C) and snap frozen. AZ3146, an MPS1 kinase inhibitor, was added to anaphase cells to a final concentration of 20 μM. After a further 30 min incubation (37°C, 5% CO_2), the cells were pelleted and snap frozen as with metaphase cells.

Lysis buffer contained: 20 mM Tris-HCl pH7.5; 150 mM NaCl; 40 mM β-glycerophosphate; 10 mM NaF; 0.3 mM $NaVO_3^-$; 1% IGEPAL; 0.1% Na-deoxycholate; 2 mM $MgCl_2$; 100 nM okadaic acid; protease inhibitors (Sigma, 1:250 dilution); and phosphatase inhibitors (Sigma, 1:100 dilution). Pellets were resuspended in lysis buffer to give ~4500 cells/μl and incubated on ice for 20 min. This should have ensured that the lysate protein concentration was approximately 3 mg/ml. DNA was digested using benzonase nuclease (40 units / 3 mg protein, 30 min each at 4°C, 25°C, 4°C). Supplementing the lysis buffer with $MgCl_2$ ensured sufficient levels of nuclease activity. Lysates were clarified (20,000 g_{av}, 20 min, 4°C) and the supernatants isolated. Protein concentrations were measured, and 3 mg of protein was used for the IP. Protein G coated beads (Sigma) were washed in 2x 1 ml lysis buffer and added to the lysates (20 μl beads/lysate). An 80 μl input sample was taken and then 3 μg of GFP antibody was added to each lysate. These were then left to incubate at 4°C for 2 hr, with mixing. After incubation, samples were spun (8000 rpm, 2 min, 4°C) and a 100 μl sample of the supernatant was taken. Beads were then washed twice in 500 μl of lysis buffer and then in 500 μl of wash buffer: 20 mM Tris-HCl pH7.5; 150 mM NaCl; 40 mM β-glycerophosphate; 10 mM NaF, 0.3 mM $NaVO_3^-$, 0.1% IGEPAL.

Proteins were then eluted from the beads, with 100 mM glycine pH 2.6, as follows: 50 µl 100 mM glycine was added to the beads and incubated at room temperature for 30 min with shaking at 1500 rpm. The samples were then spun (8000 rpm, 1 min) and added to 50 µl 1 M Tris-HCl pH 8.5 The glycine elution step was repeated, pooling the second eluate with the first. Half of the samples was taken for Western blot analysis, following addition of 3x sample buffer. 100 µl of 8 M urea was added to the remaining half, and the sample snap frozen.

4.6 Mass spectrometry protocols

4.6.1 Proteolytic digestion of timecourse samples

Time-course samples were reduced using 4 mM dithiothreitol (DTT) (Fluka) for 25 min at 56°C followed by alkylation, using 8 mM iodoacetamide (IAA) incubation, in the dark for 30 min. Excess IAA was quenched by addition of DTT to a final concentration of 8 mM. Proteins were digested first with lysyl endopeptidase (Lys-C) (Wako Pure Chemical Industries) for 4 hr at 37°C in 8 M urea. The sample was then diluted to 2 M urea, with 50 mM ammonium bicarbonate. Trypsin was then added for 12 hr at 37°C. Both enzymes were used at 1:50 ratio relative to the starting amount of protein. Digestions were quenched by acidification with 5% (vol/vol) formic acid (FA).

4.6.2 Di-methyl labelling and titanium dioxide phospho-peptide enrichment

Digested peptides, equivalent to 0.35–1.5 mg of total protein, were bound to SepPak reverse-phase C18-columns (Waters) and subjected to on-column dimethyl labelling as previously described (Boersema et al., 2009). Peptides from all timepoints of the dephosphorylation assay were labelled with cyanoborohydride and deuterated formaldehyde to generate a mass increase of 32 Da per primary amine, referred to as the ‘heavy’ label. Additionally, 6-8 mg of 0 min timepoint was

labelled with formaldehyde and cyanoborohydride to generate a mass increase of 28 Da per primary amine, referred to as the ‘light’ label, 1-2 mg of 0 min was labelled ‘heavy’. After this, 225 µg ‘light’- and ‘heavy’- labelled peptides were mixed (450 µg total). A 50 µg aliquot was dried on a speed-vac and re-suspended in 5% (vol/vol) formic acid and 5% (vol/vol) DMSO. The remainder (400 ug) was subjected to titanium dioxide enrichment.

Phospho-peptide enrichment was performed using microspin columns packed with titanium dioxide (TopTip; Glygen). All spin steps were performed at 550 rpm, equivalent to 34x g_{av}, for 5 min at room temperature (Eppendorf Centrifuge 5427 R). Columns were washed with 65 µl elution buffer (5% ammonia solution in water), then three times with 65 µl loading buffer (5% (vol/vol) trifluoroacetic acid (TFA), 1 M glycolic acid, 80% (vol/vol) acetonitrile (ACN)). An equal volume of loading buffer was added to the dimethyl labelled peptide mixtures. Phospho-peptides were then bound to the column 65 µl at a time. Following loading, columns were washed once each with loading buffer, 0.2% (vol/vol) TFA acid in 80% (vol/vol) ACN, followed by 20% (vol/vol) ACN. Phospho-peptides were eluted with three washes of 20 µl of elution buffer (5% ammonium solution) into 20 µl of 10% (vol/vol) FA and 10% (vol/vol) DMSO. This gave a total volume of 120 µl of which 20 µl was loaded onto the mass spectrometer.

4.6.3 Online nano-LC and tandem mass spectrometry

LC was performed using an EASY-nano-LC 1000 system (Proxeon) in which peptides were initially trapped on a 75 µm internal diameter guard column packed with Reprosil-Gold 120 C18, 3 µm, 120 Å pores (Dr. Maisch GmbH) in solvent A (0.1% [vol/vol] FA in water) using a constant pressure of 500 bar. Peptides were then separated on a 45°C heated EASY-Spray column (50 cm × 75 µm ID,

PepMap RSLC C18, 2 µm; Thermo Fisher Scientific) using a 3 hr linear 8–30% (vol/vol) acetonitrile gradient and constant 200 nl/min flow rate. Titanium dioxide-enriched peptides were introduced via an EASY-Spray nano-electrospray ion source into an Orbitrap Elite mass spectrometer (Thermo Fisher Scientific). Other samples were injected into Q-exactive mass spectrometers (Thermo Fischer Scientific), using linear 8-30% (vol/vol) acetonitrile gradients between 1 and 3 hours in length. Where sample concentrations were known 1 µg, 2 µg and 6 µg were loaded onto the mass spectrometer for 1 hr, 2 hr and 3 hr gradients, respectively. Spectra were acquired with resolution 30,000, m/z range 350–1,500, AGC target 10^6, maximum injection time 250 ms. The 20 most abundant peaks were fragmented using CID (AGC target 5×10^3, maximum injection time 100 ms) or ETD (AGC cation and anion target 5×10^3 and 2×10^5, respectively, maximum injection time 100 ms, normalised collision energy 35%) in a data-dependent decision tree method for titanium dioxide-enriched peptides. Peaks from other samples were fragmented using CID alone. Peptide identification and quantification of ‘heavy’ to ‘light’ phospho-peptide ratios was then performed using MaxQuant (Tyanova et al., 2016a).

4.6.4 Comparison of lysis and digestion conditions for mass spectrometry

HeLa cells were arrested in mitosis, using nocodazole, harvested by shake-off and washed three times in 1x PBS. The cells were counted, aliquoted, pelleted and snap-frozen. Each pellet contained 1.5 million cells, which were then thawed and lysed. Lysis buffer composition was as specified in Table 4.7. Each pellet was assumed to contain 1 mg of protein based on previous work, therefore one tenth of each lysate, 100 µg, was digested. When necessary samples were di-methyl labelled and phospho-enriched as described above.

Table 4.7 Lysis buffer composition

All buffers were supplemented with inhibitors as described in 4.4.1. Abbreviations are as follows: Chloroacetamide (CAA), guanidinium chloride (GdmCl), sodium deoxycholate (SDC), Tris(2-carboxyethyl)phosphine (TCEP).

Sample	Composition	Lysis
Urea (1-2)	8 M Urea, 100 mM AMBIC	Standard
Urea (3)	8 M Urea, 100 mM Tris pH 8.5, 10 mM TCEP, 40 mM CAA	Simultaneous
GdmCl (4)	6 M GdmCl, 100 mM Tris pH 8.5, 10 mM TCEP, 40 mM CAA	Simultaneous
SDC (5)	1% SDC [wt/vol], 100 mM Tris pH 8.5, 10 mM TCEP, 40 mM CAA	Simultaneous

Two separate lysis and digestion protocols were followed. Standard lysis was carried out, on samples 1 and 2, as in Methods 4.4.1. Sample 2 was not clarified prior to digestion. Simultaneous lysis (samples 3-5) was performed as follows: cells were lysed for 5 min at 95°C, then placed on ice for 15 min with sonication, then boiled again, 5 min 95°C. Reduction and alkylation occurred simultaneously with lysis due to the presence of 10 mM TCEP and 40 mM chloro-acetamide (CAA). These samples were then diluted prior to digestion**,** Table 4.8. All samples were digested as follows at 37°C; 4 hr in Lys-C and 12 hr in trypsin. Both enzymes were used at 1:50 with starting material. Following digestion samples were acidified to a final concentration of 5% FA [vol/vol]. These were then bound to C18 columns, washed in 0.6% acetic acid [vol/vol] and eluted in 400 µl 0.6% acetic acid, 80% ACN [vol:vol]. The samples were then dried in a speed-vac and resuspended in 5% FA, 5% DMSO [vol/vol] and 2 µg then run on the mass spectrometer, using a 2 hr linear 8-30% ACN [vol/vol] gradient. Where necessary sodium deoxycholate was removed following digestion, as it would precipitate at the low pH at which the column binding was performed. An equal volume of ethyl

Table 4.8 Sample dilution prior to proteolytic digestion

Dilution factors were relative to the starting sample volume

Condition	Lysis	Dilution buffer	Dilution for Lys-C digestion	Dilution for trypsin digestion
Urea	Standard	50 mM AMBIC	-	1:4
Urea	Simultaneous	10% ACN [vol/vol], 25 mM AMBIC	1:2	1:4
GdmCl	Simultaneous	10% ACN [vol/vol], 25 mM AMBIC	1:3	1:10
SDC	Simultaneous	H_2O	1:10	-

acetate was added to the sample, which was then vortexed for 60 s. The phases were separated at 15,000 g_{av} for 2 min and the organic ethyl acetate phase aspirated. This was repeated four more times, and samples acidified to 5% FA [vol/vol].

Phase-transfer surfactant buffer (PTS) was composed of 0.5% SDC, 0.35% sodium-N-lauroyl sarcosinate (SLS) [wt/vol], 100 mM TEAB supplemented with inhibitors from Methods 4.4.1. After addition of PTS samples were lysed as follows: boil 5 min, 95°C; freeze for 10 min, -80°C; and sonicate for 15 min, on ice. 10 mM DTT and 50 mM IAA were used to reduce and alkylate the sample. The samples were diluted 1:5 prior to digestion with 50 mM AMBIC. Detergent was extracted using ethyl acetate.

4.6.5 High pH fractionation of total proteome samples

Home-made in stage tips, constructed from 5 x 4G C18 discs (Empore) were used for fractionation, all spins were carried out at 3000 g_{av}, 3 min unless otherwise specified. Tips were conditioned once each with methanol, buffer 7 and buffer 1 (Table 4.9). Next 25 µg of peptides, previously resuspended in 5% FA, 5% DMSO [vol/vol], were loaded on each tip; 1500 g_{av}, 3 min. The flow-through was reapplied

twice more and the final flow-through (FT) retained. Bound peptides were washed with 20 µl buffer 1 and the flow through was then pooled with F1 to create the FT/F1 fraction. Peptides were then eluted with 20 µl of buffer 2-7, which formed fraction F2-7 respectively. Samples containing <10% ACN were diluted 1:1 whereas samples with higher concentrations of ACN were diluted to a final [ACN] of 10% and 4/5ths of the sample loaded directly on the mass spectrometer (Table 4.10). These dilutions were performed with 5% FA, 5% DMSO [vol/vol]. The gradient run-time for each fraction was as specified in Table 4.10.

4.6.6 Filter assisted sample preparation

Eluted immuno-precipitation samples were subjected to filter assisted sample preparation (FASP) for mass spectrometry analysis (Wisniewski et al., 2009). All spins were done in an Eppendorf 5427 R centrifuge for 14,500 g_{av}, 15 min at room temperature, unless otherwise stated. Vivacon 500 (Sartorius, 10,000 Da MWCO) filters were washed with 50% ACN, 0.1% TFA before thawed eluates were loaded, and spun for 30 min. Samples were then washed twice in 8 M Urea, 100 mM AMBIC before being reduced and then alkylated using 20 mM TCEP and 50 mM IAA, respectively. Each of these steps was carried out for 30 min, shaking at 700 rpm. The reagents made up in 8 M Urea, 100 mM AMBIC and filters were spun between each step. 1 M Urea, 50 mM AMBIC was then used for two further washes. Filters were then placed in a fresh collection tube. Trypsin was used at a ratio of 1:10,000 with respect to the quantity of starting lysate. Typically, this was between 150-200 ng trypsin per sample made up in 200 µl of 1 M Urea, 50 mM AMBIC. Digesting samples were left incubating at 37°C for 12 hr with gentle shaking. Digested peptides were spun for 30 min, and the filter washed once with 200 µl 0.1% TFA and once with 200 µl 50% ACN, 0.1% TFA. The flow through,

Table 4.9 High pH fractionation buffers

Buffer composition is shown as percentage proportion of two stock solutions, A and B.

Buffer	%A (20 mM NH_3 in H_2O, pH10)	%B (20 mM NH_3 in ACN)
1	100	-
2	96	4
3	92	8
4	88	12
5	80	20
6	60	40
7	20	80

Table 4.10 Fraction dilution and mass spectrometry analysis

The volume of 5% FA, 5% DMSO required to dilute each fraction is specified. Injection volumes and gradient run time for each fraction are also noted.

Fraction	Initial volume (µl)	Dilution volume (µl)	Total sample volume (µl)	Injection volume (µl)	Gradient time (min)
FTF1	40	40	80	**64**	30
F2	20	20	40	**32**	120
F3	20	20	40	**32**	120
F4	20	5	25	**20**	120
F5	20	20	40	**32**	120
F6	20	60	80	**64**	30
F7	20	140	160	**128**	30

containing tryptic peptides, from each of these three steps was collected into the same tube. The samples were then dried down in a reduced pressure centrifuge (Concentrator plus, Eppendorf) at 37°C and the peptides resuspended in 5% FA, 5% DMSO prior to mass spectrometry analysis on a 60 min gradient.

4.7 Computational analysis

Sequence alignments of protein sequences were performed in ClustalΩ (Sievers et al., 2011) and the output alignments were managed in JalView (Waterhouse et al., 2009). Accession numbers from Table 4.3 were used to generate protein sequences for alignment. Encoded graphs and statistical analysis were performed in GraphPad Prism 7.03. All figures were produced using Adobe Photoshop and Illustrator (Adobe CC 2017).

Images were processed in ImageJ. For the CCNB1-GFP fluorescence measurements over time, raw image data was opened in ImageJ using the BioFormats plug-in. Images were then Z-projected to sum the intensity across the volume of the whole cell. A region of interest was drawn around each cell in interphase, this shape was copied to a vacant region of the field of view for a measurement of background signal. The integrated density was then measured in these regions over time and the background subtracted. The corrected values were plotted either as raw intensity or as a percentage based on time 0 min.

Densitometric quantification of Western blots was also performed in ImageJ. Intensity was measured in a 60 x 30 px region of interest around each band. An adjacent region was also measured to account for background intensity.

4.7.1 Analysis of mass spectrometry timecourse data

The MaxQuant (Tyanova et al., 2016a) search output was analysed in Perseus (Tyanova et al., 2016b) as follows. Firstly, data was filtered for contaminants; identified by modification site only and identified in the reverse database only. Phospho-peptides were also filtered so that only those with a localisation score of >0.75 remained. Missing values were then replaced. If a single value was missing, it was replaced either by the average of the two adjacent values in the time series

or the adjacent value if either the first or last timepoint was missing. However, two or more consecutive missing values were not replaced as these were more likely to represent a true 0 value rather than just a missed quantification. Histograms of quantitative ratios were generated prior to replacement of missing values. Next, the t/t_0 for each timepoint was averaged across the experiments, presuming at least two valid quantificational values were observed. Protein groups and phospho-peptides were then filtered for the number of values observed over time, using CCNB1 and PRC1-pT481 as reference profiles of proteolysis and dephosphorylation. While there were a small number of dephosphorylations that were more rapid than the PRC1-pT481, these phosphorylations were less well understood and would not serve as a reliable reference. At this point any remaining missing values were replaced with the constant value, 0, to enable the clustering algorithm to function correctly. The hierarchical clustering algorithm within Perseus was used, grouping rows into four clusters and outputting a heat map. For clustering a single condition, ten iterations and one restart were allowed, this was increased to 25 iterations and two restarts when comparing two conditions.

When comparing two timecourses, cross-mixing was necessary to account for changes in the steady state level of a protein or phospho-peptide. The ratios were extracted from the cross-mixed samples and used to adjust the protein/phospho-peptide ratios relative to control. Following this a more iterative approach to clustering was required; starting from three, the number of clusters was gradually increased. This was continued until the settings were found which yielded the most clusters without producing random groupings containing very few identifications. Taking this approach allowed the comparison of complex trends

found within the large data sets from the two conditions. The heatmap shown was derived from the majority result of the clustering analysis in each case.

Clusters were exported separately from Perseus. The phospho-site sequences of each individual cluster were then aligned in iceLogo 1.2 software, using the sequences of all phospho-sites clustered as the negative set. For the percentage difference in residue enrichment to be seen in the sequence logo a p-value <0.05 was required. To determine half-lives for each cluster, the average ratio and standard error of the mean, for each timepoint, was calculated. These were adjusted to a starting ratio of one, plotted and fitted with a non-linear plateau with one phase decay curve. The half-life was the point where the curve fit crossed y=0.5.

4.7.2 Calculating the stoichiometry of PPP1CA-T320 phosphorylation

To calculate the stoichiometry of PPP1CA-T320 phosphorylation the levels of the non-phosphorylated (YGQFSGLNPGGRPI*TPPR) peptide in the total proteome samples were followed over time; where *T denotes the residue, which can be phosphorylated by CDK1. To account for changes in detection at the peptide level, the ‘heavy’ intensity for non-phosphorylated peptide were adjusted based on the average ratio of other reliably detected peptides which are not subject to modification (LLEVQGSRPGK, LNLDSIIGR, NVQLTENEIR). The adjusted ‘heavy’ intensities of 0 min and 60 min were used to calculate the percentage of dephosphorylated peptide at 0 min, from which the proportion phosphorylated could be inferred. It was assumed that 100% of PP1 was dephosphorylated 60 min after CDK inhibition. The same analysis was repeated for PPP1CB-T316 where YQYGGLNSGRPV*TPPR was the target non-phosphorylated peptide, and the reference peptides used were FLNRHDLDLICR, ICGDIHGQYTDLLR and

IVQMTEAEVR. To gauge the levels of PP1 phosphorylation during the cell cycle, the intensities of the peptides above were used to normalise phospho-peptide intensities for PPP1CA-T320 and PPP1CB-T316 generated from immuno-precipitation samples.

4.7.3 Analysis of immuno-precipitation mass spectrometry data

The MaxQuant search output of immuno-precipitation samples was loaded into Perseus and filtered as described above. Samples were grouped according to the PP1 isoform isolated and any protein identified in less than three out of nine samples in any isoform was discounted from further analysis. The intensity values were then logged to base 10. Any missing values were replaced with the number 6, representing the level of background noise. These values were averaged, and the intensities plotted to identify those which were enriched a 100 fold over control. Alternatively, the following volcano plot analysis was performed to ensure lower abundance but specific interactors were not discounted. The identified proteins were subject to a two-sample T-test, with a minimum p-value and fold change for significance of <0.05 and 10, respectively. A volcano plot was then produced, using the same significance settings, with T-test difference and –log10 p-value on the x and y-axis, respectively. The proteins found to be significant were taken forward. The averaged protein intensities were normalised by median subtraction and clustered. The correct number of clusters was found empirically, as described previously.

The observed levels of PP1 CDK phosphorylation were averaged across the three repeat experiments at each cell cycle stage. These intensities were then normalised based on the intensity of the non-modified peptides described above (Methods 4.7.2).

4.8 Annotation analysis of test digests

Protein annotations were carried out in Perseus. The GO-cellular compartment slim annotation was used to identify the relative numbers of cytoplasmic, membrane and nuclear proteins. The following annotations were grouped together for each category:

Cytoplasmic: cytosol, cytoplasm

Membrane: membrane, plasma membrane, nuclear envelope, mitochondrial envelope

Nuclear: chromosome, nucleolus, nucleoplasm, nucleosome, nucleus

4.9 Imaging

Live cell imaging was carried out in 35 mm dishes with a 14 mm No. 1.5 thickness coverglass window (MatTek Corporation). Cells were imaged in a chamber maintained at 37°C, 5% CO_2, using an Olympus Ix81 inverted microscope, 60x 1.42 NA oil immersion objective and an Ultraview Vx spinning disk confocal system (Perkin Elmer). A C9100-EM-CCD camera was used for image capture. Volocity software was used for experimental set up, image projection and exporting. Cells were excited with 488 nM lasers with 50-150 ms exposures at 4-6% laser power.

HeLa/HeLa-FRT cells for transfection were seeded at 50,000 cells/imaging dish and grown for 48 hr. Cells were transfected with 100 ng pcDNA5-NT-eGFP constructs + 700 ng pBluescript empty vector for 24 hr prior to synchronisation. HeLa-FRT cells were induced with 1 µg/ml doxycycline for 18 hr, simultaneous with synchronisation. Cells were synchronised in S phase with 18 hr treatment with 2.5 mM thymidine. Following synchronisation, cells were washed three times,

once in 1x PBS and twice in DMEM/FBS and then released into 2 ml DMEM/FBS, all of which were pre-equilibrated to 37°C, 5% CO_2. Drugs were diluted in 100 µl of pre-equilibrated media before being added dropwise when necessary during the experiment. For siRNA depletion, cells were seeded and synchronised as above, then transfected with 60 pmol siRNA duplex + 3 µl oligofectamine + 200 µl Opti-MEM for 48 hours.

5 Bibliography

Acquaviva, C., F. Herzog, C. Kraft, and J. Pines. 2004. The anaphase promoting complex/cyclosome is recruited to centromeres by the spindle assembly checkpoint. *Nature cell biology*. 6:892-898.

Afonso, O., I. Matos, A.J. Pereira, P. Aguiar, M.A. Lampson, and H. Maiato. 2014. Feedback control of chromosome separation by a midzone Aurora B gradient. *Science*. 345:332-336.

Agostinis, P., R. Derua, S. Sarno, J. Goris, and W. Merlevede. 1992. Specificity of the polycation-stimulated (type-2A) and ATP,Mg-dependent (type-1) protein phosphatases toward substrates phosphorylated by P34cdc2 kinase. *European journal of biochemistry*. 205:241-248.

Alfieri, C., L. Chang, and D. Barford. 2018. Mechanism for remodelling of the cell cycle checkpoint protein MAD2 by the ATPase TRIP13. *Nature*. 559:274-278.

Alfieri, C., L. Chang, Z. Zhang, J. Yang, S. Maslen, M. Skehel, and D. Barford. 2016. Molecular basis of APC/C regulation by the spindle assembly checkpoint. *Nature*. 536:431-436.

Alfieri, C., S. Zhang, and D. Barford. 2017. Visualizing the complex functions and mechanisms of the anaphase promoting complex/cyclosome (APC/C). *Open biology*. 7.

Alfonso-Perez, T., D. Hayward, J. Holder, U. Gruneberg, and F.A. Barr. 2018. MAD1-dependent recruitment of CDK1-CCNB1 to kinetochores promotes spindle-checkpoint signalling. *The Journal of cell biology*. Under Review.

Archambault, V., X. Zhao, H. White-Cooper, A.T. Carpenter, and D.M. Glover. 2007. Mutations in Drosophila Greatwall/Scant reveal its roles in mitosis and meiosis and interdependence with Polo kinase. *PLoS genetics*. 3:e200.

Arion, D., L. Meijer, L. Brizuela, and D. Beach. 1988. cdc2 is a component of the M phase-specific histone H1 kinase: evidence for identity with MPF. *Cell*. 55:371-378.

Bajaj, R., M. Bollen, W. Peti, and R. Page. 2018. KNL1 Binding to PP1 and Microtubules Is Mutually Exclusive. *Structure*.

Barr, F.A., P.R. Elliott, and U. Gruneberg. 2011. Protein phosphatases and the regulation of mitosis. *Journal of cell science*. 124:2323-2334.

Barr, F.A., and U. Gruneberg. 2007. Cytokinesis: placing and making the final cut. *Cell*. 131:847-860.

Barr, F.A., H.H. Sillje, and E.A. Nigg. 2004. Polo-like kinases and the orchestration of cell division. *Nature reviews. Molecular cell biology*. 5:429-440.

Bassi, Z.I., K.J. Verbrugghe, L. Capalbo, S. Gregory, E. Montembault, D.M. Glover, and P.P. D'Avino. 2011. Sticky/Citron kinase maintains proper RhoA localization at the cleavage site during cytokinesis. *The Journal of cell biology*. 195:595-603.

Bastos, R.N., M.J. Cundell, and F.A. Barr. 2014. KIF4A and PP2A-B56 form a spatially restricted feedback loop opposing Aurora B at the anaphase central spindle. *The Journal of cell biology*. 207:683-693.

Bastos, R.N., X. Penate, M. Bates, D. Hammond, and F.A. Barr. 2012. CYK4 inhibits Rac1-dependent PAK1 and ARHGEF7 effector pathways during cytokinesis. *The Journal of cell biology*. 198:865-880.

Bayliss, R., T. Sardon, I. Vernos, and E. Conti. 2003. Structural basis of Aurora-A activation by TPX2 at the mitotic spindle. *Molecular cell*. 12:851-862.

Beach, D., B. Durkacz, and P. Nurse. 1982. Functionally homologous cell cycle control genes in budding and fission yeast. *Nature*. 300:706-709.

Berdougo, E., M.V. Nachury, P.K. Jackson, and P.V. Jallepalli. 2008. The nucleolar phosphatase Cdc14B is dispensable for chromosome segregation and mitotic exit in human cells. *Cell cycle*. 7:1184-1190.

Beullens, M., V. Vulsteke, A. Van Eynde, I. Jagiello, W. Stalmans, and M. Bollen. 2000. The C-terminus of NIPP1 (nuclear inhibitor of protein phosphatase-1) contains a novel binding site for protein phosphatase-1 that is controlled by tyrosine phosphorylation and RNA binding. *The Biochemical journal*. 352 Pt 3:651-658.

Blake-Hodek, K.A., B.C. Williams, Y. Zhao, P.V. Castilho, W. Chen, Y. Mao, T.M. Yamamoto, and M.L. Goldberg. 2012. Determinants for activation of the atypical AGC kinase Greatwall during M phase entry. *Molecular and cellular biology*. 32:1337-1353.

Boekhout, M., and R. Wolthuis. 2015. Nek2A destruction marks APC/C activation at the prophase-to-prometaphase transition by spindle-checkpoint-restricted Cdc20. *Journal of cell science*. 128:1639-1653.

Boersema, P.J., R. Raijmakers, S. Lemeer, S. Mohammed, and A.J. Heck. 2009. Multiplex peptide stable isotope dimethyl labeling for quantitative proteomics. *Nature protocols*. 4:484-494.

Bollen, M. 2001. Combinatorial control of protein phosphatase-1. *Trends in biochemical sciences*. 26:426-431.

Bollen, M., W. Peti, M.J. Ragusa, and M. Beullens. 2010. The extended PP1 toolkit: designed to create specificity. *Trends in biochemical sciences*. 35:450-458.

Bonacci, T., A. Suzuki, G.D. Grant, N. Stanley, J.G. Cook, N.G. Brown, and M.J. Emanuele. 2018. Cezanne/OTUD7B is a cell cycle-regulated deubiquitinase that antagonizes the degradation of APC/C substrates. *The EMBO journal*. 37.

Brown, A.J., T. Jones, and J. Shuttleworth. 1994. Expression and activity of p40MO15, the catalytic subunit of cdk-activating kinase, during Xenopus oogenesis and embryogenesis. *Molecular biology of the cell*. 5:921-932.

Brown, N.R., S. Korolchuk, M.P. Martin, W.A. Stanley, R. Moukhametzianov, M.E. Noble, and J.A. Endicott. 2015. CDK1 structures reveal conserved and unique features of the essential cell cycle CDK. *Nature communications*. 6:6769.

Bruinsma, W., J.A. Raaijmakers, and R.H. Medema. 2012. Switching Polo-like kinase-1 on and off in time and space. *Trends in biochemical sciences*. 37:534-542.

Burgess, A., S. Vigneron, E. Brioudes, J.C. Labbe, T. Lorca, and A. Castro. 2010. Loss of human Greatwall results in G2 arrest and multiple mitotic defects due to deregulation of the cyclin B-Cdc2/PP2A balance. *Proceedings of the National Academy of Sciences of the United States of America*. 107:12564-12569.

Burton, J.L., and M.J. Solomon. 2001. D box and KEN box motifs in budding yeast Hsl1p are required for APC-mediated degradation and direct binding to Cdc20p and Cdh1p. *Genes & development*. 15:2381-2395.

Carmena, M., and W.C. Earnshaw. 2003. The cellular geography of aurora kinases. *Nature reviews. Molecular cell biology*. 4:842-854.

Carmena, M., S. Ruchaud, and W.C. Earnshaw. 2009. Making the Auroras glow: regulation of Aurora A and B kinase function by interacting proteins. *Current opinion in cell biology*. 21:796-805.

Castilho, P.V., B.C. Williams, S. Mochida, Y. Zhao, and M.L. Goldberg. 2009. The M phase kinase Greatwall (Gwl) promotes inactivation of PP2A/B55delta, a phosphatase directed against CDK phosphosites. *Molecular biology of the cell*. 20:4777-4789.

Castrillon, D.H., and S.A. Wasserman. 1994. Diaphanous is required for cytokinesis in Drosophila and shares domains of similarity with the products of the limb deformity gene. *Development*. 120:3367-3377.

Ceulemans, H., and M. Bollen. 2004. Functional diversity of protein phosphatase-1, a cellular economizer and reset button. *Physiological reviews*. 84:1-39.

Chae, H.D., J. Yun, Y.J. Bang, and D.Y. Shin. 2004. Cdk2-dependent phosphorylation of the NF-Y transcription factor is essential for the expression of the cell cycle-regulatory genes and cell cycle G1/S and G2/M transitions. *Oncogene*. 23:4084-4088.

Chang, L., Z. Zhang, J. Yang, S.H. McLaughlin, and D. Barford. 2015. Atomic structure of the APC/C and its mechanism of protein ubiquitination. *Nature*. 522:450-454.

Chao, W.C., K. Kulkarni, Z. Zhang, E.H. Kong, and D. Barford. 2012. Structure of the mitotic checkpoint complex. *Nature*. 484:208-213.

Cheeseman, I.M. 2014. The kinetochore. *Cold Spring Harbor perspectives in biology*. 6:a015826.

Cheeseman, I.M., J.S. Chappie, E.M. Wilson-Kubalek, and A. Desai. 2006. The conserved KMN network constitutes the core microtubule-binding site of the kinetochore. *Cell*. 127:983-997.

Cheng, Y.L., and R.H. Chen. 2015. Assembly and quality control of the protein phosphatase 1 holoenzyme involves the Cdc48-Shp1 chaperone. *Journal of cell science*. 128:1180-1192.

Cho, H.P., Y. Liu, M. Gomez, J. Dunlap, M. Tyers, and Y. Wang. 2005. The dual-specificity phosphatase CDC14B bundles and stabilizes microtubules. *Molecular and cellular biology*. 25:4541-4551.

Choi, E., H. Choe, J. Min, J.Y. Choi, J. Kim, and H. Lee. 2009. BubR1 acetylation at prometaphase is required for modulating APC/C activity and timing of mitosis. *The EMBO journal*. 28:2077-2089.

Choppara, S., S.K. Malonia, G. Sankaran, M.R. Green, and M.K. Santra. 2018. Degradation of FBXO31 by APC/C is regulated by AKT- and ATM-mediated phosphorylation. *Proceedings of the National Academy of Sciences of the United States of America*. 115:998-1003.

Cleveland, D.W., Y. Mao, and K.F. Sullivan. 2003. Centromeres and kinetochores: from epigenetics to mitotic checkpoint signaling. *Cell*. 112:407-421.

Clijsters, L., J. Ogink, and R. Wolthuis. 2013. The spindle checkpoint, APC/C(Cdc20), and APC/C(Cdh1) play distinct roles in connecting mitosis to S phase. *The Journal of cell biology*. 201:1013-1026.

Cohen, P.T. 2002. Protein phosphatase 1--targeted in many directions. *Journal of cell science*. 115:241-256.

Combes, G., I. Alharbi, L.G. Braga, and S. Elowe. 2017. Playing polo during mitosis: PLK1 takes the lead. *Oncogene*. 36:4819-4827.

Cornelis, S., Y. Bruynooghe, G. Denecker, S. Van Huffel, S. Tinton, and R. Beyaert. 2000. Identification and characterization of a novel cell cycle-regulated internal ribosome entry site. *Molecular cell*. 5:597-605.

Cundell, M.J., R.N. Bastos, T. Zhang, J. Holder, U. Gruneberg, B. Novak, and F.A. Barr. 2013. The BEG (PP2A-B55/ENSA/Greatwall) pathway ensures cytokinesis follows chromosome separation. *Molecular cell*. 52:393-405.

Cundell, M.J., L.H. Hutter, R. Nunes Bastos, E. Poser, J. Holder, S. Mohammed, B. Novak, and F.A. Barr. 2016. A PP2A-B55 recognition signal controls substrate dephosphorylation kinetics during mitotic exit. *The Journal of cell biology*. 214:539-554.

D'Amours, D., and A. Amon. 2004. At the interface between signaling and executing anaphase--Cdc14 and the FEAR network. *Genes & development*. 18:2581-2595.

Davey, N.E., and D.O. Morgan. 2016. Building a Regulatory Network with Short Linear Sequence Motifs: Lessons from the Degrons of the Anaphase-Promoting Complex. *Molecular cell*. 64:12-23.

De Wever, V., I. Nasa, D. Chamousset, D. Lloyd, M. Nimick, H. Xu, L. Trinkle-Mulcahy, and G.B. Moorhead. 2014. The human mitotic kinesin KIF18A binds protein phosphatase 1 (PP1) through a highly conserved docking motif. *Biochemical and biophysical research communications*. 453:432-437.

DeAntoni, A., V. Sala, and A. Musacchio. 2005. Explaining the oligomerization properties of the spindle assembly checkpoint protein Mad2. *Philosophical transactions of the Royal Society of London. Series B, Biological sciences*. 360:637-647, discussion 447-638.

Della Monica, R., R. Visconti, N. Cervone, A.F. Serpico, and D. Grieco. 2015. Fcp1 phosphatase controls Greatwall kinase to promote PP2A-B55 activation and mitotic progression. *eLife*. 4.

DeLuca, J.G., W.E. Gall, C. Ciferri, D. Cimini, A. Musacchio, and E.D. Salmon. 2006. Kinetochore microtubule dynamics and attachment stability are regulated by Hec1. *Cell*. 127:969-982.

Desai, D., H.C. Wessling, R.P. Fisher, and D.O. Morgan. 1995. Effects of phosphorylation by CAK on cyclin binding by CDC2 and CDK2. *Molecular and cellular biology*. 15:345-350.

Di Fiore, B., N.E. Davey, A. Hagting, D. Izawa, J. Mansfeld, T.J. Gibson, and J. Pines. 2015. The ABBA motif binds APC/C activators and is shared by APC/C substrates and regulators. *Developmental cell*. 32:358-372.

Di Fiore, B., and J. Pines. 2008. Defining the role of Emi1 in the DNA replication-segregation cycle. *Chromosoma*. 117:333-338.

Di Fiore, B., and J. Pines. 2010. How cyclin A destruction escapes the spindle assembly checkpoint. *The Journal of cell biology*. 190:501-509.

Dick, A.E., and D.W. Gerlich. 2013. Kinetic framework of spindle assembly checkpoint signalling. *Nature cell biology*. 15:1370-1377.

Dohadwala, M., E.F. da Cruz e Silva, F.L. Hall, R.T. Williams, D.A. Carbonaro-Hall, A.C. Nairn, P. Greengard, and N. Berndt. 1994. Phosphorylation and inactivation of protein phosphatase 1 by cyclin-dependent kinases. *Proceedings of the National Academy of Sciences of the United States of America*. 91:6408-6412.

Douglas, M.E., T. Davies, N. Joseph, and M. Mishima. 2010. Aurora B and 14-3-3 coordinately regulate clustering of centralspindlin during cytokinesis. *Current biology : CB*. 20:927-933.

Draetta, G., F. Luca, J. Westendorf, L. Brizuela, J. Ruderman, and D. Beach. 1989. Cdc2 protein kinase is complexed with both cyclin A and B: evidence for proteolytic inactivation of MPF. *Cell*. 56:829-838.

Dryden, S.C., F.A. Nahhas, J.E. Nowak, A.S. Goustin, and M.A. Tainsky. 2003. Role for human SIRT2 NAD-dependent deacetylase activity in control of mitotic exit in the cell cycle. *Molecular and cellular biology*. 23:3173-3185.

Dunphy, W.G., L. Brizuela, D. Beach, and J. Newport. 1988. The Xenopus cdc2 protein is a component of MPF, a cytoplasmic regulator of mitosis. *Cell*. 54:423-431.

Dunphy, W.G., and A. Kumagai. 1991. The cdc25 protein contains an intrinsic phosphatase activity. *Cell*. 67:189-196.

Dutertre, S., M. Cazales, M. Quaranta, C. Froment, V. Trabut, C. Dozier, G. Mirey, J.P. Bouche, N. Theis-Febvre, E. Schmitt, B. Monsarrat, C. Prigent, and B. Ducommun. 2004. Phosphorylation of CDC25B by Aurora-A at the centrosome contributes to the G2-M transition. *Journal of cell science*. 117:2523-2531.

Dynlacht, B.D., O. Flores, J.A. Lees, and E. Harlow. 1994. Differential regulation of E2F transactivation by cyclin/cdk2 complexes. *Genes & development*. 8:1772-1786.

Egloff, M.P., D.F. Johnson, G. Moorhead, P.T. Cohen, P. Cohen, and D. Barford. 1997. Structural basis for the recognition of regulatory subunits by the catalytic subunit of protein phosphatase 1. *The EMBO journal*. 16:1876-1887.

Espert, A., P. Uluocak, R.N. Bastos, D. Mangat, P. Graab, and U. Gruneberg. 2014. PP2A-B56 opposes Mps1 phosphorylation of Knl1 and thereby promotes spindle assembly checkpoint silencing. *The Journal of cell biology*. 206:833-842.

Espeut, J., D.K. Cheerambathur, L. Krenning, K. Oegema, and A. Desai. 2012. Microtubule binding by KNL-1 contributes to spindle checkpoint silencing at the kinetochore. *The Journal of cell biology*. 196:469-482.

Eto, M. 2009. Regulation of cellular protein phosphatase-1 (PP1) by phosphorylation of the CPI-17 family, C-kinase-activated PP1 inhibitors. *The Journal of biological chemistry*. 284:35273-35277.

Faesen, A.C., M. Thanasoula, S. Maffini, C. Breit, F. Muller, S. van Gerwen, T. Bange, and A. Musacchio. 2017. Basis of catalytic assembly of the mitotic checkpoint complex. *Nature*. 542:498-502.

Fan, H., and S. Penman. 1970. Regulation of protein synthesis in mammalian cells. II. Inhibition of protein synthesis at the level of initiation during mitosis. *Journal of molecular biology*. 50:655-670.

Fang, G. 2002. Checkpoint protein BubR1 acts synergistically with Mad2 to inhibit anaphase-promoting complex. *Molecular biology of the cell*. 13:755-766.

Faragher, A.J., and A.M. Fry. 2003. Nek2A kinase stimulates centrosome disjunction and is required for formation of bipolar mitotic spindles. *Molecular biology of the cell*. 14:2876-2889.

Felix, M.A., P. Cohen, and E. Karsenti. 1990. Cdc2 H1 kinase is negatively regulated by a type 2A phosphatase in the Xenopus early embryonic cell cycle: evidence from the effects of okadaic acid. *The EMBO journal*. 9:675-683.

Ferrari, S., O. Marin, M.A. Pagano, F. Meggio, D. Hess, M. El-Shemerly, A. Krystyniak, and L.A. Pinna. 2005. Aurora-A site specificity: a study with synthetic peptide substrates. *The Biochemical journal*. 390:293-302.

Floyd, S., J. Pines, and C. Lindon. 2008. APC/C Cdh1 targets aurora kinase to control reorganization of the mitotic spindle at anaphase. *Current biology : CB*. 18:1649-1658.

Foe, I.T., S.A. Foster, S.K. Cheung, S.Z. DeLuca, D.O. Morgan, and D.P. Toczyski. 2011. Ubiquitination of Cdc20 by the APC occurs through an intramolecular mechanism. *Current biology : CB*. 21:1870-1877.

Foley, E.A., M. Maldonado, and T.M. Kapoor. 2011. Formation of stable attachments between kinetochores and microtubules depends on the B56-PP2A phosphatase. *Nature cell biology*. 13:1265-1271.

Fry, A.M., T. Mayor, P. Meraldi, Y.D. Stierhof, K. Tanaka, and E.A. Nigg. 1998a. C-Nap1, a novel centrosomal coiled-coil protein and candidate substrate of the cell cycle-regulated protein kinase Nek2. *The Journal of cell biology*. 141:1563-1574.

Fry, A.M., P. Meraldi, and E.A. Nigg. 1998b. A centrosomal function for the human Nek2 protein kinase, a member of the NIMA family of cell cycle regulators. *The EMBO journal*. 17:470-481.

Frye, J.J., N.G. Brown, G. Petzold, E.R. Watson, C.R. Grace, A. Nourse, M.A. Jarvis, R.W. Kriwacki, J.M. Peters, H. Stark, and B.A. Schulman. 2013. Electron microscopy structure of human APC/C(CDH1)-EMI1 reveals multimodal mechanism of E3 ligase shutdown. *Nature structural & molecular biology*. 20:827-835.

Fu, J., M. Bian, Q. Jiang, and C. Zhang. 2007. Roles of Aurora kinases in mitosis and tumorigenesis. *Molecular cancer research : MCR*. 5:1-10.

Fu, J., M. Bian, J. Liu, Q. Jiang, and C. Zhang. 2009. A single amino acid change converts Aurora-A into Aurora-B-like kinase in terms of partner specificity and cellular function. *Proceedings of the National Academy of Sciences of the United States of America*. 106:6939-6944.

Fujimitsu, K., M. Grimaldi, and H. Yamano. 2016. Cyclin-dependent kinase 1-dependent activation of APC/C ubiquitin ligase. *Science*. 352:1121-1124.

Funabiki, H., K. Kumada, and M. Yanagida. 1996. Fission yeast Cut1 and Cut2 are essential for sister chromatid separation, concentrate along the metaphase spindle and form large complexes. *The EMBO journal*. 15:6617-6628.

Funabiki, H., and D.J. Wynne. 2013. Making an effective switch at the kinetochore by phosphorylation and dephosphorylation. *Chromosoma*. 122:135-158.

Furuno, N., N. den Elzen, and J. Pines. 1999. Human cyclin A is required for mitosis until mid prophase. *The Journal of cell biology*. 147:295-306.

Gabrielli, B.G., J.M. Clark, A.K. McCormack, and K.A. Ellem. 1997. Hyperphosphorylation of the N-terminal domain of Cdc25 regulates activity toward cyclin B1/Cdc2 but not cyclin A/Cdk2. *The Journal of biological chemistry*. 272:28607-28614.

Gabrielli, B.G., C.P. De Souza, I.D. Tonks, J.M. Clark, N.K. Hayward, and K.A. Ellem. 1996. Cytoplasmic accumulation of cdc25B phosphatase in mitosis triggers centrosomal microtubule nucleation in HeLa cells. *Journal of cell science*. 109 (Pt 5):1081-1093.

Garnett, M.J., J. Mansfeld, C. Godwin, T. Matsusaka, J. Wu, P. Russell, J. Pines, and A.R. Venkitaraman. 2009. UBE2S elongates ubiquitin chains on APC/C substrates to promote mitotic exit. *Nature cell biology*. 11:1363-1369.

Gautier, J., J. Minshull, M. Lohka, M. Glotzer, T. Hunt, and J.L. Maller. 1990. Cyclin is a component of maturation-promoting factor from Xenopus. *Cell*. 60:487-494.

Gautier, J., C. Norbury, M. Lohka, P. Nurse, and J. Maller. 1988. Purified maturation-promoting factor contains the product of a Xenopus homolog of the fission yeast cell cycle control gene cdc2+. *Cell*. 54:433-439.

Gavet, O., and J. Pines. 2010a. Activation of cyclin B1-Cdk1 synchronizes events in the nucleus and the cytoplasm at mitosis. *The Journal of cell biology*. 189:247-259.

Gavet, O., and J. Pines. 2010b. Progressive activation of CyclinB1-Cdk1 coordinates entry to mitosis. *Developmental cell*. 18:533-543.

Geley, S., E. Kramer, C. Gieffers, J. Gannon, J.M. Peters, and T. Hunt. 2001. Anaphase-promoting complex/cyclosome-dependent proteolysis of human cyclin A starts at the beginning of mitosis and is not subject to the spindle assembly checkpoint. *The Journal of cell biology*. 153:137-148.

Gharbi-Ayachi, A., J.C. Labbe, A. Burgess, S. Vigneron, J.M. Strub, E. Brioudes, A. Van-Dorsselaer, A. Castro, and T. Lorca. 2010. The substrate of Greatwall kinase, Arpp19, controls mitosis by inhibiting protein phosphatase 2A. *Science*. 330:1673-1677.

Glotzer, M. 2005. The molecular requirements for cytokinesis. *Science*. 307:1735-1739.

Glotzer, M., A.W. Murray, and M.W. Kirschner. 1991. Cyclin is degraded by the ubiquitin pathway. *Nature*. 349:132-138.

Gong, D., and J.E. Ferrell, Jr. 2010. The roles of cyclin A2, B1, and B2 in early and late mitotic events. *Molecular biology of the cell*. 21:3149-3161.

Gorr, I.H., D. Boos, and O. Stemmann. 2005. Mutual inhibition of separase and Cdk1 by two-step complex formation. *Molecular cell*. 19:135-141.

Gould, K.L., and P. Nurse. 1989. Tyrosine phosphorylation of the fission yeast cdc2+ protein kinase regulates entry into mitosis. *Nature*. 342:39-45.

Grallert, A., E. Boke, A. Hagting, B. Hodgson, Y. Connolly, J.R. Griffiths, D.L. Smith, J. Pines, and I.M. Hagan. 2015. A PP1-PP2A phosphatase relay controls mitotic progression. *Nature*. 517:94-98.

Grosskortenhaus, R., and F. Sprenger. 2002. Rca1 inhibits APC-Cdh1(Fzr) and is required to prevent cyclin degradation in G2. *Developmental cell*. 2:29-40.

Gruneberg, U., R. Neef, R. Honda, E.A. Nigg, and F.A. Barr. 2004. Relocation of Aurora B from centromeres to the central spindle at the metaphase to anaphase transition requires MKlp2. *The Journal of cell biology*. 166:167-172.

Gurden, M.D., A.J. Holland, W. van Zon, A. Tighe, M.A. Vergnolle, D.A. Andres, H.P. Spielmann, M. Malumbres, R.M. Wolthuis, D.W. Cleveland, and S.S. Taylor. 2010. Cdc20 is required for the post-anaphase, KEN-dependent degradation of centromere protein F. *Journal of cell science*. 123:321-330.

Guse, A., M. Mishima, and M. Glotzer. 2005. Phosphorylation of ZEN-4/MKLP1 by aurora B regulates completion of cytokinesis. *Current biology : CB*. 15:778-786.

Hafner, J., M.I. Mayr, M.M. Mockel, and T.U. Mayer. 2014. Pre-anaphase chromosome oscillations are regulated by the antagonistic activities of Cdk1 and PP1 on Kif18A. *Nature communications*. 5:4397.

Hagting, A., C. Karlsson, P. Clute, M. Jackman, and J. Pines. 1998. MPF localization is controlled by nuclear export. *The EMBO journal*. 17:4127-4138.

Hames, R.S., S.L. Wattam, H. Yamano, R. Bacchieri, and A.M. Fry. 2001. APC/C-mediated destruction of the centrosomal kinase Nek2A occurs in early mitosis and depends upon a cyclin A-type D-box. *The EMBO journal*. 20:7117-7127.

Hansen, D.V., A.V. Loktev, K.H. Ban, and P.K. Jackson. 2004. Plk1 regulates activation of the anaphase promoting complex by phosphorylating and triggering SCFbetaTrCP-dependent destruction of the APC Inhibitor Emi1. *Molecular biology of the cell*. 15:5623-5634.

Hauf, S., E. Roitinger, B. Koch, C.M. Dittrich, K. Mechtler, and J.M. Peters. 2005. Dissociation of cohesin from chromosome arms and loss of arm cohesion during early mitosis depends on phosphorylation of SA2. *PLoS biology*. 3:e69.

Hayes, M.J., Y. Kimata, S.L. Wattam, C. Lindon, G. Mao, H. Yamano, and A.M. Fry. 2006. Early mitotic degradation of Nek2A depends on Cdc20-independent interaction with the APC/C. *Nature cell biology*. 8:607-614.

Hayward, D., T. Alfonso-Perez, M.J. Cundell, M. Hopkins, J. Holder, J. Bancroft, L.H. Hutter, B. Novak, F.A. Barr and U. Gruneberg. 2018. CDK1-CCNB1 creates a spindle checkpoint permissive state by enabling MPS1 kinetochore localisation. *The Journal of cell biology*. Under Review.

He, E., O. Kapuy, R.A. Oliveira, F. Uhlmann, J.J. Tyson, and B. Novak. 2011. System-level feedbacks make the anaphase switch irreversible. *Proceedings of the National Academy of Sciences of the United States of America*. 108:10016-10021.

Hegarat, N., C. Vesely, P.K. Vinod, C. Ocasio, N. Peter, J. Gannon, A.W. Oliver, B. Novak, and H. Hochegger. 2014. PP2A/B55 and Fcp1 regulate Greatwall and Ensa dephosphorylation during mitotic exit. *PLoS genetics*. 10:e1004004.

Heim, A., A. Konietzny, and T.U. Mayer. 2015. Protein phosphatase 1 is essential for Greatwall inactivation at mitotic exit. *EMBO reports*. 16:1501-1510.

Hein, J.B., E.P.T. Hertz, D.H. Garvanska, T. Kruse, and J. Nilsson. 2017. Distinct kinetics of serine and threonine dephosphorylation are essential for mitosis. *Nature cell biology*. 19:1433-1440.

Hellmuth, S., F. Bottger, C. Pan, M. Mann, and O. Stemmann. 2014. PP2A delays APC/C-dependent degradation of separase-associated but not free securin. *The EMBO journal*. 33:1134-1147.

Hertz, E.P.T., T. Kruse, N.E. Davey, B. Lopez-Mendez, J.O. Sigurethsson, G. Montoya, J.V. Olsen, and J. Nilsson. 2016. A Conserved Motif Provides Binding Specificity to the PP2A-B56 Phosphatase. *Molecular cell*. 63:686-695.

Herzog, F., K. Mechtler, and J.M. Peters. 2005. Identification of cell cycle-dependent phosphorylation sites on the anaphase-promoting complex/cyclosome by mass spectrometry. *Methods in enzymology*. 398:231-245.

Herzog, F., I. Primorac, P. Dube, P. Lenart, B. Sander, K. Mechtler, H. Stark, and J.M. Peters. 2009. Structure of the anaphase-promoting complex/cyclosome interacting with a mitotic checkpoint complex. *Science*. 323:1477-1481.

Hewitt, L., A. Tighe, S. Santaguida, A.M. White, C.D. Jones, A. Musacchio, S. Green, and S.S. Taylor. 2010. Sustained Mps1 activity is required in mitosis to recruit O-Mad2 to the Mad1-C-Mad2 core complex. *The Journal of cell biology*. 190:25-34.

Hickson, G.R., A. Echard, and P.H. O'Farrell. 2006. Rho-kinase controls cell shape changes during cytokinesis. *Current biology : CB*. 16:359-370.

Hindley, J., and G.A. Phear. 1984. Sequence of the cell division gene CDC2 from Schizosaccharomyces pombe; patterns of splicing and homology to protein kinases. *Gene*. 31:129-134.

Hirota, T., N. Kunitoku, T. Sasayama, T. Marumoto, D. Zhang, M. Nitta, K. Hatakeyama, and H. Saya. 2003. Aurora-A and an interacting activator, the LIM protein Ajuba, are required for mitotic commitment in human cells. *Cell*. 114:585-598.

Hiruma, Y., C. Sacristan, S.T. Pachis, A. Adamopoulos, T. Kuijt, M. Ubbink, E. von Castelmur, A. Perrakis, and G.J. Kops. 2015. CELL DIVISION CYCLE. Competition between MPS1 and microtubules at kinetochores regulates spindle checkpoint signaling. *Science*. 348:1264-1267.

Hoffmann, I., P.R. Clarke, M.J. Marcote, E. Karsenti, and G. Draetta. 1993. Phosphorylation and activation of human cdc25-C by cdc2--cyclin B and its involvement in the self-amplification of MPF at mitosis. *The EMBO journal*. 12:53-63.

Howell, B.J., B.F. McEwen, J.C. Canman, D.B. Hoffman, E.M. Farrar, C.L. Rieder, and E.D. Salmon. 2001. Cytoplasmic dynein/dynactin drives kinetochore protein transport to the spindle poles and has a role in mitotic spindle checkpoint inactivation. *The Journal of cell biology*. 155:1159-1172.

Hsu, J.Y., J.D. Reimann, C.S. Sorensen, J. Lukas, and P.K. Jackson. 2002a. E2F-dependent accumulation of hEmi1 regulates S phase entry by inhibiting APC(Cdh1). *Nature cell biology*. 4:358-366.

Hsu, J.Y., J.D.R. Reimann, C.S. Sorensen, J. Lukas, and P.K. Jackson. 2002b. E2F-dependent accumulation of hEmi1 regulates S phase entry by inhibiting APC(Cdh1). *Nature cell biology*. 4:358-366.

Huang, X., R. Hatcher, J.P. York, and P. Zhang. 2005. Securin and separase phosphorylation act redundantly to maintain sister chromatid cohesion in mammalian cells. *Molecular biology of the cell*. 16:4725-4732.

Hummer, S., and T.U. Mayer. 2009. Cdk1 negatively regulates midzone localization of the mitotic kinesin Mklp2 and the chromosomal passenger complex. *Current biology : CB*. 19:607-612.

Hurley, T.D., J. Yang, L. Zhang, K.D. Goodwin, Q. Zou, M. Cortese, A.K. Dunker, and A.A. DePaoli-Roach. 2007. Structural basis for regulation of protein phosphatase 1 by inhibitor-2. *The Journal of biological chemistry*. 282:28874-28883.

Hutchins, J.R., Y. Toyoda, B. Hegemann, I. Poser, J.K. Heriche, M.M. Sykora, M. Augsburg, O. Hudecz, B.A. Buschhorn, J. Bulkescher, C. Conrad, D. Comartin, A. Schleiffer, M. Sarov, A. Pozniakovsky, M.M. Slabicki, S. Schloissnig, I. Steinmacher, M. Leuschner, A. Ssykor, S. Lawo, L. Pelletier, H. Stark, K. Nasmyth, J. Ellenberg, R. Durbin, F. Buchholz, K. Mechtler, A.A. Hyman, and J.M. Peters. 2010. Systematic analysis of human protein complexes identifies chromosome segregation proteins. *Science*. 328:593-599.

Imaoka, T., J.A. Lynham, and R.J. Haslam. 1983. Purification and characterization of the 47,000-dalton protein phosphorylated during degranulation of human platelets. *The Journal of biological chemistry*. 258:11404-11414.

Izawa, D., and J. Pines. 2015. The mitotic checkpoint complex binds a second CDC20 to inhibit active APC/C. *Nature*. 517:631-634.

Jacobs, H.W., E. Keidel, and C.F. Lehner. 2001. A complex degradation signal in Cyclin A required for G1 arrest, and a C-terminal region for mitosis. *The EMBO journal*. 20:2376-2386.

Janssens, V., and J. Goris. 2001. Protein phosphatase 2A: a highly regulated family of serine/threonine phosphatases implicated in cell growth and signalling. *The Biochemical journal*. 353:417-439.

Jaspersen, S.L., J.F. Charles, R.L. Tinker-Kulberg, and D.O. Morgan. 1998. A late mitotic regulatory network controlling cyclin destruction in Saccharomyces cerevisiae. *Molecular biology of the cell*. 9:2803-2817.

Jeffrey, P.D., A.A. Russo, K. Polyak, E. Gibbs, J. Hurwitz, J. Massague, and N.P. Pavletich. 1995. Mechanism of CDK activation revealed by the structure of a cyclinA-CDK2 complex. *Nature*. 376:313-320.

Jeng, J.C., Y.M. Lin, C.H. Lin, and H.M. Shih. 2009. Cdh1 controls the stability of TACC3. *Cell cycle*. 8:3537-3544.

Ji, Z., H. Gao, L. Jia, B. Li, and H. Yu. 2017. A sequential multi-target Mps1 phosphorylation cascade promotes spindle checkpoint signaling. *eLife*. 6.

Ji, Z., H. Gao, and H. Yu. 2015. CELL DIVISION CYCLE. Kinetochore attachment sensed by competitive Mps1 and microtubule binding to Ndc80C. *Science*. 348:1260-1264.

Jia, L., B. Li, and H. Yu. 2016. The Bub1-Plk1 kinase complex promotes spindle checkpoint signalling through Cdc20 phosphorylation. *Nature communications*. 7:10818.

Jiang, W., G. Jimenez, N.J. Wells, T.J. Hope, G.M. Wahl, T. Hunter, and R. Fukunaga. 1998. PRC1: a human mitotic spindle-associated CDK substrate protein required for cytokinesis. *Molecular cell*. 2:877-885.

Jin, F., H. Liu, F. Liang, R. Rizkallah, M.M. Hurt, and Y. Wang. 2008a. Temporal control of the dephosphorylation of Cdk substrates by mitotic exit pathways in budding yeast. *Proceedings of the National Academy of Sciences of the United States of America*. 105:16177-16182.

Jin, L., A. Williamson, S. Banerjee, I. Philipp, and M. Rape. 2008b. Mechanism of ubiquitin-chain formation by the human anaphase-promoting complex. *Cell*. 133:653-665.

Juang, Y.L., J. Huang, J.M. Peters, M.E. McLaughlin, C.Y. Tai, and D. Pellman. 1997. APC-mediated proteolysis of Ase1 and the morphogenesis of the mitotic spindle. *Science*. 275:1311-1314.

Kaiser, B.K., Z.A. Zimmerman, H. Charbonneau, and P.K. Jackson. 2002. Disruption of centrosome structure, chromosome segregation, and cytokinesis by misexpression of human Cdc14A phosphatase. *Molecular biology of the cell*. 13:2289-2300.

Kallio, M., J. Weinstein, J.R. Daum, D.J. Burke, and G.J. Gorbsky. 1998. Mammalian p55CDC mediates association of the spindle checkpoint protein Mad2 with the cyclosome/anaphase-promoting complex, and is involved in regulating anaphase onset and late mitotic events. *The Journal of cell biology*. 141:1393-1406.

Karaiskou, A., C. Jessus, T. Brassac, and R. Ozon. 1999. Phosphatase 2A and polo kinase, two antagonistic regulators of cdc25 activation and MPF auto-amplification. *Journal of cell science*. 112 (Pt 21):3747-3756.

Kellogg, D.R. 2003. Wee1-dependent mechanisms required for coordination of cell growth and cell division. *Journal of cell science*. 116:4883-4890.

Kelly, A., K.E. Wickliffe, L. Song, I. Fedrigo, and M. Rape. 2014. Ubiquitin chain elongation requires E3-dependent tracking of the emerging conjugate. *Molecular cell*. 56:232-245.

Kettenbach, A.N., D.K. Schweppe, B.K. Faherty, D. Pechenick, A.A. Pletnev, and S.A. Gerber. 2011. Quantitative phosphoproteomics identifies substrates and functional modules of Aurora and Polo-like kinase activities in mitotic cells. *Science signaling*. 4:rs5.

Kim, Y.M., T. Watanabe, P.B. Allen, Y.M. Kim, S.J. Lee, P. Greengard, A.C. Nairn, and Y.G. Kwon. 2003. PNUTS, a protein phosphatase 1 (PP1) nuclear targeting subunit. Characterization of its PP1- and RNA-binding domains and regulation by phosphorylation. *The Journal of biological chemistry*. 278:13819-13828.

Kimata, Y., J.E. Baxter, A.M. Fry, and H. Yamano. 2008. A role for the Fizzy/Cdc20 family of proteins in activation of the APC/C distinct from substrate recruitment. *Molecular cell*. 32:576-583.

King, R.W., M. Glotzer, and M.W. Kirschner. 1996. Mutagenic analysis of the destruction signal of mitotic cyclins and structural characterization of ubiquitinated intermediates. *Molecular biology of the cell*. 7:1343-1357.

King, R.W., J.M. Peters, S. Tugendreich, M. Rolfe, P. Hieter, and M.W. Kirschner. 1995. A 20S complex containing CDC27 and CDC16 catalyzes the mitosis-specific conjugation of ubiquitin to cyclin B. *Cell*. 81:279-288.

Kitajima, T.S., T. Sakuno, K. Ishiguro, S. Iemura, T. Natsume, S.A. Kawashima, and Y. Watanabe. 2006. Shugoshin collaborates with protein phosphatase 2A to protect cohesin. *Nature*. 441:46-52.

Koepp, D.M., L.K. Schaefer, X. Ye, K. Keyomarsi, C. Chu, J.W. Harper, and S.J. Elledge. 2001. Phosphorylation-dependent ubiquitination of cyclin E by the SCFFbw7 ubiquitin ligase. *Science*. 294:173-177.

Komander, D., and M. Rape. 2012. The ubiquitin code. *Annual review of biochemistry*. 81:203-229.

Kotani, S., H. Tanaka, H. Yasuda, and K. Todokoro. 1999. Regulation of APC activity by phosphorylation and regulatory factors. *The Journal of cell biology*. 146:791-800.

Kraft, C., F. Herzog, C. Gieffers, K. Mechtler, A. Hagting, J. Pines, and J.M. Peters. 2003. Mitotic regulation of the human anaphase-promoting complex by phosphorylation. *The EMBO journal*. 22:6598-6609.

Kraft, C., H.C. Vodermaier, S. Maurer-Stroh, F. Eisenhaber, and J.M. Peters. 2005. The WD40 propeller domain of Cdh1 functions as a destruction box receptor for APC/C substrates. *Molecular cell*. 18:543-553.

Kramer, E.R., C. Gieffers, G. Holzl, M. Hengstschlager, and J.M. Peters. 1998. Activation of the human anaphase-promoting complex by proteins of the CDC20/Fizzy family. *Current biology : CB*. 8:1207-1210.

Kramer, E.R., N. Scheuringer, A.V. Podtelejnikov, M. Mann, and J.M. Peters. 2000. Mitotic regulation of the APC activator proteins CDC20 and CDH1. *Molecular biology of the cell*. 11:1555-1569.

Kruse, T., G. Zhang, M.S. Larsen, T. Lischetti, W. Streicher, T. Kragh Nielsen, S.P. Bjorn, and J. Nilsson. 2013. Direct binding between BubR1 and B56-PP2A phosphatase complexes regulate mitotic progression. *Journal of cell science*. 126:1086-1092.

Kufer, T.A., H.H. Sillje, R. Korner, O.J. Gruss, P. Meraldi, and E.A. Nigg. 2002. Human TPX2 is required for targeting Aurora-A kinase to the spindle. *The Journal of cell biology*. 158:617-623.

Kulak, N.A., G. Pichler, I. Paron, N. Nagaraj, and M. Mann. 2014. Minimal, encapsulated proteomic-sample processing applied to copy-number estimation in eukaryotic cells. *Nature methods*. 11:319-324.

Labbe, J.C., J.P. Capony, D. Caput, J.C. Cavadore, J. Derancourt, M. Kaghad, J.M. Lelias, A. Picard, and M. Doree. 1989. MPF from starfish oocytes at first meiotic metaphase is a heterodimer containing one molecule of cdc2 and one molecule of cyclin B. *The EMBO journal*. 8:3053-3058.

Labit, H., K. Fujimitsu, N.S. Bayin, T. Takaki, J. Gannon, and H. Yamano. 2012. Dephosphorylation of Cdc20 is required for its C-box-dependent activation of the APC/C. *The EMBO journal*. 31:3351-3362.

Lammer, C., S. Wagerer, R. Saffrich, D. Mertens, W. Ansorge, and I. Hoffmann. 1998. The cdc25B phosphatase is essential for the G2/M phase transition in human cells. *Journal of cell science*. 111 (Pt 16):2445-2453.

Laoukili, J., M. Alvarez, L.A. Meijer, M. Stahl, S. Mohammed, L. Kleij, A.J. Heck, and R.H. Medema. 2008. Activation of FoxM1 during G2 requires cyclin A/Cdk-dependent relief of autorepression by the FoxM1 N-terminal domain. *Molecular and cellular biology*. 28:3076-3087.

Lara-Gonzalez, P., M.I. Scott, M. Diez, O. Sen, and S.S. Taylor. 2011. BubR1 blocks substrate recruitment to the APC/C in a KEN-box-dependent manner. *Journal of cell science*. 124:4332-4345.

Lehner, C.F., and P.H. O'Farrell. 1990. The roles of Drosophila cyclins A and B in mitotic control. *Cell*. 61:535-547.

Li, Q., L. Chang, S. Aibara, J. Yang, Z. Zhang, and D. Barford. 2016. WD40 domain of Apc1 is critical for the coactivator-induced allosteric transition that stimulates APC/C catalytic activity. *Proceedings of the National Academy of Sciences of the United States of America*. 113:10547-10552.

Lindon, C., and J. Pines. 2004. Ordered proteolysis in anaphase inactivates Plk1 to contribute to proper mitotic exit in human cells. *The Journal of cell biology*. 164:233-241.

Lindqvist, A., H. Kallstrom, A. Lundgren, E. Barsoum, and C.K. Rosenthal. 2005. Cdc25B cooperates with Cdc25A to induce mitosis but has a unique role in activating cyclin B1-Cdk1 at the centrosome. *The Journal of cell biology*. 171:35-45.

Lischetti, T., G. Zhang, G.G. Sedgwick, V.M. Bolanos-Garcia, and J. Nilsson. 2014. The internal Cdc20 binding site in BubR1 facilitates both spindle assembly checkpoint signalling and silencing. *Nature communications*. 5:5563.

Liu, D., and M.A. Lampson. 2009. Regulation of kinetochore-microtubule attachments by Aurora B kinase. *Biochemical Society transactions*. 37:976-980.

Liu, D., M. Vleugel, C.B. Backer, T. Hori, T. Fukagawa, I.M. Cheeseman, and M.A. Lampson. 2010. Regulated targeting of protein phosphatase 1 to the outer kinetochore by KNL1 opposes Aurora B kinase. *The Journal of cell biology*. 188:809-820.

London, N., S. Ceto, J.A. Ranish, and S. Biggins. 2012. Phosphoregulation of Spc105 by Mps1 and PP1 regulates Bub1 localization to kinetochores. *Current biology : CB*. 22:900-906.

Lu, D., J.R. Girard, W. Li, A. Mizrak, and D.O. Morgan. 2015. Quantitative framework for ordered degradation of APC/C substrates. *BMC biology*. 13:96.

Lu, D., J.Y. Hsiao, N.E. Davey, V.A. Van Voorhis, S.A. Foster, C. Tang, and D.O. Morgan. 2014. Multiple mechanisms determine the order of APC/C substrate degradation in mitosis. *The Journal of cell biology*. 207:23-39.

Lucocq, J., G. Warren, and J. Pryde. 1991. Okadaic acid induces Golgi apparatus fragmentation and arrest of intracellular transport. *Journal of cell science*. 100 (Pt 4):753-759.

Luo, X., Z. Tang, G. Xia, K. Wassmann, T. Matsumoto, J. Rizo, and H. Yu. 2004. The Mad2 spindle checkpoint protein has two distinct natively folded states. *Nature structural & molecular biology*. 11:338-345.

Madaule, P., M. Eda, N. Watanabe, K. Fujisawa, T. Matsuoka, H. Bito, T. Ishizaki, and S. Narumiya. 1998. Role of citron kinase as a target of the small GTPase Rho in cytokinesis. *Nature*. 394:491-494.

Mailand, N., C. Lukas, B.K. Kaiser, P.K. Jackson, J. Bartek, and J. Lukas. 2002. Deregulated human Cdc14A phosphatase disrupts centrosome separation and chromosome segregation. *Nature cell biology*. 4:317-322.

Major, M.L., R. Lepe, and R.H. Costa. 2004. Forkhead box M1B transcriptional activity requires binding of Cdk-cyclin complexes for phosphorylation-dependent recruitment of p300/CBP coactivators. *Molecular and cellular biology*. 24:2649-2661.

Manning, G., D.B. Whyte, R. Martinez, T. Hunter, and S. Sudarsanam. 2002. The protein kinase complement of the human genome. *Science*. 298:1912-1934.

Mansfeld, J., P. Collin, M.O. Collins, J.S. Choudhary, and J. Pines. 2011. APC15 drives the turnover of MCC-CDC20 to make the spindle assembly checkpoint responsive to kinetochore attachment. *Nature cell biology*. 13:1234-1243.

Margottin-Goguet, F., J.Y. Hsu, A. Loktev, H.M. Hsieh, J.D. Reimann, and P.K. Jackson. 2003. Prophase destruction of Emi1 by the SCF(betaTrCP/Slimb) ubiquitin ligase activates the anaphase promoting complex to allow progression beyond prometaphase. *Developmental cell*. 4:813-826.

Marx, H., S. Lemeer, J.E. Schliep, L. Matheron, S. Mohammed, J. Cox, M. Mann, A.J. Heck, and B. Kuster. 2013. A large synthetic peptide and phosphopeptide reference library for mass spectrometry-based proteomics. *Nature biotechnology*. 31:557-564.

Masuda, T., N. Saito, M. Tomita, and Y. Ishihama. 2009. Unbiased quantitation of Escherichia coli membrane proteome using phase transfer surfactants. *Molecular & cellular proteomics : MCP*. 8:2770-2777.

Matsumoto, M.L., K.E. Wickliffe, K.C. Dong, C. Yu, I. Bosanac, D. Bustos, L. Phu, D.S. Kirkpatrick, S.G. Hymowitz, M. Rape, R.F. Kelley, and V.M. Dixit. 2010. K11-linked polyubiquitination in cell cycle control revealed by a K11 linkage-specific antibody. *Molecular cell*. 39:477-484.

McGarry, T.J., and M.W. Kirschner. 1998. Geminin, an inhibitor of DNA replication, is degraded during mitosis. *Cell*. 93:1043-1053.

Meadows, J.C., L.A. Shepperd, V. Vanoosthuyse, T.C. Lancaster, A.M. Sochaj, G.J. Buttrick, K.G. Hardwick, and J.B. Millar. 2011. Spindle checkpoint silencing

requires association of PP1 to both Spc7 and kinesin-8 motors. *Developmental cell*. 20:739-750.
Meijer, L., D. Arion, R. Golsteyn, J. Pines, L. Brizuela, T. Hunt, and D. Beach. 1989. Cyclin is a component of the sea urchin egg M-phase specific histone H1 kinase. *The EMBO journal*. 8:2275-2282.
Meraldi, P., A.D. McAinsh, E. Rheinbay, and P.K. Sorger. 2006. Phylogenetic and structural analysis of centromeric DNA and kinetochore proteins. *Genome biology*. 7:R23.
Meyer, H.J., and M. Rape. 2011. Processive ubiquitin chain formation by the anaphase-promoting complex. *Seminars in cell & developmental biology*. 22:544-550.
Miller, J.J., M.K. Summers, D.V. Hansen, M.V. Nachury, N.L. Lehman, A. Loktev, and P.K. Jackson. 2006. Emi1 stably binds and inhibits the anaphase-promoting complex/cyclosome as a pseudosubstrate inhibitor. *Genes & development*. 20:2410-2420.
Minshull, J., R. Golsteyn, C.S. Hill, and T. Hunt. 1990. The A- and B-type cyclin associated cdc2 kinases in Xenopus turn on and off at different times in the cell cycle. *The EMBO journal*. 9:2865-2875.
Mishima, M., V. Pavicic, U. Gruneberg, E.A. Nigg, and M. Glotzer. 2004. Cell cycle regulation of central spindle assembly. *Nature*. 430:908-913.
Mitsuhashi, S., N. Matsuura, M. Ubukata, H. Oikawa, H. Shima, and K. Kikuchi. 2001. Tautomycetin is a novel and specific inhibitor of serine/threonine protein phosphatase type 1, PP1. *Biochemical and biophysical research communications*. 287:328-331.
Mitsuhashi, S., H. Shima, N. Tanuma, N. Matsuura, M. Takekawa, T. Urano, T. Kataoka, M. Ubukata, and K. Kikuchi. 2003. Usage of tautomycetin, a novel inhibitor of protein phosphatase 1 (PP1), reveals that PP1 is a positive regulator of Raf-1 in vivo. *The Journal of biological chemistry*. 278:82-88.
Mocciaro, A., E. Berdougo, K. Zeng, E. Black, P. Vagnarelli, W. Earnshaw, D. Gillespie, P. Jallepalli, and E. Schiebel. 2010. Vertebrate cells genetically deficient for Cdc14A or Cdc14B retain DNA damage checkpoint proficiency but are impaired in DNA repair. *The Journal of cell biology*. 189:631-639.
Mocciaro, A., and E. Schiebel. 2010. Cdc14: a highly conserved family of phosphatases with non-conserved functions? *Journal of cell science*. 123:2867-2876.
Mochida, S., S. Ikeo, J. Gannon, and T. Hunt. 2009. Regulated activity of PP2A-B55 delta is crucial for controlling entry into and exit from mitosis in Xenopus egg extracts. *The EMBO journal*. 28:2777-2785.
Mochida, S., S.L. Maslen, M. Skehel, and T. Hunt. 2010. Greatwall phosphorylates an inhibitor of protein phosphatase 2A that is essential for mitosis. *Science*. 330:1670-1673.
Mochida, S., S. Rata, H. Hino, T. Nagai, and B. Novak. 2016. Two Bistable Switches Govern M Phase Entry. *Current biology : CB*. 26:3361-3367.
Mollinari, C., J.P. Kleman, W. Jiang, G. Schoehn, T. Hunter, and R.L. Margolis. 2002. PRC1 is a microtubule binding and bundling protein essential to maintain the mitotic spindle midzone. *The Journal of cell biology*. 157:1175-1186.
Morgan, D.O. 1995. Principles of CDK regulation. *Nature*. 374:131-134.

Morin, V., S. Prieto, S. Melines, S. Hem, M. Rossignol, T. Lorca, J. Espeut, N. Morin, and A. Abrieu. 2012. CDK-dependent potentiation of MPS1 kinase activity is essential to the mitotic checkpoint. *Current biology : CB*. 22:289-295.

Morla, A.O., G. Draetta, D. Beach, and J.Y. Wang. 1989. Reversible tyrosine phosphorylation of cdc2: dephosphorylation accompanies activation during entry into mitosis. *Cell*. 58:193-203.

Moura, M., M. Osswald, N. Leca, J. Barbosa, A.J. Pereira, H. Maiato, C.E. Sunkel, and C. Conde. 2017. Protein Phosphatase 1 inactivates Mps1 to ensure efficient Spindle Assembly Checkpoint silencing. *eLife*. 6.

Mumby, M.C., K.L. Russell, L.J. Garrard, and D.D. Green. 1987. Cardiac contractile protein phosphatases. Purification of two enzyme forms and their characterization with subunit-specific antibodies. *The Journal of biological chemistry*. 262:6257-6265.

Murnion, M.E., R.R. Adams, D.M. Callister, C.D. Allis, W.C. Earnshaw, and J.R. Swedlow. 2001. Chromatin-associated protein phosphatase 1 regulates aurora-B and histone H3 phosphorylation. *The Journal of biological chemistry*. 276:26656-26665.

Murray, A.W., M.J. Solomon, and M.W. Kirschner. 1989. The role of cyclin synthesis and degradation in the control of maturation promoting factor activity. *Nature*. 339:280-286.

Musacchio, A. 2015. The Molecular Biology of Spindle Assembly Checkpoint Signaling Dynamics. *Current biology : CB*. 25:R1002-1018.

Musacchio, A., and E.D. Salmon. 2007. The spindle-assembly checkpoint in space and time. *Nature reviews. Molecular cell biology*. 8:379-393.

Nasa, I., S.F. Rusin, A.N. Kettenbach, and G.B. Moorhead. 2018. Aurora B opposes PP1 function in mitosis by phosphorylating the conserved PP1-binding RVxF motif in PP1 regulatory proteins. *Science signaling*. 11.

Neef, R., U. Gruneberg, R. Kopajtich, X. Li, E.A. Nigg, H. Sillje, and F.A. Barr. 2007. Choice of Plk1 docking partners during mitosis and cytokinesis is controlled by the activation state of Cdk1. *Nature cell biology*. 9:436-444.

Neef, R., U.R. Klein, R. Kopajtich, and F.A. Barr. 2006. Cooperation between mitotic kinesins controls the late stages of cytokinesis. *Current biology : CB*. 16:301-307.

Nicklas, R.B. 1997. How cells get the right chromosomes. *Science*. 275:632-637.

Nicklas, R.B., S.C. Ward, and G.J. Gorbsky. 1995. Kinetochore chemistry is sensitive to tension and may link mitotic forces to a cell cycle checkpoint. *The Journal of cell biology*. 130:929-939.

Nigg, E.A. 1993. Cellular substrates of p34(cdc2) and its companion cyclin-dependent kinases. *Trends in cell biology*. 3:296-301.

Nijenhuis, W., G. Vallardi, A. Teixeira, G.J. Kops, and A.T. Saurin. 2014. Negative feedback at kinetochores underlies a responsive spindle checkpoint signal. *Nature cell biology*. 16:1257-1264.

Nilsson, J., M. Yekezare, J. Minshull, and J. Pines. 2008. The APC/C maintains the spindle assembly checkpoint by targeting Cdc20 for destruction. *Nature cell biology*. 10:1411-1420.

Novak, B., and J.J. Tyson. 1993. Numerical analysis of a comprehensive model of M-phase control in Xenopus oocyte extracts and intact embryos. *Journal of cell science*. 106 (Pt 4):1153-1168.

Palozola, K.C., G. Donahue, H. Liu, G.R. Grant, J.S. Becker, A. Cote, H. Yu, A. Raj, and K.S. Zaret. 2017. Mitotic transcription and waves of gene reactivation during mitotic exit. *Science*. 358:119-122.

Park, J.E., N.K. Soung, Y. Johmura, Y.H. Kang, C. Liao, K.H. Lee, C.H. Park, M.C. Nicklaus, and K.S. Lee. 2010. Polo-box domain: a versatile mediator of polo-like kinase function. *Cellular and molecular life sciences : CMLS*. 67:1957-1970.

Passmore, L.A., E.A. McCormack, S.W. Au, A. Paul, K.R. Willison, J.W. Harper, and D. Barford. 2003. Doc1 mediates the activity of the anaphase-promoting complex by contributing to substrate recognition. *The EMBO journal*. 22:786-796.

Peeper, D.S., L.L. Parker, M.E. Ewen, M. Toebes, F.L. Hall, M. Xu, A. Zantema, A.J. van der Eb, and H. Piwnica-Worms. 1993. A- and B-type cyclins differentially modulate substrate specificity of cyclin-cdk complexes. *The EMBO journal*. 12:1947-1954.

Petronczki, M., M. Glotzer, N. Kraut, and J.M. Peters. 2007. Polo-like kinase 1 triggers the initiation of cytokinesis in human cells by promoting recruitment of the RhoGEF Ect2 to the central spindle. *Developmental cell*. 12:713-725.

Pfleger, C.M., and M.W. Kirschner. 2000. The KEN box: an APC recognition signal distinct from the D box targeted by Cdh1. *Genes & development*. 14:655-665.

Pfleger, C.M., E. Lee, and M.W. Kirschner. 2001. Substrate recognition by the Cdc20 and Cdh1 components of the anaphase-promoting complex. *Genes & development*. 15:2396-2407.

Picard, A., J.P. Capony, D.L. Brautigan, and M. Doree. 1989. Involvement of protein phosphatases 1 and 2A in the control of M phase-promoting factor activity in starfish. *The Journal of cell biology*. 109:3347-3354.

Pines, J., and T. Hunt. 1987. Molecular cloning and characterization of the mRNA for cyclin from sea urchin eggs. *The EMBO journal*. 6:2987-2995.

Pines, J., and T. Hunter. 1989. Isolation of a human cyclin cDNA: evidence for cyclin mRNA and protein regulation in the cell cycle and for interaction with p34cdc2. *Cell*. 58:833-846.

Pinsky, B.A., C.R. Nelson, and S. Biggins. 2009. Protein phosphatase 1 regulates exit from the spindle checkpoint in budding yeast. *Current biology : CB*. 19:1182-1187.

Pomerening, J.R., E.D. Sontag, and J.E. Ferrell, Jr. 2003. Building a cell cycle oscillator: hysteresis and bistability in the activation of Cdc2. *Nature cell biology*. 5:346-351.

Poon, R.Y., K. Yamashita, M. Howell, M.A. Ershler, A. Belyavsky, and T. Hunt. 1994. Cell cycle regulation of the p34cdc2/p33cdk2-activating kinase p40MO15. *Journal of cell science*. 107 (Pt 10):2789-2799.

Potel, C.M., M.H. Lin, A.J.R. Heck, and S. Lemeer. 2018. Defeating Major Contaminants in Fe(3+)- Immobilized Metal Ion Affinity Chromatography (IMAC) Phosphopeptide Enrichment. *Molecular & cellular proteomics : MCP*. 17:1028-1034.

Presler, M., E. Van Itallie, A.M. Klein, R. Kunz, M.L. Coughlin, L. Peshkin, S.P. Gygi, M. Wuhr, and M.W. Kirschner. 2017. Proteomics of phosphorylation and protein dynamics during fertilization and meiotic exit in the Xenopus egg. *Proceedings of the National Academy of Sciences of the United States of America*. 114:E10838-E10847.

Pyronnet, S., L. Pradayrol, and N. Sonenberg. 2000. A cell cycle-dependent internal ribosome entry site. *Molecular cell*. 5:607-616.

Qian, J., M. Beullens, J. Huang, S. De Munter, B. Lesage, and M. Bollen. 2015. Cdk1 orders mitotic events through coordination of a chromosome-associated phosphatase switch. *Nature communications*. 6:10215.

Qian, J., M. Beullens, B. Lesage, and M. Bollen. 2013. Aurora B defines its own chromosomal targeting by opposing the recruitment of the phosphatase scaffold Repo-Man. *Current biology : CB*. 23:1136-1143.

Qiao, R., F. Weissmann, M. Yamaguchi, N.G. Brown, R. VanderLinden, R. Imre, M.A. Jarvis, M.R. Brunner, I.F. Davidson, G. Litos, D. Haselbach, K. Mechtler, H. Stark, B.A. Schulman, and J.M. Peters. 2016. Mechanism of APC/CCDC20 activation by mitotic phosphorylation. *Proceedings of the National Academy of Sciences of the United States of America*. 113:E2570-2578.

Qin, X., and P. Sarnow. 2004. Preferential translation of internal ribosome entry site-containing mRNAs during the mitotic cycle in mammalian cells. *The Journal of biological chemistry*. 279:13721-13728.

Queralt, E., C. Lehane, B. Novak, and F. Uhlmann. 2006. Downregulation of PP2A(Cdc55) phosphatase by separase initiates mitotic exit in budding yeast. *Cell*. 125:719-732.

Queralt, E., and F. Uhlmann. 2008. Cdk-counteracting phosphatases unlock mitotic exit. *Current opinion in cell biology*. 20:661-668.

Ragusa, M.J., B. Dancheck, D.A. Critton, A.C. Nairn, R. Page, and W. Peti. 2010. Spinophilin directs protein phosphatase 1 specificity by blocking substrate binding sites. *Nature structural & molecular biology*. 17:459-464.

Rattani, A., P.K. Vinod, J. Godwin, K. Tachibana-Konwalski, M. Wolna, M. Malumbres, B. Novak, and K. Nasmyth. 2014. Dependency of the spindle assembly checkpoint on Cdk1 renders the anaphase transition irreversible. *Current biology : CB*. 24:630-637.

Reddy, S.K., M. Rape, W.A. Margansky, and M.W. Kirschner. 2007. Ubiquitination by the anaphase-promoting complex drives spindle checkpoint inactivation. *Nature*. 446:921-925.

Reed, S.I., J.A. Hadwiger, and A.T. Lorincz. 1985. Protein kinase activity associated with the product of the yeast cell division cycle gene CDC28. *Proceedings of the National Academy of Sciences of the United States of America*. 82:4055-4059.

Riedel, C.G., V.L. Katis, Y. Katou, S. Mori, T. Itoh, W. Helmhart, M. Galova, M. Petronczki, J. Gregan, B. Cetin, I. Mudrak, E. Ogris, K. Mechtler, L. Pelletier, F. Buchholz, K. Shirahige, and K. Nasmyth. 2006. Protein phosphatase 2A protects centromeric sister chromatid cohesion during meiosis I. *Nature*. 441:53-61.

Rodier, G., P. Coulombe, P.L. Tanguay, C. Boutonnet, and S. Meloche. 2008. Phosphorylation of Skp2 regulated by CDK2 and Cdc14B protects it from degradation by APC(Cdh1) in G1 phase. *The EMBO journal*. 27:679-691.

Rodrigues, N.T., S. Lekomtsev, S. Jananji, J. Kriston-Vizi, G.R. Hickson, and B. Baum. 2015. Kinetochore-localized PP1-Sds22 couples chromosome segregation to polar relaxation. *Nature*. 524:489-492.

Rogers, S., D. Fey, R.A. McCloy, B.L. Parker, N.J. Mitchell, R.J. Payne, R.J. Daly, D.E. James, C.E. Caldon, D.N. Watkins, D.R. Croucher, and A. Burgess.

2016. PP1 initiates the dephosphorylation of MASTL, triggering mitotic exit and bistability in human cells. *Journal of cell science*. 129:1340-1354.
Rosenberg, J.S., F.R. Cross, and H. Funabiki. 2011. KNL1/Spc105 recruits PP1 to silence the spindle assembly checkpoint. *Current biology : CB*. 21:942-947.
Roshak, A.K., E.A. Capper, C. Imburgia, J. Fornwald, G. Scott, and L.A. Marshall. 2000. The human polo-like kinase, PLK, regulates cdc2/cyclin B through phosphorylation and activation of the cdc25C phosphatase. *Cellular signalling*. 12:405-411.
Ruchaud, S., M. Carmena, and W.C. Earnshaw. 2007. Chromosomal passengers: conducting cell division. *Nature reviews. Molecular cell biology*. 8:798-812.
Russo, A.A., P.D. Jeffrey, and N.P. Pavletich. 1996. Structural basis of cyclin-dependent kinase activation by phosphorylation. *Nature structural biology*. 3:696-700.
Sackton, K.L., N. Dimova, X. Zeng, W. Tian, M. Zhang, T.B. Sackton, J. Meaders, K.L. Pfaff, F. Sigoillot, H. Yu, X. Luo, and R.W. King. 2014. Synergistic blockade of mitotic exit by two chemical inhibitors of the APC/C. *Nature*. 514:646-649.
Samwer, M., M.W.G. Schneider, R. Hoefler, P.S. Schmalhorst, J.G. Jude, J. Zuber, and D.W. Gerlich. 2017. DNA Cross-Bridging Shapes a Single Nucleus from a Set of Mitotic Chromosomes. *Cell*. 170:956-972 e923.
Saurin, A.T., M.S. van der Waal, R.H. Medema, S.M. Lens, and G.J. Kops. 2011. Aurora B potentiates Mps1 activation to ensure rapid checkpoint establishment at the onset of mitosis. *Nature communications*. 2:316.
Saville, M.K., and R.J. Watson. 1998. The cell-cycle regulated transcription factor B-Myb is phosphorylated by cyclin A/Cdk2 at sites that enhance its transactivation properties. *Oncogene*. 17:2679-2689.
Seki, A., and G. Fang. 2007. CKAP2 is a spindle-associated protein degraded by APC/C-Cdh1 during mitotic exit. *The Journal of biological chemistry*. 282:15103-15113.
Sharma, K., R.C. D'Souza, S. Tyanova, C. Schaab, J.R. Wisniewski, J. Cox, and M. Mann. 2014. Ultradeep human phosphoproteome reveals a distinct regulatory nature of Tyr and Ser/Thr-based signaling. *Cell reports*. 8:1583-1594.
Shepperd, L.A., J.C. Meadows, A.M. Sochaj, T.C. Lancaster, J. Zou, G.J. Buttrick, J. Rappsilber, K.G. Hardwick, and J.B. Millar. 2012. Phosphodependent recruitment of Bub1 and Bub3 to Spc7/KNL1 by Mph1 kinase maintains the spindle checkpoint. *Current biology : CB*. 22:891-899.
Shuda, M., C. Velasquez, E. Cheng, D.G. Cordek, H.J. Kwun, Y. Chang, and P.S. Moore. 2015. CDK1 substitutes for mTOR kinase to activate mitotic cap-dependent protein translation. *Proceedings of the National Academy of Sciences of the United States of America*. 112:5875-5882.
Sievers, F., A. Wilm, D. Dineen, T.J. Gibson, K. Karplus, W. Li, R. Lopez, H. McWilliam, M. Remmert, J. Soding, J.D. Thompson, and D.G. Higgins. 2011. Fast, scalable generation of high-quality protein multiple sequence alignments using Clustal Omega. *Molecular systems biology*. 7:539.
Skaar, J.R., J.K. Pagan, and M. Pagano. 2013. Mechanisms and function of substrate recruitment by F-box proteins. *Nature reviews. Molecular cell biology*. 14:369-381.
Skaar, J.R., J.K. Pagan, and M. Pagano. 2014. SCF ubiquitin ligase-targeted therapies. *Nature reviews. Drug discovery*. 13:889-903.

Skoko, D., M. Li, Y. Huang, M. Mizuuchi, M. Cai, C.M. Bradley, P.J. Pease, B. Xiao, J.F. Marko, R. Craigie, and K. Mizuuchi. 2009. Barrier-to-autointegration factor (BAF) condenses DNA by looping. *Proceedings of the National Academy of Sciences of the United States of America*. 106:16610-16615.

Skoufias, D.A., P.R. Andreassen, F.B. Lacroix, L. Wilson, and R.L. Margolis. 2001. Mammalian mad2 and bub1/bubR1 recognize distinct spindle-attachment and kinetochore-tension checkpoints. *Proceedings of the National Academy of Sciences of the United States of America*. 98:4492-4497.

Solomon, M.J., M. Glotzer, T.H. Lee, M. Philippe, and M.W. Kirschner. 1990. Cyclin activation of p34cdc2. *Cell*. 63:1013-1024.

Song, L., and M. Rape. 2010. Regulated degradation of spindle assembly factors by the anaphase-promoting complex. *Molecular cell*. 38:369-382.

Stefansson, B., and D.L. Brautigan. 2006. Protein phosphatase 6 subunit with conserved Sit4-associated protein domain targets IkappaBepsilon. *The Journal of biological chemistry*. 281:22624-22634.

Stefansson, B., T. Ohama, A.E. Daugherty, and D.L. Brautigan. 2008. Protein phosphatase 6 regulatory subunits composed of ankyrin repeat domains. *Biochemistry*. 47:1442-1451.

Stegmeier, F., and A. Amon. 2004. Closing mitosis: the functions of the Cdc14 phosphatase and its regulation. *Annual review of genetics*. 38:203-232.

Stegmeier, F., M. Rape, V.M. Draviam, G. Nalepa, M.E. Sowa, X.L. Ang, E.R. McDonald, 3rd, M.Z. Li, G.J. Hannon, P.K. Sorger, M.W. Kirschner, J.W. Harper, and S.J. Elledge. 2007. Anaphase initiation is regulated by antagonistic ubiquitination and deubiquitination activities. *Nature*. 446:876-881.

Stegmeier, F., R. Visintin, and A. Amon. 2002. Separase, polo kinase, the kinetochore protein Slk19, and Spo12 function in a network that controls Cdc14 localization during early anaphase. *Cell*. 108:207-220.

Stemmann, O., I.H. Gorr, and D. Boos. 2006. Anaphase topsy-turvy: Cdk1 a securin, separase a CKI. *Cell cycle*. 5:11-13.

Stern, B., and P. Nurse. 1996. A quantitative model for the cdc2 control of S phase and mitosis in fission yeast. *Trends in genetics : TIG*. 12:345-350.

Stewart, S., and G. Fang. 2005a. Anaphase-promoting complex/cyclosome controls the stability of TPX2 during mitotic exit. *Molecular and cellular biology*. 25:10516-10527.

Stewart, S., and G. Fang. 2005b. Destruction box-dependent degradation of aurora B is mediated by the anaphase-promoting complex/cyclosome and Cdh1. *Cancer research*. 65:8730-8735.

Su, K.C., T. Takaki, and M. Petronczki. 2011. Targeting of the RhoGEF Ect2 to the equatorial membrane controls cleavage furrow formation during cytokinesis. *Developmental cell*. 21:1104-1115.

Sudakin, V., D. Ganoth, A. Dahan, H. Heller, J. Hershko, F.C. Luca, J.V. Ruderman, and A. Hershko. 1995. The cyclosome, a large complex containing cyclin-selective ubiquitin ligase activity, targets cyclins for destruction at the end of mitosis. *Molecular biology of the cell*. 6:185-197.

Suijkerbuijk, S.J., M. Vleugel, A. Teixeira, and G.J. Kops. 2012. Integration of kinase and phosphatase activities by BUBR1 ensures formation of stable kinetochore-microtubule attachments. *Developmental cell*. 23:745-755.

Swenson, K.I., K.M. Farrell, and J.V. Ruderman. 1986. The clam embryo protein cyclin A induces entry into M phase and the resumption of meiosis in Xenopus oocytes. *Cell*. 47:861-870.

Takaki, T., M. Montagner, M.P. Serres, M. Le Berre, M. Russell, L. Collinson, K. Szuhai, M. Howell, S.J. Boulton, E. Sahai, and M. Petronczki. 2017. Actomyosin drives cancer cell nuclear dysmorphia and threatens genome stability. *Nature communications*. 8:16013.

Tang, Z., B. Li, R. Bharadwaj, H. Zhu, E. Ozkan, K. Hakala, J. Deisenhofer, and H. Yu. 2001. APC2 Cullin protein and APC11 RING protein comprise the minimal ubiquitin ligase module of the anaphase-promoting complex. *Molecular biology of the cell*. 12:3839-3851.

Tang, Z., H. Shu, W. Qi, N.A. Mahmood, M.C. Mumby, and H. Yu. 2006. PP2A is required for centromeric localization of Sgo1 and proper chromosome segregation. *Developmental cell*. 10:575-585.

Tassan, J.P., M. Jaquenoud, A.M. Fry, S. Frutiger, G.J. Hughes, and E.A. Nigg. 1995. In vitro assembly of a functional human CDK7-cyclin H complex requires MAT1, a novel 36 kDa RING finger protein. *The EMBO journal*. 14:5608-5617.

Tassan, J.P., S.J. Schultz, J. Bartek, and E.A. Nigg. 1994. Cell cycle analysis of the activity, subcellular localization, and subunit composition of human CAK (CDK-activating kinase). *The Journal of cell biology*. 127:467-478.

Taylor, S., and J.M. Peters. 2008. Polo and Aurora kinases: lessons derived from chemical biology. *Current opinion in cell biology*. 20:77-84.

Terrak, M., F. Kerff, K. Langsetmo, T. Tao, and R. Dominguez. 2004. Structural basis of protein phosphatase 1 regulation. *Nature*. 429:780-784.

Tipton, A.R., W. Ji, B. Sturt-Gillespie, M.E. Bekier, 2nd, K. Wang, W.R. Taylor, and S.T. Liu. 2013. Monopolar spindle 1 (MPS1) kinase promotes production of closed MAD2 (C-MAD2) conformer and assembly of the mitotic checkpoint complex. *The Journal of biological chemistry*. 288:35149-35158.

Tipton, A.R., K. Wang, L. Link, J.J. Bellizzi, H. Huang, T. Yen, and S.T. Liu. 2011. BUBR1 and closed MAD2 (C-MAD2) interact directly to assemble a functional mitotic checkpoint complex. *The Journal of biological chemistry*. 286:21173-21179.

Tonks, N.K. 2006. Protein tyrosine phosphatases: from genes, to function, to disease. *Nature reviews. Molecular cell biology*. 7:833-846.

Toyoshima, F., T. Moriguchi, A. Wada, M. Fukuda, and E. Nishida. 1998. Nuclear export of cyclin B1 and its possible role in the DNA damage-induced G2 checkpoint. *The EMBO journal*. 17:2728-2735.

Trinkle-Mulcahy, L., J. Andersen, Y.W. Lam, G. Moorhead, M. Mann, and A.I. Lamond. 2006. Repo-Man recruits PP1 gamma to chromatin and is essential for cell viability. *The Journal of cell biology*. 172:679-692.

Tyanova, S., T. Temu, and J. Cox. 2016a. The MaxQuant computational platform for mass spectrometry-based shotgun proteomics. *Nature protocols*. 11:2301-2319.

Tyanova, S., T. Temu, P. Sinitcyn, A. Carlson, M.Y. Hein, T. Geiger, M. Mann, and J. Cox. 2016b. The Perseus computational platform for comprehensive analysis of (prote)omics data. *Nature methods*. 13:731-740.

Uhlmann, F., C. Bouchoux, and S. Lopez-Aviles. 2011. A quantitative model for cyclin-dependent kinase control of the cell cycle: revisited. *Philosophical*

transactions of the Royal Society of London. Series B, Biological sciences. 366:3572-3583.

Uzunova, K., B.T. Dye, H. Schutz, R. Ladurner, G. Petzold, Y. Toyoda, M.A. Jarvis, N.G. Brown, I. Poser, M. Novatchkova, K. Mechtler, A.A. Hyman, H. Stark, B.A. Schulman, and J.M. Peters. 2012. APC15 mediates CDC20 autoubiquitylation by APC/C(MCC) and disassembly of the mitotic checkpoint complex. *Nature structural & molecular biology*. 19:1116-1123.

Vagnarelli, P., S. Ribeiro, L. Sennels, L. Sanchez-Pulido, F. de Lima Alves, T. Verheyen, D.A. Kelly, C.P. Ponting, J. Rappsilber, and W.C. Earnshaw. 2011. Repo-Man coordinates chromosomal reorganization with nuclear envelope reassembly during mitotic exit. *Developmental cell*. 21:328-342.

van Leuken, R., L. Clijsters, W. van Zon, D. Lim, X. Yao, R.M. Wolthuis, M.B. Yaffe, R.H. Medema, and M.A. van Vugt. 2009. Polo-like kinase-1 controls Aurora A destruction by activating APC/C-Cdh1. *PloS one*. 4:e5282.

Van Voorhis, V.A., and D.O. Morgan. 2014. Activation of the APC/C ubiquitin ligase by enhanced E2 efficiency. *Current biology : CB*. 24:1556-1562.

van Zon, W., J. Ogink, B. ter Riet, R.H. Medema, H. te Riele, and R.M. Wolthuis. 2010. The APC/C recruits cyclin B1-Cdk1-Cks in prometaphase before D box recognition to control mitotic exit. *The Journal of cell biology*. 190:587-602.

Vandre, D.D., and V.L. Wills. 1992. Inhibition of mitosis by okadaic acid: possible involvement of a protein phosphatase 2A in the transition from metaphase to anaphase. *Journal of cell science*. 101 (Pt 1):79-91.

Vankova Hausnerova, V., and C. Lanctot. 2017. Transcriptional Output Transiently Spikes Upon Mitotic Exit. *Scientific reports*. 7:12607.

Vanoosthuyse, V., and K.G. Hardwick. 2009. A novel protein phosphatase 1-dependent spindle checkpoint silencing mechanism. *Current biology : CB*. 19:1176-1181.

Vazquez-Novelle, M.D., V. Esteban, A. Bueno, and M.P. Sacristan. 2005. Functional homology among human and fission yeast Cdc14 phosphatases. *The Journal of biological chemistry*. 280:29144-29150.

Vazquez-Novelle, M.D., L. Sansregret, A.E. Dick, C.A. Smith, A.D. McAinsh, D.W. Gerlich, and M. Petronczki. 2014. Cdk1 inactivation terminates mitotic checkpoint surveillance and stabilizes kinetochore attachments in anaphase. *Current biology : CB*. 24:638-645.

Vigneron, S., E. Brioudes, A. Burgess, J.C. Labbe, T. Lorca, and A. Castro. 2009. Greatwall maintains mitosis through regulation of PP2A. *The EMBO journal*. 28:2786-2793.

Vigneron, S., A. Gharbi-Ayachi, A.A. Raymond, A. Burgess, J.C. Labbe, G. Labesse, B. Monsarrat, T. Lorca, and A. Castro. 2011. Characterization of the mechanisms controlling Greatwall activity. *Molecular and cellular biology*. 31:2262-2275.

Visconti, R., L. Palazzo, R. Della Monica, and D. Grieco. 2012. Fcp1-dependent dephosphorylation is required for M-phase-promoting factor inactivation at mitosis exit. *Nature communications*. 3:894.

Visintin, R., K. Craig, E.S. Hwang, S. Prinz, M. Tyers, and A. Amon. 1998. The phosphatase Cdc14 triggers mitotic exit by reversal of Cdk-dependent phosphorylation. *Molecular cell*. 2:709-718.

Visintin, R., S. Prinz, and A. Amon. 1997. CDC20 and CDH1: a family of substrate-specific activators of APC-dependent proteolysis. *Science*. 278:460-463.

Voets, E., and R.M. Wolthuis. 2010. MASTL is the human orthologue of Greatwall kinase that facilitates mitotic entry, anaphase and cytokinesis. *Cell cycle*. 9:3591-3601.

Wakula, P., M. Beullens, H. Ceulemans, W. Stalmans, and M. Bollen. 2003. Degeneracy and function of the ubiquitous RVXF motif that mediates binding to protein phosphatase-1. *The Journal of biological chemistry*. 278:18817-18823.

Walczak, C.E., and S.L. Shaw. 2010. A MAP for bundling microtubules. *Cell*. 142:364-367.

Wang, W., and M.W. Kirschner. 2013. Emi1 preferentially inhibits ubiquitin chain elongation by the anaphase-promoting complex. *Nature cell biology*. 15:797-806.

Wang, X., R. Bajaj, M. Bollen, W. Peti, and R. Page. 2016. Expanding the PP2A Interactome by Defining a B56-Specific SLiM. *Structure*. 24:2174-2181.

Wang, Z., P. Liu, H. Inuzuka, and W. Wei. 2014. Roles of F-box proteins in cancer. *Nature reviews. Cancer*. 14:233-247.

Watanabe, N., H. Arai, J. Iwasaki, M. Shiina, K. Ogata, T. Hunter, and H. Osada. 2005. Cyclin-dependent kinase (CDK) phosphorylation destabilizes somatic Wee1 via multiple pathways. *Proceedings of the National Academy of Sciences of the United States of America*. 102:11663-11668.

Watanabe, N., H. Arai, Y. Nishihara, M. Taniguchi, N. Watanabe, T. Hunter, and H. Osada. 2004. M-phase kinases induce phospho-dependent ubiquitination of somatic Wee1 by SCFbeta-TrCP. *Proceedings of the National Academy of Sciences of the United States of America*. 101:4419-4424.

Watanabe, T., E.F. da Cruz e Silva, H.B. Huang, N. Starkova, Y.G. Kwon, A. Horiuchi, P. Greengard, and A.C. Nairn. 2003. Preparation and characterization of recombinant protein phosphatase 1. *Methods in enzymology*. 366:321-338.

Waterhouse, A.M., J.B. Procter, D.M. Martin, M. Clamp, and G.J. Barton. 2009. Jalview Version 2--a multiple sequence alignment editor and analysis workbench. *Bioinformatics*. 25:1189-1191.

Wei, R.R., J. Al-Bassam, and S.C. Harrison. 2007. The Ndc80/HEC1 complex is a contact point for kinetochore-microtubule attachment. *Nature structural & molecular biology*. 14:54-59.

Wei, S., H.C. Yang, H.C. Chuang, J. Yang, S.K. Kulp, P.J. Lu, M.D. Lai, and C.S. Chen. 2008. A novel mechanism by which thiazolidinediones facilitate the proteasomal degradation of cyclin D1 in cancer cells. *The Journal of biological chemistry*. 283:26759-26770.

Welburn, J.P., M. Vleugel, D. Liu, J.R. Yates, 3rd, M.A. Lampson, T. Fukagawa, and I.M. Cheeseman. 2010. Aurora B phosphorylates spatially distinct targets to differentially regulate the kinetochore-microtubule interface. *Molecular cell*. 38:383-392.

Welcker, M., and B.E. Clurman. 2008. FBW7 ubiquitin ligase: a tumour suppressor at the crossroads of cell division, growth and differentiation. *Nature reviews. Cancer*. 8:83-93.

Wertz, I.E., S. Kusam, C. Lam, T. Okamoto, W. Sandoval, D.J. Anderson, E. Helgason, J.A. Ernst, M. Eby, J. Liu, L.D. Belmont, J.S. Kaminker, K.M. O'Rourke, K. Pujara, P.B. Kohli, A.R. Johnson, M.L. Chiu, J.R. Lill, P.K. Jackson, W.J. Fairbrother, S. Seshagiri, M.J. Ludlam, K.G. Leong, E.C. Dueber, H. Maecker, D.C. Huang, and V.M. Dixit. 2011. Sensitivity to

antitubulin chemotherapeutics is regulated by MCL1 and FBW7. *Nature*. 471:110-114.

Whitfield, M.L., G. Sherlock, A.J. Saldanha, J.I. Murray, C.A. Ball, K.E. Alexander, J.C. Matese, C.M. Perou, M.M. Hurt, P.O. Brown, and D. Botstein. 2002. Identification of genes periodically expressed in the human cell cycle and their expression in tumors. *Molecular biology of the cell*. 13:1977-2000.

Wickliffe, K.E., S. Lorenz, D.E. Wemmer, J. Kuriyan, and M. Rape. 2011. The mechanism of linkage-specific ubiquitin chain elongation by a single-subunit E2. *Cell*. 144:769-781.

Wilker, E.W., M.A. van Vugt, S.A. Artim, P.H. Huang, C.P. Petersen, H.C. Reinhardt, Y. Feng, P.A. Sharp, N. Sonenberg, F.M. White, and M.B. Yaffe. 2007. 14-3-3sigma controls mitotic translation to facilitate cytokinesis. *Nature*. 446:329-332.

Williams, B.C., J.J. Filter, K.A. Blake-Hodek, B.E. Wadzinski, N.J. Fuda, D. Shalloway, and M.L. Goldberg. 2014. Greatwall-phosphorylated Endosulfine is both an inhibitor and a substrate of PP2A-B55 heterotrimers. *eLife*. 3:e01695.

Williamson, A., K.E. Wickliffe, B.G. Mellone, L. Song, G.H. Karpen, and M. Rape. 2009. Identification of a physiological E2 module for the human anaphase-promoting complex. *Proceedings of the National Academy of Sciences of the United States of America*. 106:18213-18218.

Winkler, C., S. De Munter, N. Van Dessel, B. Lesage, E. Heroes, S. Boens, M. Beullens, A. Van Eynde, and M. Bollen. 2015. The selective inhibition of protein phosphatase-1 results in mitotic catastrophe and impaired tumor growth. *Journal of cell science*. 128:4526-4537.

Wisniewski, J.R., A. Zougman, N. Nagaraj, and M. Mann. 2009. Universal sample preparation method for proteome analysis. *Nature methods*. 6:359-362.

Wojcik, E., R. Basto, M. Serr, F. Scaerou, R. Karess, and T. Hays. 2001. Kinetochore dynein: its dynamics and role in the transport of the Rough deal checkpoint protein. *Nature cell biology*. 3:1001-1007.

Wolfe, B.A., T. Takaki, M. Petronczki, and M. Glotzer. 2009. Polo-like kinase 1 directs assembly of the HsCyk-4 RhoGAP/Ect2 RhoGEF complex to initiate cleavage furrow formation. *PLoS biology*. 7:e1000110.

Wu, J., H.P. Cho, D.B. Rhee, D.K. Johnson, J. Dunlap, Y. Liu, and Y. Wang. 2008. Cdc14B depletion leads to centriole amplification, and its overexpression prevents unscheduled centriole duplication. *The Journal of cell biology*. 181:475-483.

Wu, J.Q., J.Y. Guo, W. Tang, C.S. Yang, C.D. Freel, C. Chen, A.C. Nairn, and S. Kornbluth. 2009. PP1-mediated dephosphorylation of phosphoproteins at mitotic exit is controlled by inhibitor-1 and PP1 phosphorylation. *Nature cell biology*. 11:644-651.

Wurzenberger, C., and D.W. Gerlich. 2011. Phosphatases: providing safe passage through mitotic exit. *Nature reviews. Molecular cell biology*. 12:469-482.

Xing, Y., Y. Xu, Y. Chen, P.D. Jeffrey, Y. Chao, Z. Lin, Z. Li, S. Strack, J.B. Stock, and Y. Shi. 2006. Structure of protein phosphatase 2A core enzyme bound to tumor-inducing toxins. *Cell*. 127:341-353.

Xu, Y., Y. Chen, P. Zhang, P.D. Jeffrey, and Y. Shi. 2008. Structure of a protein phosphatase 2A holoenzyme: insights into B55-mediated Tau dephosphorylation. *Molecular cell*. 31:873-885.

Xu, Y., Y. Xing, Y. Chen, Y. Chao, Z. Lin, E. Fan, J.W. Yu, S. Strack, P.D. Jeffrey, and Y. Shi. 2006. Structure of the protein phosphatase 2A holoenzyme. *Cell*. 127:1239-1251.

Xu, Z., B. Cetin, M. Anger, U.S. Cho, W. Helmhart, K. Nasmyth, and W. Xu. 2009. Structure and function of the PP2A-shugoshin interaction. *Molecular cell*. 35:426-441.

Yamagishi, Y., C.H. Yang, Y. Tanno, and Y. Watanabe. 2012. MPS1/Mph1 phosphorylates the kinetochore protein KNL1/Spc7 to recruit SAC components. *Nature cell biology*. 14:746-752.

Yamaguchi, M., R. VanderLinden, F. Weissmann, R. Qiao, P. Dube, N.G. Brown, D. Haselbach, W. Zhang, S.S. Sidhu, J.M. Peters, H. Stark, and B.A. Schulman. 2016. Cryo-EM of Mitotic Checkpoint Complex-Bound APC/C Reveals Reciprocal and Conformational Regulation of Ubiquitin Ligation. *Molecular cell*. 63:593-607.

Yamano, H., K. Ishii, and M. Yanagida. 1994. Phosphorylation of dis2 protein phosphatase at the C-terminal cdc2 consensus and its potential role in cell cycle regulation. *The EMBO journal*. 13:5310-5318.

Yamashita, K., H. Yasuda, J. Pines, K. Yasumoto, H. Nishitani, M. Ohtsubo, T. Hunter, T. Sugimura, and T. Nishimoto. 1990. Okadaic acid, a potent inhibitor of type 1 and type 2A protein phosphatases, activates cdc2/H1 kinase and transiently induces a premature mitosis-like state in BHK21 cells. *The EMBO journal*. 9:4331-4338.

Yang, J., E.S. Bardes, J.D. Moore, J. Brennan, M.A. Powers, and S. Kornbluth. 1998. Control of cyclin B1 localization through regulated binding of the nuclear export factor CRM1. *Genes & development*. 12:2131-2143.

Yu, J., S.L. Fleming, B. Williams, E.V. Williams, Z. Li, P. Somma, C.L. Rieder, and M.L. Goldberg. 2004. Greatwall kinase: a nuclear protein required for proper chromosome condensation and mitotic progression in Drosophila. *The Journal of cell biology*. 164:487-492.

Yu, J., Y. Zhao, Z. Li, S. Galas, and M.L. Goldberg. 2006. Greatwall kinase participates in the Cdc2 autoregulatory loop in Xenopus egg extracts. *Molecular cell*. 22:83-91.

Yuce, O., A. Piekny, and M. Glotzer. 2005. An ECT2-centralspindlin complex regulates the localization and function of RhoA. *The Journal of cell biology*. 170:571-582.

Zachariae, W., M. Schwab, K. Nasmyth, and W. Seufert. 1998. Control of cyclin ubiquitination by CDK-regulated binding of Hct1 to the anaphase promoting complex. *Science*. 282:1721-1724.

Zachariae, W., T.H. Shin, M. Galova, B. Obermaier, and K. Nasmyth. 1996. Identification of subunits of the anaphase-promoting complex of Saccharomyces cerevisiae. *Science*. 274:1201-1204.

Zeng, K., R.N. Bastos, F.A. Barr, and U. Gruneberg. 2010a. Protein phosphatase 6 regulates mitotic spindle formation by controlling the T-loop phosphorylation state of Aurora A bound to its activator TPX2. *The Journal of cell biology*. 191:1315-1332.

Zeng, X., and R.W. King. 2012. An APC/C inhibitor stabilizes cyclin B1 by prematurely terminating ubiquitination. *Nature chemical biology*. 8:383-392.

Zeng, X., F. Sigoillot, S. Gaur, S. Choi, K.L. Pfaff, D.C. Oh, N. Hathaway, N. Dimova, G.D. Cuny, and R.W. King. 2010b. Pharmacologic inhibition of the anaphase-

promoting complex induces a spindle checkpoint-dependent mitotic arrest in the absence of spindle damage. *Cancer cell*. 18:382-395.

Zhang, S., L. Chang, C. Alfieri, Z. Zhang, J. Yang, S. Maslen, M. Skehel, and D. Barford. 2016. Molecular mechanism of APC/C activation by mitotic phosphorylation. *Nature*. 533:260-264.

Zhang, Y., J. van Deursen, and P.J. Galardy. 2011. Overexpression of ubiquitin specific protease 44 (USP44) induces chromosomal instability and is frequently observed in human T-cell leukemia. *PloS one*. 6:e23389.

Zhao, W.M., J.A. Coppinger, A. Seki, X.L. Cheng, J.R. Yates, 3rd, and G. Fang. 2008a. RCS1, a substrate of APC/C, controls the metaphase to anaphase transition. *Proceedings of the National Academy of Sciences of the United States of America*. 105:13415-13420.

Zhao, W.M., and G. Fang. 2005. Anillin is a substrate of anaphase-promoting complex/cyclosome (APC/C) that controls spatial contractility of myosin during late cytokinesis. *The Journal of biological chemistry*. 280:33516-33524.

Zhao, Y., O. Haccard, R. Wang, J. Yu, J. Kuang, C. Jessus, and M.L. Goldberg. 2008b. Roles of Greatwall kinase in the regulation of cdc25 phosphatase. *Molecular biology of the cell*. 19:1317-1327.

Zheng, N., Q. Zhou, Z. Wang, and W. Wei. 2016. Recent advances in SCF ubiquitin ligase complex: Clinical implications. *Biochimica et biophysica acta*. 1866:12-22.

Zhu, T., Z. Dou, B. Qin, C. Jin, X. Wang, L. Xu, Z. Wang, L. Zhu, F. Liu, X. Gao, Y. Ke, Z. Wang, F. Aikhionbare, C. Fu, X. Ding, and X. Yao. 2013. Phosphorylation of microtubule-binding protein Hec1 by mitotic kinase Aurora B specifies spindle checkpoint kinase Mps1 signaling at the kinetochore. *The Journal of biological chemistry*. 288:36149-36159.